YEAR-END TECHNICAL REPORT
August 29, 2015 to August 28, 2016

Environmental Remediation Science and Technology

Date submitted:

October 21, 2016

Principal Investigator:

Leonel E. Lagos, Ph.D., PMP®

Florida International University Collaborators:

Yelena Katsenovich, Ph.D.
Ravi Gudavalli, Ph.D.
Angelique Lawrence, M.S., GISP
Reinaldo Garcia, Ph.D.
Shimelis Setegn, Ph.D.
David Roelant, Ph.D.
Vasileios Anagnostopoulos, Ph.D.
Hilary P. Emerson, Ph.D.
Mehrnoosh Mahmoudi, Ph.D.
Alberto Abarca, Graduate Research Assistant
DOE Fellows

Prepared for:

U.S. Department of Energy
Office of Environmental Management
Under Cooperative Agreement # DE-EM0000598

Addendum:

This document represents one (1) of four (4) reports that comprise the Year End Reports for the period of August 29, 2015 to August 28, 2016 prepared by the Applied Research Center at Florida International University for the U.S. Department of Energy Office of Environmental Management (DOE-EM) under Cooperative Agreement No. DE-EM0000598.

The complete set of FIU's Year End Reports for this reporting period includes the following documents:

Project 1: Chemical Process Alternatives for Radioactive Waste
Document number: FIU-ARC-2016-800006470-04b-249

Project 2: Environmental Remediation Science and Technology
Document number: FIU-ARC-2016-800006471-04b-250

Project 3: Waste and D&D Engineering and Technology Development
Document number: FIU-ARC-2016-800006472-04b-238

Project 4: DOE-FIU Science & Technology Workforce Development Initiative
Document number: FIU-ARC-2016-800006473-04b-251

Each document will be submitted to OSTI separately under the respective project title and document number as shown above.

TABLE OF CONTENTS

LIST OF FIGURES

LIST OF TABLES

PROJECT 2 OVERVIEW

Nuclear weapons production and other defense-related activities at U.S. Department of Energy (DOE) sites have resulted in radionuclide and heavy metal contamination in surface and subsurface environments nationwide. Florida International University (FIU) is conducting applied research in collaboration with Pacific Northwest National Laboratory (PNNL), Savannah River National Laboratory (SRNL) and Savannah River Ecology Laboratory (SREL) scientists to support environmental remediation efforts at the Hanford Site and Savannah River Site (SRS), which are focused on cleanup technologies for contaminated soil and groundwater and the assessment of the fate and transport of contaminants in the environment. FIU is also teaming with scientists at Los Alamos National Laboratory (LANL) and the DOE Carlsbad Field Office (CBFO) to address potential contamination issues and update risk assessment models associated with the disposal of large quantities of defense-related, transuranic waste at the Waste Isolation Pilot Plant (WIPP). The aim of FIU's research is to reduce the potential for contaminant mobility or toxicity in the surface and subsurface through the development and application of state-of-the-art scientific and environmental remediation technologies at DOE sites.

Project 2, Environmental Remediation Science & Technology, focuses on providing assistance to Hanford Site and Savannah River Site (SRS) in environmental cleanup of soil and groundwater and to the WIPP in predicting the potential for release of contaminants from the deep geologic repository. During FIU Performance Year 6 (2015-2016), FIU ARC worked on five tasks:

Task 1: Remediation Research and Technical Support for the Hanford Site

Legacy waste from the development of atomic weapons at the Hanford Site has left significant radionuclide contamination in soil and groundwater. There is a need to further investigate the environmental fate of uranium and technetium under natural conditions and following remediation. For example, a significant residual mass of uranium still resides in the deep vadose zone (VZ) following release of over 200,000 kg of uranium from improper waste disposal and accidental spills (Szecsody et al. 2013).

During FIU Performance Year 6, ammonia gas and tripolyphosphate injection as a remediation strategy for uranium were investigated further with laboratory-scale experiments. Ammonia gas injection is currently being considered for uranium remediation at the pilot scale in the 200 Area of the Hanford Site. Previous work has shown that the injection of NH_3 gas to the vadose zone is a viable method to decrease uranium mobility in the contaminated subsurface via pH manipulation and co-precipitation processes (Szecsody et al. 2012a, Zhong et al. 2015). However, batch experiments focused on understanding the mechanisms leading to removal of uranium in the presence and absence of minerals and sediments as well as the mineral dissolution caused by weak base treatment. Furthermore, isopiestic and spectroscopic methods were a significant focus to better characterize these systems.

Pilot scale testing of tripolyphosphate injection for the formation of apatite and autunite minerals in the 300 Area subsurface was completed in 2009 (Vermeul et al. 2009). Although it was initially found to be an effective remediation technology, there was a rebound in aqueous uranium concentrations after several months. Therefore, there is a need to better understand the dissolution of autunite minerals especially through microbial pathways. Autunite and meta-autunite minerals, as $(X^m)_{2/m}[(UO_2)(PO_4)]_2 \cdot xH_2O$ where X is a monovalent or divalent cation, are

an important group of uranyl minerals acting as a sink for dissolved U(VI) in soils. Even small quantities of phosphate present in groundwater can promote the formation of autunite group minerals that can persist over geologic periods (De Vivo et al. 1984).

Bacteria may dissolve uranyl-phosphate minerals in an effort to obtain phosphorous, thus liberating uranium from the solid phase. In addition to the biological activity, the presence of bicarbonate ions enhances the release of U(VI) into the aqueous phase (Gudavalli et al., 2013). Experiments in Year 6 focused on understanding of the effect of *Shewanella* cells on the biodissolution of natural Ca-autunite minerals. A new subtask was also initiated with a PNNL internship (DOE Fellow Alejandro Garcia) in spring of 2016. This task strives to utilize spectral induced polarization (SIP) geophysical measurements to detect the formation of biofilms based on their changes to the physical and electrical properties of the subsurface.

Currently, four graduate students are involved in this research, including DOE Fellows Robert Lapierre and Alejandro Garcia, working towards their master's degrees and DOE Fellows Silvina Di Pietro and Claudia Cardona working towards their PhDs.

Task 2. Remediation Research and Technical Support for Savannah River Site

The F/H Area Seepage Basins located in the center of SRS received approximately 1.8 billion gallons of acidic waste solutions (pH from 3.2 to 5.5) contaminated with a variety of radionuclides and dissolved metals. The acidic nature of the basin waste solutions caused the mobilization of metals and radionuclides, resulting in contaminated groundwater plumes. The primary focus of this investigation is uranium (VI), which is a key contaminant of concern in the basin's groundwater. During FIU Performance Year 6, the main objectives of this research was to assess whether sodium silicate has sufficient alkalinity to restore the natural pH of the groundwater and to investigate via batch and column experiments humic substances abilities to affect the mobility of actinides in natural systems. Currently, four students are supporting this research including DOE Fellow Hansell Gonzalez working towards his Ph.D.

This task also conducted microcosm studies mimicking conditions after the ARCADIS demonstration at the SRS F-Area. The experiments were based on molasses injections in the F/H Area wells to create anaerobic conditions in the subsurface. The sample analysis and speciation modeling predictions did not suggest the formation of reduced iron phases such as siderite or pyrite.

Task 3: Surface Water Modeling of Tims Branch

The principal objective of this task is to develop an integrated hydrology/transport model as a tool to estimate flow and transport parameters and predict the spatial and temporal distribution of contaminants during extreme storm events. Results from this study are key to evaluating the effectiveness of tin(II)-based mercury treatment at the SRS site, and are also relevant to evaluating the potential of using water treatment and novel remediation technologies in other mercury-contaminated streams.

Task 4: Sustainability Plan for the A/M Area Groundwater Remediation System

DOE sites are developing sustainability programs, projects and initiatives in order to help meet the goals as set out in individual Site Sustainability Plans (SSPs) and the overall U.S. DOE 2013 Strategic Sustainability Performance Plan. There are many benefits of implementing sustainable practices, including reducing costs as well as fostering better engagement and acceptance of

improved remediation strategies and sustainable practices by regulators, the public, and other stakeholders. These benefits are in addition to the more obvious ones of reducing energy consumption, improving air and water quality, minimizing impact to the environment, reducing carbon footprints, and reducing waste generation. The research and analysis performed under this task was performed under the direction of Mr. Albes Gaona, program lead for DOE's Sustainable Remediation Program. The analysis was focused on the M1 Air Stripper: its mechanical systems, volume flow rate of water and contaminant concentration, performance of the packing material, and the blower motor. During FIU Performance Year 6, FIU analyzed the equipment, processes, hydraulic containment of contamination, and developed a set of recommendations for the existing infrastructure of the groundwater remediation system that will reduce the environmental burden of the A/M Area groundwater remediation system. This task and associated research was completed and a technical report was submitted to SRNL and DOE.

Task 5: Remediation Research and Technical Support for the WIPP

A new collaboration was begun in spring 2016 with Los Alamos National Laboratory's field office at the Carlsbad Environmental Monitoring and Research Center (LANL CEMRC) which is a part of New Mexico State University. Hilary Emerson spent ten weeks working at the LANL CEMRC laboratories to kick off this new task in collaboration with Drs. Tim Dittrich and Donald Reed. The goal is to generate accurate sorption data for the actinides to minerals and under conditions relevant to the Waste Isolation Pilot Plant as previous risk assessment models are based on conservative assumptions. During FIU Performance Year 6, batch and mini column experiments were initiated to understand sorption of neodymium as an analog for the trivalent actinides at ionic strength from 0.1 - 5.0 M. DOE Fellow Frances Zengotita (B.S. Chemistry and English) also supported this project.

TASK 1: SEQUESTERING URANIUM AT THE HANFORD 200 AREA BY IN SITU SUBSURFACE PH MANIPULATION USING AMMONIA (NH$_3$) GAS

TASK 1: EXECUTIVE SUMMARY

During FIU Performance Year 6, research focused on the speciation modeling simulations to correlate results with SEM/EDS and XRD analysis on the selected precipitate samples. Another focus of this research was to investigate the stability of the multicomponent uranium-bearing precipitates mimicking those created in sediments as a result of alkaline ammonia gas treatment in the vadose zone. The amount of water adsorbed on uranium-bearing precipitates was determined gravimetrically by the isopiestic method. The results indicate that gravimetric measurements of moisture uptake as a function of increasing relative humidity can provide reasonable estimates of the deliquescence point of solid phases or its components. This research was the basis for a manuscript accepted for the publication in the *Applied Geochemistry Journal.* The results of these studies were also summarized in the abstract "Removal of U(VI) in the Alkaline Conditions Created by NH$_3$ Gas" submitted to the Waste Management in March 2017.

During FIU Performance Year 6, new experiments were begun to understand the partitioning of uranium and dissolution of minerals following base treatment. This work is helping to understand the mechanisms controlling the fate of uranium during and after base treatment as a potential remediation technique. Silvina Di Pietro, a DOE Fellow and Ph.D. student within the chemistry department, began working on this project in August 2015. In March 2016, she was awarded the Roy G. Post scholarship at the Waste Management Conference and presented a student poster on the research work entitled "A comparison of NH$_4$OH and NaOH treatments for uranium immobilization in the presence of kaolinite."

In addition, FIU submitted a technical report to DOE-EM on June 22, 2016 entitled, "Effects of ammonia on uranium partitioning and kaolinite mineral dissolution." An updated version of this report was submitted for publication in the *Journal of Environmental Radioactivity* in August 2016 and is currently being revised for final publication. Hilary P. Emerson, a FIU-ARC postdoctoral scholar, also presented an oral presentation and a Sci-Mix poster at the American Chemical Society fall meeting in August 2016. Her presentation was entitled "Investigation of ammonia gas treatment for the immobilization of uranium in the presence of pure minerals." Di Pietro has also submitted to present during the professional section at Waste Management in March 2017 with an abstract entitled "Ammonia gas treatment for uranium immobilization at DOE Hanford's Site."

This task also investigated autunite biodissolution by focusing on the bacterial strains of *Shewanella oneidensis* MR1 sp. Additional sets of batch experiments were conducted in an anaerobic glove box to explain mechanisms of biodissolution by replicating the exact conditions (U, Ca and P concentration, three different bicarbonate concentrations) before inoculation with bacteria in the absence of autunite (mineral free).

Subtask 1.1: Sequestering Uranium at the Hanford 200 Area Vadose Zone by In Situ Subsurface pH Manipulation Using NH₃ Gas

Subtask 1.1: Introduction

At the Hanford Site, a significant residual mass of the disposed uranium inventory still resides in the deep vadose (Szecsody et al. 2013). The mobility of uranium in the oxidizing, carbonate-rich Hanford subsurface at pH ~8.0 is relatively high, with a low U(VI) adsorption distribution coefficient (K_d) averaging 0.11 - 4 L/kg (Zachara et al. 2007, Szecsody et al. 2013, Zachara et al. 2005). The mobility of U(VI) is explained by the formation of highly soluble and stable uranyl-carbonato complexes ($UO_2CO_3^0$, $UO_2(CO_3)_2^{2-}$ and $UO_2(CO_3)_3^{4-}$) (Langmuir 1997, Guillaumont et al. 2003). Remediation techniques for the deep VZ contaminated with radionuclides have so far received less attention although such methods are critical for protection of water resources from contaminants historically accumulated in the unsaturated subsurface environments. Remediation of deep vadose zone contamination of radionuclides can potentially be done *in situ* by converting aqueous U-carbonate mobile phases to lower solubility precipitates that are stable in the natural environment.

Injection of NH₃ gas to the vadose zone is a viable method to decrease uranium mobility in the contaminated subsurface via pH manipulation and creation of alkaline conditions (Szecsody et al. 2012, Zhong et al. 2015). Ammonia is a highly soluble gas and its injection in the vadose zone can cause the formation of NH_4^+ (which consumes H^+) in pore water followed by a subsequent increase in pH up 11.87 (3.1 mol/L NH₃ (aq)) for 5% NH₃ or pH 11.02 for 0.1% NH₃ (0.063 mol/L). This manipulation can significantly alter the pore water chemistry due to dissolution of the dominant soil minerals such as calcite, feldspar, iron oxides, and quartz present in the VZ soil. These dissolution reactions in alkaline conditions potentially induce the release of cations including Si, Al, Ca, Mg, Na, and K from soil minerals to pore water (Zhong et al. 2015). Then, upon the re-establishment of natural pH conditions, various silica and aluminosilicate solid phases would precipitate as a uranium-silicate such as Na-boltwoodite (Szecsody et al. 2013) or decrease U mobility by a coating of U-bearing phases forming a low solubility, non-U precipitate, such as cancrinite (Bickmore et al. 2001), sodalite, hydrobiotite, brucite, and goethite, as observed in water-saturated systems (Qafoku et al. 2004, Qafoku and Icenhower 2008). These chemical reactions can potentially control the mobility of uranyl cations and limit their downward migration to the underlying groundwater aquifer (Szecsody et al. 2012). However, there is a lack of knowledge on how pore water constituencies in alkaline conditions where soil minerals dissolution contributes to the solution ions may affect uranium removal or precipitation.

This year, research focused on the speciation modeling simulations to correlate results with SEM/EDS and XRD analysis on the selected precipitate samples. The speciation modeling for the prediction on the uranium aqueous species and solid phases has included a literature search to manually edit thermodynamic datasets for speciation modeling simulations via Geochemist Workbench (GWB) software. This research was extended to obtain SEM/EDS images for uranium elevated samples following by XRD analysis to find a correlation with speciation modeling predictions. The report on this subtask also presents results on gravimetric measurements of moisture uptake on uranium-bearing precipitates as a function of increasing relative humidity to provide reasonable estimates of the deliquescence point of solid phases or its components. The primary focus of this research was to investigate the stability of the multicomponent uranium-bearing precipitates mimicking those created in sediments as a result

of alkaline ammonia gas treatment in the vadose zone. The amount of water adsorbed on uranium-bearing precipitates was determined gravimetrically by the isopiestic method. The results indicate that gravimetric measurements of moisture uptake as a function of increasing relative humidity can provide reasonable estimates of the deliquescence point of solid phases or its components.

Subtask 1.1: Material and Methods

Sample Preparation

The composition of pore water at the Hanford Site has been previously characterized in terms of concentrations of major cations, anions, and pH (Serne et al. 2008). For the purpose of this research, the pore water composition was simplified to have five major components in the test solutions: uranium, silica, aluminum, calcium and bicarbonate. The concentration of uranium in all experiments was kept constant at 0.0084 mM (2 mg/L) (Katsenovich et al. 2016) and the bicarbonate concentrations varied from 0 to 100 mM (0, 2.9, 25, 50, 75 and 100 mM). The silica concentration was tested in the range of 5 mM to 250 mM (5, 50, 100, 150, 200, 250 mM) given past observations of 30 mM in 5% NH_3 treated sediment (Szecsody et al. 2012), and reached up to100 mM in 10% NH_3 treated sediment (Zhong et al. 2015). The same highest Si concentration of 100 mM with the total cation values of 250 mM was noted by (Szecsody et al. 2010). Past observations also showed that the concentration of Al released during the soil treatment by 1 mol L^{-1} NaOH is relatively small, resulting in ~5.1 mM of Al in the soil solution (Qafoku et al. 2003), justifying the fact that Al concentrations are smaller than Si. Both Si and Al concentrations tested for experiments are orders of magnitude greater than U; that can lead to the potential U precipitation as U-silicates from the Si and Al amended synthetic solutions.

Calcite mineral is abundant in Hanford soil and it exists as a mineralogical component in all of subsurface sediments (Liu et al. 2004). Groundwater and pore waters are in equilibrium with calcite, which exists in the form of caliche layers. The concentration of calcium carbonate in these layers varies over a wide range (Serne et al. 2004) justifying a wide range of bicarbonate concentrations tested in the experiments. Stock solutions of Al (50 mM), Si (422 mM), and HCO_3^- (400 mM) were first prepared in deionized water (DIW) from the salts $Al(NO_3)_3 \cdot 9H_2O$, $Na_2SiO_3 \cdot 9H_2O$, and $KHCO_3$, respectively, reaching the desired concentrations in 50 mL volume. Sodium metasilicate, $Na_2SiO_3 \cdot 9H_2O$, and potassium bicarbonate, $KHCO_3$, were also served as a source of sodium and potassium in the solution mixture. Experimental results on the removal of uranium were presented in previous reports and publications (Katsenovich et al. 2016, Lagos et al. 2014).

In addition, a set of samples was prepared with elevated uranium concentrations for XRD and SEM/EDS analysis. The procedures for sample preparation followed the same routine as previously described for samples containing 2 ppm of U. However, for this set, the uranium concentration that was injected was 400 ppm. The composition of six samples was comprised of the salt solutions described in Table 1. These solutions were consistent across the samples with the only difference being the bicarbonate (HCO_3^-) and calcium (Ca^{2+}) content added. The concentrated stock solutions were prepared such that the desired concentration would be reached after mixing in the solutions.

Geochemical Modeling for Speciation Prediction

The Geochemist Workbench (GWB) version 10.0.04 (Bethke 2007) was used to predict aqueous speciation and solid phases likely to be saturated in the post-treated synthetic pore water after ammonia gas injections. The synthetic pore water formulations containing 2 ppm of uranium used for the GWB speciation modeling are shown in Table 1.

Table 1.Synthetic Pore Water Formulation used for the Speciation Modeling

Sample ID	Targeting Concentration in Samples (mM)			
	Bicarbonate [HCO_3^-]	Silicate [Si]	Aluminum [Al^{3+}]	Calcium [Ca^{2+}]
1	2.9	50	5	0
2	2.9	50	5	5
3	2.9	50	5	10
4	50	50	5	0
5	50	50	5	5
6	50	50	5	10

The GWB software compiles four thermodynamic databases for speciation models. The Visual MINTEQ version 2.40 thermodynamic database, thermo-minteq.tdat, formatted for the GWB by Jon Petter Gustafsson (KTH Royal Institute of Technology), was chosen to run simulations. This database was manually updated to include some uranyl aqueous species and uranyl mineral phases to adjust their stability constants and the solubility products (log K's) obtained at 25ºC. The task to assemble a dataset of thermodynamic data that compiles most of the thermodynamic properties of uranyl minerals obtained under alkaline conditions is challenging because experimental data are still limited, especially with respect to ternary aqueous complexes and solid phases (Altmaier, Gaona and Fanghänel 2013). In addition, reliable solubility measurements are lacking for many uranyl minerals and results from a large number of solubility studies don't show reliable thermodynamic parameters due to inappropriate experimental design or incomplete analyses (Gorman-Lewis, Burns and Fein 2008).

Critically reviewed thermodynamic databases with a reliable data selection on uranium aqueous and solid phases were taken from the National Cooperative for the Disposal of Radioactive Waste (Hummel et al. 2002) and the Thermodynamic Reference Database (THEREDA) for Nuclear Waste Disposal (Richter, Bok and Brendler 2015), which reviewed the most recently published peer reviewed publications (Grenthe et al. 1992, Kalmykov and Choppin 2000, Bernhard et al. 2001, Guillaumont and Mompean 2003, Dong and Brooks 2006, Gorman-Lewis et al. 2008, Thoenen et al. 2014). These literature sources provided thermodynamic data on uranyl carbonates, uranyl oxides hydrates, and uranyl silicates aqueous species and uranyl minerals phases that were required to complete the speciation modeling for this study. The basic components considered for simulation were the same as for the synthetic pore water compositions and included $HSiO_4$, Na^+, K^+, HCO_3^-, Al^{3+}, NO_3^-, Ca^+, Cl^-, UO_2^{2+}, and $NH_3(g)$. Therefore, the revised uranyl aqueous species and uranyl minerals phases included in the dataset accounted for all of these components. The concentration of U(VI) was maintained at a constant 2 mg/L in all simulations.

The speciation modeling was conducted with the assumption that ammonia would not reduce U(VI) to U(IV). The process of uranium reduction by ammonia is strongly impeded by the presence of air, which is 21% oxygen, in the headspace of capped vials, the addition of nitrate with uranyl standard and pH adjustment solutions, and by the stabilizing effect of bicarbonate in the bicarbonate-amended solutions due to the formation of uranyl-carbonate complexes (Campbell et al., 2015). Based on this assumption, the aqueous U(IV) species were not predicted in this study.

However, the magnitude of the equilibrium constant for the U(IV) carbonate complexes $U(CO_3)_4^{4-}$ and $U(CO_3)_5^{6-}$ depends on the value of the standard potential of UO_2^{2+}/U_4^+. Since $U(CO_3)_5^{6-}$ species is already present in the thermo-minteq database, only the $U(CO_3)_4^{4-}$ thermodynamic parameters were incorporated (Hummel et al. 2002, Richter et al. 2015).

The polynuclear mixed U(VI) hydroxide-carbonate complex, $(UO_2)_{11}(CO_3)_6(OH)_{12}^2$ was found by Grenthe et al. (1992) to be a minor aqueous species. In addition, Richter et al. (2015) revised and included the $(UO_2)_2CO_3(OH)_3^-$ and $(UO_2)_3CO_3(OH)_3^+$ U(VI) complexes, which are now a part of the thermo_minteq database.

The major U(VI) carbonate complexes, $UO_2CO_3(aq)$, $UO_2(CO_3)_2^{2-}$ and $UO_2(CO_3)_3^{4-}$, were reported by Grenthe et al. (1992). Later, a technical report by the National Cooperative for the Disposal of Radioactive Waste (Hummel et al. 2002) found that the criteria to evaluate the stability constants $(\log_{10}\beta^0)$ for the reactions at 298.15^0K (25^0C) were not the same for the three complexes. In the case of $UO_2CO_3(aq)$, the $\log_{10}\beta^0$ was calculated using the SIT (Specific Ion Interaction Theory) coefficient, but corrected each value of the experimental data to zero ionic strength and selected an average as the $\log_{10}\beta^0$. In the cases of $UO_2(CO_3)_2^{2-}$ and $UO_2(CO_3)_3^{4-}$, linear regressions were used to calculate the respective stability constants. The inconsistency was noted when a linear regression applied to calculate the $\log_{10}\beta^0$ for $UO_2CO_3(aq)$ resulted in a SIT interaction coefficient far from zero. This result is not in agreement with the National Energy Agency (NEA 2004; Grenthe et al. 2004), which established the SIT interaction coefficients of neutral species as zero. This evaluation helped to revise the stability constants for the $UO_2(CO_3)_3^{4-}$, $UO_2CO_3(aq)$, and $UO_2(CO_3)_2^{2-}$ complexes, which have changed from 21.60 ± 0.05 to 21.84 ± 0.04, from 9.68 ± 0.0411 to 9.94 ± 0.03, and from log 16.94 ± 0.12 to log 16.61 ± 0.09, respectively (Grenthe et al. 1992, Guillaumont and Mompean 2003, Guillaumont et al. 2003). The thermodynamic stability constants for $UO_2CO_3(aq)$ and $UO_2(CO_3)_2^2$ were modified accordingly in the thermo-minteq database.

Ternary complexes of uranyl and carbonate with alkaline earth metals, $Ca_2UO_2(CO_3)_3(aq)$ and $CaUO_2(CO_3)_3^{2-}$, play an important role in the aqueous speciation of uranium. Bernhard (Bernhard et al. 1996) was the first who reported neutral $Ca_2UO_2(CO_3)_3(aq)$. Further studies evaluated the stability constants for calcium uranyl- carbonato complexes and introduced $CaUO_2(CO_3)_3^{2-}$ (Kalmykov and Choppin 2000, Bernhard et al. 2001, Guillaumont et al. 2003, Dong and Brooks 2006). Due to the discrepancies found between values, the formation constants for these species were not recommended for databases and served only as evidence of the species existence. However, the thermo-minteq database compiles these complexes in the database, including the stability constants that correspond to the first published data at 25ºC, -30.55 for $Ca_2UO_2(CO_3)_3(aq)$ and -25.40 for $CaUO_2(CO_3)_3^{2-}$ (Bernhard et al. 1996). In this study conducted at alkaline pH, the thermodynamic data for aqueous calcium-uranyl-carbonate species are essential to evaluate the presence of these complexes in the corresponding synthetic pore water systems since the $Ca_2UO_2(CO_3)_3(aq)$ complex is a major aqueous U(VI) species in the vadose

zone (Liu et al. 2004). Recently, the THEREDA database (Richter et al. 2015) was revised and the recommended stability constants for the reactions were -30.60 ± 0.09 for $Ca_2UO_2(CO_3)_3(aq)$ and -27.18 ± 0.06 for $CaUO_2(CO_3)_3^{2-}$. These values were replaced in the database.

In the evaluated synthetic porewater systems, the distribution of the aqueous and solid phases is essential for the formation of uranyl minerals; so, the thermodynamic parameters are necessary to determine the existing uranyl minerals. Previous studies of UO_2 in Si-rich water under oxidation conditions have showed the formation of the uranyl-silicates (Wronkiewicz et al. 1992, Wronkiewicz et al. 1996). In addition, boltwoodite and uranophane were found as uranium-bearing precipitates in the vadose zone of the Hanford Site (Catalano et al. 2004, Um et al. 2009). The Hanford subsurface is also rich with carbonates and calcite. Thus, thermodynamic parameters of relevant uranyl silicates, uranyl carbonates and uranyl oxides hydrates phases were reviewed to be included or modified in the database. The uranyl-silicate minerals, boltwoodite [(Na, K)$(UO_2(HSiO_4)_2$ $3H_2O$], uranophane [$Ca(UO_2)_2(HSiO_4)_2(H_2O)_5$] and soddyite [$(UO2)_2SiO_4(H_2O)_2$] were included following the thermodynamic parameters found by (Shvareva et al. 2011) and confirmed by THEDERA (Richter et al. 2015). The uranyl-carbonate mineral parameters for grimselite [$NaK_3UO_2(CO_3)_3$], rutherfordine [UO_2CO_3], liebigite [$Ca_2UO_2(CO_3)_3.10H_2O$ (cr)], and andersonite [$Na_2CaUO_2(CO_3)_3.6H_2O$] were taken from the values reviewed and summarized by (Gorman-Lewis et al. 2008); but ceikaite mineral [$Na_4UO_2(CO_3)_3$] parameters followed the recommendations presented in THEDERA Database (Richter et al. 2015). The uranyl oxides hydrates (becquerelite, clarkeite and schoepite) were also carefully reviewed and updated with the values suggested by NEA (Grenthe et al. 2004) and confirmed by THEREDA (Richter et al. 2015). In the updated database, metaschoepite replaced the schoepite species based on its similarity to the schoepite species (Guillaumont et al. 2003, Gorman-Lewis et al. 2008, Shvareva et al. 2011).

SEM-EDS Analysis

Scanning electron microscopy and energy dispersive spectroscopy (SEM-EDS) were used to study the surface morphology and composition of precipitates formed during sample preparation. The recovered solids were allowed to dry in preparation for SEM-EDS and X-ray diffraction analysis. Small specimens were taken from the solid precipitates and mounted to aluminum studs covered with double-sided carbon tape. These studs were evaluated for alpha emission, in accordance with the guidance of the campus Radiation Safety Officer, prior to transferring for analysis to the Florida Center for Analytical Electron Microscopy located on the Florida International University Modesto A. Maidique Campus (MMC).

The SEM system used was a JOEL-5910-LV with acceleration potentials ranging from 10 to 20 kV. EDS analysis was produced using an EDAX Sapphire detector with UTW Window controlled through Genesis software. Any required gold coating was done with an SPI-Module Control and Sputter unit for 2 minutes to produce a thin layer of gold. The specimens were coated with gold and palladium to enhance conductivity and analyzed in backscatter electron capture mode, which is preferred for distinguishing the differences in average atomic weight in an area. This was of particular use to this study for identifying areas of elevated uranium content. The uranium content was also associated with other elements in the sample composition, such as silica, sodium or calcium.

XRD Analysis

After SEM-EDS analysis, samples selected based on the detection of uranium were carefully ground by pestle and mortar for powder X-ray diffraction analysis. A custom sample holder designed specifically for holding the small quantities of sample available in this experiment was used. Analyses were performed on the dried precipitates at 35 kV and 40 mA via a Bruker 5000D XRD instrument. Diffraction patterns were obtained using a copper Cu Kα radiation source (λ=0.154056 nm) with a tungsten filter. The XRD was programmed to run over a 2-theta (2θ) range from 10° to 75° with a 0.02° step size and 2 second counting per step. XRD patterns were compared with the diffraction data of uranium-bearing pure minerals and accessory as calcite taken from the online American Mineralogist Crystal Structure Database to determine the phases present.

Measurements of Water Adsorption via Isopiestic Method

Water adsorption occurs when a solid surface is exposed to a water vapor or liquid. The adsorption process is divided into two categories depending on the kinds of forces that are involved in the interaction. For physical sorption (physisorption), the molecules are kept on the surface by weak van der Waals forces; whereas for chemical adsorption (chemisorption), the molecules become part of the solid and involve true chemical bonding of the vapor with the surface. Thus, physisorption is typically a reversible process. The amount of fluid adsorbed on a surface at equilibrium conditions is dependent on the fluid-solid interactions and the external parameters such as temperature, relative humidity (RH), and vapor pressure (Rouquerol, Rouquerol and Sing 1999). Water molecules adsorb onto the surface of dry solids, forming a monomolecular layer, and as more molecules adhere to the surface, moisture starts transferring into the material via diffusional forces (Kontny and Zografi 1995). So, the total amount of water adsorbed by a solid is usually a sum of the fractions held by different mechanisms. These include chemical bonding with the solid; multilayer adsorption; pore or capillarity condensation, responsible for creation of curved interfaces (menisci); and micropore filling (Gruszkiewicz et al. 2000). Usually, adsorbed water doesn't affect the solid before water vapor starts to condensate onto the surface at high humidity. Water condensation can trigger a deliquescent process for water-soluble precipitates or their components forming a saturated solution (Van Campen, Amidon and Zografi 1983, Kontny and Zografi 1995).

Understanding the mechanism of water adsorption on precipitates in the Hanford vadose zone would help to explain the processes leading to the dissolution of water soluble uranium species incorporated in the uranium-bearing precipitates created as a result of ammonia treatment of the vadose zone sediments. It can also help to identify the RH where uranium-bearing precipitates start dissolving water soluble uranium phases. The occurrence of these mechanisms depends on the chemical composition of the precipitates as well as many other factors such as temperature and surface characteristics. For this study, only one temperature was considered (25°C) with more focus given to the differences occurring between precipitate compositions. Previously, Gruszkiewicz et al. (2001) measurements of water adsorption on geothermal rocks indicated a correlation between the mineral composition of the rocks and their water adsorption capacities.

The ability of solids to uptake water vapor is best measured by sorption or desorption as a function of relative humidity under constant temperature at equilibrium conditions where sorption or desorption is occurring independently of time. RH is defined through the partial pressure of water vapor as follows:

$$RH = p_w/p_w^o \qquad\qquad \text{Eq 1}$$

Where p_w is the partial pressure of water vapor over an aqueous solution and p_w^0 is the partial pressure of water vapor over pure water. The ratio p_w/p_w^o is referred to as the relative pressure. The activity of water in aqueous solutions relates to its fugacity by equation (Rard and Clegg 1997):

$$a_w = f_w / f_w^o \qquad\qquad \text{Eq 2}$$

Where f_w is the fugacity of water vapor over an aqueous solution and f_w^0 is the fugacity of water vapor over pure water. It is usually assumed that, in ambient temperature and moderate pressure, water vapor behaves ideally and the fugacities can be replaced by partial pressure (Reid, Prausnitz and Poling 1987):

$$f_w/f_w^o = p_w/p_w^o \qquad\qquad \text{Eq 3}$$

yielding:

$$RH = a_w \qquad\qquad \text{Eq 4}$$

The RH is commonly expressed as a percentage; thus $RH\% = 100*a_w$.

At equilibrium conditions, the water activity of solids is equal to the RH of the atmosphere in which it is stored and relative humidity should be the same for sorption or desorption measurements. However, one of the most characteristic features of the physisorption process is the hysteresis loop that is associated with the capillary condensation. This may occur irreversibly and the fluid amounts adsorbed do not necessary coincide with increasing or decreasing vapor pressure over a certain interval (Rouquerol et al. 1999, Lowell et al. 2012).

Water moisture uptake by uranium-bearing precipitates as a function of increasing relative humidity was measured at 25°C via the isopiestic method. This method can provide estimates of water quantity retained within precipitates conducted in the range of water activities or pressure, $0 \leq p/p_o \leq 0.9$, where p_o is the saturated water pressure.

The experimental approach for this study included weighing the solid samples after equilibration in the isopiestic chamber (Figure 1, Figure 2, and Figure 3).
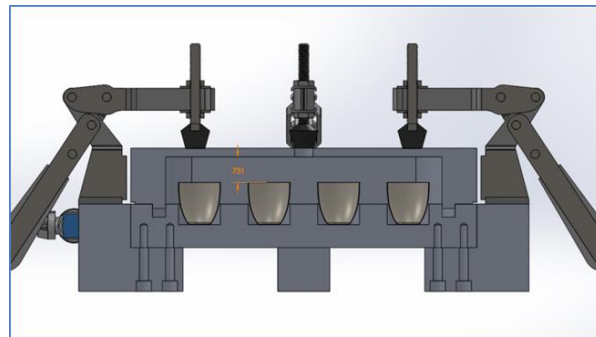
Figure 1. The full assembly of the isopiestic chamber with crucibles inside.

Figure 2. Isopiestic chambers for the solubility experiments fabricated in ARC's machine shop.

The new isopiestic chamber set-up that includes an environmental chamber, vacuum pump and balances was established in the radiation lab to allow for the conduction of experiments with uranium-bearing samples (Figure 3).

Figure 3. Isopiestic chamber set up in the FIU-ARC radiation laboratory.

The apparatus was originally designed for measuring isopiestic molalities of aqueous solutions and featured the same principle to quantify water adsorption on solids at constant temperature. The basic features of the method include isothermal equilibration of samples of known masses and known initial concentrations through a common vapor phase. In the closed system, the solvent is distilled isothermally from one crucible to another until each solution reaches the same chemical potential. All of the solutions at equal vapor pressure or isopiestic equilibrium have the same solvent activities. These conditions can be rewritten as $\ln a_s = \ln a_{ref}$ (Rard and Platford 2000).

Samples to measure water adsorption were prepared using two different bicarbonate concentrations (3 mM and 50 mM) and four different Ca concentrations (0 mM, 5 mM, 10 mM and 15 mM). The composition of the samples is presented in Table 2. Eight samples were prepared using "low" bicarbonate concentrations of 3 mM HCO_3 and 0-15 mM of Ca and "high" bicarbonate concentrations of 50 mM HCO_3 and 0-15 mM of Ca. Each sample composition was amended with 2 ppm uranium in tarred crucibles and then, after drying at 40°C until attaining a constant weight, placed in the isopiestic apparatus.

Table 2. Targeted Concentrations of Constituencies to Prepare 50 mL of Samples

Stock Solution	Salts Used	Molecular Weight (g/mol)	Stock Solution Concentration (mM)	Amount to Prepare 50 mL (g)	Target Concentrations in Samples (mM)
Bicarbonate	$KHCO_3$	100.114	400	2.002	3, 50
Metasilicate	$Na_2SiO_3 \cdot 9H_2O$	284.196	422.24	5.998	100
Aluminum	$Al(NO_3)_3 \cdot 9H_2O$	375.129	50	0.938	5
Calcium	$CaCl_2 . H_2O$	219.08	2500	27.385	0, 5, 10, 15

The initial weights of the samples and the amount of uranium per gram of precipitate are presented in Table 3.

Table 3. Initial Sample Weight

Sample number	Standard Sample	Solute Initial Weight (g)	Solute Content (moles)	ug U/g Precipitate
1	100 mM Si, 5 mM Al, 2 ppm U, 3 mM HCO_3, 0 mM Ca	0.18931	0.00024	105.65
2	100 mM Si, 5 mM Al, 2 ppm U, 3 mM HCO_3, 5 mM Ca	0.19113	0.00024	104.64
3	100 mM Si, 5 mM Al, 2 ppm U, 3 mM HCO_3, 10 mM Ca	0.20101	0.00024	99.50
4	100 mM Si, 5 mM Al, 2 ppm U, 3 mM HCO_3, 15 mM Ca	0.19627	0.00024	101.90
5	100 mM Si, 5 mM Al, 2 ppm U, 50 mM HCO_3, 0 mM Ca	0.22623	0.00030	88.41
6	100 mM Si, 5 mM Al, 2 ppm U, 50 mM HCO_3, 5 mM Ca	0.23957	0.00030	83.48
7	100 mM Si, 5 mM Al, 2 ppm U, 50 mM HCO_3, 10 mM Ca	0.23168	0.00030	86.33
8	100 mM Si, 5 mM Al, 2 ppm U, 50 mM HCO_3, 15 mM Ca	0.23467	0.00031	85.23

Based on the composition, silica gel was the major component of the precipitates; so, it was important to compare silica gel water retention capacity with multicomponent precipitates. To attain this, two crucibles contained 10 mL samples of 100 mM sodium silicate were placed in the isopiestic apparatus after drying until achieving a constant weight. The results on water retaining

capacities obtained on pure silica gel samples were compared with the multicomponent samples. A solution of calcium chloride was used as a standard to evaluate the samples' water activity. The apparatus was sealed, degassed and left at 25°C in the environmental chamber. The isopiestic apparatus was opened every 2-3 weeks for weighing the samples after the system reached equilibrium. In the experiments, 15-mL nickel cups were used; to avoid evaporation losses, tightly fitted light nickel lids were immediately added when the apparatus was open. Then, the crucibles with lids were placed on balances for weighing. Metler Toledo analytical balances XS205DU with a precision of no less than 1×10^{-5} g were used for weighing the crucible cups covered with lids. The measurements obtained were used to calculate the water adsorption and water activity values. The percent of water loss during the weighing process was estimated to be in the range of 3.5-5%. After weighing of the samples was complete, about 0.4 mL of degassed DIW was distributed between the standards and the samples and the chamber was closed again; the air was evacuated until the pressure reached around 4.5 kPa (Blanco, Amado and Avellaneda 2006).

The direct weighing method has the following advantages:

- The mass of the sample is determined in comparison with standard weights. The result is not sensitive to errors in pressure measurement.
- With the direct weighing method, all of the points on an isotherm are measured independently; so, the errors for data points obtained earlier do not affect the following points. This allows for monitoring the weight of the sample over long time periods (Gruszkiewicz et al. 2000).

The desorption portion of the isotherm was obtained by progressively decreasing the water activity or relative pressure in the isopiestic chamber while monitoring the equilibrium amount of moisture sorbed at each relative pressure. This was accomplished by the addition in the chamber another crucible with a few drops of concentrated H_2S0_4 that created an excellent "sink" for water vapor. Obtained water sorption-desorption isotherms for uranium-bearing precipitates can provide insight on the nature of precipitate-water interactions. This information is obtained from the amount of moisture sorbed at certain humidities and, in addition, suggests if the process is reversible or not. This can be found from the hysteresis between sorption and desorption and from the shape of the hysteresis loop (Kontny and Zografi 1995).

Subtask 1.1: Results and Discussion

Geochemical Modeling Results, Ca-free synthetic solutions

GWB speciation modeling helped to predict uranium aqueous species and uranium-mineral phases that might form in varied pore-water compositions after ammonia gas injections in the subsurface. The predominant aqueous species and the mineral saturation indices (Q/K) with UO_2^{2+} were displayed as a function of pH. According to the speciation modeling, in bicarbonate–free synthetic solutions, $UO_2(OH)_3^-$ and $UO_2(OH)_4^{2-}$ were the predominant aqueous uranium species. In the presence of bicarbonate, aqueous uranium carbonates species, $UO_2(CO_3)_3^{4-}$ and $UO_2(CO_3)_2^{2-}$, dominated uranium speciation at both 0.1% (0.063 mol/L NH3(aq) and 5% (3.1 mol/L NH3(aq) of NH_3. However, the concentration of uranyl carbonates species was noted to decrease above pH 9.5; the decrease of $UO_2(CO_3)_3^{4-}$ and $UO_2(CO_3)_2^{2-}$ was more pronounced at 2.9 mM HCO_3^- when using 0.1% of NH_3(Figure 4-B1) compared to 5% of NH_3 (Figure 5-B1). At higher bicarbonate concentrations, the concentration of $UO_2(CO_3)_3^{4-}$ species was almost unchanged over a pH range from 8 to 11 in both ammonia gas concentrations but, at the pH

above 11.5, their concentrations were slightly decreased with treatment of 5% NH_3 (Figure 4C1, Figure 5(C1)).
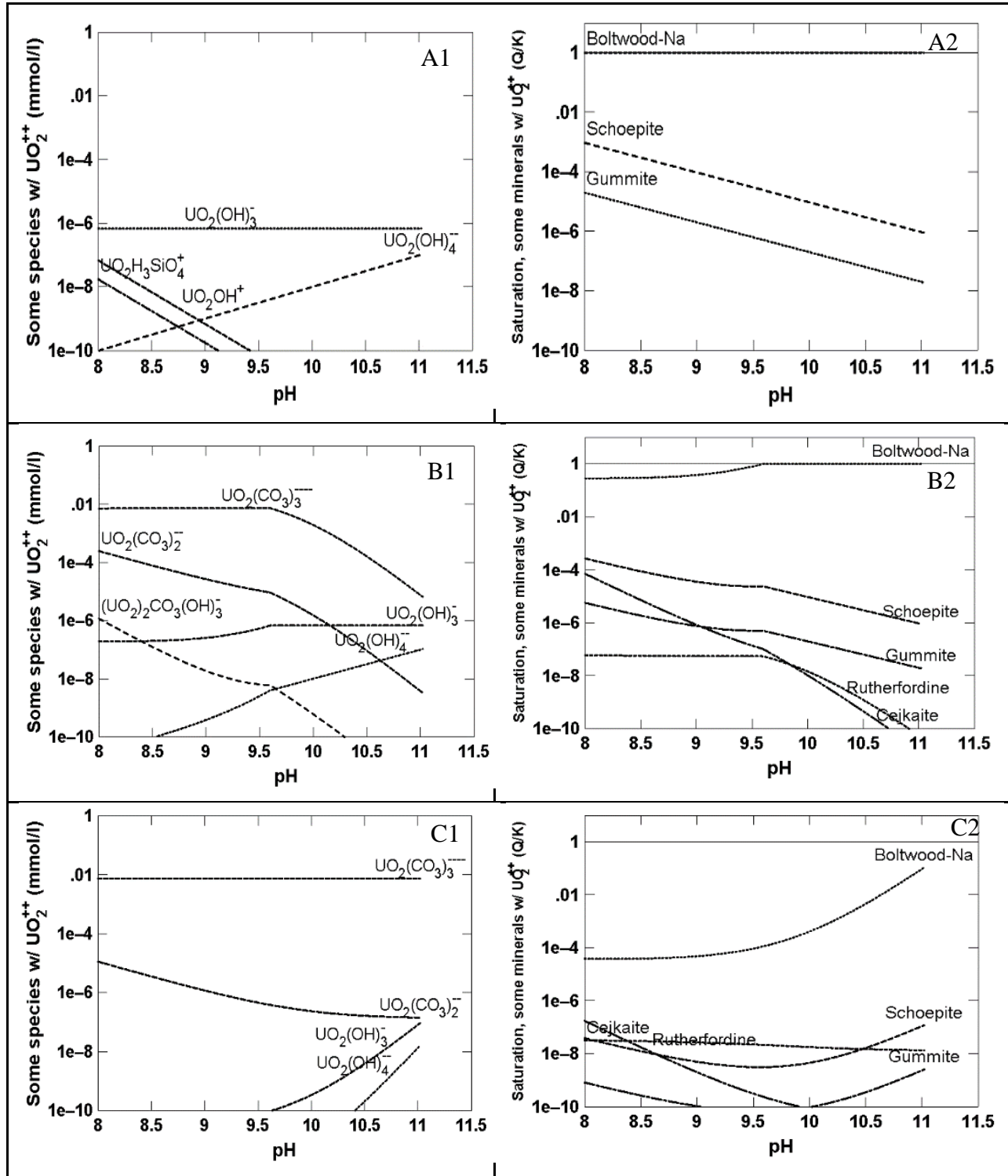
Figure 4. Diagrams of uranium aqueous species and saturation indices of some of uranium-bearing mineral phases plotted as a function of pH for 0.1% of NH_3 (0.063 mol/L NH_3(aq)). Sample composition includes 50 mM of Si and varied HCO_3^- concentrations. The first row shows diagrams for HCO_3—free samples (A1, A2), the 2nd and 3rd row show the diagrams for 2.9 mM (B1, B2) and 50 mM of HCO_3^- (C1, C2).
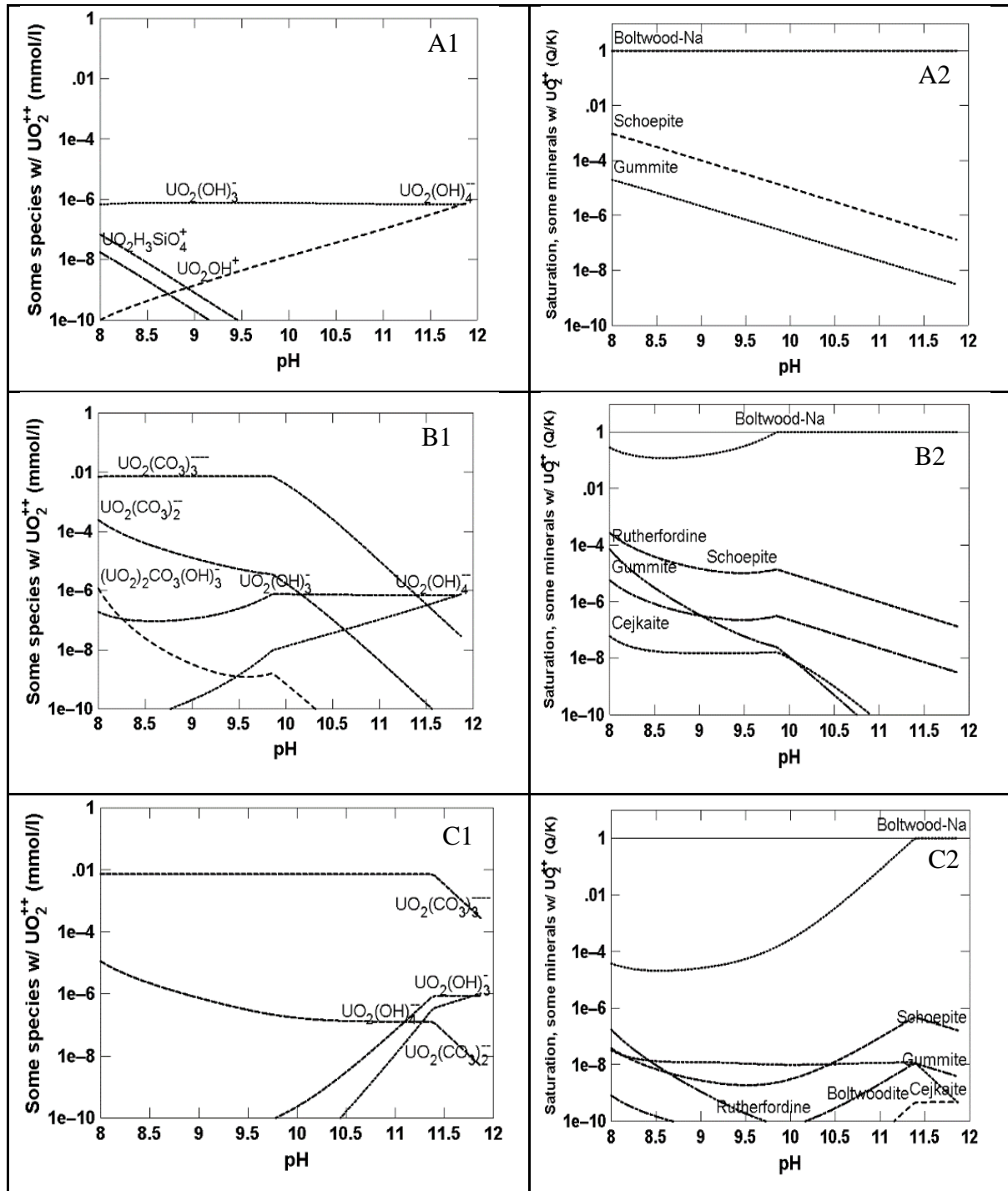
Figure 5. Diagrams of uranium aqueous species and saturation indices of some of uranium-bearing mineral phases plotted as a function of pH for 5% of NH$_3$ (3.1mol/L NH$_3$(aq)). Sample composition includes 50 mM of Si and varied HCO$_3^-$ concentrations. The first row shows diagrams for HCO$_3^-$free samples (A1, A2), the 2nd and 3rd row show the diagrams for 2.9 mM (B1, B2) and 50 mM of HCO$_3^-$ (C1, C2).

Modeling also predicted the formation of relevant uranium mineral phases. For the Ca –free samples, modeling identified the formation of uranyl silicate Na-boltwoodite [(Na)(UO$_2$)(HSiO$_4$)·0.5H$_2$O] and uranyl carbonate solid phases such as cejkaite [Na$_4$ (UO$_2$)(CO$_3$)$_3$ and rutherfordine [UO$_2$(CO$_3$)] in addition to gummite, schoepite

[$(UO_2)_8O_2(OH)_{12}(H_2O)_{12}$] and [$UO_2(OH)_3$ (beta)]. Na-boltwoodite, cejkaite, gummite, schoepite, and [$UO_2(OH)_3$ (beta)] were present in all of the conditions tested, while rutherfordine was seen only in the presence of bicarbonate in the solution. The formation of uranyl hydroxide minerals, schoepite and [$UO_2(OH)_3$ (beta)], were favored under bicarbonate-free and low 2.9 mM bicarbonate concentrations; however, according to the modeling simulation done for both 0.1% and 5% of NH_3 their saturation indices decreased as the concentration of bicarbonate ions increased. Overall, saturation indices for Na-boltwoodite were found to be the highest for all of the conditions tested. This correlates with previous results obtained by (Szecsody et al. 2013) based on the samples analyzed 24 h after NH_3 treatment. They also suggested that Na-boltwoodite is the predominant phases even in the presence of high carbonate concentration. The increase in silica concentration from 50 mM to 100 mM has not affected the speciation and the saturation indices of formed minerals (Figure 6, Figure 7).
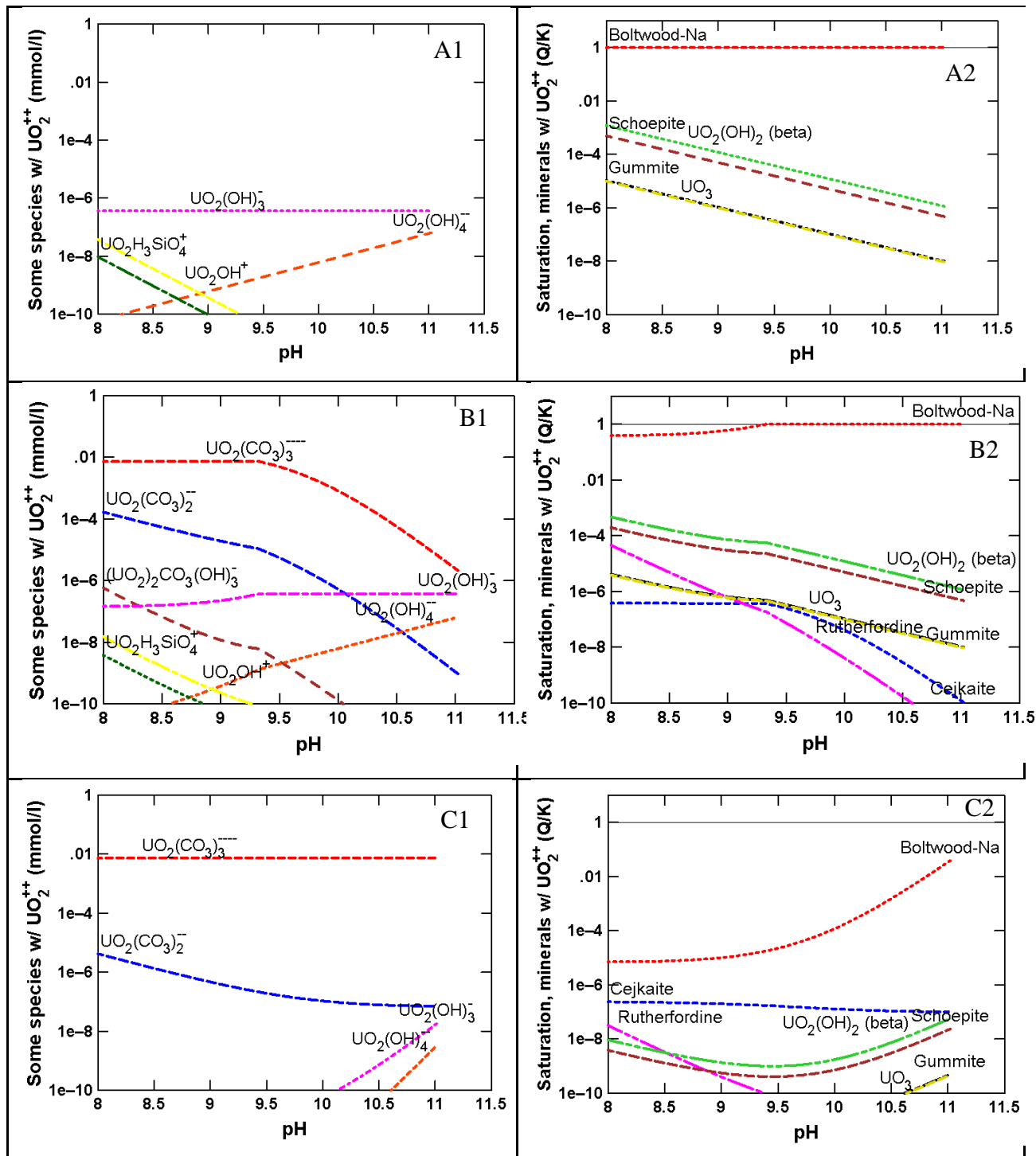
Figure 6. The diagrams showing uranium species concentrations and saturation indices of some uranium minerals plotted as a function of pH for sample composition of 100 mM Si , 5 mM Al and 2 ppm of U(VI). Injected NH₃ concentration is 0.1% (0.063 mg/L). Left- aqueous uranium species; right- saturation indeces of formed uranium solid phases. The first row shows diagrams for HCO₃⁻ free samples (A1, A2), the 2nd and 3rd row show the diagrams for 2.9 mM (B1, B2) and 50 mM of HCO₃⁻ (C1, C2).

Figure 7. The diagrams showing uranium species concentrations and saturation indices of some uranium minerals plotted as a function of pH for bicarbonate-free sample composition of 100 mM Si, 5 mM Al and 2 ppm of U(VI). Injected NH₃ concentration is 5% (3.1 mg/L). Left- aqueous uranium species; right- saturation indeces of formed uranium solid phases. The first row shows diagrams for HCO₃⁻free samples (A1, A2), the 2ⁿᵈ and 3ʳᵈ row show the diagrams for 2.9 mM (B1, B2) and 50 mM of HCO₃⁻ (C1, C2).

Speciation modeling for Ca-amended synthetic solutions

GWB simulations were conducted for synthetic mixtures composed of 50 mM Si and 10 mM Ca. Three bicarbonate concentrations were chosen for the experiments-0 mM, "low" bicarbonate

concentration of 2.9 mM and "high" bicarbonate concentration of 50 mM. The Al concentration of 5 mM was constant for all simulations.
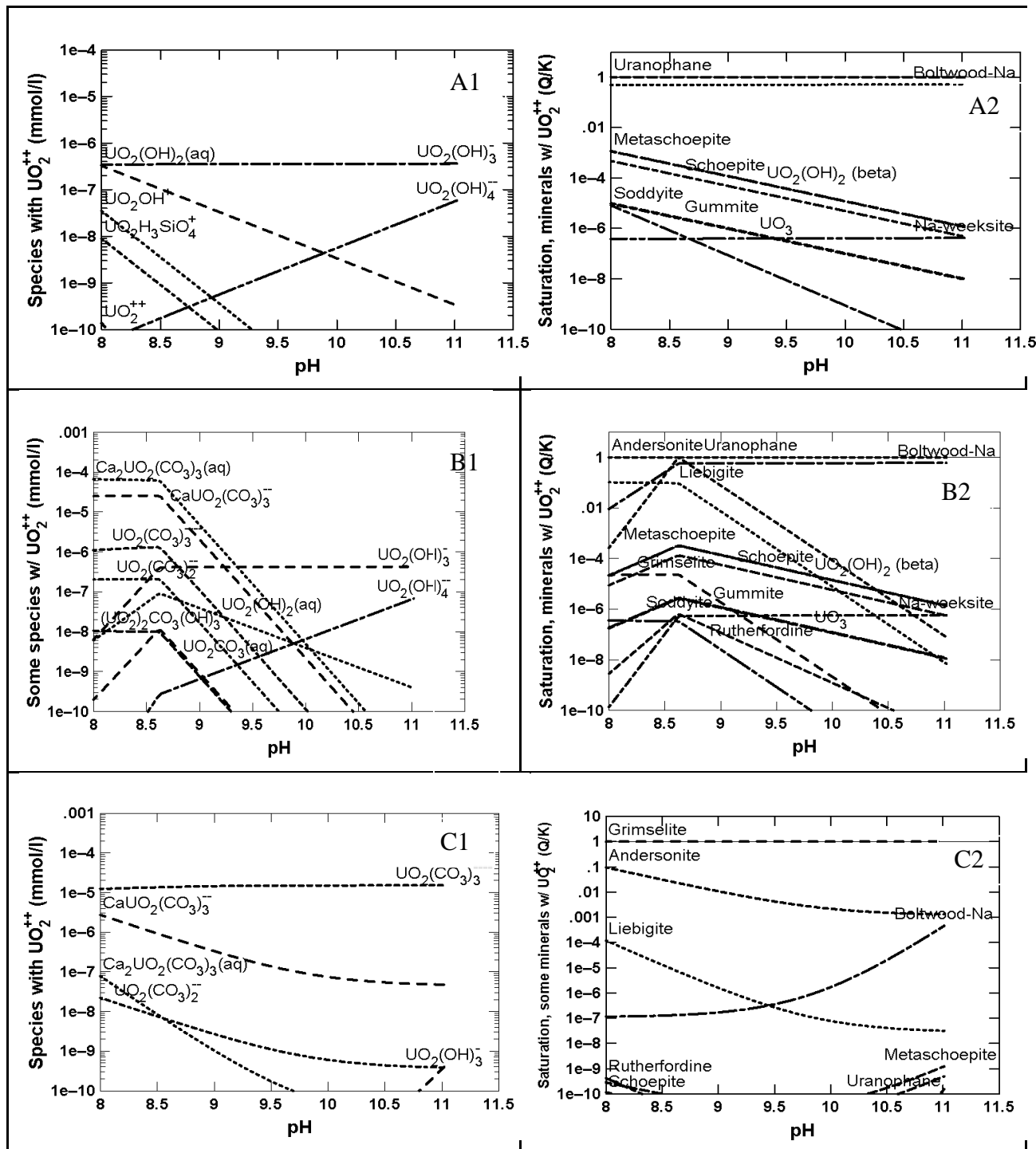
Figure 8. Diagrams of uranium aqueous species and saturation indices of some of uranium-bearing mineral phases plotted as a function of pH for 0.1% of NH₃ (0.063 mol/L NH₃(aq)). Sample composition includes 50 mM of Si, 10 mM of Ca and varied HCO₃⁻ concentrations. The first row shows diagrams for HCO₃—free samples (A1, A2), the 2nd and 3rd row show the diagrams for 2.9 mM (B1, B2) and 50 mM of HCO₃⁻ (C1, C2).

Modeling simulations predicted the highest saturation indices values for uranyl silicate solid phases, Na-boltwoodite [$(Na)(UO_2)(HSiO_4) \cdot 0.5H_2O$] and uranophane $Ca(UO_2)2SiO_3(OH)_2 \cdot 5(H_2O)$. In an aqueous phase uranyl hydroxide species were prevailing in all pHs. At "low" bicarbonate concentrations, in addition to uranyl silicates, the highest saturation indices were found for uranyl carbonate mineral, andersonite, $Na_2Ca(UO_2)(CO_3)_3 \cdot 6H_2O$. Aqueous speciation at pH 11 after the injection of ammonia was dominated by uranyl hydroxide species (Figure 8- B1, B2). As concentration of bicarbonate was increased in the sample composition up to 50 mM, grimselite, $K_3Na(UO_2)(CO_3)_3 \cdot (H_2O)$, was predicted as a prevailing uranium-bearing solid phase in the precipitate (Figure 8-C1, C2).
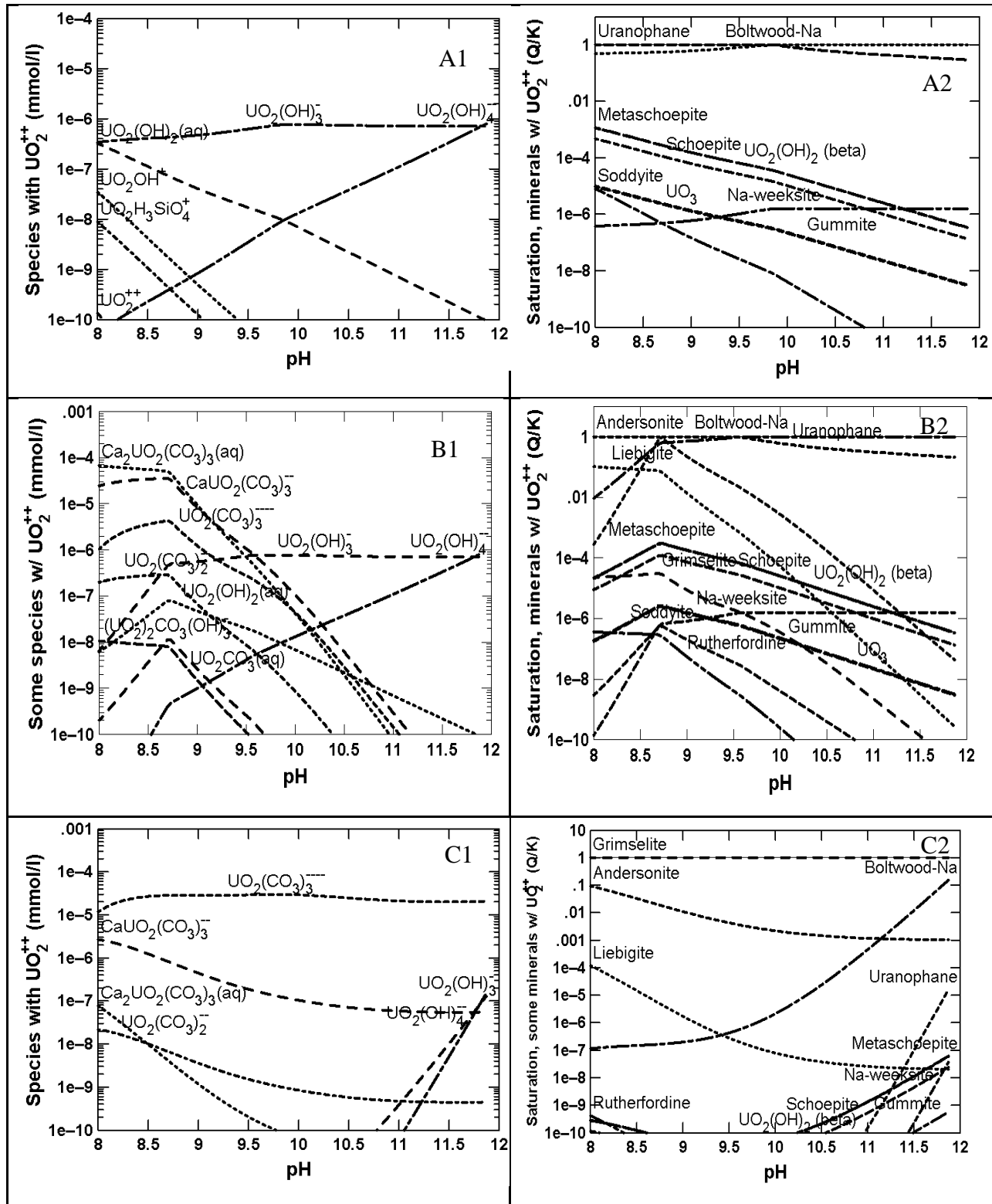
Figure 9. Diagrams of uranium aqueous species and saturation indices of some of uranium-bearing mineral phases plotted as a function of pH for 5% of NH$_3$ (3.1 mol/L NH$_3$(aq)). Sample composition includes 50 mM of Si, 10 mM Ca and varied HCO$_3^-$ concentrations. The first row shows diagrams for HCO$_3$—free samples (A1, A2), the 2nd and 3rd row show the diagrams for 2.9 mM (B1, B2) and 50 mM HCO$_3^-$ (C1, C2).

Modeling simulations for samples containing 10 mM of Ca in the solution mixture after injection of 5% ammonia gas followed the same trend as samples treated with 0.1% of ammonia. The highest saturation indices values were predicted for uranyl silicate solid phases, Na-boltwoodite $[(Na)(UO_2)(HSiO_4) \cdot 0.5H_2O]$ and uranophane $Ca(UO_2)2SiO_3(OH)_2 \cdot 5(H_2O)$ for bicarbonate free samples. In an aqueous phase uranyl hydroxide species were prevailing in all pHs. At "low" bicarbonate concentrations, in addition to uranyl silicates, the highest saturation indices were found for uranyl carbonate mineral, andersonite, $Na_2Ca(UO_2)(CO_3)_3 \cdot 6H_2O$. Aqueous speciation at pH 11 after the injection of ammonia was dominated by uranyl hydroxide species (Figure 9-B1, B2). At "high" bicarbonate concentration of 50mM, the highest saturation indices were found for uranyl carbonate mineral, grimselite, $K_3Na(UO_2)(CO_3)_3 \cdot H_2O$.

Studies also attempted to determine the morphological and mineralogical characteristics of the uranium solid phases produced during ammonia treatment. SEM and EDS analysis were used for the observation of uranium phases (Figure 10, Figure 12) to select samples for XRD analysis. The samples prepared with high bicarbonate concentrations (50 mM) showed the uranium-bearing crystal-like structures or uranium dense regions of amorphous collection. EDS analysis of these areas resulted in uranium atomic percentages between 14.8% - 29.7% (Figure 10, Figure 12). The diffraction analysis of those samples having only difference in a concentration of calcium in a composition, 15 mM (Figure 10) and 10 mM (Figure 12), revealed potential matches for grimselite ($K_3Na(UO_2)(CO_3)_3 \cdot H_2O$), along with calcite and the overwhelming presence of nitratine ($NaNO_3$) (pure mineral intensity is not shown on the graph) (Figure 11, Figure 13).

Element	Wt%	At%
CK	14.94	27.31
NK	08.46	13.25
OK	30.96	42.48
NaK	12.75	12.17
AlK	00.10	00.08
SiK	00.85	00.66
ClK	00.55	00.34
KK	01.28	00.72
CaK	00.46	00.25
UL	29.66	02.74
Matrix	Correction	ZAF
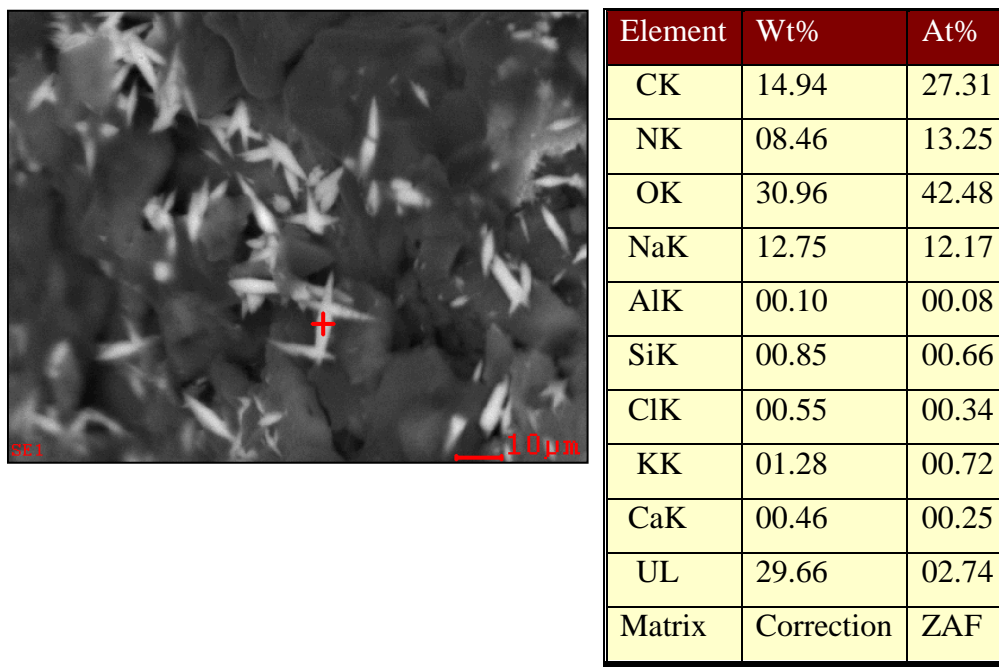
Figure 10. SEM image showing the crystalline uranium phases and the spot chemical composition using EDS. Sample was composed using 50 mM of Si, 5 mM of Al, 15 mM of Ca and 50 mM HCO₃.
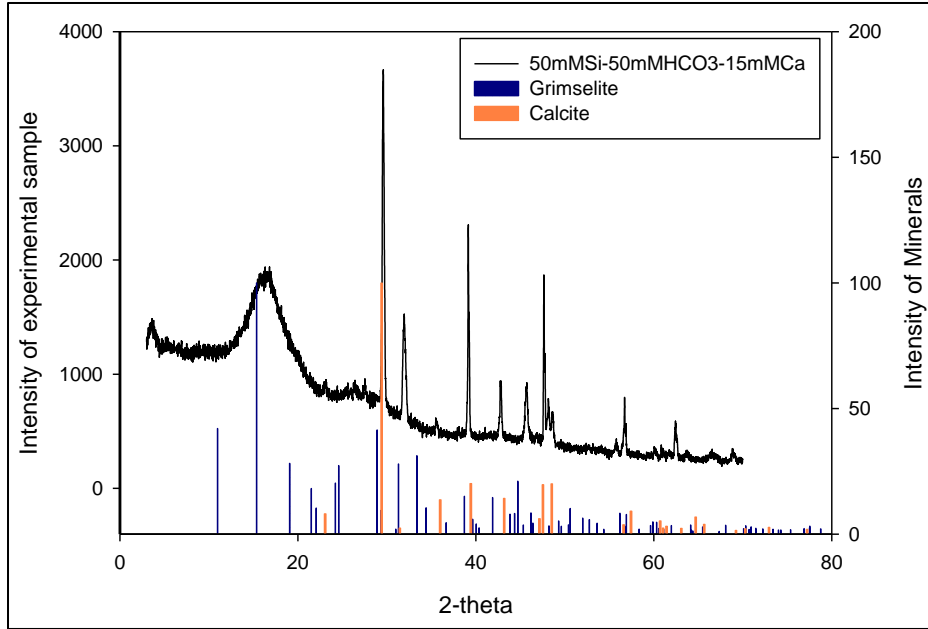
Figure 11. XRD pattern for uranium bearing precipitate prepared with 50 mM Si, 5 mMAl, 15 mM Ca and 50 mM HCO₃.

A grounded sample composed of 50 mM Si, 5 mM Al, 10 mM of Ca and 50 mM HCO₃, shown on Figure 12, doesn't display the crystal-like phases. However, the XRD analysis of this sample (Figure 13) suggested the presence of grimselite mineral, which correlates with the mineral composition displayed on Figure 11. In addition, the finding of grimselite mineral in the sample composition matches with the speciation modeling results conducted for "high" bicarbonate samples.
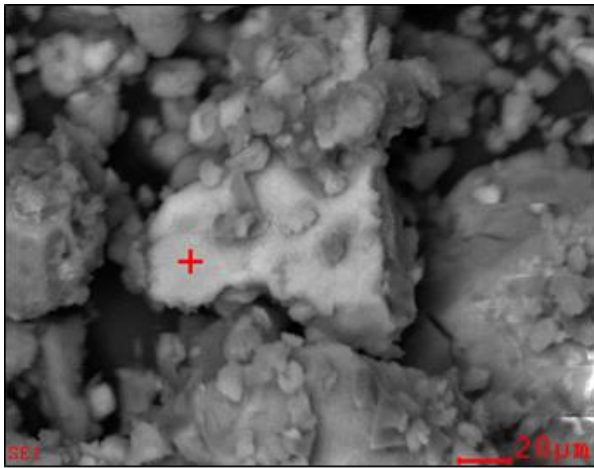
Element	Wt%	At%
CK	08.24	15.18
NK	04.13	06.53
OK	32.78	45.37
NaK	08.81	08.48
AlK	02.19	01.80
SiK	20.51	16.17
ClK	04.57	02.85
KK	01.53	00.87
CaK	02.46	01.36
UL	14.78	01.37
Matrix	Correction	ZAF

Figure 12. SEM image of the grounded precipitate sample and the spot composition using EDS. Sample was composed using 50 mM of Si, 5 mM Al, 10 mM of Ca and 50 mM HCO₃.
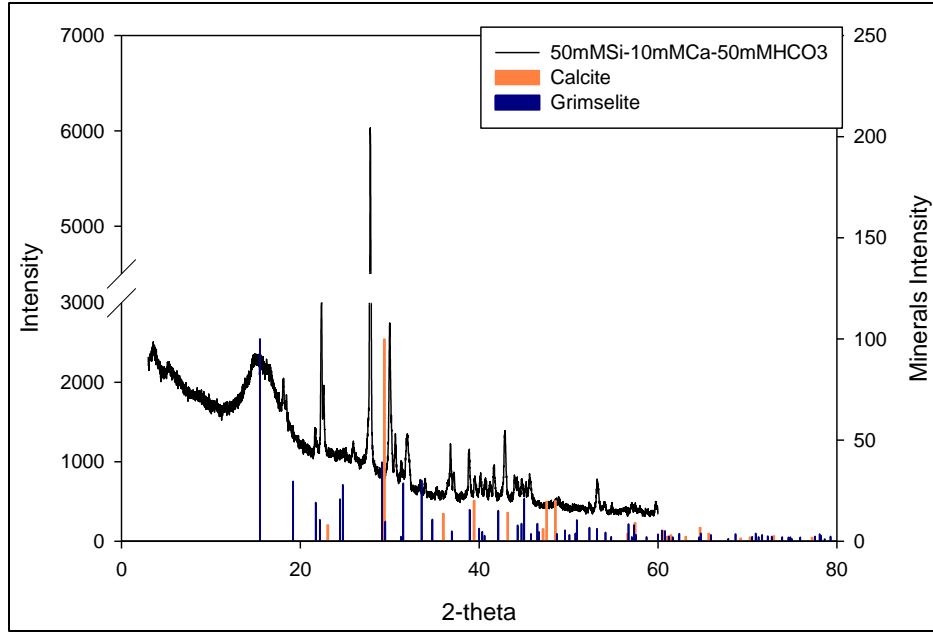
Figure 13. XRD pattern for uranium bearing precipitates prepared with 50 mM of Si, 5 mM Al, 10 mM of Ca and 50 mM HCO₃.

While the high bicarbonate (50 mM) samples showed uranium-bearing crystal-like formations, the low bicarbonate version showed only significant amorphous uranium-dense areas with U atomic percentages ranging between 11.4%-14.0% (Figure 14, Figure 15). These areas coincided with higher Si weight percentage on the level of 19-21%.

Element	Wt%	At%
CK	14.60	31.53
OK	10.80	17.50
NaK	02.51	02.83
AlK	02.14	02.05
SiK	21.06	19.45
ClK	12.13	08.87
UM	11.42	01.24
KK	06.10	04.05
CaK	19.26	12.46
Matrix	Correction	ZAF
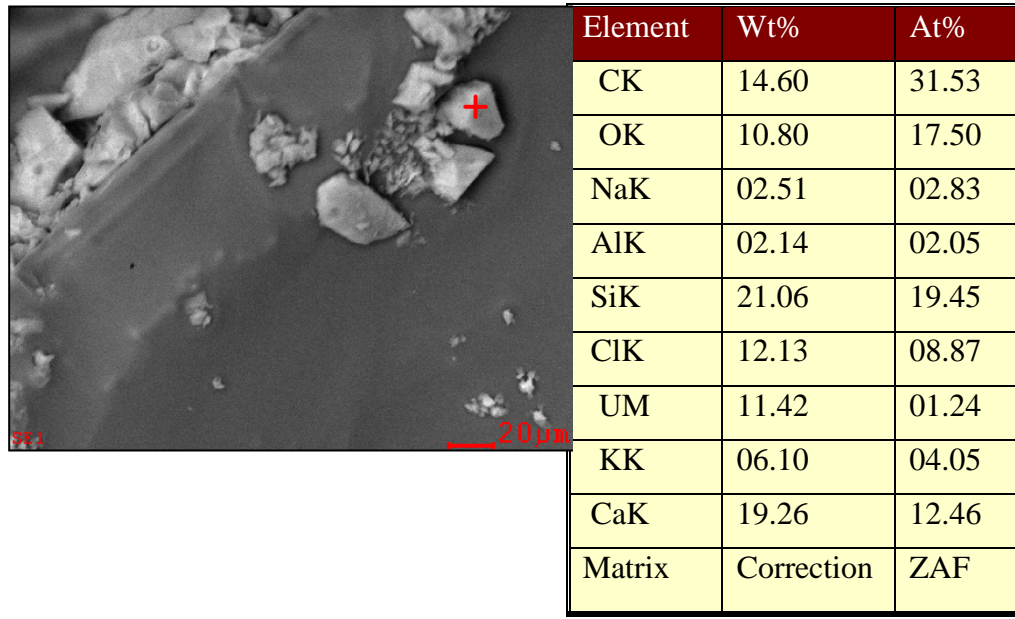
Figure 14. SEM image of the grounded precipitate sample and the spot composition using EDS. Sample was composed using 50 mM of Si, 5 mM Al, 10 mM of Ca and 3 mM HCO₃.
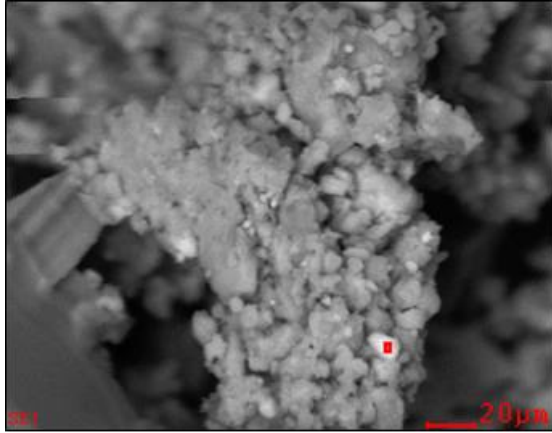
Element	Wt%	At%
CK	09.22	16.88
NK	04.64	07.28
OK	32.72	44.96
NaK	06.30	06.02
AlK	02.14	01.74
SiK	19.40	15.18
ClK	03.83	02.37
KK	02.57	01.44
CaK	05.14	02.82
UL	14.05	01.30
Matrix	Correction	ZAF

Figure 15. SEM image of the grounded precipitate sample and the spot composition using EDS. Sample was composed using 50 mM of Si, 5 mM Al, 15 mM of Ca and 3 mM HCO₃.

The XRD pattern produced a broad undefined single peak between 2Θ between 12 and 22 suggesting the presence in the sample of amorphous materials as well as well-defined peaks representative for crystalline forms. The presence of boltwoodite and uranophane were predicted by the speciation modeling and SEM/EDS identified areas of concentrated uranium and Si. However, uranyl silicates were not detected with any certainty by powder XRD perhaps due to amorphous nature of these solid phases.
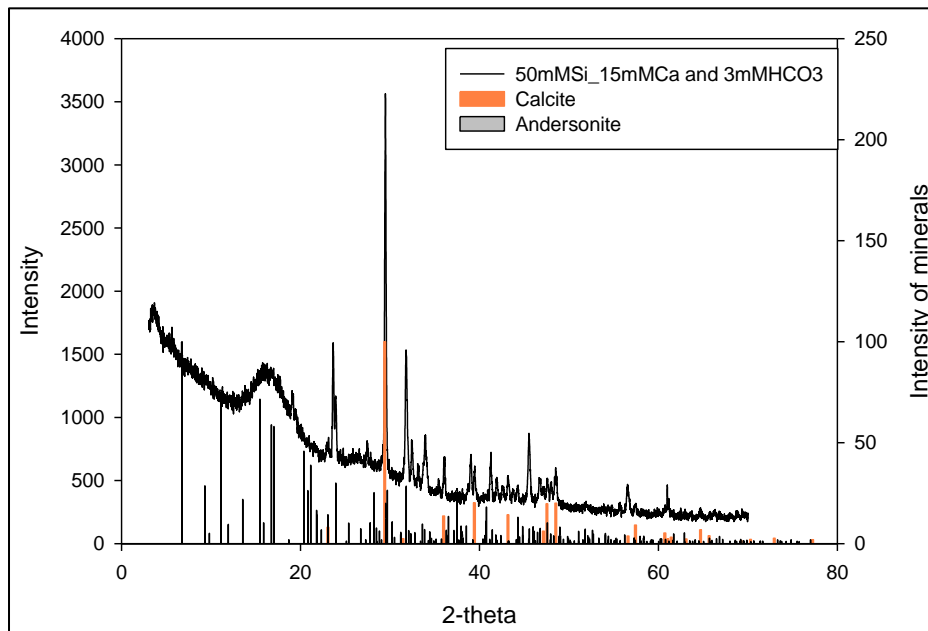
Figure 16. XRD patterns for uranium bearing precipitates prepared with 50 mM of Si, 5 mM Al, 15 mM of Ca and 3 mM HCO₃.

Measurements of Water Adsorption on Multicomponent Solids via Isopiestic Method

The amount of vapor adsorbed by the precipitate solids is proportional to the mass of the sample and depends on the relative pressure inside the chamber and temperature (Afonso and Silveira Jr 2005). Since the experiments were conducted at a constant temperature of 25ºC, temperature variations were not considered during the current study. The conditions for each isotherm (g of water/g of solids) were calculated by a division of the amount of adsorbed moisture (g) by the amount of dry precipitate samples (g).

Figure 17 shows water adsorption and desorption isotherms for all U-bearing precipitate compositions tested at 25ºC.
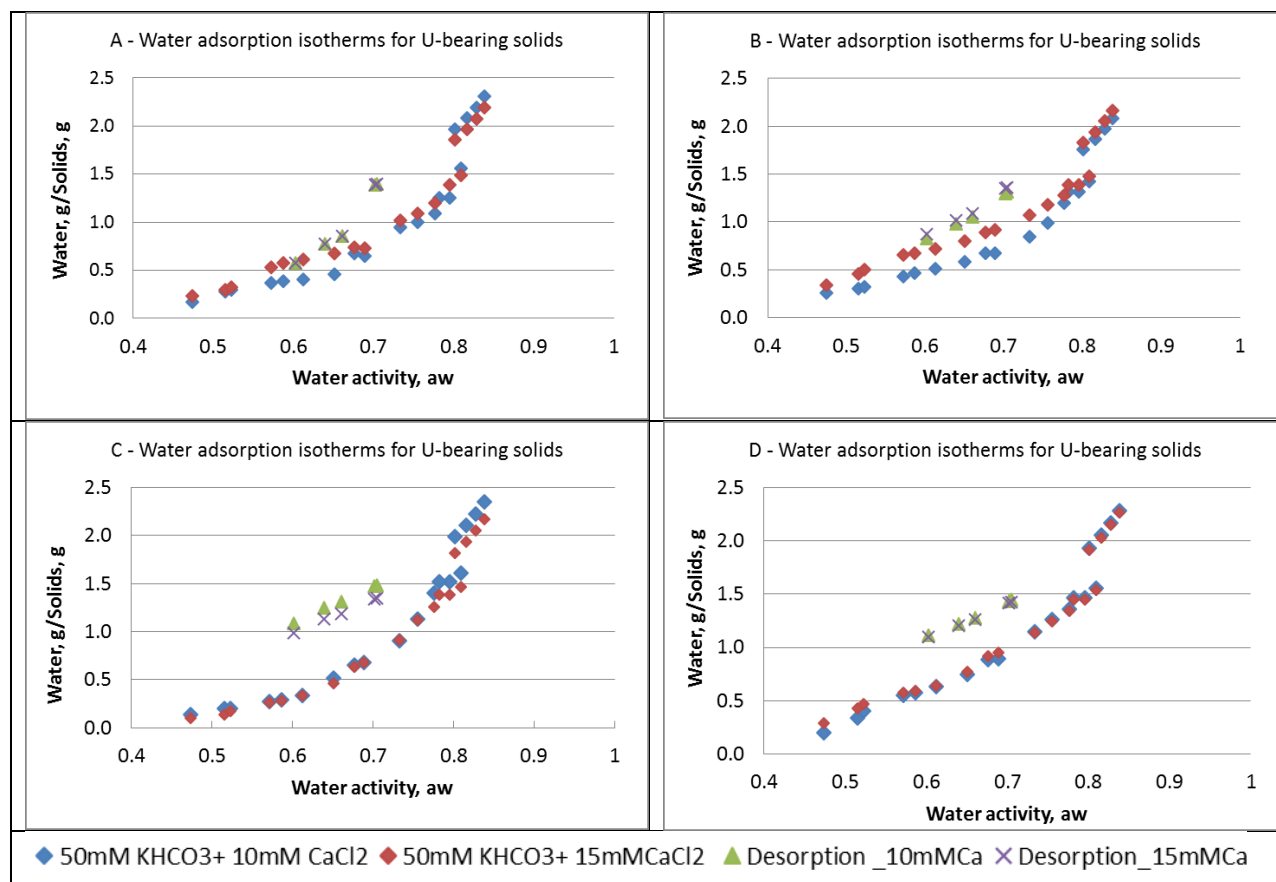
Figure 17. Water adsorption isotherms for U-bearing solids; A) Samples prepared with 3 mM HCO₃ and 0 mM and 5 mM of Ca; B) Samples prepared with 3 mM HCO₃ and 10 mM and 15 mM of Ca; C) Samples prepared with 50 mM HCO₃ and 0 mM and 5 mM of Ca; D) Samples prepared with 50 mM HCO₃ and 10 mM and 15 mM of Ca.

The shape of the adsorption isotherms reflects a Type II sorption isotherm curve according to the recommended classification (Sing 1985). This type of isotherm is characterized by monolayer-multilayer sorption on the nonporous or macroporous surface of a precipitate. This isotherm is characterized by a hysteresis loop that shows the difference between adsorption and desorption isotherms. A hysteresis loop is commonly associated with a capillary condensation taking place in mesopores. The initial part of the Type II isotherm is characterized by a linear increase in water retention until reaching a formation of a well-defined monolayer at which monolayer coverage is complete and multilayer adsorption starts to occur (Sing 1985, Lowell et al. 2012).

At high water activities, a steep upward increase of water retention is noted due to vapor condensation (Figure 17). So, at high humidity, solid water-soluble components at the surface of precipitates can start to dissolve in adsorbed water vapor forming a saturated solution (Kontny and Zografi 1995). This will eventually lead to the deliquescence of the solid or its components and the formation of a liquid phase. Figure 18 shows a solution on the bottom of crucibles formed as results of vapor condensation at water activity higher than 0.79.

Figure 18. Condensation of water vapor forming a saturated solution on the bottom of crucibles.

All experimental data obtained were grouped in Figure 19 to present isotherms for samples composed of 3 mM HCO_3 and 50 mM HCO_3, both prepared with 0 mM, 5 mM, 10 mM, and 15 mM Ca concentrations. Each figure also includes results for the samples prepared using pure 100 mM sodium silicate for comparison.
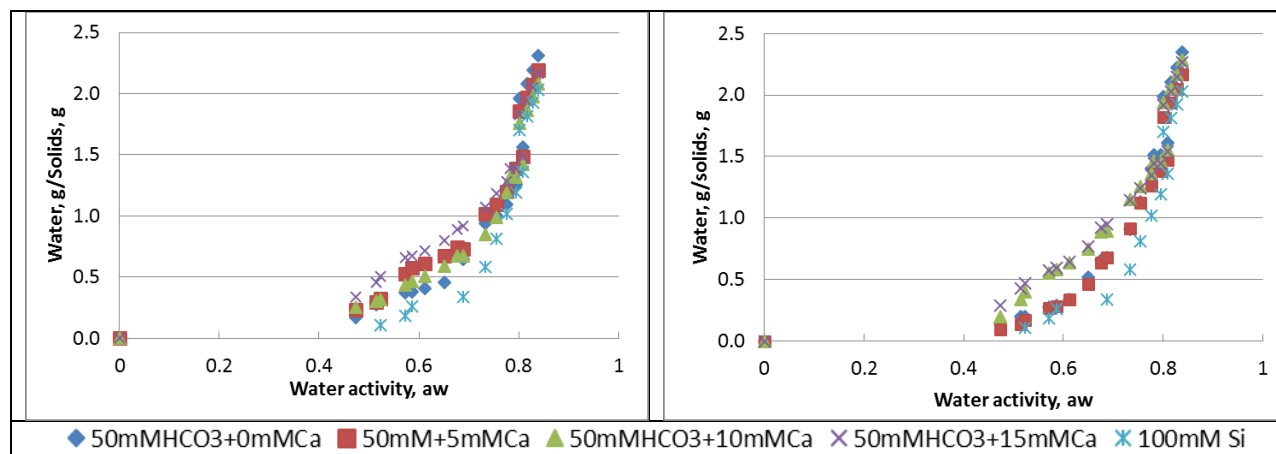
Figure 19. Water adsorption isotherms for U-bearing solids: A) Samples prepared with 3 mM HCO_3; B) Samples prepared with 50 mM HCO_3.

The amount of water adsorbed by multicomponent precipitates at $a_w = 0.67$ ranged between 0.63-0.77 g water/g precipitate. The water retention capability was generally greater for multicomponent samples compared to dry silicate gel. In addition, the samples prepared with higher Ca concentrations exhibited higher abilities for water retention.

Silica is the major constituent of the uranium-bearing precipitates, which are mainly amorphous upon formation. For an example, silica-gel produced from sodium silicate is considered to be a highly porous solid. It consists of porous particles with diameters varying between 2-20 nm (Iler 1979) that account for a surface area of about 2.8×10^7 m^2 per m^3 of silica gel (Saha, Akisawa and Kashiwagi 2001). Due to these properties, the silica-gel has a great capacity to adsorb water vapor (Ng et al. 2001, Tahat 2001). In FIU's experiments, the amount of water adsorbed on the

silica samples at a_w =0.67 averaged up to 58% of the dry mass of the silica gel samples, which is higher than observed by (Ng et al. 2001).

The surface properties of amorphous silica in many cases depend on the presence of hydroxyl silanol groups, $\equiv$Si-OH, which are formed on the surface by the condensation polymerization of $Si(OH)_4$ and as a result of rehydroxylation of dehydroxylated silica when it is treated with water or aqueous solutions. Supersaturated solutions of monomeric $Si(OH)_4$ are formed when an aqueous solution of soluble silicate is acidified.

$$Na_2SiO_3 + H_2O + 2HCI = Si(OH)_4 + 2NaCl \qquad \qquad Eq\ 5$$

This also leads to the formation of colloidal particles of silica, which are highly porous with an extensive internal surface covered with $\equiv$Si-OH groups. The sufficient concentration of silanol groups makes such a surface hydrophilic (Iler 1979). The H_2O molecule always interacts with the hydroxyl groups through H-bonding (Yang and Wang 2006). After drying some of the silanol groups remain on the surface (Zhuravlev 2000).

Measurements of desorption hysteresis loops down to low water activity suggested that adsorption and desorption isotherms did not coincide for any of sample compositions and the desorption branch is steeper than the adsorption (Figure 17). Initial measurements exhibited hysteresis loop between sorption and desorption isotherms, suggesting that precipitates are most likely porous in nature able for sorbing water via capillary condensation (Kontny and Zografi 1995). In addition, samples prepared with "high" bicarbonate content exhibited broader hysteresis loop formed by adsorption/desorption isotherms compared to samples containing 3 mM HCO_3 (Figure 17). Experiments on water desorption are still ongoing.

Subtask 1.1: Acknowledgements

Subtask 1.1: References

Afonso, M. & V. Silveira Jr (2005) Characterization of equilibrium conditions of adsorbed silica–gel/water bed according to Dubinin–Astakhov and Freundlich. *Revista de Engenharia Térmica,* 4.

Altmaier, M., X. Gaona & T. Fanghänel (2013) Recent advances in aqueous actinide chemistry and thermodynamics. *Chemical reviews,* 113**,** 901-943.

Bernhard, G., G. Geipel, V. Brendler & H. Nitsche (1996) Speciation of uranium in seepage waters of a mine tailing pile studied by time-resolved laser-induced fluorescence spectroscopy (TRLFS). *Radiochimica Acta,* 74**,** 87-92.

Bernhard, G., G. Geipel, T. Reich, V. Brendler, S. Amayri & H. Nitsche (2001) Uranyl (VI) carbonate complex formation: Validation of the Ca2UO2 (CO3) 3 (aq.) species. *Radiochimica Acta International journal for chemical aspects of nuclear science and technology,* 89**,** 511.

Bethke, C. M. 2007. *Geochemical and biogeochemical reaction modeling*. Cambridge University Press.

Bickmore, B. R., K. L. Nagy, J. S. Young & J. W. Drexler (2001) Nitrate-cancrinite precipitation on quartz sand in simulated Hanford tank solutions. *Environmental science & technology,* 35**,** 4481-4486.

Blanco, L. H., E. Amado & J. A. Avellaneda (2006) Isopiestic determination of the osmotic and activity coefficients of dilute aqueous solutions of the series MeEt 3 NI to HepEt 3 NI at 298.15 K. *Fluid phase equilibria,* 249**,** 147-152.

Catalano, J. G., S. M. Heald, J. M. Zachara & G. E. Brown (2004) Spectroscopic and diffraction study of uranium speciation in contaminated vadose zone sediments from the Hanford Site, Washington State. *Environmental science & technology,* 38**,** 2822-2828.

Dong, W. & S. C. Brooks (2006) Determination of the formation constants of ternary complexes of uranyl and carbonate with alkaline earth metals (Mg2+, Ca2+, Sr2+, and Ba2+) using anion exchange method. *Environmental science & technology,* 40**,** 4689-4695.

Felmy, A. R., H. Cho, J. R. Rustad & M. J. Mason (2001) An aqueous thermodynamic model for polymerized silica species to high ionic strength. *Journal of Solution Chemistry,* 30**,** 509-525.

Gorman-Lewis, D., P. C. Burns & J. B. Fein (2008) Review of uranyl mineral solubility measurements. *The Journal of Chemical Thermodynamics,* 40**,** 335-352.

Grenthe, I., J. Fuger, R. J. Konings, R. J. Lemire, A. B. Muller, C. Nguyen-Trung & H. Wanner. 1992. *Chemical thermodynamics of uranium*. North-Holland Amsterdam.

Gruszkiewicz, M., J. Horita, M. Simonson & E. Mesmer. 2000. High temperature water adsorption on geothermal reservoir rocks. In *Proceedings of the World Geothermal Conference*.

Gruszkiewicz, M. S., J. Horita, J. M. Simonson, R. E. Mesmer & J. B. Hulen (2001) Water adsorption at high temperature on core samples from The Geysers geothermal field, California, USA. *Geothermics,* 30**,** 269-302.

Guillaumont, R., T. Fanghänel, J. Fuger, I. Grenthe, V. Neck, D. Palmer & M. Rand (2003) Update on the chemical thermodynamics of U, Np, Pu, Am and Tc. *Chemical Thermodynamics,* 5.

Guillaumont, R. & F. J. Mompean (2003) Update on the chemical thermodynamics of uranium, neptunium, plutonium, americium and technetium.

Hummel, W., U. Berner, E. Curti, F. Pearson & T. Thoenen. 2002. Nagra/PSI chemical thermodynamic data base 01/01, National Cooperative for the Disposal of Radioactive Waste in Switzerland (Nagra). Technical Report 02-16.

Iler, R. K. (1979) The chemistry of silica: solubility, polymerization, colloid and surface properties, and biochemistry. *Canada: John Wiley &Sons Inc*.

Kalmykov, S. N. & G. R. Choppin (2000) Mixed Ca2+/UO22+/CO32-complex formation at different ionic strengths. *Radiochimica Acta International journal for chemical aspects of nuclear science and technology,* 88**,** 603.

Katsenovich, Y. P., C. Cardona, R. Lapierre, J. Szecsody & L. E. Lagos (2016) The effect of Si and Al concentrations on the removal of U (VI) in the alkaline conditions created by NH 3 gas. *Applied Geochemistry,* 73**,** 109-117.

Kontny, M. J. & G. Zografi. 1995. Sorption of Water by Solids. In *Physical Characterization of Pharmaceutical Solids*, 387-418. CRC Press.

Langmuir, D. 1997. *Aqueous Environmental Geochemistry*. Upper Saddle River, New Jersey: Prentice Hall.

Liu, C., J. M. Zachara, O. Qafoku, J. P. McKinley, S. M. Heald & Z. Wang (2004) Dissolution of uranyl microprecipitates in subsurface sediments at Hanford Site, USA. *Geochimica et Cosmochimica Acta,* 68**,** 4519-4537.

Lowell, S., J. E. Shields, M. A. Thomas & M. Thommes. 2012. *Characterization of porous solids and powders: surface area, pore size and density*. Springer Science & Business Media.

Ng, K., H. Chua, C. Chung, C. Loke, T. Kashiwagi, A. Akisawa & B. Saha (2001) Experimental investigation of the silica gel–water adsorption isotherm characteristics. *Applied Thermal Engineering,* 21**,** 1631-1642.

Qafoku, N. P., C. C. Ainsworth, J. E. Szecsody & O. S. Qafoku (2003) Aluminum Effect on Dissolution and Precipitation under Hyperalkaline Conditions. *Journal of environmental quality,* 32**,** 2354-2363.

Qafoku, N.P., C. C. Ainsworth, J. E. Szecsody & O. S. Qafoku (2004) Transport-controlled kinetics of dissolution and precipitation in the sediments under alkaline and saline conditions. *Geochimica et Cosmochimica Acta,* 68**,** 2981-2995.

Qafoku, N. P. & J. P. Icenhower (2008) Interactions of aqueous U (VI) with soil minerals in slightly alkaline natural systems. *Reviews in Environmental Science and Bio/Technology,* 7**,** 355-380.

Rard, J. A. & S. L. Clegg (1997) Critical Evaluation of the Thermodynamic Properties of Aqueous Calcium Chloride. 1. Osmotic and Activity Coefficients of 0−10.77 mol·kg-1 Aqueous Calcium Chloride Solutions at 298.15 K and Correlation with Extended Pitzer Ion-Interaction Models. *Journal of Chemical & Engineering Data,* 42**,** 819-849.

Reid, R. C., J. M. Prausnitz & B. E. Poling (1987) The properties of gases and liquids.

Richter, A., F. Bok & V. Brendler (2015) Data compilation and evaluation for U (IV) and U (VI) for the Thermodynamic Reference Database THEREDA.

Rouquerol, F., J. Rouquerol & K. Sing. 1999. In Adsorption by Powders and Porous Solids: Principles, Methodology and Applications, 1-626. London: Academic Press.

Saha, B., A. Akisawa & T. Kashiwagi (2001) Solar/waste heat driven two-stage adsorption chiller: the prototype. *Renewable Energy,* 23**,** 93-101.

Serne, R., B. Bjornstad, D. Horton, D. Lanigan, C. Lindenmeier, M. Lindberg, R. Clayton, V. LeGore, R. O. I. Kutnyakov & S. Baum (2004) Characterization of Vadose Zone Sediments Below the TX Tank Farm: Boreholes C3830, C3831, C3832 and RCRA Borehole 299-W10-27. *Pacific Northwest National Laboratory (PNNL): Richland, WA*.

Serne, R. J., G. V. Last, G. W. Gee, H. T. Schaef, D. C. Lanigan, C. W. Lindenmeier, M. J. Lindberg, R. E. Clayton, V. L. Legore & R. D. Orr. 2008. Characterization of vadose zone sediment: Borehole 299-E33-45 near BX-102 in the B-BX-BY waste management area. Pacific Northwest National Laboratory (PNNL), Richland, WA (US).

Shvareva, T. Y., L. Mazeina, D. Gorman-Lewis, P. C. Burns, J. E. Szymanowski, J. B. Fein & A. Navrotsky (2011) Thermodynamic characterization of boltwoodite and uranophane: Enthalpy of formation and aqueous solubility. *Geochimica et Cosmochimica Acta,* 75**,** 5269-5282.

Sing, K. S. (1985) Reporting physisorption data for gas/solid systems with special reference to the determination of surface area and porosity (Recommendations 1984). *Pure and applied chemistry,* 57**,** 603-619.

Szecsody, J. E., M. J. Truex, N. P. Qafoku, D. M. Wellman, T. Resch & L. R. Zhong (2013) Influence of acidic and alkaline waste solution properties on uranium migration in subsurface sediments. *Journal of Contaminant Hydrology,* 151**,** 155-175.

Szecsody, J. E., M. J. Truex, L. Zhong, N. Qafoku, M. D. Williams, J. P. McKinley, Z. Wang, J. Bargar, D. K. Faurie, C. T. Resch & J. L. Phillips. 2010. Remediation of Uranium in the Hanford Vadose Zone Using Ammonia Gas: FY 2010 Laboratory-Scale Experiments. Medium: ED; Size: PDFN.

Szecsody, J. E., M. J. Truex, M. J. Zhong, T. C. Johnson, N. P. Qafoku, M. D. Williams, W. J. Greenwood, E. L. Wallin, J. D. Bargar & D. K. Faurie (2012) Geochemical and Geophysical Changes during Ammonia Gas Treatment of Vadose Zone Sediments for Uranium Remediation. *Vadose Zone Journal***,** 1-13.

Tahat, M. (2001) Heat-pump/energy-store using silica gel and water as a working pair. *Applied energy,* 69**,** 19-27.

Thoenen, T., W. Hummel, U. Berner & E. Curti (2014) The PSI/Nagra Chemical Thermodynamic Database 12/07.

Um, W., Z. Wang, R. J. Serne, B. D. Williams, C. F. Brown, C. J. Dodge & A. J. Francis (2009) Uranium phases in contaminated sediments below Hanford's U tank farm. *Environmental science & technology,* 43**,** 4280-4286.

Van Campen, L., G. Amidon & G. Zografi (1983) Moisture sorption kinetics for water-soluble substances I: Theoretical considerations of heat transport control. *Journal of pharmaceutical sciences,* 72**,** 1381-1388.

Wronkiewicz, D. J., J. K. Bates, T. J. Gerding, E. Veleckis & B. S. Tani (1992) Uranium release and secondary phase formation during unsaturated testing of UO 2 at 90 C. *Journal of Nuclear Materials,* 190**,** 107-127.

Wronkiewicz, D. J., J. K. Bates, S. F. Wolf & E. C. Buck (1996) Ten-year results from unsaturated drip tests with UO 2 at 90 C: implications for the corrosion of spent nuclear fuel. *Journal of Nuclear Materials,* 238**,** 78-95.

Yang, J. & E. Wang (2006) Reaction of water on silica surfaces. *Current Opinion in Solid State and Materials Science,* 10**,** 33-39.

Zachara, J. M., C. Brown, J. Christensen, J. A. Davis, E. Dresel, C. Liu, S. Kelly, J. Mckinley, J. Serne & W. Um (2007) A site-wide perspective on uranium geochemistry at the Hanford Site.

Zachara, J. M., J. A. Davis, J. P. McKinley, D. M. Wellman, C. Liu, N. P. Qafoku & S. Yabusaki. 2005. Uranium Geochemistry in Vadose Zone and Aquifer Sediments from the 300 Area Uranium Plume. ed. U. S. DOE. Hanford, WA: Pacific Northwest National Laboratory.

Zhong, L., J. E. Szecsody, M. J. Truex, M. D. Williams & Y. Liu (2015) Ammonia gas transport and reactions in unsaturated sediments: Implications for use as an amendment to immobilize inorganic contaminants. *Journal of Hazardous Materials,* 289**,** 118-129.

Zhuravlev, L. (2000) The surface chemistry of amorphous silica. Zhuravlev model. *Colloids and Surfaces A: Physicochemical and Engineering Aspects,* 173**,** 1-38.

Subtask 1.1.1: Characterization of the Uranium-Bearing Samples

Subtask 1.1.1: Introduction

The release of hazardous waste accumulated with the production of the earliest nuclear weapons has threatened the long-term health of the ecosystem surrounding the Hanford Site. Among the particular concerns is a risk posed to the Colombia River by the potential mobilization of the radiochemical species, such as uranium, which contaminate the subsurface. Of the *in situ* amendments considered for the remediation of uranium contamination in the Hanford vadose zone, the research for the injection of ammonia gas (NH_3) has shown much promise for the reduction of contaminant mobility (Szecsody et al. 2010).

This remediation technology relies on the subsurface chemistry change associated with the injection of the reactive ammonia gas into the Hanford vadose zone. The partitioning and dissolution of the gas into the pore water, which resides and migrates through the soil's interstitial space, causes the elevation of the pH from the typical near neutral value to much more alkaline levels. These post-injection conditions encourage the partial dissolution of a variety of subsurface minerals that make up the soil. As the system re-establishes the natural pH conditions, the mobility of uranium phases is reduced, likely due to the re-precipitation of the aforementioned mineral phases physically containing the contaminant. This is supported by the findings of Pacific Northwest National Laboratory research, which showed the reduction of uranium mobility in contaminated sediments (Szecsody et al. 2012).

Laboratory scale experiments to investigate the ammonia gas remediation technology were completed using an array of synthetic pore water solutions designed to be representative of conditions within the Hanford 200 Area vadose zone. The analysis of these prior samples, using a combination of scanning electron microscopy with energy dispersive spectroscopy (SEM with EDS) and X-ray diffraction (XRD), revealed the presence of crystal-like uranium-rich solid phases (Figure 20), which came to be the focal point of the investigation moving forward. The comparison of the diffraction patterns for the select samples with reference patterns for the most likely mineral phases resulted in a tentative match for the uranium species cejkaite ($Na_4(UO_2)(CO_3)_3$), though this result could not be confirmed. It was theorized that the overwhelming presence of nitratine ($NaNO_3$), which appears to be clearly defined in the diffraction pattern, hindered the detection of any other mineral phases present in the sample.
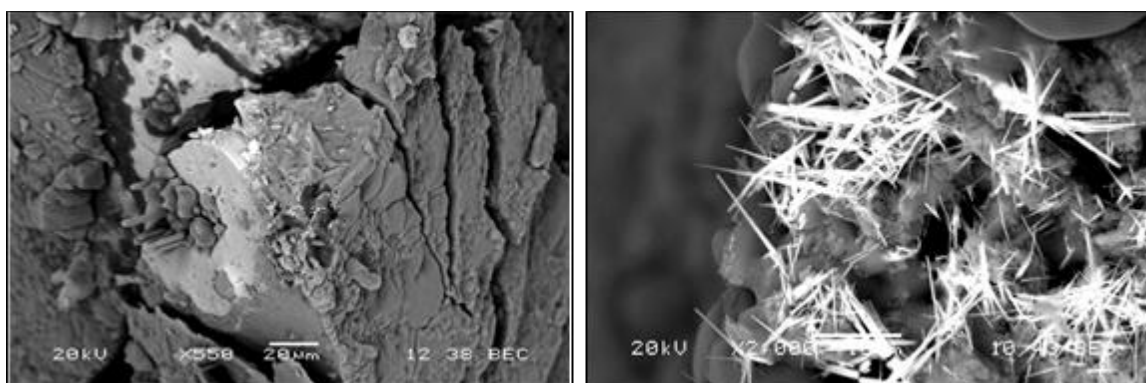
Figure 20. SEM images showing uranium phases of interest in past sample analysis.

In addition to the presumed analytical inference, the presence of a species like nitratine is problematic because the highly soluble crystal should not precipitate under the experimental

conditions. It was thereby determined that the formation was likely due evaporation of the residual supernatant when drying the sample precipitate. In order to avoid this obstacle, a new batch of experimental samples was prepared with a method modified to include filtration and deionized water (DIW) rinse steps.

The modifications in sample preparation were coupled with enhancements to the overall experimental design in order to better evaluate the contribution of the variable bicarbonate and calcium concentrations on sample characterization. These included a synthetic pore water optimization study which, paired with the results of SEM-EDS analysis of the precipitate phase, would be used for selecting samples, which would advance to further analysis. The selected samples would be treated to a sequential extraction procedure for characterizing the likely uranium phases present in precipitates based on their affinities to various solutions.

Subtask 1.1.1 Materials and Methods

The modified sample preparation methods closely follow the main components of the procedure, which have been described in prior reports. An array of synthetic pore water solutions was put together using stock solutions of their component salts and combined to achieve the desired final concentrations when diluted to volume (Table 4). Samples were prepared in duplicate for comparison solid phases with and without the DIW rinse.

Table 4. Stock Solution & Synthetic Pore Water Concentrations for Sample Preparation

Stock Solution	Concentration (mM)	Synthetic Pore Water Concentrations (mM)
$CaCl_2 \cdot 6H_2O$	500.00	0/5/10
$NaHCO_3$	400.00	5/25/50
$Na_2SiO_3 \cdot 9H_2O$	422.24	100
$Al(NO_3)_3 \cdot 9H_2O$	50.00	5
$UO_2(NO_3)_2 \cdot 6H_2O$	210.06	2.1 (500 ppm U)
5% NH_3 in N_2 (gas)	Bubbled into solution until pH ≈ 11	

The procedure begins with concentrated solutions of $KHCO_3$, Na_2SiO_3, and $Al(NO_3)_3$ combined in a 50-mL vial to form the base of the various synthetic pore water solutions. The base solution would then be pH adjusted using nitric acid to reach a value of about 8, consistent with the pH of pore water in the Hanford vadose zone. The synthetic pore water solutions were then bubbled with ammonia gas until the system reached a treatment pH range around 11 (Figure 21). Immediately following this step, the base solutions were broken up into 10-mL aliquots in 15-mL vials with caps perforated to allow some air exchange. The final components, $CaCl_2$ and $UO_2(NO_3)_2$, were added in small volumes of highly concentrated solutions in order to reach desired concentrations when diluted. The previously reported increase in uranium concentration, from 200 ppm to 500 ppm, was retained in these samples.

Figure 21. NH₃ injection of the low, mid, and high bicarbonate synthetic pore water base solutions.

The synthetic pore water pH was monitored as the samples re-established the pre-treatment pH range through the partitioning and liberation of the dissolved NH_3 gas. The change in pH was very slow initially, dropping by less than 0.5 in the first week. After three weeks of slow change, the samples were transferred to an orbital shaker and agitated gently for a fourth week before reaching the desired post-treatment pH range of 8-9. The solid precipitate phase and supernatant were separated by vacuum filtration using disposable 0.22 μm nitrocellulose filters. The collected precipitates of sample duplicates, prepared identically to this point, were rinsed with 5-mL of deionized water. The filtered precipitates were dried at 30°C over 3 days while the supernatant filtrates and rinse solutions were labeled and stored for further analysis.

Samples were labeled using the two digits of the bicarbonate concentration followed by the two digits of the calcium concentration. Either an A or B was affixed to the end of the label to distinguish the unrinsed and rinsed samples, respectively.

Synthetic Pore Water Optimization Study

In order to facilitate the analysis of the precipitates produced with the treatment of the synthetic pore water solutions, an optimization study was done to maximize the presence of uranium in the precipitate phase for analysis. A 3^2 full-factorial experimental design was used in order to cover all combinations of the two factor, three level experiment. This involved preparing synthetic pore water solutions with a range of concentrations for the experimental variables, bicarbonate (HCO_3^-) and calcium (Ca^{2+}) resulting in a total of 9 samples and their duplicates (Table 5). For this study, the concentration of uranium retained in the supernatant filtrate solution was used to deduce, by difference, which precipitates contained the most uranium. This required the assumption of negligible analyte loss to the filter. For duplicate samples, the uranium concentration of the DIW rinse was not considered.

Supernatant solutions were diluted up to 10,000 times in 1% nitric acid to make sure that uranium fell into the analytical range for analysis by kinetic phosphorescence analyzer (KPA). The results of this analysis were used as the primary basis for determining which samples advanced to further analysis.

Table 5. Synthetic Pore Water Solution Concentrations & Labels

Primary Constituents	Component Concentrations								
	Low Bicarbonate			Mid Bicarbonate			High Bicarbonate		
HCO_3^-	5			25			50		
Al	5			5			5		
Si	100			100			100		
Ca	0	5	10	0	5	10	0	5	10
Label	05-00	05-05	05-10	25-00	25-05	25-10	50-00	50-05	50-10

Solid Phase Characterization

SEM-EDS Analysis

Sample specimens were taken from all samples for solid phases analysis by scanning electron microscopy with energy dispersive spectroscopy (SEM-EDS). This analysis was used, together with the results of the synthetic pore water optimization study, to determine what samples would move on to further analysis.

Samples were mounted to aluminum studs using double-sided carbon tape and sputter coated with a thin layer of gold using an SPI-Module Control and Sputter unit to enhance surface conductivity for better imaging. Analysis was done using a JEOL-5910-LV SEM with acceleration potentials between 10 and 20 kV. EDS analysis was done using an EDAX Sapphire detector with UTW Window and Genesis EDS microanalysis software. Micrographs were completed primarily using backscatter electron capture mode in order to better discern the areas with higher average atomic mass, which would be most likely to be rich in uranium.

Sequential Extraction

Though it is typically reserved for soil samples, a sequential extraction procedure for sample precipitates was added to the precipitate phase characterization strategy. This method made use of a series of increasingly aggressive extractions, each intended to target increasingly more difficult to remove uranium phases. Each extraction step utilized solutions and conditions chosen specifically to selectively target uranium associated with various phases within the precipitate sample (Table 6).

It is important to note that a number of sequential extraction procedures have been reported using a wide variety of conditions. While some differences are simply adjustments to fit the sample composition and analyte being targeted, there are many variations for comparable extractions. The procedure employed in this study is an amalgam based in particular on a combination of the procedures published by Tessier et al. (1979), Szecsody et al. (2010), Szecsody et al. (2012), and Kohler et al. (2004). The principal difference from the source material was the choice of distilled deionized water (DDIW) for the initial extraction (Step I), rather than a synthetic ground water solution. Additionally, after each extraction step, samples were rinsed with 5 mL of deionized water (DIW) which functioned to help remove any lingering extractant. For analytical purposes, this rinse solution was considered a part of the preceding extraction.

Table 6. Sequential Extraction Procedure

Extraction Step	Extraction Solution	Concentrations/Notes	Extraction Time	Target
I	DDI-Water	-	1 hour	Aqueous species
II	Carbonate Buffer	0.0144M NaHCO$_3$ and 0.0028M Na$_2$CO$_3$, pH 9.3	1 hour	Adsorbed species
III	Acetate Buffer	1M CH$_3$COO-Na (Adjusted to pH 5 by Acetic Acid)	1 hour	Some carbonates
IV	Acetic Acid	Concentrated CH$_3$COOH, pH 2.3	5 days	Carbonates and hydrated silicates
V	Nitric Acid	8M HNO$_3$, at 95 °C	2 hours	Difficult to remove phases

Like other aspects of the procedure, a variety of methods for selecting the volume of extraction solution has been published (Tessier et al. 1979, Ariza et al. 2000, Galán et al. 2003). These range from using a consistent volume to applying any of a number to solid-to-solution ratios. For the purpose of this study, the extraction volume was selected using a 40-to-1 solid (mg) to solution (mL) ratio which was used in a PNNL extraction study on uranium in Hanford sediment (Smith and Szecsody 2011).

Table 7. Extraction Solution Volumes – by Sample

Sample Label	Sample Weight (mg)	40:1 Extraction Volume (mL)
05 – 00A	26.4	0.6600
05 – 00B	16.6	0.4150
05 – 10A	38.2	0.9550
05 – 10B	45.8	1.145
50 – 00A	25.0	0.6250
50 – 00B	19.1	0.4775
50 – 10A	32.1	0.8025
50 – 10B	39.4	0.9850

The extraction procedure began with the addition of a known mass of precipitate to a labeled vial, to which the corresponding volume of extraction solution would be added (Table 7). The mixture was briefly vortexed before being transferred to an orbital shaker where the vessel was agitated at 150 rpm for the duration of the extraction. After extraction, samples were centrifuged at 5000 rpm for 30 minutes in order to separate the extractant and remaining precipitate. The extraction was followed by a 10 minute DI water rinse which, like the extraction, was accompanied with agitation and centrifugation. This process of extraction and rinse was repeated

for extraction steps I through IV with each of their specified extraction times. The final extraction (Step V), intended to target hard to extract uranium species, differed in that its extraction solution used 8 M nitric acid (HNO_3) maintained at 95°C using a water bath.

In some sequential extraction procedures (Smith and Szecsody 2011), an oxalate extraction solution is used prior to the nitric acid step. This was omitted from the procedure due to the fact that it was meant to target iron oxides from soils, which this system does not contain (Chao and Zhou 1983).

Subtask 1.1.1. Results and Discussion

Synthetic Pore Water Optimization

The results of previous attempts to characterize the precipitates produced by application of the remediation method to synthetic pore water solutions showed that solid phase analysis was largely hindered by the relatively small amount of uranium analyte in the precipitate. To counter this, this optimization study focused on what component concentrations would maximize the fraction of uranium in the precipitate phase based on the concentrations of uranium left in their supernatants. This relied on the assumption that all uranium introduced to the sample solutions was either retained in solution or precipitated/adsorbed onto the solid phase.

The optimization experiments were designed such that the results of the KPA analysis of the filtered supernatant solutions could be visualized using response surface diagrams (Figure 22). The full factorial experimental design took into account all test concentrations to display the relationship between the two variable concentrations and the concentration of uranium in the supernatant phase. Though the duplicate sample set was rinsed after vacuum filtration, the data used in the response surface does not take into account that rinse solution.

The results of both sample sets present a clear and demonstrative positive correlation between the increasing concentration of bicarbonate in synthetic porewater solutions and the concentration of uranium in the filtered post-treatment supernatant solution. This finding suggests that with increasing sample bicarbonate concentration, the amount of uranium in the precipitate decreases. It is therefore safe to conclude that the high bicarbonate samples (50-00, 50-05, & 50-10) would be least likely to precipitate the uranium analyte.
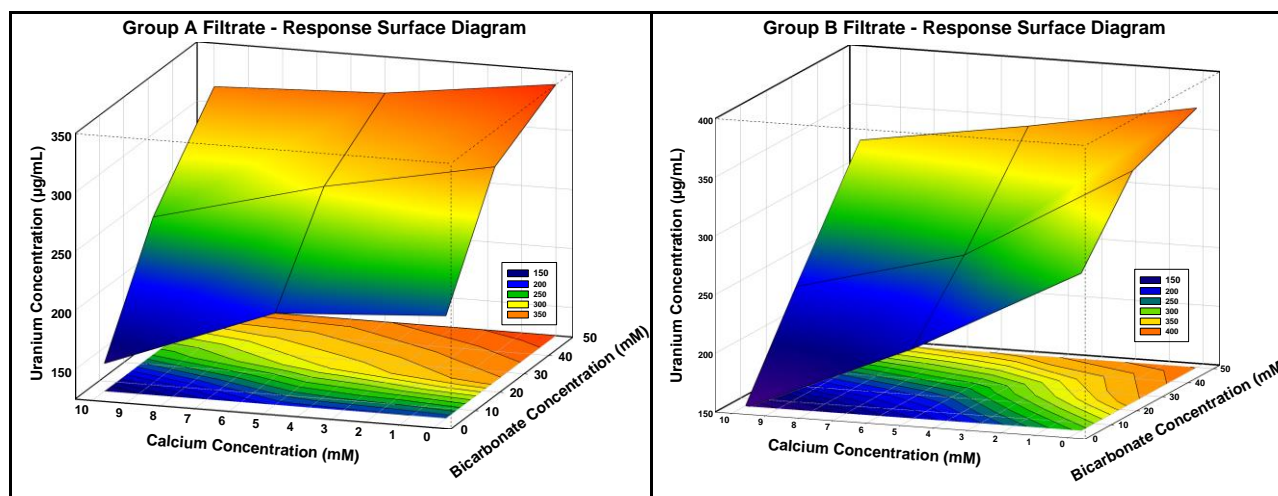
Figure 22. Response surface diagrams displaying filtrate solution uranium retention for the original (Group A) and duplicate/rinsed (Group B) samples.

This observed trend of uranium in the supernatant solutions increasing with added bicarbonate is likely indicative of conditions increasingly favoring the formation of uranyl carbonate. These species, which are highly soluble in aqueous solutions, form charged complexes, which can adsorb to the surface solid minerals under the right pH conditions. This data conflicts with past results of scanning electron microscope analysis for similar samples (Lagos et al. 2014) where uranium-rich crystalline solid phases were largely limited to the high bicarbonate (50 mM) samples (Figure 20). Within that same sample set, no samples showed these crystalline structures, though a scarce few did show amorphous uranium phases observable by SEM analysis. This previous finding also runs counter to what is expected of low bicarbonate samples based on the response surface. The trends in Figure 22 show that low bicarbonate samples (05-00, 05-25, & 05-50) have the least uranium remaining in the supernatant solutions and should, therefore, have the most in the precipitate phase.

Though much less pronounced, there is correlation between the increasing calcium concentrations in sample solution and the concentration of uranium in the supernatant. Unlike bicarbonate, however, the increasing calcium is associated with a decrease of uranium concentration in solution and, therefore, a reciprocal increase in the uranium precipitated out. It is theorized that the increase in calcium could favor the removal or uranium in one of two ways. There is evidence to suggest that presence of calcium ions in the system could facilitate the formation of calcium-uranyl precipitate phases (Figure 9). Another possible explanation is that the increase in calcium results in the precipitation of less soluble solids, such as calcium carbonate or calcium silicates, which could serve as nucleation sites provoking Si polymerization reactions and precipitation of silica (Iler 1979). When silica precipitate, this can also lead to co-precipitation of uranium.

Despite the initial aim of simply determining which sample conditions most favored the partitioning of uranium from the sample solutions to the resulting precipitates, all samples continued on to the surface analysis by scanning electron microscope. In this continued analysis, particular attention was paid to the samples corresponding to the vertices of the response surface diagrams (05-00, 05-10, 50-00, & 50-10).

Solid Phase Characterization

The analysis of the solid precipitate phase relied, in part, on scanning electron microscopy with energy dispersive spectroscopy for the qualitative analysis of the sample surface. This, combined with the results of supernatant analysis in the preceding optimization study, would be used to narrow the range of samples used for more laborious experiments.
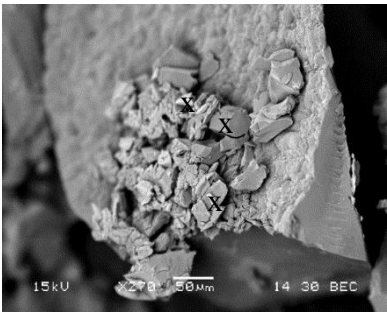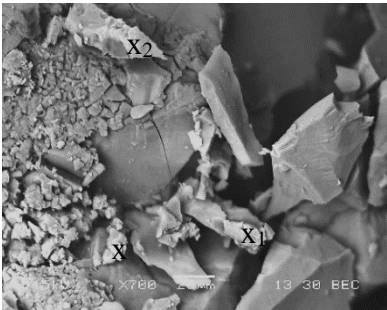
Scanning Electron Microscopy with Energy Dispersive Spectroscopy (SEM w. EDS)
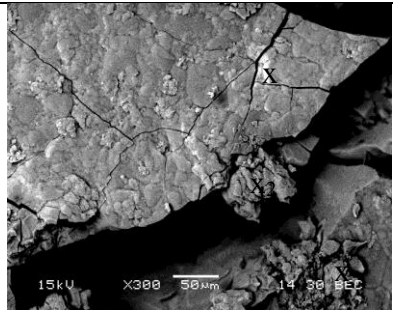
The SEM-EDS analysis of past samples played an important part in the evaluation these precipitates, including providing an idea of how to visually distinguish areas likely to have the highest atomic percentage of uranium. Primary areas of interest included crystal-like structures and areas of higher average atomic mass, identified as bright spots using backscatter electron capture mode. Energy dispersive spectroscopy was used to confirm the presence and estimate the abundance of uranium in these analysis points using primarily the atomic percentage (At%).

Surface morphological and compositional analysis started with low bicarbonate samples due to the relatively high removal of uranium from sample solutions and, presumably, into the

precipitate which was observed in supernatant analysis. This trend strongly implies that these precipitates would have the most abundant uranium phases for identification by SEM-EDS analysis. To the contrary, of the low bicarbonate samples across the spectrum of calcium concentrations, both unrinsed (Table 8) and rinsed (Table 9), no point analysis showed atomic percentages of uranium reaching or exceeding even 1%. This arbitrary value is one that was regularly exceeded in similar samples, where uranium-phases regularly reached $1 - 5\%$.
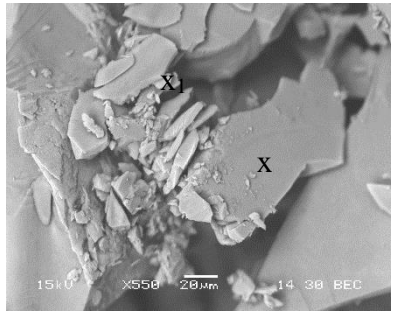
Table 8. SEM Images and EDS Data for Unrinsed Low Bicarbonate Samples

Sample SEM	EDS Point Analysis					
	X_1		**X_2**		**X_3**	
05-00A	*Element*	*At%*	*Element*	*At%*	*Element*	*At%*
	$C - K_\alpha$	13.62	$C - K_\alpha$	08.43	$C - K_\alpha$	10.48
	$O - K_\alpha$	52.09	$O - K_\alpha$	56.13	$O - K_\alpha$	52.75
	$Na - K_\alpha$	09.06	$Na - K_\alpha$	18.40	$Na - K_\alpha$	06.39
	$Al - K_\alpha$	01.63	$Al - K_\alpha$	01.50	$Al - K_\alpha$	02.54
	$Si - K_\alpha$	21.57	$Si - K_\alpha$	14.49	$Si - K_\alpha$	25.76
	$Au - M_\alpha$	01.60	$Au - M_\alpha$	00.80	$Au - M_\alpha$	01.68
			$U - M_\alpha$	00.25		
	$U - M_\alpha$	00.43			$U - M_\alpha$	00.40
05-05A	*Element*	*At%*	*Element*	*At%*	*Element*	*At%*
	$C - K_\alpha$	08.58	$C - K_\alpha$	12.23	$C - K_\alpha$	17.17
	$N - K_\alpha$	05.70	$N - K_\alpha$	06.34	$N - K_\alpha$	06.02
	$O - K_\alpha$	41.75	$O - K_\alpha$	48.14	$O - K_\alpha$	49.45
	$Na - K_\alpha$	06.32	$Na - K_\alpha$	09.54	$Na - K_\alpha$	05.06
	$Al - K_\alpha$	02.11	$Al - K_\alpha$	01.49	$Al - K_\alpha$	01.62
	$Si - K_\alpha$	33.77	$Si - K_\alpha$	21.36	$Si - K_\alpha$	20.07
	$U - M_\alpha$	00.77	$U - M_\alpha$	00.42	$U - M_\alpha$	00.25
	$Ca - K_\alpha$	01.01	$Ca - K_\alpha$	00.48	$Ca - K_\alpha$	00.36
05-10A	*Element*	*At%*	*Element*	*At%*	*Element*	*At%*
	$C - K_\alpha$	10.17	$C - K_\alpha$	21.16	$C - K_\alpha$	26.41
	$N - K_\alpha$	04.33	$N - K_\alpha$	04.36	$N - K_\alpha$	04.02
	$O - K_\alpha$	53.07	$O - K_\alpha$	45.67	$O - K_\alpha$	52.11

Sample SEM	EDS Point Analysis					
	X₁		**X₂**		**X₃**	
	$Na - K_\alpha$	04.89	$Na - K_\alpha$	00.85	$Na - K_\alpha$	00.62
	$Al - K_\alpha$	01.88	$Al - K_\alpha$	00.43	$Al - K_\alpha$	00.14
	$Si - K_\alpha$	24.99	$Si - K_\alpha$	00.79	$Si - K_\alpha$	00.47
	$U - M_\alpha$	00.33	$U - M_\alpha$	00.10	$U - M_\alpha$	00.04
	$Ca - K_\alpha$	00.35	$Ca - K_\alpha$	26.64	$Ca - K_\alpha$	16.19

There are several possible explanations for the discrepancy between the expectation of finding uranium-rich phases and the lack there of in solid phase analysis. The simplest reasoning is that the sample specimens extracted for SEM-EDS analysis did not contain any of the uranium phases present in the sample. More likely though is that the uranium phases present were highly distributed throughout the sample and indistinguishable by backscatter SEM.

Table 9. SEM Images and EDS Data for Rinsed Low Bicarbonate Samples

Sample SEM	EDS Point Analysis				**X₃**
	X₁		**X₂**		
05-00B	*Element*	*At%*	*Element*	*At%*	
	$C - K_\alpha$	08.30	$C - K_\alpha$	07.97	
	$N - K_\alpha$	07.70	$N - K_\alpha$	07.19	
	$O - K_\alpha$	48.39	$O - K_\alpha$	45.36	
	$Na - K_\alpha$	08.15	$Na - K_\alpha$	13.95	
	$Al - K_\alpha$	01.98	$Al - K_\alpha$	01.66	
	$Si - K_\alpha$	24.88	$Si - K_\alpha$	23.42	
	$U - M_\alpha$	00.59	$U - M_\alpha$	00.45	

Sample SEM	EDS Point Analysis					
	X₁		X₂		X₃	

	X_1		X_2		X_3	
05-05B	*Element*	*At%*	*Element*	*At%*	*Element*	*At%*
	$C - K_\alpha$	10.65	$C - K_\alpha$	12.84	$C - K_\alpha$	11.27
	$N - K_\alpha$	05.81	$N - K_\alpha$	05.78	$N - K_\alpha$	05.39
	$O - K_\alpha$	52.74	$O - K_\alpha$	46.27	$O - K_\alpha$	52.24
	$Na - K_\alpha$	03.42	$Na - K_\alpha$	05.70	$Na - K_\alpha$	06.64
	$Al - K_\alpha$	00.60	$Al - K_\alpha$	01.01	$Al - K_\alpha$	01.56
	$Si - K_\alpha$	26.36	$Si - K_\alpha$	27.48	$Si - K_\alpha$	22.18
	$U - M_\alpha$	00.25	$U - M_\alpha$	00.38	$U - M_\alpha$	00.30
	$Ca - K_\alpha$	00.17	$Ca - K_\alpha$	00.53	$Ca - K_\alpha$	00.41
05-10B	*Element*	*At%*	*Element*	*At%*	*Element*	*At%*
	$C - K_\alpha$	07.82	$C - K_\alpha$	11.15	$C - K_\alpha$	07.30
	$N - K_\alpha$	03.31	$N - K_\alpha$	05.62	$N - K_\alpha$	04.96
	$O - K_\alpha$	50.83	$O - K_\alpha$	33.47	$O - K_\alpha$	46.45
	$Na - K_\alpha$	04.65	$Na - K_\alpha$	01.20	$Na - K_\alpha$	07.88
	$Al - K_\alpha$	01.60	$Al - K_\alpha$	00.47	$Al - K_\alpha$	01.82
	$Si - K_\alpha$	30.46	$Si - K_\alpha$	02.25	$Si - K_\alpha$	29.43
	$U - M_\alpha$	00.56	$U - M_\alpha$	00.20	$U - M_\alpha$	00.66
	$Ca - K_\alpha$	00.77	$Ca - K_\alpha$	45.64	$Ca - K_\alpha$	01.50

The SEM imaging and EDS analysis (not shown) of the mid-range 25 mM samples were largely the same across the range of calcium concentrations with a similar lack of uranium-rich areas of interest. The most likely reason for this is the same as with low bicarbonate samples. The exceptions were small regions in the 25-00B and 25-05A samples (Figure 23) which were the only ones to show uranium atomic percentages that exceeded 1%. These areas of interest were different from past uranium-rich locations in that they appeared as flat, dark areas rather than the bright, crystal-like phases observed in past samples (Figure 20). This deviation is likely associated with the increased silicon, the percentage of which is twice that of the EDS analysis of uranium phases typically spotted on similar samples.

25-00B		25-05A	
Element	At%	Element	At%
C – Kα	03.17	C – Kα	04.64
N – Kα	13.94	N – Kα	10.27
O – Kα	33.25	O – Kα	32.18
Na – Kα	11.96	Na – Kα	08.77
Al – Kα	01.77	Al – Kα	02.14
Si – Kα	34.90	Si – Kα	39.27
U – Mα	01.01	U – Mα	01.66
		Ca – Kα	01.08
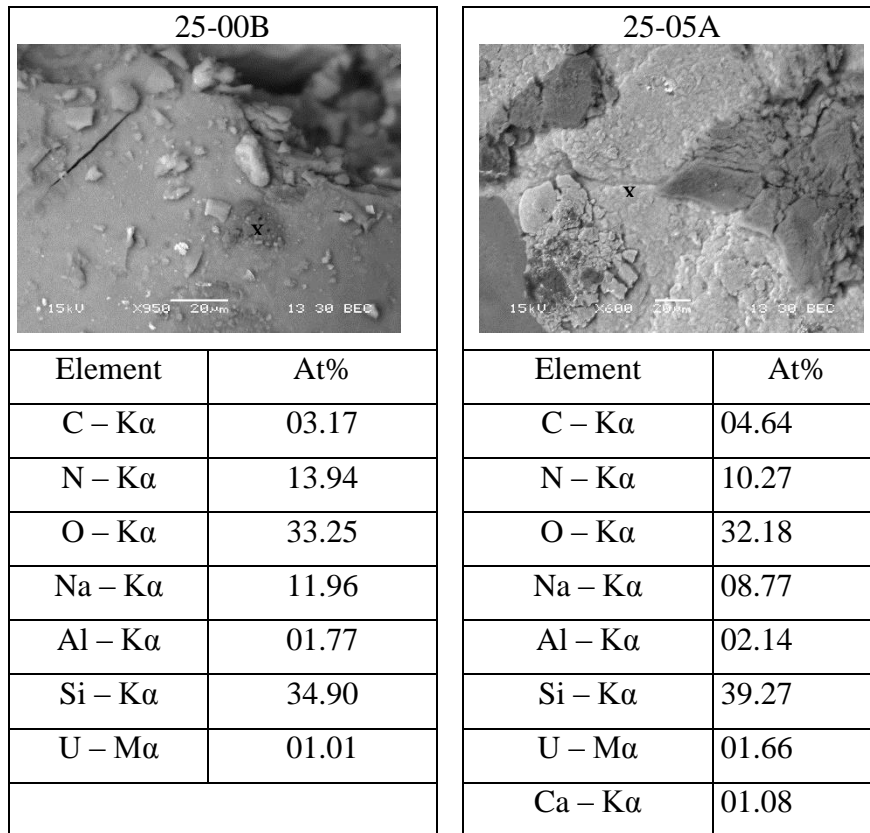
Figure 23. SEM image and EDS data for point analysis of specimens from the rinsed, 25 mM bicarbonate, zero calcium precipitate (left) and the unrinsed, 25 mM bicarbonate, 5 mM calcium precipitate (right).

50-00A	50-05A

Element	At%
$C - K_\alpha$	11.22
$N - K_\alpha$	05.48
$O - K_\alpha$	55.08
$Na - K_\alpha$	06.11
$Al - K_\alpha$	01.40
$Si - K_\alpha$	19.38
$U - M_\alpha$	01.31

Element	At%
$C - K_\alpha$	12.37
$N - K_\alpha$	07.13
$O - K_\alpha$	52.44
$Na - K_\alpha$	10.22
$Al - K_\alpha$	01.26
$Si - K_\alpha$	14.48
$U - M_\alpha$	01.47
$Ca - K_\alpha$	00.06
$Cl - K_\alpha$	00.55
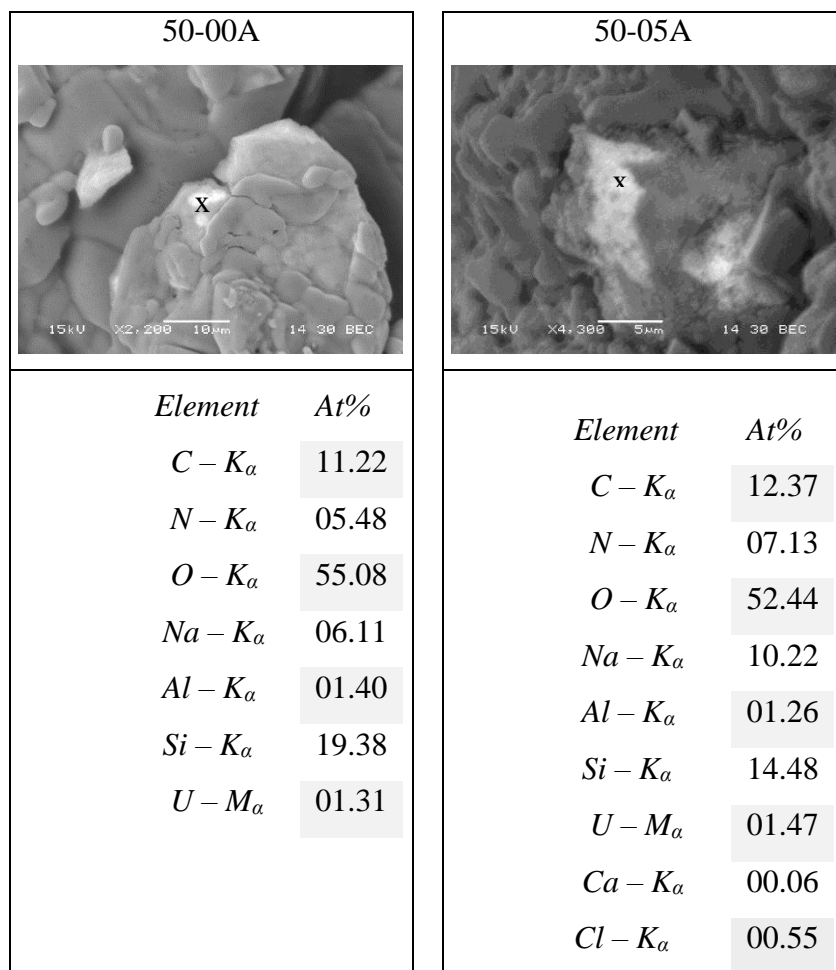
Figure 24. SEM image and EDS data for point analysis of specimens from the unrinsed, 50 mM bicarbonate, zero calcium precipitate (left) and the unrinsed, 50 mM bicarbonate, 5 mM calcium precipitate (right).

Although the overt trend in the optimization study suggesting that uranium's distribution into the precipitate would be favored in low bicarbonate samples, SEM-EDS analysis showed the distinct, bright, uranium-rich hotspots that were anticipated nearly exclusively in the high bicarbonate samples. These uranium phases, though they lacked the structure observed in Figure 20, were consistent with those observed in past analysis of similar samples. It is possible that, despite the addition of the vacuum filtration step, the evaporation of residual supernatant solution resulted in the precipitation of otherwise soluble uranium species. A comparison of the rinsed and unrinsed samples could be used to support this theory if the rinsed samples lacked the uranium phases observed in their unrinsed counterparts. The samples were reserved to conduct these analysis.

Sequential Extraction

The combination of supernatant analysis in the optimization study and SEM-EDS analysis of the sample precipitates was used to determine which samples would move on to the more extensive sequential extraction procedure. Though supernatant analysis suggested that uranium in the precipitate phase would be maximized in the low bicarbonate samples, SEM-EDS analysis primarily revealed uranium-rich phases in the high bicarbonate samples. While calcium concentration did appear to have an impact on uranium removal in the optimization study, the

effect was much less pronounced than that of bicarbonate concentration. Based on these observations, specimens from all low bicarbonate (5 mM) and high bicarbonate (50 mM) samples were taken for the sequential extraction study.

The KPA data collected from the study was graphed to display the mass of uranium removed with each extraction step based on the determined uranium concentration and the volume that it was extracted into (Figure 25). Despite the disagreement with the preceding SEM-EDS observations, the results of the sequential extraction were consistent with expectations based on the supernatant analysis. Although its SEM-EDS analysis showed no observable uranium-rich phases, the total mass of uranium extracted shows that each of the low bicarbonate samples had more uranium removed than their high bicarbonate counterparts. The difference is especially pronounced in the high calcium samples, corresponding to the supernatant analysis, which suggest that these would have the most uranium partitioning into the solid phase.
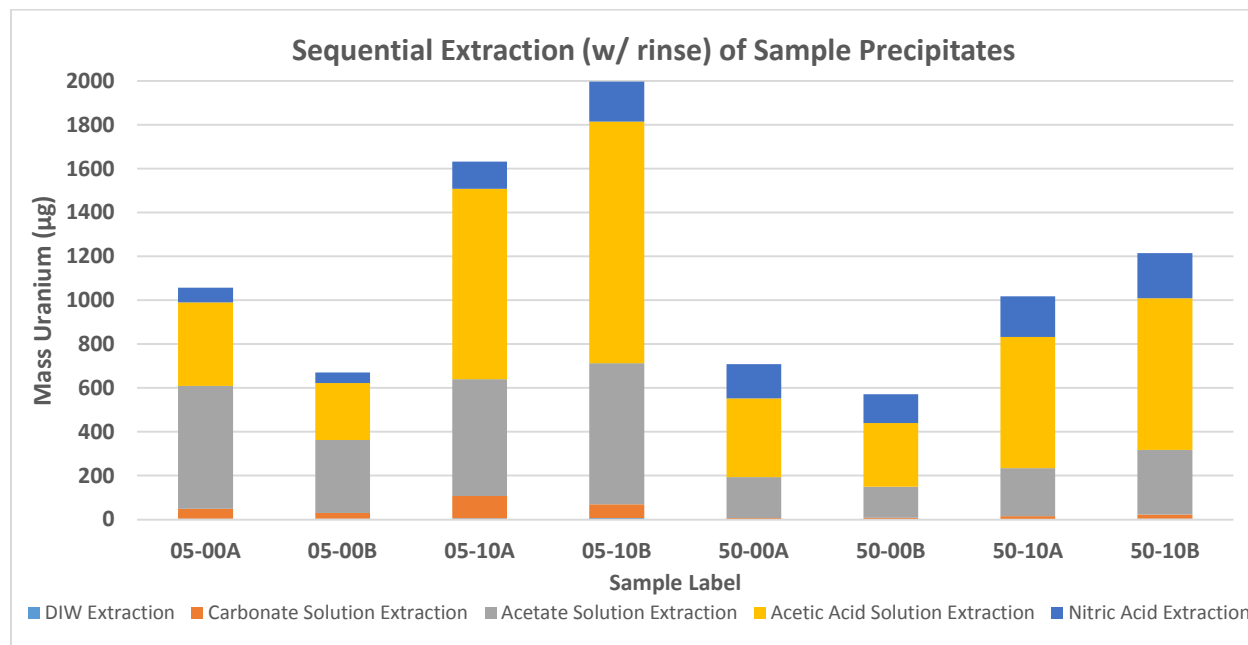
Figure 25. Sequential uranium extraction of sample precipitates with the addition of mass extracted by rinse.

The increased total uranium extraction in the high calcium containing samples, as compared to the calcium-free ones, is a trend that is consistent with the inverse relationship observed in supernatant analysis for synthetic pore water optimization. The fact that it consistent in both the unrinsed and rinsed samples,

The next most telling tendency displayed in this sequential extraction data was the increased total removal of uranium in the calcium containing samples compared to the calcium-free samples. This finding is consistent with the trends observed in the supernatant analysis that showed an inverse relationship between the calcium included in synthetic pore water solutions and the concentration of uranium retained in solution. In that experiment, the high calcium samples had the lowest uranium concentrations at each bicarbonate level evaluated.

A comparison of the relative removal of uranium between the various extraction steps reveals how each extracting solution was favored in the varying samples. This is useful for developing an assumption of the types of uranium phases which are most prevalent based on the "targeted"

extraction phase (Table 6) and the relative mass of the analyte removed by its corresponding solution.
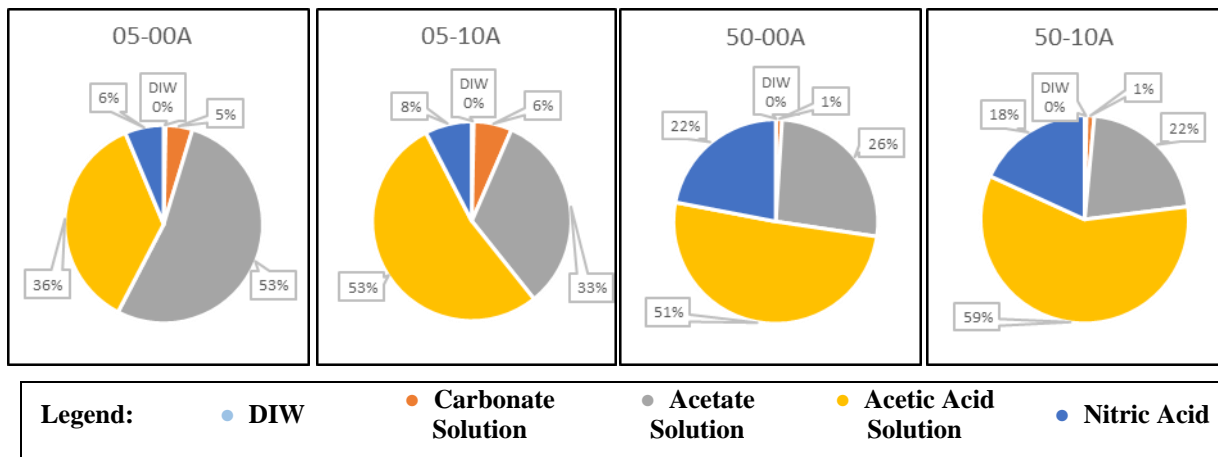
Figure 26. Uranium Extraction Distribution for Unrinsed (Group A) Samples.
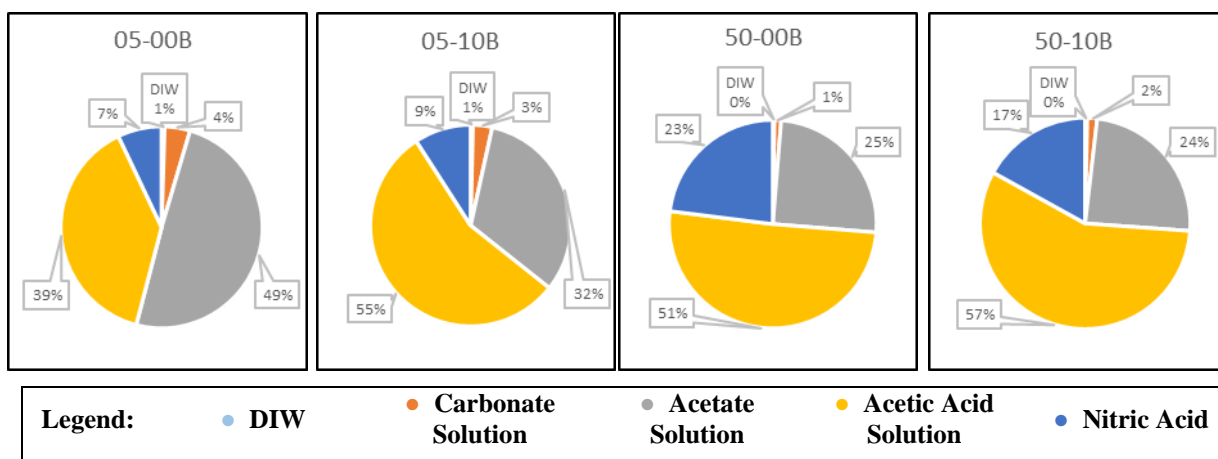
Figure 27. Uranium Extraction Distribution for Rinsed (Group B) Samples.

The sequential extraction distribution charts make clear that in both the rinsed (Figure 27) and unrinsed (Figure 28) samples, there is a near insignificant mass removal in the less aggressive DIW extraction. The most reasonable explanation for this extraction, which targets aqueous species, is likely that these species were largely prevented from forming by isolating the supernatant and precipitate in the vacuum filtration step of sample preparation.

Between equivalent low and high bicarbonate samples, the carbonate extraction, which targets the adsorbed species, had a significant decrease. The relative uranium removal decreased from 5-6% to 1%, about an 80% decrease of its relative abundance.

The majority of uranium was removed in the acetate solution (step 3) and acetic acid solution (step 4) extractions, making a strong case for suggesting that the uranyl carbonates and silicates make up the bulk of the extracted analyte.

Subtask 1.1.1 Future Work

Sample precipitates were cold mounted in epoxy in order to prepare for electron microprobe analysis (EPMA). This involved preparing 1-inch cylindrical epoxy molds which had ¼" holes drilled into their centers (Figure 28a). Promising samples, selected based on the results of prior

analysis (Table 10), were crushed and mixed with small amounts of epoxy before being poured into the hole of the cured molds (Figure 28b). Samples then spent 5 minutes in a vacuum chamber at 25 in. Hg to evacuate any air bubbles before curing over 24 hours.

Table 10. Samples Elected for Epoxy Fixing and Analysis
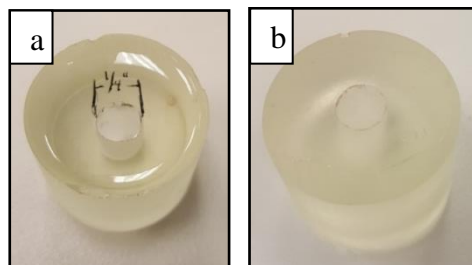
Figure 28. Epoxy mold before (a) and after (b) filling with resin + sample mixture.

Sample Labels		Key Variables
• 05-00A	• 05-00B	5 mM HCO_3^- and no Ca^{2+}
• 05-10A	• 05-10B	5 mM HCO_3^- and 10 mM Ca^{2+}
• 50-00A	• 50-00B	50 mM HCO_3^- and no Ca^{2+}
• 50-10A	• 50-10B	50 mM HCO_3^- and 10 mM Ca^{2+}

*Samples labeled "B" are duplicate precipitates which were rinsed with DIW

The eight samples selected for electron microprobe analysis were shipped to collaborators at Pacific Northwest National Laboratory for cutting, grinding, and polishing steps which require specialized rad-sample compatible equipment. Once this preparation process is completed, future work would include the EPMA analysis and mapping of elements associated with uranium on the sample surface. It is anticipated that this high resolution mapping and elemental analysis will provide valuable insight into the likely uranium phases present.

Subtask 1.1.1 Acknowledgements

Subtask 1.1.1 References

Ariza, J. G., I. Giraldez, D. Sanchez-Rodas & E. Morales (2000) Metal sequential extraction procedure optimized for heavily polluted and iron oxide rich sediments. *Analytica Chimica Acta,* 414**,** 151-164.

Chao, T. & L. Zhou (1983) Extraction techniques for selective dissolution of amorphous iron oxides from soils and sediments. *Soil Science Society of America Journal,* 47**,** 225-232.

Galán, E., J. L. Gómez-Ariza, I. González, J. C. Fernández-Caliani, E. Morales & I. Giráldez (2003) Heavy metal partitioning in river sediments severely polluted by acid mine drainage in the Iberian Pyrite Belt. *Applied Geochemistry,* 18**,** 409-421.

Iler, R. K. (1979) The chemistry of silica: solubility, polymerization, colloid and surface properties, and biochemistry. *Canada: John Wiley &Sons Inc.*

Kohler, M., G. P. Curtis, D. E. Meece & J. A. Davis (2004) Methods for Estimating Adsorbed Uranium(VI) and Distribution Coefficients of Contaminated Sediments. *Environmental Science & Technology,* 38**,** 240-247.

Lagos, L., Y. Katsenovich, R. Gudavalli, C. Cardona, R. Lapierre, P. Sepulveda, J. McGill, H. Gonzalez, V. Padilla & C. Pino. 2014. Rapid Deployment of Engineered Solutions for Environmental. Florida International University, Applied Research Center.

Smith, S. C. & J. E. Szecsody (2011) Influence of contact time on the extraction of 233uranyl spike and contaminant uranium from Hanford Site sediment. *Radiochimica Acta International journal for chemical aspects of nuclear science and technology,* 99**,** 693-704.

Szecsody, J. E., M. J. Truex, L. Zhong, N. Qafoku, M. D. Williams, J. P. McKinley, Z. Wang, J. Bargar, D. K. Faurie, C. T. Resch & J. L. Phillips. 2010. Remediation of Uranium in the Hanford Vadose Zone Using Ammonia Gas: FY 2010 Laboratory-Scale Experiments. Medium: ED; Size: PDFN.

Szecsody, J. E., M. J. Truex, M. J. Zhong, T. C. Johnson, N. P. Qafoku, M. D. Williams, W. J. Greenwood, E. L. Wallin, J. D. Bargar & D. K. Faurie (2012) Geochemical and Geophysical Changes during Ammonia Gas Treatment of Vadose Zone Sediments for Uranium Remediation. *Vadose Zone Journal***,** 1-13.

Tessier, A., P. G. Campbell & M. Bisson (1979) Sequential extraction procedure for the speciation of particulate trace metals. *Analytical chemistry,* 51**,** 844-851.

Subtask 1.2: Investigation on Microbial Meta-Autunite Interactions - Effect of Bicarbonate

Task 1.2: Introduction

Uranium is a key soil and groundwater contaminant at many U.S. Department of Energy sites, serving a leading role in the nation's defense for over 50 years. Uranium contamination of soil and groundwater is of great environmental concern due to the toxicological properties of the uranyl species. The behavior of uranium and its mobility in the subsurface is affected by various factors such as porewater and groundwater chemical composition, soil mineralogy, and microorganisms that thrive under these conditions. Uranium exists in four oxidation states but, under oxidizing conditions, it dominates as a highly soluble and stable uranyl ion, $UO2^{2+}$. In neutral or basic pH conditions, uranium undergoes hydrolysis in aqueous solutions and can readily complex with a wide variety of ligands such as carbonate, nitrate and phosphate. In a bicarbonate-rich environment, carbonate anions are an important complexing agent for U(VI), and soluble uranyl-carbonate complexes are formed, such as negatively charged $UO2(CO_3)_2^{2-}$ and $UO_2(CO_3)_3^{4-}$, as well as neutral complexes such as UO_2CO_3 (Bachmaf et al., 2008). The presence of carbonates clearly affects the dissolution of actinides and facilitates uranium desorption reactions from soil and sediments, thus increasing uranium mobility in natural waters (Langmuir, 1978). The above mentioned complexes have been identified in contaminated pore water at the Hanford Site, Washington State, and have been shown to inhibit the microbial reduction of U(VI) (Bernhard et al., 2001; Brooks et al., 2003).

The addition of tripolyphosphate amendments is one of the methods used to decrease the concentration of soluble uranium in contaminated plumes. The introduction of sodium tripolyphosphate into uranium-bearing saturated porous media results in the formation of uranyl phosphate solid phases (autunite) of general formula {X1-2[(UO$_2$)(PO$_4$)]2-1·nH$_2$O}, where X is a monovalent or divalent cation. The stability of the uranyl phosphate solids in the subsurface is a critical factor that allows for determining the long-term effectiveness of the sodium tripolyphosphate remediation strategy. The presence of soil bacteria can affect uranium mobility significantly. Bacteria, in an effort to obtain phosphorous, a vital nutrient for their metabolism, may dissolve uranyl-phosphate minerals, thus liberating uranium in the aqueous phase. In addition to the biological activity, the presence of bicarbonate ions seems to enhance the release of U(VI) into the aqueous phase (Gudavalli et al., 2013). Natural systems are complex and their behavior is dictated by the synergistic and/or antagonistic effect of both biotic and physicochemical factors.

The Columbia River, adjacent to the Hanford Site, exhibits large stage variations, causing fluctuations in the water table. These water table fluctuations and multiple rise-and-fall cycles in the river created an oxic-anoxic interface in this region. Previous assessments of Hanford sediment samples collected from this area noted a decline in cultivable aerobic bacteria and suggested the presence of facultative anaerobic bacteria (Lin et al., 2012; Marshall et al., 2008). Therefore, understanding the role of facultative and anaerobic bacteria (e.g., *Shewanella*) as one of the factors affecting the stability of autunite solids is very important for designing a successful environmental remediation strategy.

Task 1.2: Objectives

The objective of this research is to investigate autunite dissolution under anaerobic conditions by focusing on the bacterial strains of *Shewanella oneidensis* MR1 sp. There have been a few

studies on the microbial dissolution of autunite in the anaerobic conditions examining dissimilatory metal-reducing bacteria (DMRB) (*Shewanella putrefaciens* 200R) (Smeaton et al., 2008) and *Shewanella oneidensis* MR1 (Sheng & Fein, 2013; Sheng & Fein, 2014b). Previous experiments with aerobic *Arthrobacter oxydans* strains illustrated a bio-enhanced release of U(VI) from natural Ca-autunite in the presence of various concentrations of bicarbonate. *Arthrobacter* strains, G968 and G975, which exhibited various degrees of tolerance to U(VI) toxicity, were able to bio-enhance the release of U(VI) from natural Ca-autunite at almost the same capacity (Katsenovich et al., 2013). Previous research by Bencheikh-Latmani and Leckie (Bencheikh-Latmani & Leckie, 2003) and Katsenovich (Katsenovich et al., 2012) has also suggested that uranyl-carbonate complexes formed in the solution do not strongly interact with the negatively charged bacterial surface, which in turn can mitigate U(VI) toxicity on cells.

Mineral-free batch experiments that replicate the exact conditions (U, Ca and P concentrations along with three different bicarbonate concentrations) before inoculation with bacteria were conducted. The objective of this experiment was to identify the mechanism of secondary mineral formation in the presence of *Shewanella oneidensis* under anaerobic conditions. It compliments the first objective by investigating the different mechanisms that co-exist: autunuite dissolution, secondary mineral formation and potentially U(VI) bio-reduction.

Task 1.2: Materials and Methods

Bicarbonate media solution preparation

The media solution was prepared in 1 L of DIW buffered with 0.02 M Na-Hepes buffer with pH adjusted to 7.1 with 0.1 mol/L HCl or NaOH. Sodium lactate ($C_3H_5NaO_3$, 60% w/w) was added to the solution with a concentration of 0.024 mol/L. The solution was divided into three bottles and sterilized by autoclaving at 121°C, 15 psi for 15 min and cooled at room temperature. As the experiment is based on the investigation of bacteria interactions in the presence of different bicarbonate concentrations, potassium bicarbonate salt was added to the autoclaved bottles to obtain 3 mM and 10 mM bicarbonate; the remaining bottle was kept bicarbonate-free. This accounts for a total of three concentrations of bicarbonate for the experiment tested. Next, the solutions were filter-sterilized and the sterile bottles were stored in the anaerobic chamber until the beginning of the experiment.

Shewanella oneidensis MR-1 growth conditions

Shewanella oneidensis MR1 strains were obtained from the Pacific Northwest National Laboratory (PNNL) and stored at −80°C in 25% glycerol prior to use. A starter culture was grown on sterile hard and liquid Luria-Bertani (LB) media prepared with 10.0 g of tryptone, 5.0 g of yeast extract, and 10.0 g of sodium chloride, with a pH of 7.0. Hard media required an addition of 15.0 g of agar. A fresh culture was grown in 15-mL tubes placed in the incubator at 30°C while being shaken at 100 rpm (C24KC refrigerated incubator shaker; New Brunswick Scientific). Bacterial cells were grown overnight in an LB liquid medium and then harvested for the cell density (cells/mL) calculations using a glass hemocytometer (Fisher Scientific, Pittsburg, PA) or INCYTO C-Chip disposable hemocytometer (SKC America). Once the average cell count was obtained, it was multiplied by the dilution factor and the volume factor (10^4) in order to calculate the final concentration of cells per mL. The number of cells/mL in the stock suspension was used to estimate a desired volume (mL) of a bacterial suspension needed for the inoculation of each bottle. To account for viable bacteria, a well-mixed homogeneous aliquot (0.01 mL - 0.1 mL) of the suspension from each test vial was uniformly spread on the sterile

Petri dishes containing a LB growth media mixed with 15 g/L of agar. Inoculated plates were kept inverted in an incubator at 30°C. Viable microorganisms were calculated from the number of colony-forming units (CFU) found on a specific dilution.

Autunite biodissolution experiments

The autunite biodissolution experiments were performed by using 20-mL sacrificial glass scintillation vials as opposed to past experiments where sampling was periodically conducted from the same 100-mL sealed bottle containing 50 mL of sterile medium. The sacrificial vials approach was chosen to avoid microbial cross-contamination during sampling events. Each vial was filled with 18 mg of autunite powder to provide a final U(VI) concentration of 4.4 mmol/L (Figure 29), which is similar to concentrations previously used in the mixed bioreactors. All prepared glass vials with autunite were covered with plastic caps and autoclaved for 15 min at 121°C to ensure sterile conditions. Each vial was amended with 10 mL of sterile media solution containing 0, 3, and 10 mM KHCO$_3$. After autunite equilibration, the samples were inoculated with the desired volume of bacterial suspension to obtain an initial cell density of 10^6 cells/mL. In addition, abiotic control vials were kept for each bicarbonate concentration and sampled in parallel with the experimental vials. Each set, prepared using a specific bicarbonate concentration, includes duplicate sacrificial biotic vials and an abiotic control. Samples were sacrificed at specific time intervals according to the sampling schedule. In addition, to allow the media solutions to equilibrate with the autunite, three abiotic samples were prepared at each bicarbonate concentration and sampled every 5 days before bacteria inoculation. The interval of time between sampling events after the media equilibrated with the autunite and bacteria inoculation was about 4-5 days, as shown in Figure 30. The total number of sacrificial vials for the duration of the experiment was calculated as 99.

Figure 29. 20-mL glass scintillation vial prepared with media amended with KHCO$_3$ and autunite mineral.

Figure 30. Sampling schedule before and after inoculation.

Experimental vials and bottles with the media solutions amended with bicarbonate were kept in an anaerobic chamber for the entire duration of the experiment (Figure 31).

Figure 31. Sacrificial vials inside the anaerobic glove box filled with nitrogen gas, prepared to conduct the autunite biodissolution experiment.

Mineral-free experiments

Mineral-free experiments were performed by using 20-mL sacrificial glass vials that contained 200 ppb, 400 ppb and 1.5 ppm of U(VI) for bicarbonate-free samples as well as samples amended with 3 and 10 mM of bicarbonate. The samples were spiked with the appropriate amount from a uranyl-acetate stock solution ($UO_2(CH_3COO)_2 \cdot 2H_2O$, Electron Microscopy Sciences). The initial concentration of Ca and P was kept constant across the samples, 40 ppm and 500 ppm, respectively. Sodium lactate ($C_3H_5NaO_3$, 60% w/w) was added to the solution with a concentration of 0.024 mol/L. All prepared glass vials were autoclaved and were inoculated with the desired volume of bacterial suspension to obtain an initial cell density of 10^6 cells/mL. For each bicarbonate concentration, abiotic controls were created (containing all elements and no bacteria) and controls containing only uranium in DI water were prepared as a reference of initial uranium concentration. Each vial was sacrificed at specific time intervals for a period of 45 days and the interval of time between sampling events was about 4-5 days.

Protein analysis

For cell protein determination, a BCA (Pierce) protein analysis kit was used. For the preliminary assessment, a calibration curve was built using albumin as a standard solution and the absorbance was measured at 562 nm spectrophotometrically. The BCA protein assay is based on the highly selective colorimetric detection of the cuprous cation (Cu^+) by bicinchoninic acid (BCA) as a result of the reduction of Cu^{2+} to Cu^+ by protein in an alkaline medium. A fresh culture of facultative anaerobic bacteria *Shewanella oneidensis* MR1 was grown in two 15-mL tubes filled with LB liquid media to determine the relationship between the protein content and cell density. The tubes were placed in the incubator for two days at 30°C. After two days, the tubes were centrifuged and the pellet was washed with deionized water and re-suspended in 1.5 mL of DIW. The washing procedures were repeated twice. After washing, the cells were counted via hemocytometer and 1.2 mL from each vial was extracted into the 1.5-mL microcentrifuge tubes to be used for the bicinchoninic acid protein assay. The stock cell density concentrations in vial #1 and vial #2 were calculated as 884,210,526 cells/mL and 877,419,355 cells/mL, respectively. Following the protocol procedures, the cells were lysed by boiling at 100°C for 10 min and then cooled on ice. The addition of an alkaline medium followed and the samples were placed in a water bath (60°C) for 30 minutes. Several aliquots were taken from the stock cell solutions and a calibration curve was prepared by using albumin as a standard for the protein

content and the absorbance was measured at 562 nm spectrophotometrically. Testing of this protocol yielded a detection limit of $10^{5.9}$ cell/mL.

Sampling and elemental analysis

Prior to any further manipulation, the pH of the samples was recorded. Then, 1-mL aliquots were isolated from each vial and stored in the laboratory refrigerator for further uranium analysis by the kinetic phosphorescence analysis (KPA-11, Chemchek Instruments Inc.) instrument. The presence of organic content in the solutions can interfere with KPA measurements; hence, samples collected during the experiments were pre-processed by wet ashing followed by dry ashing procedures. A modified ashing technique described by Ejnik (Ejnik et al., 2000) was used for wet and dry ashing. Wet digestion was performed by the addition of 500 μL of concentrated nitric acid (HNO_3) and 500 μL of concentrated hydrogen peroxide (H_2O_2) to each vial; the vials were placed on a heating plate until full evaporation was achieved and a white solid residue was acquired. Occasionally, some samples turned yellow while ashing; 0.5 mL of peroxide was added to these samples and the process was continued until a white precipitate was obtained. The dry samples were placed in a furnace preheated to 450°C for 15 min and then allowed to cool at room temperature. Finally, precipitates obtained in the drying step were dissolved in 1 mL of 2 mol/L nitric acid and analyzed by means of the KPA instrument to determine uranium concentrations released into the aqueous phase as a function of time. In addition, calcium and phosphorous were determined by means of inductively coupled plasma - optical emission spectroscopy (ICP-OES 7300 Optima, Perkin Elmer) using calcium and phosphorous standards (Spex CertiPrep). ANOVA statistics were used to examine the results on the release of U(VI) due to varying concentrations of bicarbonate ions. The significance level was set at $\alpha = 0.05$. The results from elemental analysis were used in speciation modeling calculations by means of Visual Minteq and Hydra speciation software.

SEM-EDS analysis

The autunite samples, after isolation of aliquots for chemical analysis and protein analysis, were prepared for SEM-EDS analysis. Cells attached on autunite were first treated with 4 ml of 2% glutaraldehyde in 0.1 M HEPES at 4°C for 2h. Samples were then centrifuged, supernatant was decanted and the material was washed with 4 ml of 0.05 M HEPES for 10 min. After discarding the supernatant, the material was "dehydrated" in 4 consecutive steps: treatment with 35%, 70%, 90% and 100% of ethanol for 10 min at room temperature. Finally, a small quantity of hexamethyldisilazane (HMDS) (Pierce Biotechnology, Inc, obtained from Fisher Scientific) was introduced two times and the material was left to air-dry at room temperature for 10 min before being stored in a desiccator until SEM-EDS analysis (Braet et al., 1997; Hazrin-Chong & Manefield, 2012).

Task 1.2: Results and Discussion

Elemental analysis

Figure 32, Figure 33, and Figure 34 present concentrations of uranium measured by means of KPA in bicarbonate-free samples and samples amended with 3 mM and 10 mM of bicarbonate, respectively.
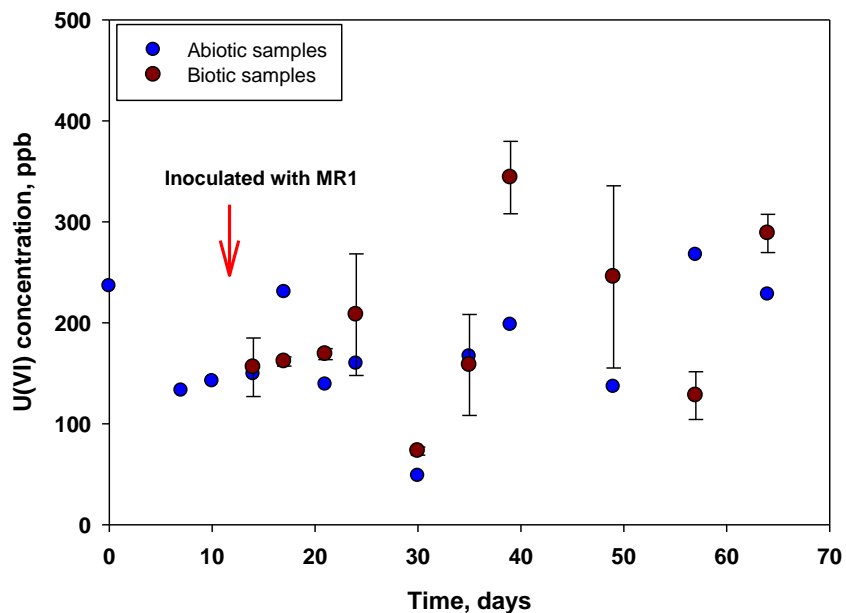
Figure 32. Uranium concentration as a function of time for bicarbonate-free samples.

In the case of bicarbonate-free samples, the amount of uranium released in the aqueous phase didn't show any statistically significant difference between abiotic and biotic samples (confidence level 95%, p=0.468), denoting that the presence of *Shewanella oneidensis* does not contribute to the release of uranium in the aqueous phase (Figure 32). It seems that the release of U(VI) in the aqueous phase is the outcome of the autunite mineral dissolution by the aqueous phase. Furthermore, no decrease in uranium was observed in the biotic samples after inoculation with *Shewanella oneidensis* (day 10), a fact that implies that there is no bioreduction of U(VI) to U(IV). On the other hand, in the samples amended with 3 and 10 mM bicarbonate, the inoculation with bacteria cells incurs a sharp increase in uranium concentration in the aqueous phase, most probably due to bacterial activity of dissolving autunite in order to obtain the metabolically necessary phosphorous. The steady state maximum concentrations of U(VI) detected were 3-6 fold higher compared to the corresponding bicarbonate-bearing abiotic controls at steady state. However, despite anaerobic conditions, no bioreduction of uranium was observed in the bicarbonate-amended samples and the concentration of uranium in the media solutions remained stable throughout the experiment (63 days) (Figure 33, Figure 34).
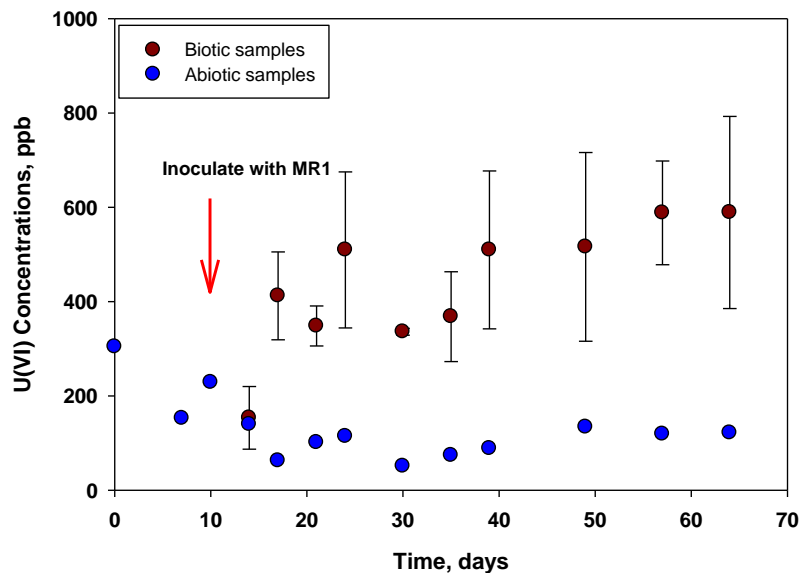
Figure 33. Uranium concentration as a function of time for samples amended with 3 mM bicarbonate.
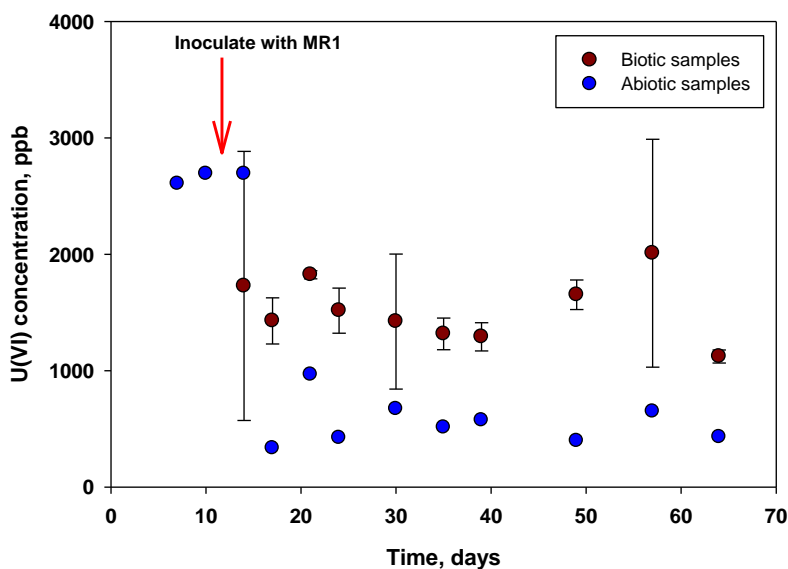
Figure 34. Uranium concentration as a function of time for samples amended with 10 mM bicarbonate.

Despite the fact that no bioreduction of U(VI) was observed in any of the conditions studied, the degree of uranium release among the different conditions in the presence of *Shewanella oneidensis* differed significantly (Figure 35). There was a progressive increase in uranium release as the concentration of bicarbonate in the sample increased ($p=0.001$ among all groups for confidence intervals 95%).
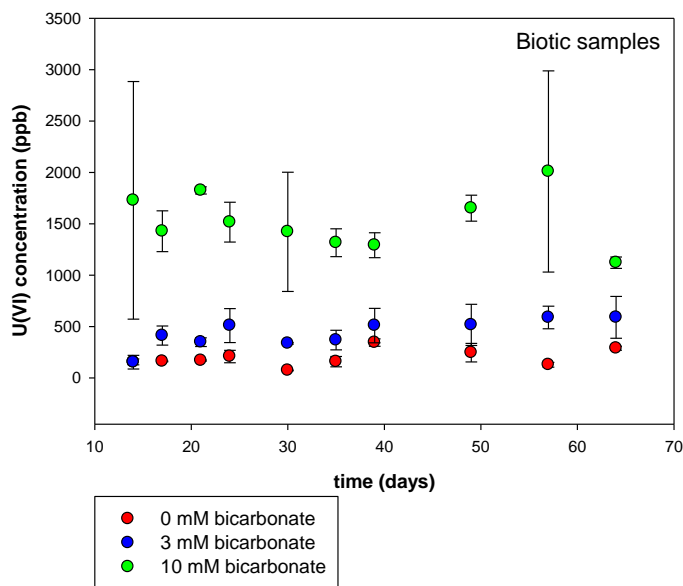
Figure 35. Uranium concentration in the aqueous phase in the presence of *Shewanella oneidensis* as a function of time, for three different bicarbonate conditions.

The dissolution of autunite also resulted in the release of calcium and phosphorous in the aqueous phase. The results for calcium analysis are presented in Figure 36- Figure 38.
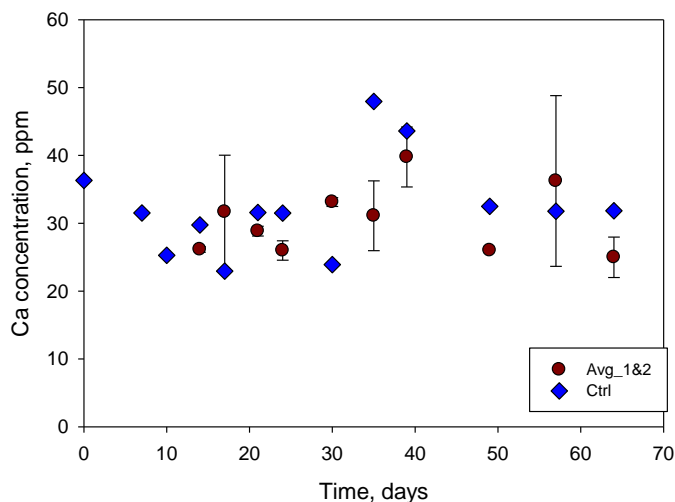
Figure 36. Calcium concentration as a function of time for bicarbonate-free samples. Red points represent biotic samples while blue points represent abiotic samples.
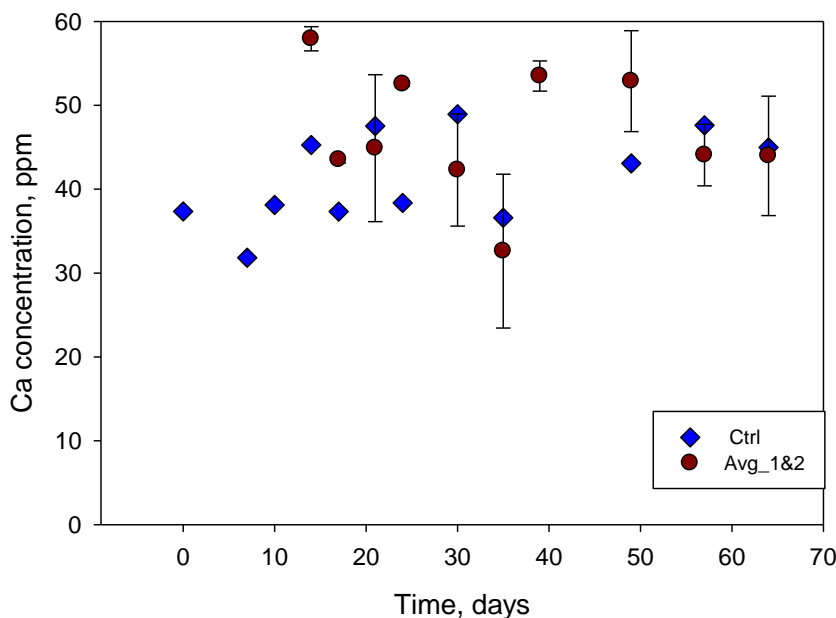
Figure 37. Calcium concentration as a function of time for samples amended with 3 mM bicarbonate. Red points represent biotic samples while blue points represent abiotic samples.
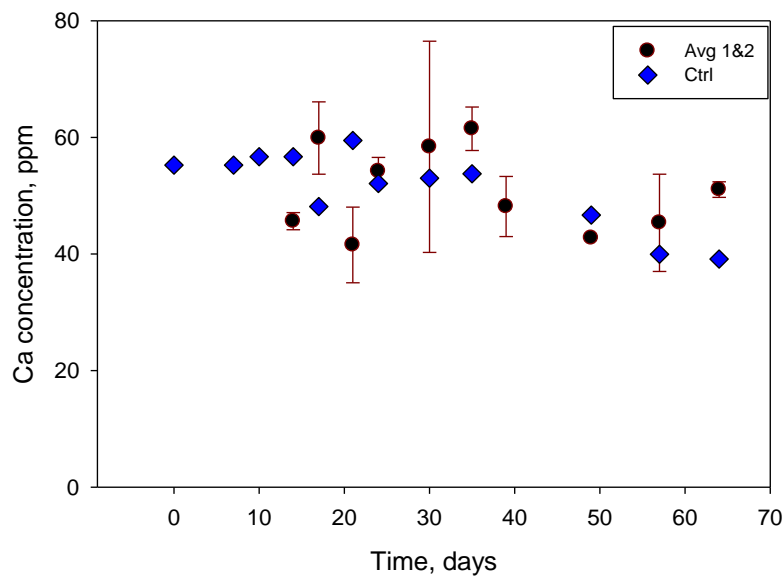
Figure 38. Calcium concentration as a function of time for samples amended with 10 mM bicarbonate. Red points represent biotic samples while blue points represent abiotic samples.

In bicarbonate-free samples, results revealed a similar trend between biotic and abiotic samples. Statistical evaluation suggested that there is not a significant difference between abiotic and biotic samples (p=0.476). A similar trend was observed in the samples amended with 3 mM bicarbonate (p=0.965) and with 10 mM bicarbonate (p=0.867, confidence interval 95%). In accordance with uranium results, higher concentrations of bicarbonate ions in the media solutions resulted in higher calcium release in the aqueous phase. Despite the high variability of

phosphorous concentrations between biotic duplicates, the results were similar to that tested for calcium; there was no significant difference between biotic and abiotic samples in all three categories (p=0.784, p= 0.793 and p=0.644 when comparing biotic and abiotic samples for bicarbonate-free, 3 mM and 10 mM amended samples, respectively, confidence interval 95%).
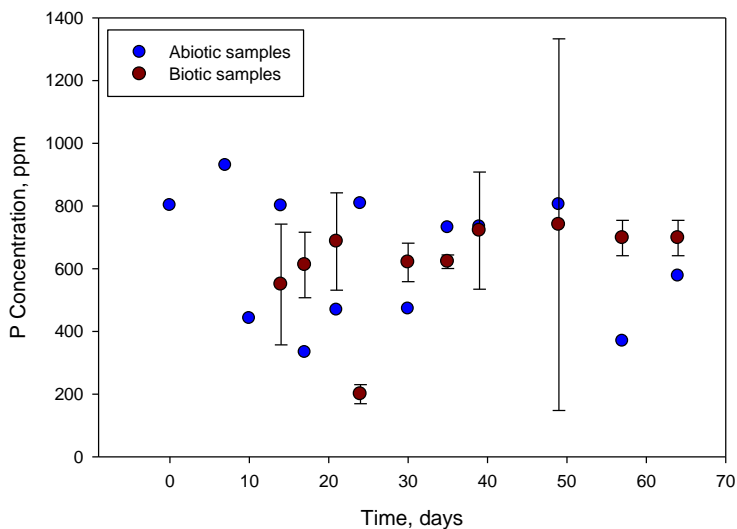
Figure 39. Phosphorous concentration as a function of time for bicarbonate-free samples. Red points represent biotic samples while blue points represent abiotic samples.
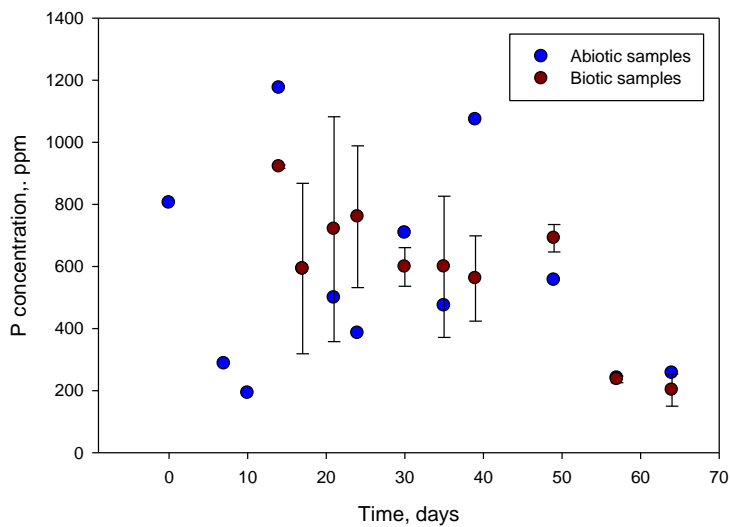
Figure 40. Phosphorous concentration as a function of time for samples amended with 3 mM bicarbonate. Red points represent biotic samples while blue points represent abiotic samples.
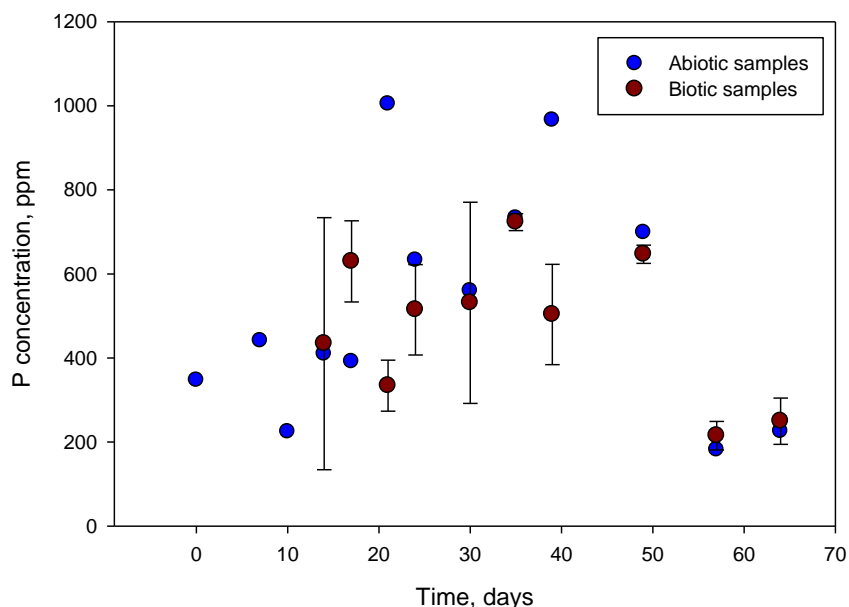
Figure 41. Phosphorous concentration as a function of time for samples amended with 10 mM bicarbonate. Red points represent biotic samples while blue points represent abiotic samples.

Cell density and cell viability per plates

Direct visual cell counting using a hemocytometer combined with a cell viability analysis using the spread plate method was conducted for each sampling event. The initial inoculation cell density was 10^6 cells/mL (log 6 cells/mL) for all biotic samples. In bicarbonate-free samples, cell densities for the duration of the experiment showed almost no change from the initial concentration (Figure 14). In contrast, samples amended with 3 mM and 10 mM of bicarbonate demonstrated almost 10-14 fold increases in cell density and values stabilized in the range of log 6.9- log 7.3 cell/mL by the end of experiment (Figure 42).

Cell viability, determined via counts of colony forming units (CFU/mL), was compared to the cell density obtained via direct cell counting. Samples containing 0 mM bicarbonate yielded on average about 11.1% of viable cells out of a total cell density that correlates to only $1.1^5 \pm 1.0^5$ CFU/mL. In addition, viable cells showed a tendency to decrease with time. In samples amended with 3 mM and 10 mM of HCO_3, the ratio between viable cells and total cell density increased to 30-31%. Since the cell density in bicarbonate-amended solutions increased in average to 1.0^7-1.4^7 cells/mL, the quantity of viable cells was determined to be on the order of 2.2^6-2.3^6 CFU/mL, which is significantly higher than was observed in the bicarbonate-free solutions. The increase in total cell density and the quantity of viable cells might be an indication that the cells have acclimated to withstand uranium toxicity in the presence of bicarbonate ions. Figure 43 presents results for the total cell density versus viable cells for the three bicarbonate concentrations tested.
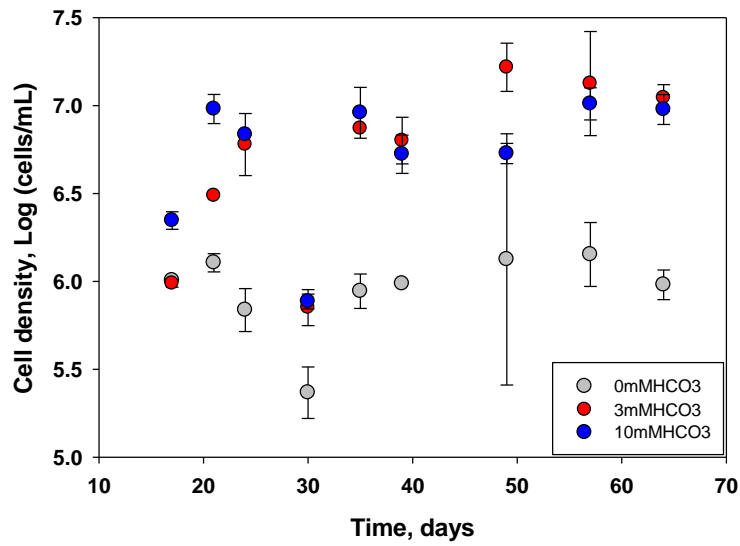
Figure 42. Changes in the direct cell counts for samples containing varying concentrations of bicarbonate.
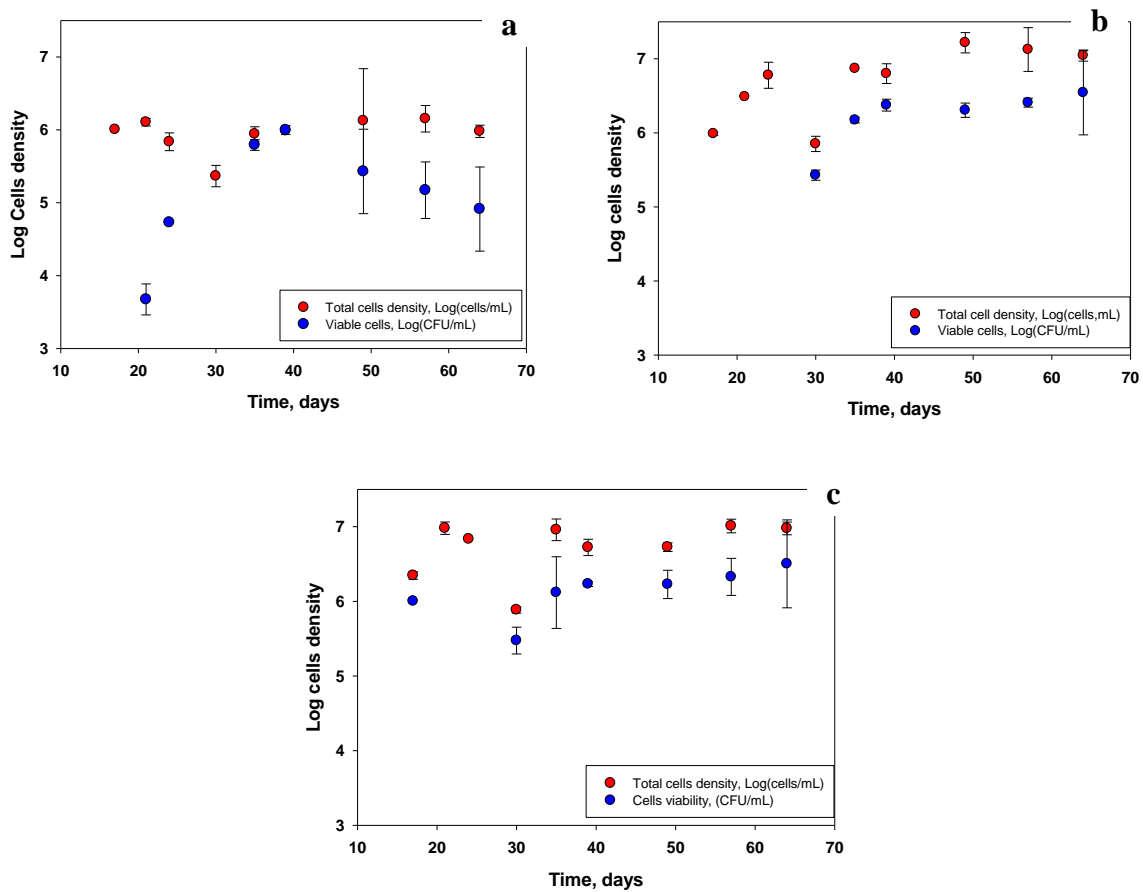
Figure 43. Results for the total cell density versus viable cells for a) 0 mM HCO₃; b) 3 mM HCO₃; c) 10 mM HCO₃.

pH monitoring and protein analysis

pH monitoring was conducted for every sampling event. For all the samples, bicarbonate-free and the ones amended with 3 and 10 mM bicarbonate, an increase in pH (0.7 pH units) was observed at day 21. However, there was no similar trend observed for the control abiotic samples, where pH remained practically unchanged until the end of the experiment (Figure 44). Facultative anaerobic bacteria in the presence of a terminal electron donor (O_2) can convert sugars to CO_2 through respiration (Lin et al., 2005), whereas in the absence of a terminal electron donor, sugars can be converted into organic molecules through fermentation reactions (Sánchez et al., 2005). In the case of *Shewanella oneidensis* MR-1, the bacteria under aerobic conditions have been reported in literature to produce no other by products than CO_2 (Pinchuk et al., 2011), which when dissolved in water forms carbonic acid, hence decreasing the pH. On the other hand, *Shewanella oneidensis* has been reported to metabolically excrete acetate and formate when grown on lactate as a sole carbon source under anaerobic conditions and the production of CO_2 was very limited (Claessens et al., 2006; Meshulam-Simon et al., 2007; Pinchuk et al., 2011; Tang et al., 2006). Assuming that the release of CO_2 is the determining factor for pH fluctuation, the limited release of CO_2 scenario may be a possible explanation for the experimental results presented in Figure 44.
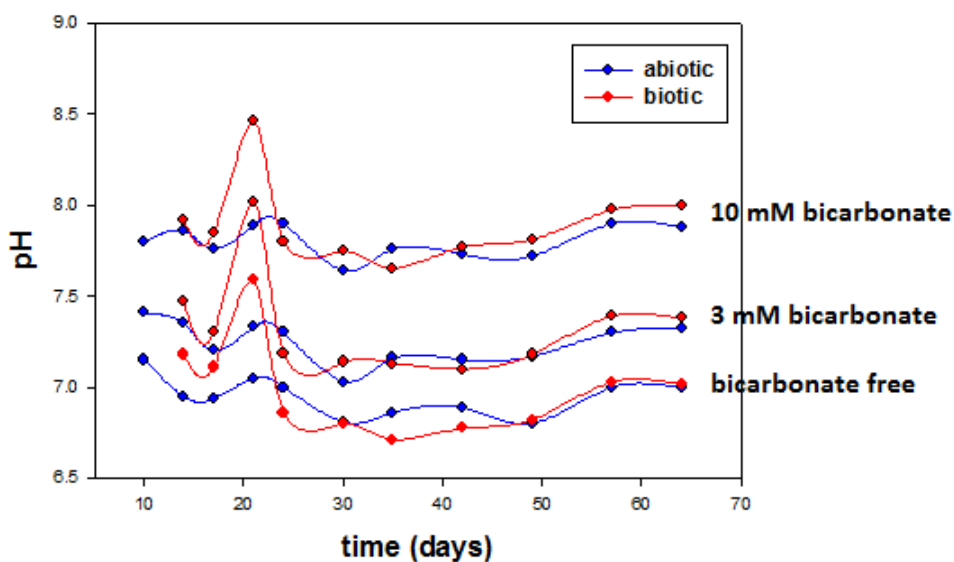
Figure 44. pH of autunite suspensions as a function of time. Red lines represent biotic samples and blue lines abiotic samples.

Interestingly, the protein analysis revealed a very similar trend with a sharp increase of protein content at day 21, and the increase was more profound in the samples amended with 3 and 10 mM bicarbonate (Figure 45). A correlation between cell density of fresh *Shewanella oneidensis* suspensions and protein content fits to a linear regression (Figure 46). Based on the estimated regression function, the experimentally determined protein content was converted to the cell density for all bicarbonate concentrations tested (Figure 47). The correlation coefficient between the protein content and the calculated amount of cells present in the medium suggested an increase in cell growth at day 21. Cells cultivated in media amended with 10 mM HCO_3 demonstrated almost 3 times higher density than that in bicarbonate-free solutions. This vigorous cell growth demonstrated through a sharp increase in protein concentration in the medium

coincided with the pH increase. In the case of bicarbonate-free samples, the cell density reached $10^{7.5}$ from 10^6 cells/ml, whereas in the case of samples amended with 3 mM and 10 mM bicarbonate, the change in cell density was much greater, from 10^6 cells/ml to 10^{10} cells/mL.
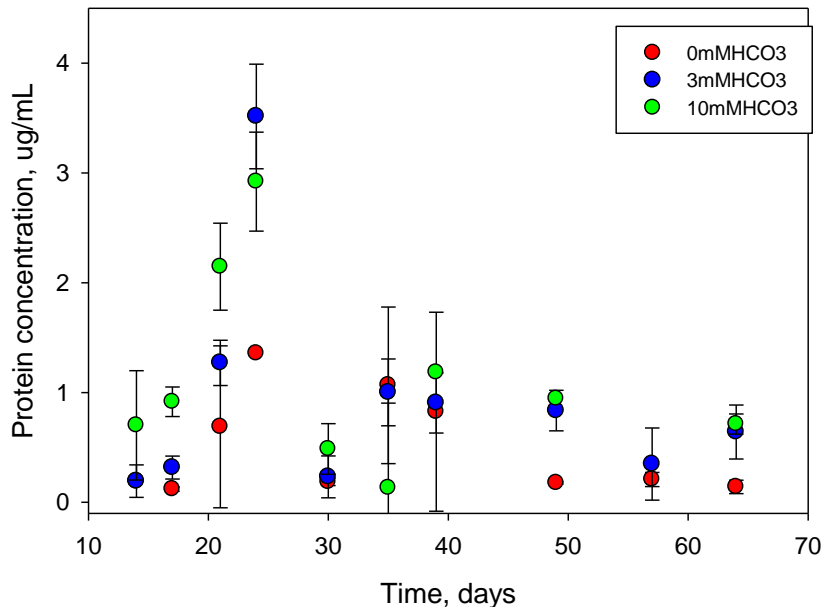
Figure 45. Protein concentration as a function of time for *Shewanella oneidensis* grown under anaerobic conditions.
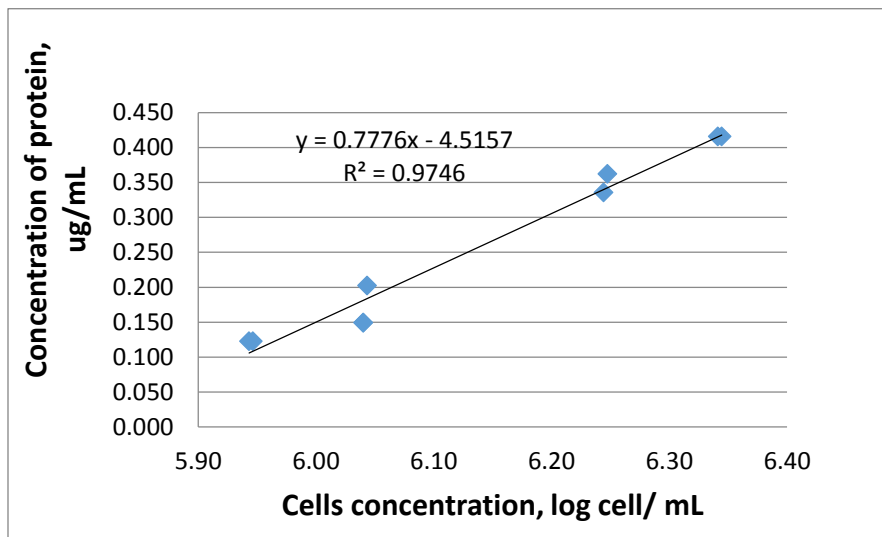
Figure 46. Correlation between cell density of *Shewanella oneidensis* MR1 and protein content.
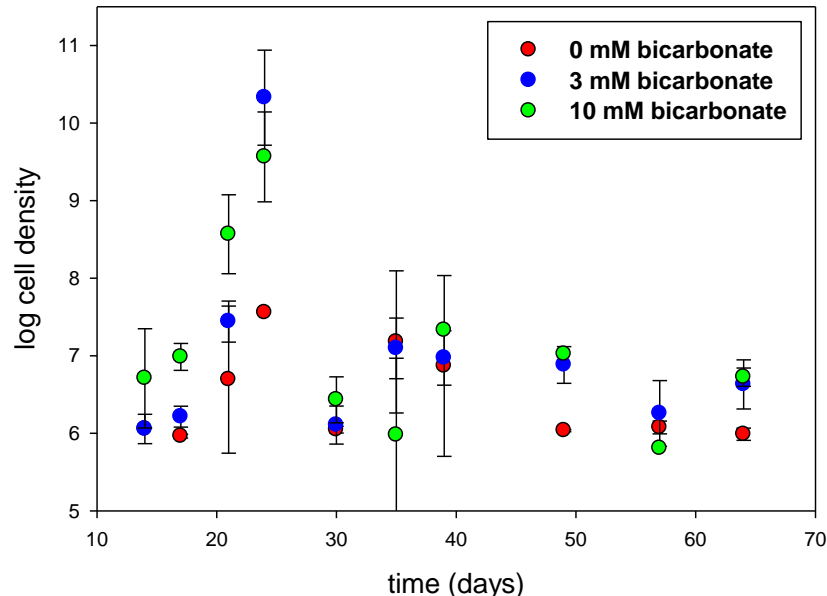
Figure 47. The variation of cell density (logarithmic scale) as function of time.

The theoretically calculated cell density values presented in Figure 47 correspond to the total cell density, which is a sum of both viable and non-viable cells. The nature of the protein determination protocol does not allow estimating the amount of viable and non-viable cells. Overall, the theoretically calculated total cell density looks overestimated compared to the direct visual cell density counting. This might be due to the fact that Figure 47 calculations were based on *Shewanella oneidensis* cells grown in the bacteria culture medium. There is a possibility that exposure to uranium affected the cell physiology and protein content, which might have resulted in changes of protein masses (Khemiri et al., 2014). So, the correlation between cell density and protein content obtained for the control cells grown in culture media might not be valid for cells exposed to uranium. Further experiments on uranium-bacteria interactions conducted without autunite solids will help to investigate changes in protein content as a result of uranium exposure.

SEM-EDS analysis and speciation studies

Images of autunite solids taken by means of SEM revealed the destruction of autunite as a consequence of bicarbonate effect and bacterial activity (Figure 48). In the bicarbonate-free samples, no bacteria were observed on the autunite surface. This finding may explain the fact that there was not any uranium release in the aqueous phase due to bacterial activity in the bicarbonate-free samples (Figure 38). On the other hand, bacteria were clearly observed on the mineral's surface in the case of samples amended with 3 mM and 10 mM bicarbonate (Figure 49). Bacteria can attach on the mineral surfaces through specific structures called extracellular polymeric substances (EPS), comprised mostly of saccharides and proteins and secondarily DNA and lipids (Donlan, 2002). Nevertheless, no extensive (covering most of the surface or creating vertical multilayer formations) biofilm was observed in these samples. The formation of an extensive film has been reported to be crucial for metal reduction by *Shewanella* and is regulated by the presence of oxygen (McLean et al., 2008; Wu et al., 2013). FIU's experiments were

performed in the absence of oxygen, hence the absence of an extensive biofilm, as well as bioreduction, may be justifiable.
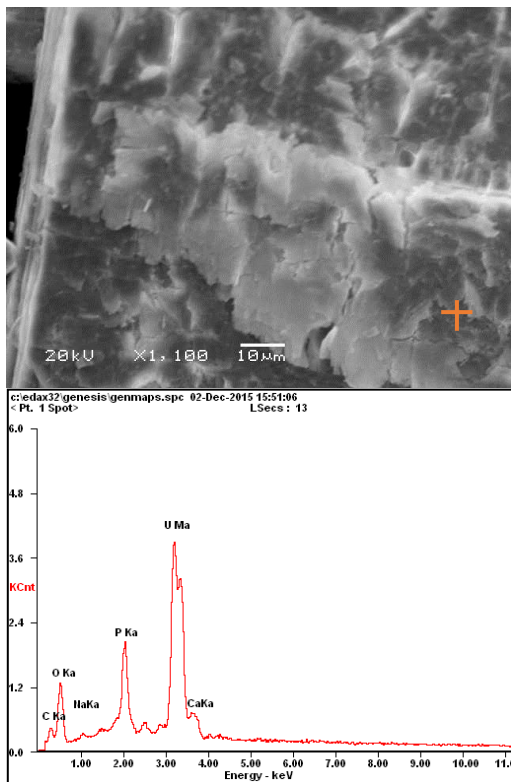
Element	Wt%	At%
CK	01.43	07.80
OK	14.19	57.90
NaK	00.55	01.57
PK	04.28	09.03
CaK	01.39	02.26
UL	78.15	21.44
Matrix	Correction	ZAF

Figure 48. SEM image revealing structural damage of autunite and associated elemental composition by EDS analysis.
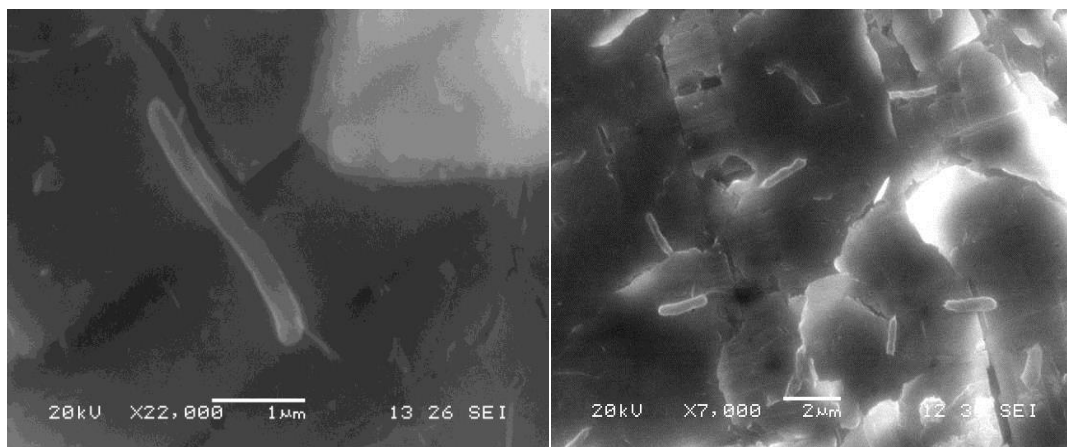
Figure 49. Bacterial activity on the surface of autunite.

A study by Thormann investigated the biofilm formation by *Shewanella* and reported the formation of a layer of biofilm initially with the coverage of the surface and, consequently, the formation of vertical towering biofilm structures (Thormann et al., 2004). Furthermore, acetate and lactate have been reported to be less effective stimulants for U(VI) reduction, whereas more complex organic electron donors have been directly correlated to the ability of DMRB to reduce U(VI) (Barlett, 2014). The SEM photos also revealed the formation of secondary minerals, mainly uranyl phosphates and uranyl carbonates, coating the surface of autunite (

Figure 50). These secondary minerals are a result of saturation of the aqueous phase due to the release uranium, calcium and phosphorous under the conditions studied.
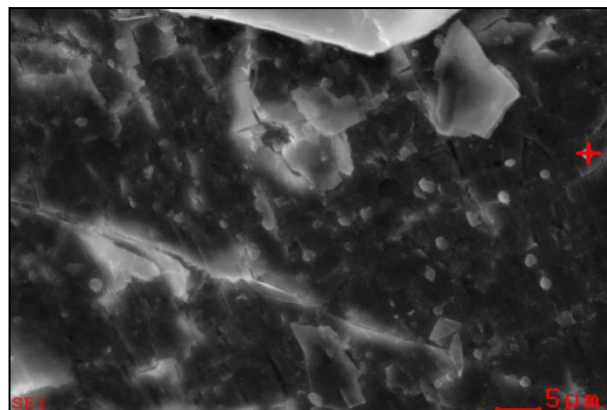
Figure 50. Secondary mineral particles coating on the surface of autunite and EDS analysis.

Element	Wt%	At%
CK	06.22	14.63
NK	09.87	19.91
OK	28.16	49.76
NaK	00.65	00.80
PK	05.92	05.40
UM	42.96	05.10
CaK	06.23	04.39

The formation of the secondary minerals was predicted by the calculations performed by means of speciation software (Visual Minteq and Hydra). The soluble species were also predicted by the speciation software under the experimental conditions; the results are presented in Table 11. As can be seen, the saturation of hydroxylapatite (calcium phosphate mineral) and uranyl-phopshate minerals is predicted in all cases. Nevertheless, the elemental analysis results did not reveal a decrease in any of these elements throughout the duration of the experiment; on the contrary, uranium, calcium and phosphorous seem to be unaffected. A decrease in the concentration of those elements could be associated with the formation of secondary minerals (and bioreduction, only in the case of uranium). A possible explanation could be that the rate of release of those elements in the aqueous phase is very similar to the rate of micro-precipitation of secondary minerals, which removes these elements from the aqueous phase; hence, the apparent concentration of those elements remains the same.

Table 11. Soluble and Saturated Species for All Three Conditions Studied (bicarbonate-free samples and samples amended with 3 and 10 mM bicarbonate)

0 mM bicarbonate		3 mM bicarbonate		10 mM bicarbonate	
Soluble	**Precipitates**	**Soluble**	**Precipitates**	**Soluble**	**Precipitates**
20% UO_2HPO_4	Hydroxylapatite	50% $Ca_2UO_2(CO_3)_3$	Hydroxylapatite	92% $UO_2(CO_3)_3^{-4}$	Hydroxylapatite
80% $UO_2PO_4^-$	Uranyl-phosphate	44% $CaUO_2(CO_3)_3^{-2}$	Uranyl-phosphate	6% $CaUO_2(CO_3)_3^{-2}$	Uranyl-phosphate
	autunite	~6% negatively charged uranyl carbonates	autunite		autunite

On the other hand, the soluble species are primarily negatively charged entities in the case of bicarbonate-free samples and samples that contain 10 mM of bicarbonate; whereas in the case of

samples amended with 3 mM of bicarbonate, the negatively charged and the neutral U(VI) complexes are almost 50-50%. It has been suggested in literature that negatively charged uranyl complexes are less bioavailable to the cells and the least readily reducible fraction, mostly due to electrostatic repulsions between negatively charged uranyl complexes and the bacterial cell surface (Belli et al., 2015; Sheng & Fein, 2014). This scenario provides an additional potential explanation for the absence of bioreduction, especially in the case of bicarbonate-free samples and samples amended with 10 mM of bicarbonate, where the majority of uranyl complexes are negatively charged. On the other hand, the point of zero charge (pzc) of aututnite is 5-6 (Wellman et al., 2007), which makes the net surface charge of aututnite at pH 7.5 negative. Hence, one would expect electrostatic repulsion between negatively charged bacterial surfaces and the autunite surface. Bacteria were detected on the surface of autunite in the samples amended with 3 and 10 mM bicarbonate, implying that under phosphorus-limiting conditions, bacteria may overcome the electrostatic repulsion and liberate P from uranyl mineral phases to meet metabolic needs. It is not clear though to what degree this takes place, since the amount of bacteria detected on the surface was not very high. Although uranyl phosphates are considered to be sinks of uranium and therefore strong candidates for remediation strategies (Beazley et al., 2007), the experimental findings demonstrate their liability in the presence of bacteria.

Mineral-free experiments

pH monitoring & Elemental Analysis

The fluctuation of pH as a function time is presented at Figure 23. pH levels for each category of samples (bicarbonate free and 3mM and 10mM amended samples) remain stable throughout the experiment; no significant change is observed due to the presence of bacteria or other chemical reactions taking place.
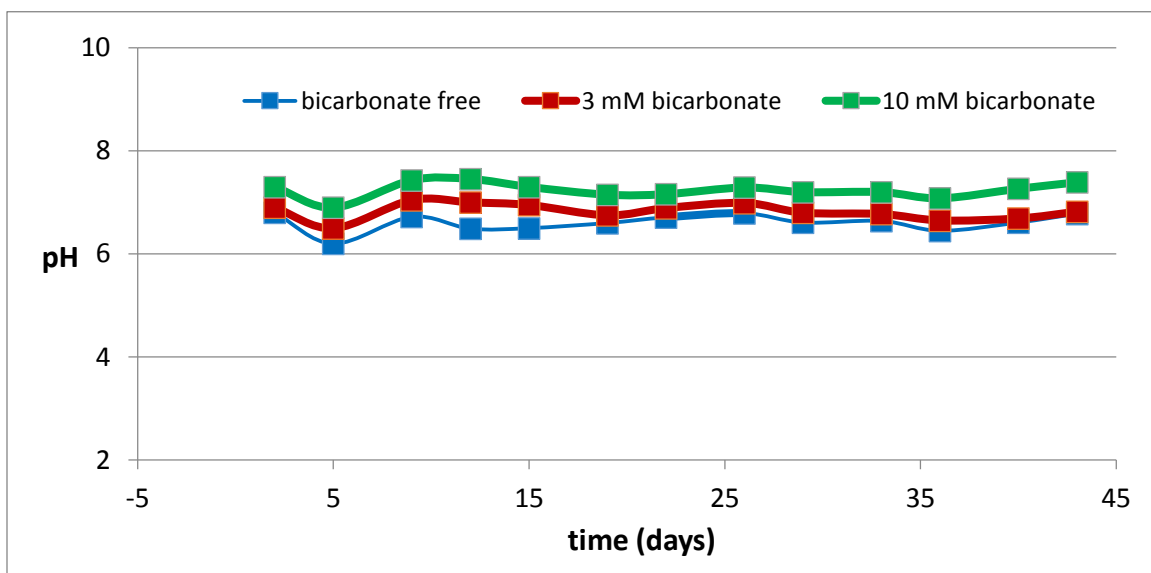
Figure 51. pH as a function of time for biotic, mineral free samples (bicarbonate free and 3 mM and 10 mM bicarbonate amended samples).

The experimental results of the mineral free experiments are presented in Figure 52-Figure 55. The concentrations of Ca, P and U in the aqueous phase as a function of time were recorded.
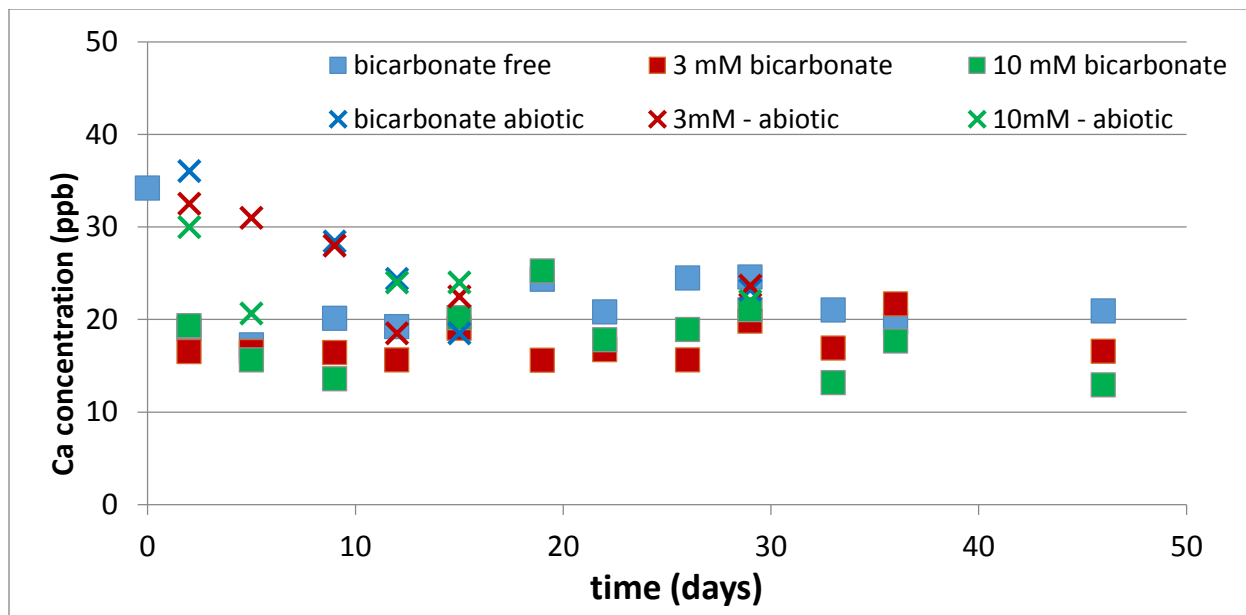
Figure 52. Concentration of Ca in the aqueous phase as a function of time for bicarbonate free, as well as samples amended with 3 and 10 mM bicarbonates (biotic and abiotic).
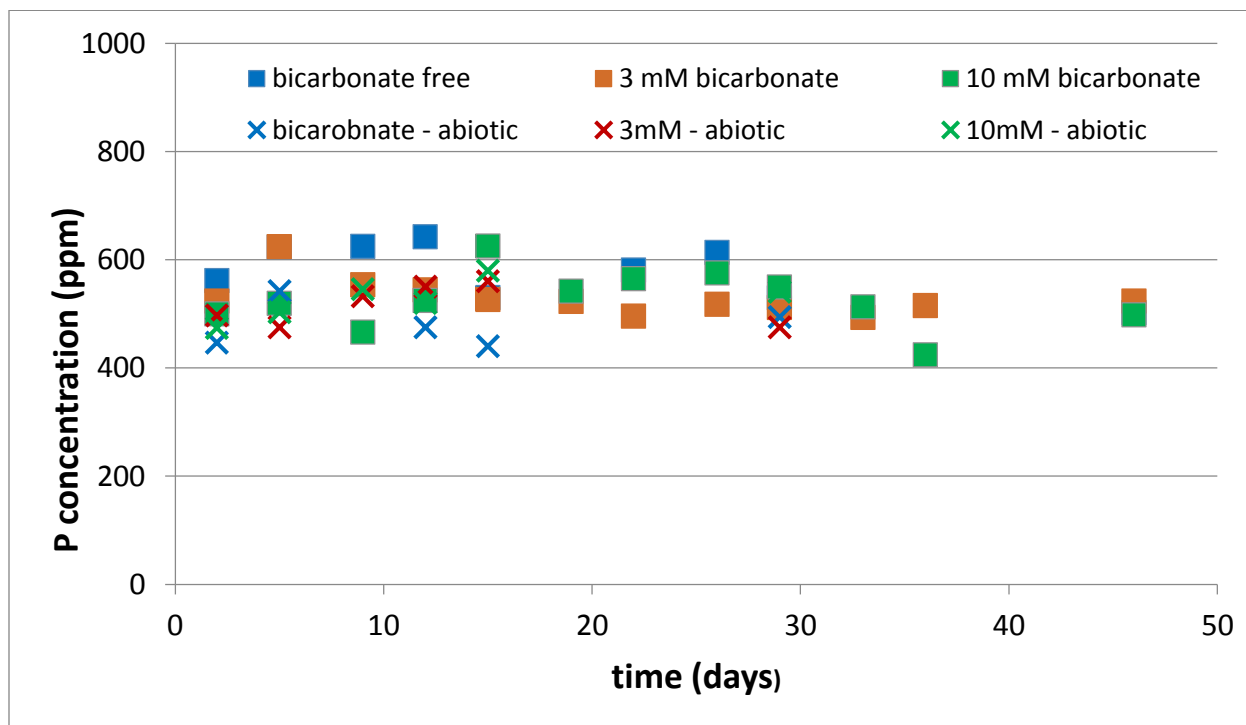
Figure 53. Concentration of P in the aqueous phase as a function of time for bicarbonate free, as well as samples amended with 3 and 10 mM bicarbonates.
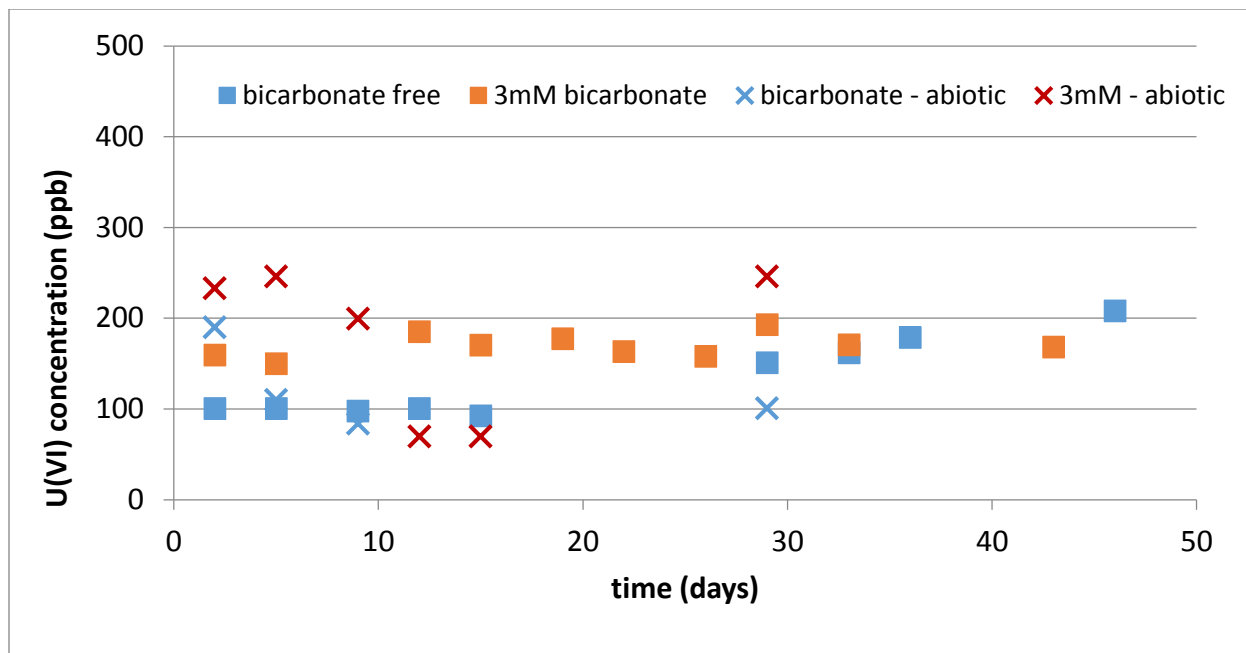
Figure 54. Concentration of U(VI) in the aqueous phase as a function of time for bicarbonate free, as well as samples amended with 3 mM bicarbonates.
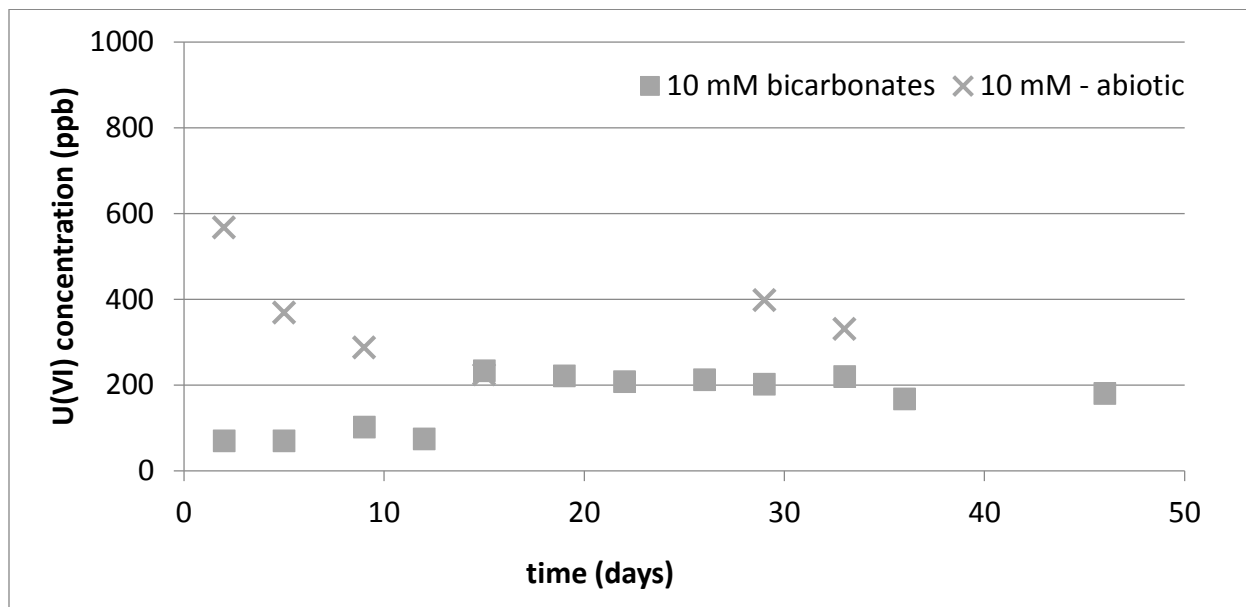
Figure 55. Concentration of U(VI) in the aqueous phase as a function of time for samples amended with 10 mM bicarbonates.

For all samples, the levels of phosphorous in the aqueous phase remained stable and very close to the initial phosphorus concentration (551±26 ppm), denoting that phosphorous may have limited participation in the formation of secondary minerals. Furthermore, the bacterial population does not seem to be using significant amounts of phosphorus for its metabolic needs, despite the fact that phosphates have been cited in literature as a source of phosphorus for *Shewanella oneidensis* (Pinchuk et al., 2008; Pinchuk et al., 2010). The average concentrations of phosphorous in the aqueous phase were found to be 568±48 ppm, 529±33 ppm and 524±40

ppm for bicarbonate-free samples and samples amended with 3 mM and 10 mM, respectively. On the other hand, calcium levels may be similar for all cases (21 ± 2 ppm for bicarbonate-free samples and 18 ± 2 ppm and 18 ± 4 ppm for samples amended with 3 mM and 10 mM bicarbonates, respectively), but the concentration is significantly lower than the initial concentration introduced in the sample (31 ± 3 ppm). This is an indication of calcium participating in secondary mineral formation and, consequently, removal from the aqueous phase. In the case of uranium, there seems to be some fluctuation in U(VI) concentration, especially in the case of bicarbonate-free samples and in the samples amended with 10 mM bicarbonate throughout the period the experiment lasted (Figure 54, Figure 55). Nevertheless, for bicarbonate-free samples, U(VI) concentration between biotic and abiotic (control) samples were at similar levels: the average U(VI) concentrations were determined to be 117 ± 31 ppb and 123 ± 57 ppb, respectively. Hence, it seems that in the case of bicarbonate-free samples, any uranium removal (the final concentrations are very close to the initial concentration of 220 ± 30 ppb) may be due mostly to chemical reactions (e.g. uranium co-precipitation with calcite) and not to bio-reduction. The absence (or very limited bio-reduction) in the case of bicarbonate-free samples is in accordance with literature where it is mentioned that negatively charged uranyl complexes are less bioavailable to the cells and the least readily reducible fraction. In the case of samples amended with 3 and 10 mM bicarbonate, the final uranium concentration was found to be 170 ± 13 ppb and 163 ± 62 ppb, respectively, which are significantly lower than the initial uranium concentrations introduced in the samples (341 ± 38 ppm and 704 ± 28 for 3 and 10 mM bicarbonate amendment, respectively). The corresponding values for abiotic samples are 180 ± 78 ppb and 406 ± 158 ppb for samples amended with 3 and 10 mM bicarbonates. Hence, in the case of samples amended with 3 mM bicarbonate, chemical reactions seem to dominate the phenomenon, whereas in the case of samples amended with 10 mM bicarbonate, despite the larger standard deviation, the average value between biotic and abiotic samples is statistically different ($p<0.0001$ for confidence levels 95%). In conclusion, it seems that in the cases of bicarbonate-free samples and samples amended with 3 mM bicarbonate, mineral dissolution is the driving force of the phenomenon. On the other hand, in the case of samples that contain 10 mM bicarobnate, bio-reduction may be contributing to the decrease of uranium from the aqueous phase. In other words, all three mechanisms (mineral dissolution, secondary mineral formation and bio-reduction) seem to be part of the process in the presence of 10 mM bicarbonate. This is more obvious in the beginning of the process (days 2-10) where the concentration of uranium in the aqueous phase in abiotic samples is quite higher that in the equivalent samples that contain bacteria. Hence, the hypothesis that in experiments that contain minerals, different mechanisms (mineral dissolution releasing calcium, uranium and phosphorous into the aqueous phase while secondary mineral formation and bio-reduction remove those elements from the aqueous phase) seem to contribute to the apparent equilibrium in elemental concentration may be true depending on the bicarbonate concentration.

Cell counting

Collected samples were evaluated for the cell density via direct count using hemocytometer and cell viability analysis using the spread plate method. The initial inoculation cells density for biotic samples was 10^6 cells/mL (log 6 cells/mL), a similar concentration to the experiment with autunite amended samples.
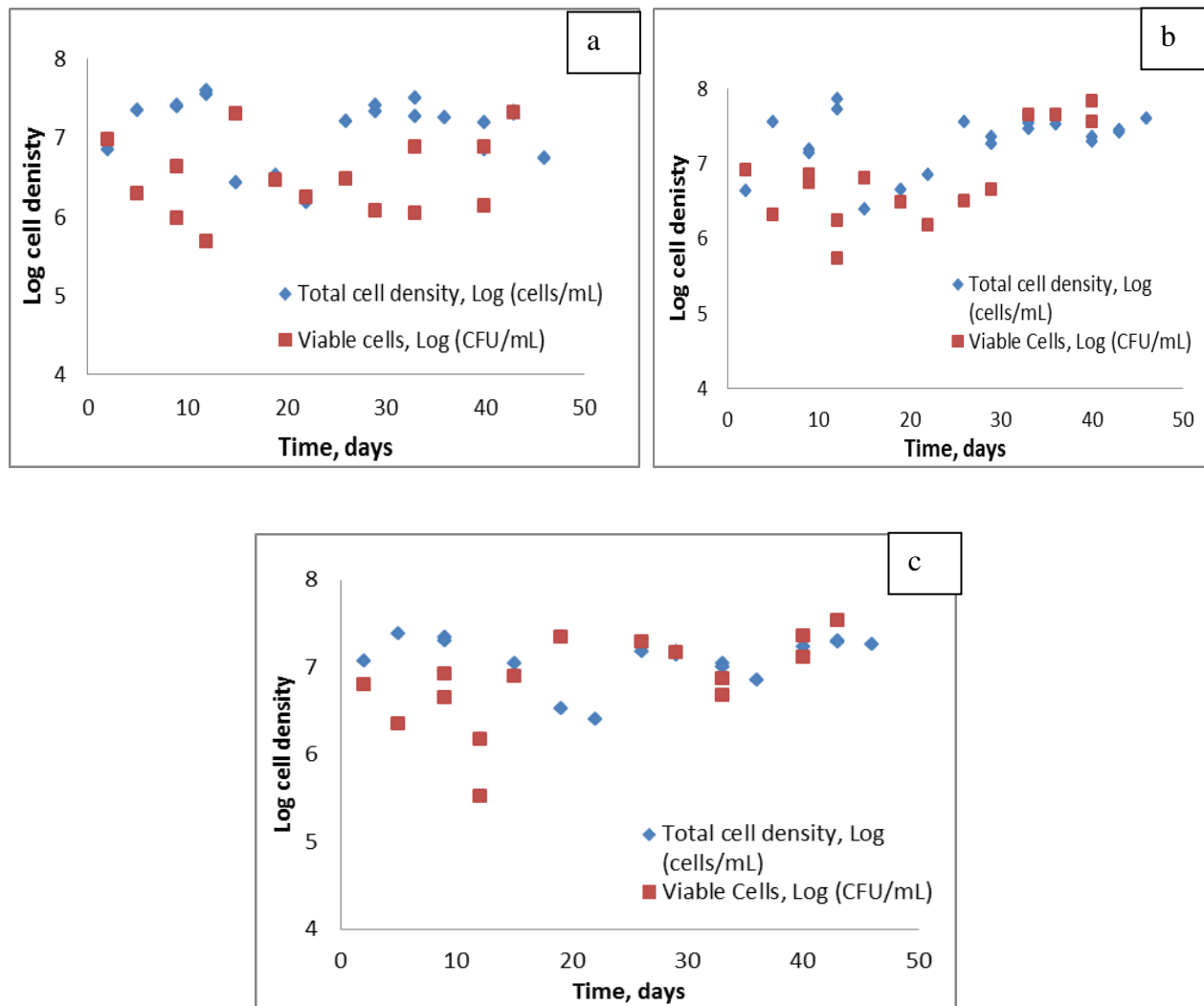
Figure 56. Results for the total cell density versus viable cells for mineral-free samples; a) 0 mM HCO₃; b) 3 mM HCO₃; c) 10 mM HCO₃.

In bicarbonate-free samples, total cell densities increased at the beginning of the experiment to log 7.5 cells/mL and then stabilized at the level of log 6.7- 7.2 cells/mL (Figure 56a). The cell density values in the mineral-free experiment were observed to be much higher than in the presence of autunite mineral. Samples amended with 3 mM of bicarbonate showed slightly higher results in cell density and values stabilized by the end of experiment in the range of log 7.4 -7.5 cell/mL (Figure 56b). The increase in cell density in the solutions amended with 3 mM HCO₃ was noted at higher uranium concentrations (Figure 54) compared to bicarbonate-free samples, justifying the fact that the presence of bicarbonate ions can mitigate uranium toxicity. Cell densities in samples amended with 10 mM HCO₃ were around log 7.2 cell/mL (Figure 56c). These cell density values are slightly lower than those observed in samples amended with 3 mM MHCO₃. Perhaps the higher uranium concentrations measured in the samples contributed to the slight decrease in cell densities (Figure 55).

Cell viability was determined via counts of colonies forming units (CFU/mL) and values were compared to the cell densities obtained via direct cell counting. At the beginning of the

experiment, bicarbonate-free samples yielded an average 3-18% of viable cells out of the total cell density. By the end of the experiments, cell viability increased and stabilized at the level of ~32%. In samples amended with 3 mM and 10 mM HCO_3, the viability of cells in the first 10 days was averaged at the level of 20% but increased significantly by the end of the experiments at the level of total density concentrations. A similar effect was noted for samples amended with 10 mM HCO_3 but with a larger percentage of cell viability. After 10 days, the viability was noted to be about 32%, and then increased to the level of total cell density concentrations. Overall, mineral-free samples exhibited much higher total cell density and cell viability compared to mineral-amended samples.

Task 1.2: Acknowledgments

Task 1.2: References

Bachmaf, S., Planer-Friedrich, B., Merkel, B.J. 2008. Effect of sulfate, carbonate, and phosphate on the uranium(VI) sorption behavior onto bentonite. *Radiochimica Acta*, **96**(359-366).

Barlett, M. 2014. Uranium reduction and microbial community development in response to stimulation with different electron donors.

Beazley, M.J., Martinez, R.J., Sobecky, P.A., Webb, S.M., Taillefert, M. 2007. Uranium Biomineralization as a Result of Bacterial Phosphatase Activity: Insights from Bacterial Isolates from a Contaminated Subsurface. *Environmental Science & Technology*, **41**(16), 5701-5707.

Belli, K.M., DiChristina, T.J., Van Cappellen, P., Taillefert, M. 2015. Effects of aqueous uranyl speciation on the kinetics of microbial uranium reduction. *Geochimica et Cosmochimica Acta*, **157**, 109-124.

Bencheikh-Latmani, R., Leckie, J.O. 2003. Association of uranyl with the cell wall of Pseudomonas fluorescens inhibits metabolism. *Geochimica et Cosmochimica Acta*, **67**(21), 4057-4066.

Bernhard, G., Geipel, G., Reich, T., Brendler, V., Amayri, S., Nitsche, H. 2001. Uranyl(VI) carbonate complex formation: Validation of the Ca2UO2(CO3)3(aq.) species. in: *Radiochimica Acta International journal for chemical aspects of nuclear science and technology*, Vol. 89, pp. 511.

Braet, F., De Zanger, R., Wisse, E. 1997. Drying cells for SEM, AFM and TEM by hexamethyldisilazane: a study on hepatic endothelial cells. *Journal of Microscopy*, **186**(1), 84-87.

Brooks, S.C., Fredrickson, J.K., Carroll, S.L., Kennedy, D.W., Zachara, J.M., Plymale, A.E., Kelly, S.D., Kemner, K.M., Fendorf, S. 2003. Inhibition of Bacterial U(VI) Reduction by Calcium. *Environmental Science & Technology*, **37**(9), 1850-1858.

Claessens, J., van Lith, Y., Laverman, A.M., Van Cappellen, P. 2006. Acid–base activity of live bacteria: Implications for quantifying cell wall charge. *Geochimica et Cosmochimica Acta*, **70**(2), 267-276.

Donlan, R.M. 2002. Biofilms: Microbial Life on Surfaces. in: *Emerg Infect Dis*, Vol. 8.

Ejnik, J.W., Hamilton, M.M., Adams, P.R., Carmichael, A.J. 2000. Optimal sample preparation conditions for the determination of uranium in biological samples by kinetic phosphorescence analysis (KPA). *Journal of Pharmaceutical and Biomedical Analysis*, **24**(2), 227-235.

Gudavalli, R.K.P., Katsenovich, Y.P., Wellman, D.M., Idarraga, M., Lagos, L.E., Tansel, B. 2013. Comparison of the kinetic rate law parameters for the dissolution of natural and synthetic autunite in the presence of aqueous bicarbonate ions. *Chemical Geology*, **351**, 299-309.

Hazrin-Chong, N.H., Manefield, M. 2012. An alternative SEM drying method using hexamethyldisilazane (HMDS) for microbial cell attachment studies on sub-bituminous coal. *Journal of Microbiological Methods*, **90**(2), 96-99.

Katsenovich, Y., Carvajal, D., Guduru, R., Lagos, L., Li, C.-Z. 2013. Assessment of the Resistance to Uranium (VI) Exposure by Arthrobacter sp. Isolated from Hanford Site Soil. *Geomicrobiology Journal*, **30**(2), 120-130.

Katsenovich, Y.P., Carvajal, D.A., Wellman, D.M., Lagos, L.E. 2012. Enhanced U(VI) release from autunite mineral by aerobic Arthrobacter sp. in the presence of aqueous bicarbonate. *Chemical Geology*, **308–309**, 1-9.

Langmuir, D. 1978. Uranium solution- mineral equilibria at low temperatures with application to sedimentary ore deposits. *Geochimica et Cosmochimica Acta*, **42**, 547-569.

Lin, H., Bennett, G.N., San, K.-Y. 2005. Chemostat culture characterization of Escherichia coli mutant strains metabolically engineered for aerobic succinate production: A study of the modified metabolic network based on metabolite profile, enzyme activity, and gene expression profile. *Metabolic Engineering*, **7**(5–6), 337-352.

Lin, X., Kennedy, D., Peacock, A., McKinley, J., Resch, C.T., Fredrickson, J., Konopka, A. 2012. Distribution of Microbial Biomass and Potential for Anaerobic Respiration in Hanford Site 300 Area Subsurface Sediment. *Applied and Environmental Microbiology*, **78**(3), 759-767.

Marshall, M., Plymale, A., Kennedy, D., Shi, L., Wang, Z., Reed, S., Dohnalkova, A., Simonson, C., Liu, C., Saffarini, D., Romine, M., Zachara, J., Beliaev, A., Fredrickson, J. 2008. Hydrogenase- and outer membrane c-type cytochrome-facilitated reduction of technetium(VII) by *Shewanella oneidensis MR-1*. *Environmental Microbiology*, **10**(1), 125-136.

McLean, J.S., Pinchuk, G.E., Geydebrekht, O.V., Bilskis, C.L., Zakrajsek, B.A., Hill, E.A., Saffarini, D.A., Romine, M.F., Gorby, Y.A., Fredrickson, J.K., Beliaev, A.S. 2008. Oxygen-dependent autoaggregation in Shewanella oneidensis MR-1. *Environmental Microbiology*, **10**(7), 1861-1876.

Meshulam-Simon, G., Behrens, S., Choo, A.D., Spormann, A.M. 2007. Hydrogen Metabolism in Shewanella oneidensis MR-1. *Applied and Environmental Microbiology*, **73**(4), 1153-1165.

Pinchuk, G.E., Ammons, C., Culley, D.E., Li, S.-M.W., McLean, J.S., Romine, M.F., Nealson, K.H., Fredrickson, J.K., Beliaev, A.S. 2008. Utilization of DNA as a Sole Source of Phosphorus, Carbon, and Energy by Shewanella spp.: Ecological and Physiological Implications for Dissimilatory Metal Reduction. *Applied and Environmental Microbiology*, **74**(4), 1198-1208.

Pinchuk, G.E., Geydebrekht, O.V., Hill, E.A., Reed, J.L., Konopka, A.E., Beliaev, A.S., Fredrickson, J.K. 2011. Pyruvate and Lactate Metabolism by Shewanella oneidensis MR-1 under

Fermentation, Oxygen Limitation, and Fumarate Respiration Conditions. *Applied and Environmental Microbiology*, **77**(23), 8234-8240.

Pinchuk, G.E., Hill, E.A., Geydebrekht, O.V., De Ingeniis, J., Zhang, X., Osterman, A., Scott, J.H., Reed, S.B., Romine, M.F., Konopka, A.E., Beliaev, A.S., Fredrickson, J.K., Reed, J.L. 2010. Constraint-Based Model of Shewanella oneidensis MR-1 Metabolism: A Tool for Data Analysis and Hypothesis Generation. *PLoS Computational Biology*, **6**(6), e1000822.

Sánchez, A.M., Bennett, G.N., San, K.-Y. 2005. Novel pathway engineering design of the anaerobic central metabolic pathway in Escherichia coli to increase succinate yield and productivity. *Metabolic Engineering*, **7**(3), 229-239.

Sheng, L., Fein, J.B. 2013. Uranium adsorption by Shewanella oneidensis MR-1 as a function of dissolved inorganic carbon concentration. *Chemical Geology*, **358**, 15-22.

Sheng, L., Fein, J.B. 2014. Uranium Reduction by Shewanella oneidensis MR-1 as a function of NaHCO3 concentration: surface complexation control of reduction kinetics. *Environmental Science & Technology*, **48**(7), 3768-3775.

Smeaton, C.M., Weisener, C.G., Burns, P.C., Fryer, B.J., Fowle, D.A. 2008. Bacterially enhanced dissolution of meta-autunite. *American mineralogist*, **93**, 1858-1864.

Tang, Y.J., Laidlaw, D., Gani, K., Keasling, J.D. 2006. Evaluation of the effects of various culture conditions on Cr(VI) reduction by Shewanella oneidensis MR-1 in a novel high-throughput mini-bioreactor. *Biotechnology and Bioengineering*, **95**(1), 176-184.

Thormann, K.M., Saville, R.M., Shukla, S., Pelletier, D.A., Spormann, A.M. 2004. Initial Phases of Biofilm Formation in Shewanella oneidensis MR-1. *Journal of Bacteriology*, **186**(23), 8096-8104.

Wellman, D.M., Gunderson, K.M., Icenhower, J.P., Forrester, S.W. 2007. Dissolution kinetics of synthetic and natural meta-autunite minerals, X3−n(n)+ [(UO2)(PO4)]2 · xH2O, under acidic conditions. *Geochemistry, Geophysics, Geosystems*, **8**(11), n/a-n/a.

Wu, C., Cheng, Y.-Y., Yin, H., Song, X.-N., Li, W.-W., Zhou, X.-X., Zhao, L.-P., Tian, L.-J., Han, J.-C., Yu, H.-Q. 2013. Oxygen promotes biofilm formation of Shewanella putrefaciens CN32 through a diguanylate cyclase and an adhesin. *Scientific Reports*, **3**, 1945.

Subtask 1.3: Evaluation of Ammonia Fate and Biological Contributions During and After Ammonia Injection for Uranium Treatment

Subtask 1.3.1: Evaluation of Ammonia and Uranium Fate and Biological Contributions During and After Ammonia Injection for Uranium Treatment

Subtask 1.3.1: Introduction

The Department of Energy's (DOE) Hanford Site, located in Washington state, has over 200,000 kg of uranium (U) deposited into the vadose zone (Corbin, Simpson et al. 2005, Zachara, Brown et al. 2007). This release occurred as a result of improper disposal of waste from plutonium production during World War II and the Cold War. U is highly mobile in the Hanford vadose zone due to the oxidizing conditions and the presence of carbonate creating highly mobile uranyl carbonate species. The partitioning coefficient (K_d) for U was previously measured in the range of $0.11 - 4$ mL/g at pH 8 for Hanford sediments and groundwater (Zachara, Brown et al. 2007, Szecsody, Truex et al. 2013) and the retardation factor was measured at 1.43 (Szecsody, Truex et al. 2013).

Moreover, the Hanford vadose zone is up to 255 feet thick with contamination measured down to 170 feet below the ground surface (Serne, Last et al. 2008). Therefore, there is a desire to create a remediation option that does not input additional liquid to the vadose zone as this could increase U flux to the groundwater below. Of the remediation methods that DOE is currently considering, ammonia gas injection appears to be a favorable option. Gas injection has been previously described as a viable remediation technique for inorganic radionuclides because they are highly affected by solution chemistry (Denham and Looney 2005, Dresel, Wellman et al. 2011).

The goal of the remediation technique is to remove U from the aqueous phase by raising the pH of the system, leading to immobilization as insoluble precipitates or strongly sorbed species. However, it must be noted that geochemical changes within the subsurface are often temporary unless they are moving the system towards its natural equilibrium. Therefore, the injection of ammonia gas for remediation is designed to temporarily raise the pH of the aqueous phase to dissolve natural aluminosilicate minerals. Based on preliminary laboratory scale experiments, it is expected that the system may reach a pH of $11 - 13$ (Szecsody, Truex et al. 2012).

Basic injections, including the injection of the weak base NH_3 gas, may lead to the slow dissolution of silica-containing minerals such as quartz, montmorillonite, muscovite and kaolinite (Wan, Tokunaga et al. 2004, Wan, Tokunaga et al. 2004, Szecsody, Truex et al. 2012, Szecsody, Truex et al. 2013). This results in an increase in dissolved Si^+ and Al^{3+} as well as small increases in Na^+, K^+, $Fe^{2+/3+}$, Cl^-, F^- and SO_4^{2-} (Szecsody, Truex et al. 2012, Szecsody, Truex et al. 2013). Moreover, Ca^{2+} increases in the aqueous phase were reported in column experiments following injection of $U + 0.1$ M NaOH $+ 1$ M $NaNO_3$ (Szecsody, Truex et al. 2013). The dissolution of these minerals will ultimately buffer the pH of the system (Qafoku, Ainsworth et al. 2003, Szecsody, Truex et al. 2013).

Then, as the system returns to a neutral pH as the ammonia escapes, U is expected to be immobilized as part of a co-precipitation process with aluminosilicate minerals. As ammonia leaves the aqueous phase and the pH returns to neutral, there are two phenomena that are expected to decrease the mobility of U: 1) U precipitation as solubility of Si, Al and similar ions decreases; and 2) U (co)precipitates are coated with non-U, low solubility precipitates. Some of

the low solubility precipitates that are expected to form include cancrinite, sodalite, hydrobiotite, brucite and goethite (Bickmore, Nagy et al. 2001, Qafoku, Ainsworth et al. 2004, Zhao, Deng et al. 2004, Qafoku and Icenhower 2008).

A decrease in the pH of approximately two units occurred after six months in previous column experiments following ammonia gas injection (Szecsody, Truex et al. 2012). Further, Szecsody et al. reported that as much as 93% less U mass may be leached with 5% ammonia gas injection versus untreated sediments as evaluated in column experiments after 100 pore volumes. Similar work by Zhong et al. reported that 85% less U is mobilized for columns treated with 5 and 15% v/v ammonia gas (Zhong, Szecsody et al. 2015).

Nonetheless, there is a lack of understanding of the fate of U under the transient conditions caused by ammonia gas injection. Szecsody et al. has shown that basic solutions co-disposed with U may lead to an increase in retardation (1.76 compared to 1.43 at neutral pH) within the subsurface and that precipitation is likely (Szecsody, Truex et al. 2013). However, the high ionic strength conditions caused by mineral dissolution and the greater likelihood of carbonate complexation may lead to desorption and mobilization of U. Szecsody et al. (2013) has shown an increase in column effluent concentrations for pH 8 versus 0.1 M NaOH with concentrations of U measured at 6.0 and 9.1 µM, respectively. There is still a need to understand the mechanisms with the greatest effect on U mobility under these conditions.

The objective of this work is to understand the partitioning of U and the mineral dissolution caused by injection of ammonia in simplified experiments. Further, samples will be prepared with a baseline (a neutral pH representative of natural conditions), a base treatment with NaOH and a base treatment with NH_4OH. This allows for a comparison with the mainstream remediation technique of sodium hydroxide (NaOH) injection and natural conditions at the Hanford Site. Sequential extractions will also investigate the lability of U in the solid phase following treatments.

Subtask 1.3.1: Experimental Methods

Materials

The following minerals were chosen for the experiments based on the mineralogy of the site as summarized in Table 12 with data from Serne et al. (2008), discussions with the PNNL collaborators Drs. Jim Szecsody and Nik Qafoku, and previous work (Qafoku, Ainsworth et al. 2004, Szecsody, Truex et al. 2010, Zhong, Szecsody et al. 2015). The minerals chosen for the experiments include: quartz (Ottawa Sand Standard pass through 20-30 mesh, Fisher), kaolinite (Alfa Aesar), montmorillonite (SWy-2, Clay Minerals Society), illite (Imt-2, Clay Minerals Society), muscovite (Ward Scientific, <2 mm size fraction), calcite (Alfa Aesar, 0.06-0.19" diameter) and Hanford sediments. The Hanford sediment samples were received from Dr. Jim Szecsody at PNNL and came from the ERDF pit at a depth of 6.1 meters. Further characterization of this sediment has been published previously (Szecsody, Truex et al. 2013). BET surface area measurements were collected for each of the minerals investigated with the exception of calcite and are shown in Table 13.

Table 12. Major Minerals in the 200 Area (Serne, Last et al. 2008)

Mineral	Bulk Fraction	Clay-sized Fraction
Quartz	30-80	5-10
Feldspar	10-30	<5
Smectite	ND	30-35
Illite	ND	15-40
Chlorite	ND	15-20
Kaolinite	ND	ND-10
Calcite	ND-5	15-20

Table 13. BET Surface Area for Relevant Minerals and Hanford Sediment

Mineral ID	m^2/g
Quartz	0.046
Kaolinite	17.9
Illite	19.1
Montmorillonite	23.8
Hanford Sediment	17.4
Muscovite	0.096

Two solutions were formulated to describe the Hanford groundwater: 1) a simplified synthetic groundwater (SGW) as described in Table 14; and 2) a NaCl solution of similar ionic strength for comparison. The simplified SGW in Table 14 is based on correspondence with Dr. Szecsody and previous work (Szecsody, Cantrell et al. 1998).

Table 14. Synthetic Groundwater (SGW) Composition with Total Ionic Strength of 7.2 mM

Element	(mmol/L)
Na^+	1.1
K^+	0.22
Ca^{2+}	1.4
Mg^{2+}	0.6
HCO_3^-	1.32
Cl^-	3.9

Batch experimental protocols

Initial batch experiments were conducted in triplicate at pH ~7.5 in the presence of mineral and either synthetic groundwater (Table 14) or NaCl at similar ionic strength (~0.0032 M). Batch

experiments were conducted separately for each of the minerals described in the Materials section at the following concentrations: 5 g/L for kaolinite, illite, montmorillonite, and calcite, 25 g/L for muscovite and Hanford 200 Area sediments and 100 g/L for quartz. Prior to addition of pure minerals to the batch experiments, they were washed based on the methods outlined in Table 15.

An aliquot of U (Spex Certiprep, New Jersey) was added following equilibration of samples at pH ~7.5 to reach 500 ppb U. After equilibration with U for three days on an end over end tube revolver at 40 rpm (Thermo Scientific), a homogenous aliquot was removed for analysis for both controls (without kaolinite) and samples. pH (Thermo Scientific, 8175BNWP) and redox conditions (for only select samples, Microelectrodes) were analyzed for each sample.

All samples (except for montmorillonite) were centrifuged at 5000 rpm for 30 minutes (18100 rcf, Thermo Scientific, Corvall ST 16R centrifuge) to remove particles >100 nm based on Stoke's law as described by Jackson (Jackson 1985). Montmorillonite was subjected to a longer centrifugation step for three hours to remove particles <40 nm due to the greater likelihood of colloid formation based on previous work (Lagaly and Ziesmer 2003). Then, the supernatant was acidified in 1% HNO_3 (Fisher, ACS Plus) for analysis by kinetic phosphorescence analyzer (KPA-11, Chemchek) for U and inductively coupled plasma optical emission spectroscopy (ICP-OES, Perkin Elmer, Optima 7300 DV) for major cations (Ca, Mg, Fe, Al and Si). The cation concentrations in the aqueous phase were analyzed to track dissolution of the kaolinite mineral throughout these experiments. In addition, appropriate control samples without the solid were prepared with negligible losses (within error of the measurements) to the vial walls at pH ~7.5.

Following equilibration at pH ~7.5, the pH of each sample was raised with either 2.5 M NH_4OH or 2.5 M $NaClO_4$ + 0.025 M NaOH. Samples adjusted with NH_4OH were immediately capped and wrapped with Para film following addition to reduce volatilization of NH_3 gas. It should be noted that ammonia volatilization increases by an order of magnitude for every unit above pH 6.0 and, therefore, is expected to be higher in alkaline soils (Vlek and Craswell 1981, Singandhupe and Rajput 1989). The pH adjust solutions were prepared to allow for similar ionic strength and base adjusting power. In addition, the adjustment by either NH_4OH or NaOH allows for comparison of both options as a possible step to raise the pH during remediation of the subsurface. After adjustment, samples were equilibrated for three days before analysis as described above for U, Al, and Si and additional analysis for total ammonia. Control samples analyzed at elevated pH showed considerable losses from the aqueous phase for synthetic groundwater conditions and will be discussed with the results below.

Table 15. Summary of Mineral Washing Methods

Mineral	Method	Reference
Quartz (Ottawa Sand)	(1) Mix 100 g/L suspension in 0.01 M NaOH for 60 minutes, (2) Centrifuge, decant, replace liquid with 0.01 M HCl, mix 60 minutes, (3) Centrifuge, decant, replace with Nanopure (>18 MΩ) H_2O and mix 3 minutes, (4) repeat step three two more times, (5) Dry solid at 35°C for ~3 days	(Powell, Kersting et al. 2008, Zavarin, Powell et al. 2012, Boggs, Dai et al. 2015)
Montmorillonite	(1) Mix 100 g/L suspension in 0.001 M HCl for 30 minutes, (2) Add 0.5 mL H_2O_2 and mix an additional 30 minutes, (3) Centrifuge 6 hours at 4500 rpm, decant aqueous and replace with 0.01 M NaCl (or synthetic porewater for synthetic porewater experiments) and mix overnight, (4) Repeat four times, (5) Centrifuge, decant and replace with Nanopure H_2O, (6) Repeat at least four times (until excess ions are removed), (7) Dry solid at 35°C for ~3 days, (8) Lightly crush with a mortar and pestle to homogenize	(Powell, Kersting et al. 2008, Zavarin, Powell et al. 2012, Boggs, Dai et al. 2015)
Kaolinite	(1) Mix 100 g/L suspension in 1 M NaCl (synthetic pore water for synthetic porewater experiments) for 30 minutes, (2) Centrifuge, decant and repeat four more times, (3) Centrifuge, decant and replace with Nanopure H_2O, (4) repeat four more times, (5) Dry solid at 35°C for ~3 days, (6) Lightly crush with a mortar and pestle to homogenize	(Heidmann, Christl et al. 2005, Heidmann, Christl et al. 2005)
Illite	(1) Mix 100 g/L suspension with 1 M NaCl (or synthetic porewater) for three hours and allow to flocculate overnight, (2) Decant and replace with 1 M NaCl (or synthetic porewater) and mix, (3) Repeat two more times, (4) Decant and replace with Nanopure H_2O, (5) Repeat until excess ions are removed, (6) Dry solid at 35°C for ~3 days, (7) Lightly crush with a mortar and pestle to homogenize	(Baeyens and Bradbury 2004)

Geochemical speciation modeling in Geochemist's Workbench (GWB)

Geochemist Workbench Standard version 10.0.04 (GWB) was used to model the aqueous speciation of uranium within these systems. The Visual Minteq database that was previously converted for GWB by Jon Petter Gustafsson was used for modeling with several additions to update uranium species based on new thermodynamic data. Specifically, several aqueous and solid species were updated based on recent reviews (Guillamont, Fanghanel et al. 2003, Gorman-Lewis, Burns et al. 2008, Thoenen, Hummel et al. 2014, Richter, Bok et al. 2015). However, the thermodynamic data for aqueous and solid actinide species under alkaline and hyperalkaline

conditions are still incomplete, especially with respect to ternary aqueous complexes and solid phases (Altmaier, Gaona et al. 2013).

The neutral calcium - uranyl - carbonate species $[Ca_2UO_2(CO_3)_3]$ was modified based on previous work (Kalmykov and Choppin 2000, Bernhard, Geipel et al. 2001, Dong and Brooks 2006). This neutral species was first reported in literature by Bernhard (Bernhard, Geipel et al. 1996). Additional complexes for ternary uranyl carbonate complexes with alkaline earth metals were also included based on previous work (Dong and Brooks 2006). Notably, the $MgUO_2(CO_3)_3^{-2}$ species was added based on Dong and Brooks (2006) as it was absent from the original database. It should be noted that the neutral calcium - uranyl - carbonate species measured by Kalmykov et al., Dong and Brooks, and Bernhard et al. are all within the experimental error of each other with the $Log\beta_{213} = 29.8\pm0.7$, 30.7 ± 0.05, and 30.55 ± 0.25, respectively. In addition, several uranyl hydroxide and uranyl carbonate species were added or updated based on the OECD NEA update and confirmed by the THEREDA and PSI/NAGRA database updates with only minor differences (Guillamont, Fanghanel et al. 2003, Thoenen, Hummel et al. 2014, Richter, Bok et al. 2015).

Although several researchers have previously investigated the thermodynamic properties of the becquerelite $[Ca(UO_2)_6O_4(OH)_6(H_2O)_8]$ solid based on the review by Gorman-Lewis et al. (2008), there is still a significant error between measurements (> 6 log units for the K_{sp}). However, Richter et al. (2015) confirmed the suggested value from Guillamont et al. (2003) based on a new study (Gorman-Lewis, Fein et al. 2008). Therefore, it is included in the database. Metaschoepite was also included in the database but replaced the schoepite species based on its similarity to the schoepite species from the OECD NEA update (Guillamont, Fanghanel et al. 2003, Gorman-Lewis, Shvareva et al., 2008). Further, the species measured in these works are better defined as metaschoepite (Guillamont, Fanghanel et al. 2003, Richter, Bok et al. 2015).

The most recent thermodynamic data added to the database includes several uranium silicate and oxide minerals. The values for K-boltwoodite, uranophane and coffinite were added based on recent research (Shvareva, Mazeina et al. 2011, Szenknect, Mesbah et al. 2016). Shvareva et al. (2011) also measured parameters for Na-boltwoodite which were within the error of the previous value reported in the updated OECD NEA database (Guillamont, Fanghanel et al. 2003). Therefore, these values for K-boltwoodite and uranophane are expected to be accurate measurements. K-boltwoodite and uranophane are common uranyl silicates in oxidiating conditions and have been previously identified in the Hanford vadose zone where uranium waste was historically released (Catalano, Heald et al. 2004, Um, Icenhower et al. 2010).

The uranophane K_{sp} replaced the highly variable measurements previously summarized by Gorman-Lewis et al. (2008). Further, the coffinite K_{sp} value from Szenknect et al. (2016) is an important addition because it has been reported in many reducing, low-temperature aquatic systems (Guo, Szenknect et al. 2015). Szenknect et al. (2016) reported a standard free energy of formation for coffinite of -1862.3 ± 7.8 kJ/mol which compares well with the previously measured values ranging from -1872 ± 6 to -1886 ± 6 kJ/mol (Langmuir 1978, Grenthe, Wanner et al. 1992, Guo, Szenknect et al. 2015). In addition, the size of the coffinite grains used in the study are considered representative of coffinite in nature and as an alteration product of spent nuclear fuel (Szenknect, Mesbah et al. 2016).

Alwan and Williams previously measured the dissolution of swartzite and liebigite (Alwan and Williams 1980). The authors did not state whether or not the solids were checked for stability

and it was assumed but not confirmed that dissolution of major cations was stoichiometric (Gorman-Lewis, Burns et al. 2008). Therefore, this data was not selected for the OECD database (Guillamont, Fanghanel et al. 2003). However, it is included in some of the simulations in this work for comparison.

The Davies equation was used for calculation of activity coefficients because the Visual Minteq database was used with GWB. The Davies method is generally considered to be applicable up to 0.7 mol/kg (Langmuir 1997). Moreover, the solutions in this work are within this range with the highest ionic strength near 0.5 mol/L for the highest pH treatments. The total carbonate concentration was fixed at 0.22 mM in the model to represent initial equilibrium with the atmosphere at pH 7.5 for the 3.2 mM NaCl solutions and at 1.3 mM for the synthetic groundwater based on the recipe. The modeling of the treated samples (with either NaOH or NH_4OH) is assumed to be closed from the atmosphere and, therefore, maintains the total carbonate from the initial conditions. Models were run utilizing the sliding feature to add the appropriate chemical.

Subtask 1.3.1: Results and Discussion

Because a significant amount of the work completed during FIU Performance Year 6 was submitted as a technical report and for peer-reviewed publication, it will not be included in this year-end summary report. The previous report includes all of the data collected in the presence of kaolinite for equilibrium batch experiments and sequential extractions. This report will present the batch experiments for additional pure minerals and Hanford sediments. Some of the equilibrium data for kaolinite will still be included in summary figures when comparing different minerals.

Uranium Fate

The recovery of U in the aqueous phase in control (without mineral) samples prepared in triplicate for the SGW (Table 14) and 3.2 mM NaCl is presented in Figure 59. The fraction of U remaining in the aqueous phase for the initial samples at neutral pH (~7.5) are nearly 100% (96±6% for SGW and 70±2% for NaCl). Therefore, the batch data presented in Figure 60 and Figure 61 is corrected for the control recovery for the initial conditions as pH ~7.5 as it is assumed these are losses due to sorption to vial walls and/or pH adjustment.

However, in the SGW controls, the aqueous phase recovery after treatment at pH near 11.5 is similar to or less than the recovery in the presence of the mineral. For comparison, aqueous phase recovery was 1.2±0.2% versus 2.5±0.4% for the NH_4OH treatment for the control and with kaolinite, respectively. For the NaOH treatment, recovery was 9±6% and 12±4%, respectively. These samples were not corrected for the recovery of U in the controls at elevated pH as the system appears more complex with precipitation and sorption occurring simultaneously and likely at different levels than samples with kaolinite.

In addition, in the presence of SGW, precipitation of several different uranyl minerals is expected. At neutral pH, formation of swartzite is predicted by GWB. However, it is likely that the solubility constant for swartzite measured by Alwan and Williams (1980) is not accurate because precipitation was not observed in control samples at neutral pH. In addition, their solubility constants were not used in the previous OECD database for reasons discussed in the modeling section of the Materials and Methods.

It should be noted that the 3.2 mM NaCl control samples had approximately 70% recovery at neutral pH and 90% recovery for both treatments to reach pH ~11.5 as shown in Figure 61. Further, speciation modeling in GWB did not predict solid minerals to dominate the system until pH 11 (Figure 60). However, the software did predict precipitation of clarkeite above pH 10 for the NaOH + NaClO$_4$ treatment but not as a major mineral as shown by the Pourbaix diagrams in Figure 60 (data not shown). Because precipitation was not significant in these samples, it is likely that more aqueous carbonate was present in the system than expected and complexed U at higher pH.

Because of the likelihood of precipitation in both controls and in the presence of kaolinite, the batch equilibrium data presented below represents an apparent K$_d$ as it includes both precipitation and sorption processes in the overall partitioning coefficient. It is notable that precipitation is significant in the control samples for SGW and removal is greater in controls than in the presence of kaolinite. This shows that there are likely additional reactions occurring in the system with minerals present. It is possible that a decrease of precipitation in the presence of the mineral is due to sorption of cations that would otherwise precipitate and remove U as part of a co-precipitation process. However, this process cannot be predicted with GWB.
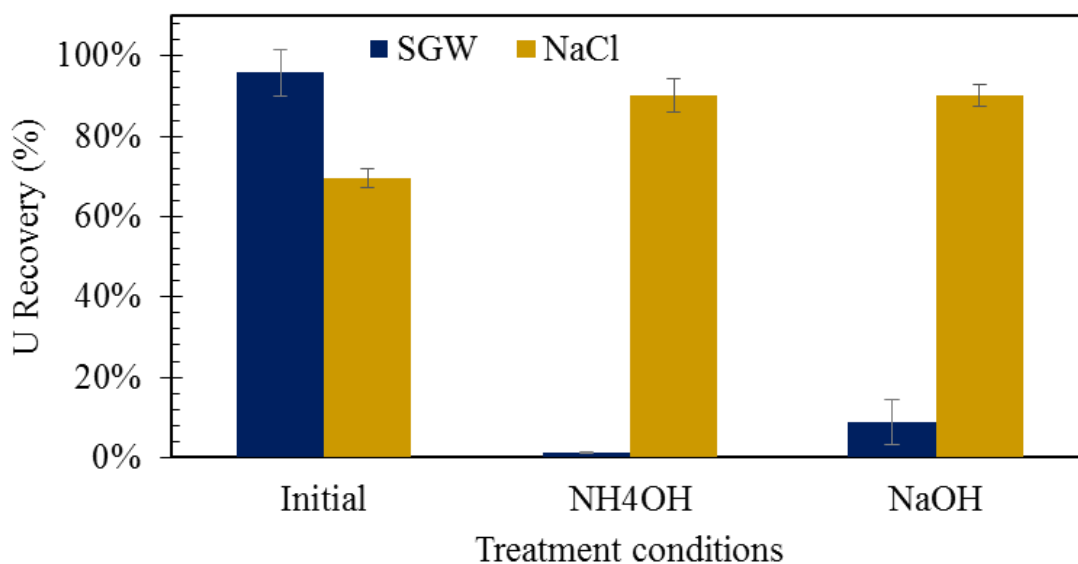
Figure 57. Uranium recovery in the aqueous phase for control samples (no solids/minerals) for synthetic groundwater (blue) and 3.2 mM NaCl (yellow).
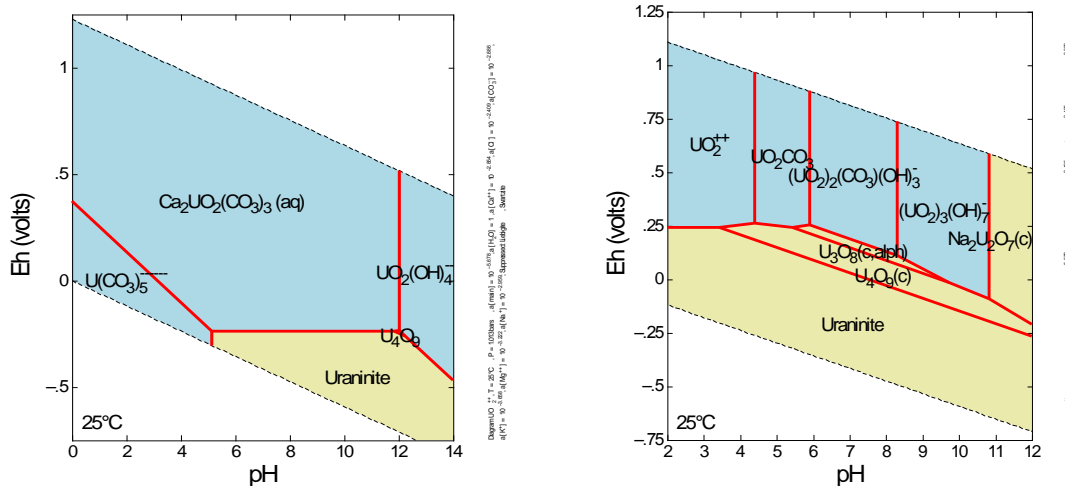
Figure 58. Uranium speciation as Pourbaix diagrams via GWB modeling for control samples (no solids/minerals) for synthetic groundwater (*right*) and 3.2 mM NaCl (*left*), Note: blue species are aqueous species and yellow species are solid minerals.

Figure 61and Figure 62 summarize the partitioning of U in SGW in the presence of the suite of minerals and Hanford sediments. Figure 61 represents K_d values normalized with respect to the mass of mineral and Figure 62 represents K_d values normalized with respect to surface area based on BET measurements taken prior to the experiments. Remarkably, the removal of U from the aqueous phase increases with base treatment in the presence of SGW for each of the minerals investigated with the exception of muscovite. Further, the removal appears to be slightly greater for silicate layer clays (kaolinite, illite, montmorillonite and muscovite) with the exception again being muscovite.

The removal is also slightly greater for NH_4^+ as a base treatment than Na^+ for the silicate layer clays for the SGW experiments. For kaolinite, illite, and montmorillonite this seems to confirm that the ions present in each of the treatments (Na^+ or NH_4^+) are impacting the removal of uranium in the presence of these clays in slightly different ways. Therefore, it is likely that removal of U is partially due to ion exchange processes. However, muscovite, although still a silicate layer clay, reacts differently. Previous XAS work has shown that U removal may occur through surface precipitation on muscovite and this could explain the consistent removal of U in the presence of muscovite with varying pH and ionic strengths (Moyes, Parkman et al. 2000).

Quartz and calcite exhibit increased removal with both basic treatments but not a significant difference between the two treatments in the presence of SGW. This indicates that either precipitation or strong, inner-sphere sorption are occurring. However, further work will be conducted to investigate the solid phase species present following treatment. Remarkably, when surface area is accounted for, the removal of U is greatest for muscovite and quartz. Assuming that surface precipitation is responsible for removal in the presence of muscovite as reported previously, the quartz would be predicted to be the strongest adsorbent of the pure minerals investigated in the presence of SGW. However, calcite cannot be compared at this time because BET analysis has not yet been conducted.

In the presence of the Hanford sediment, sorption is the lowest especially when surface area is accounted for in the minerals. This implies that there are fewer available sorption sites within the heterogeneous mixture of minerals in the sediments possibly because minerals are coating one

another and blocking sorption sites. In addition, the greatest difference between the two base treatments is observed for the Hanford sediments suggesting that the different ions within the treatments had an exceptionally significant impact on sorption of U likely due to the difference in ion exchange for Na^+ versus NH_4^+ and their impact on U sorption site availability.

U partitioning was also analyzed in the presence of 0.0032 M NaCl solution for four different minerals: kaolinite, illite, quartz and montmorillonite. This was performed as a comparison with the SGW solution (Figure 61). Figure 63 represents K_d values normalized with respect to the mass for the above mentioned minerals and Figure 64 represents equivalent experiments normalized with respect to surface area (Table 13). Unlike SGW samples, minerals in the presence of the simpler NaCl solution show a greater apparent K_d at initial conditions and then, after treatment, a decrease in apparent K_d or increase in environmental availability. This opposite behavior can be attributed to the difference in chemical species for each solution. For the simpler NaCl system, the aqueous fraction of U is expected to increase since more uranyl carbonates species are forming under this system. Such carbonates are either neutral or negatively charged, and will likely be repelled by the negative surface of the pure minerals at these neutral and basic pH ranges. This repulsion causes a decreased likelihood of U sorption. However, the exception can be seen for montmorillonite. Possible explanations can be sorption to vials or losses during pH adjustment. For quartz, NaOH treatment is still being analyzed and analysis of initial condition should be re-run since the error between measurements is significant.
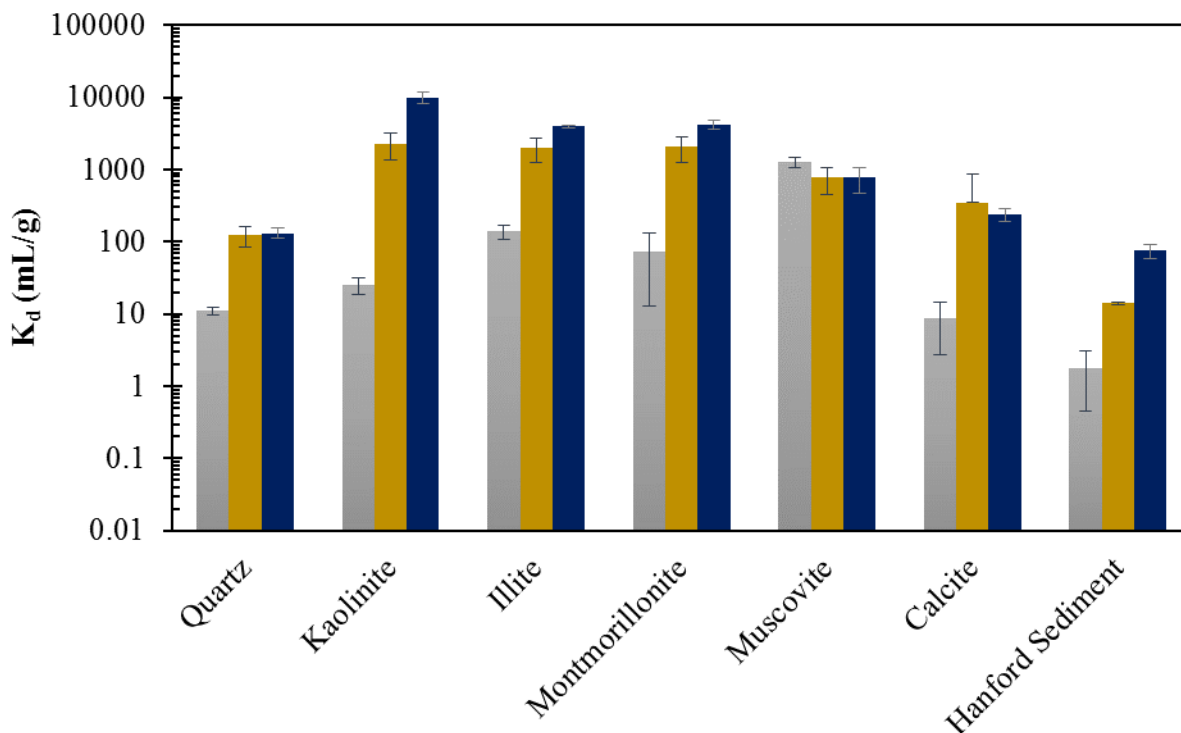
Figure 59. K_d (mL/g) for pure minerals and Hanford sediments for initial (gray), NaOH (yellow) and NH₄OH (blue) treated samples in SGW.
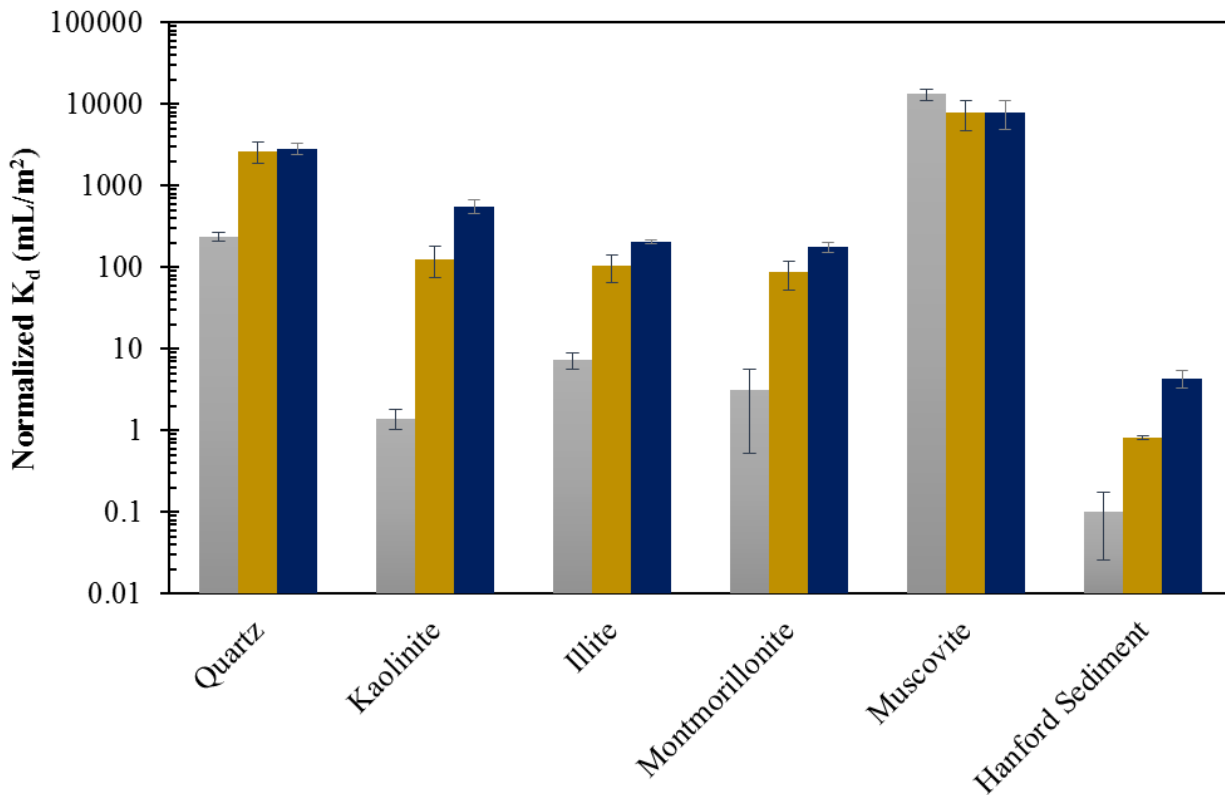
Figure 60. Surface area normalized K_d (mL/m^2) for pure minerals and Hanford sediments for initial (*gray*), NaOH (*yellow*) and NH$_4$OH (*blue*) treated samples in SGW, Note: calcite was not included because BET surface area has not yet been measured on this mineral.
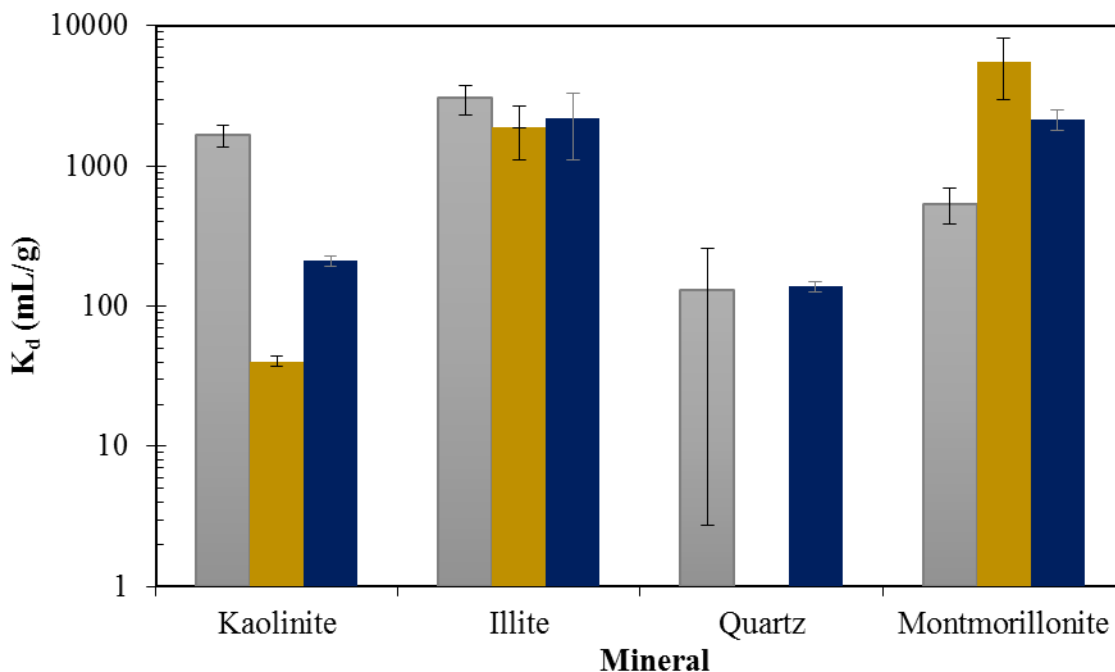
Figure 61. K_d (mL/g) for pure minerals for initial (*gray*), NaOH (*yellow*) and NH$_4$OH (*blue*) treated samples in 0.0032 M NaCl solution. Note: NaOH treatment for quartz is still being analyzed.
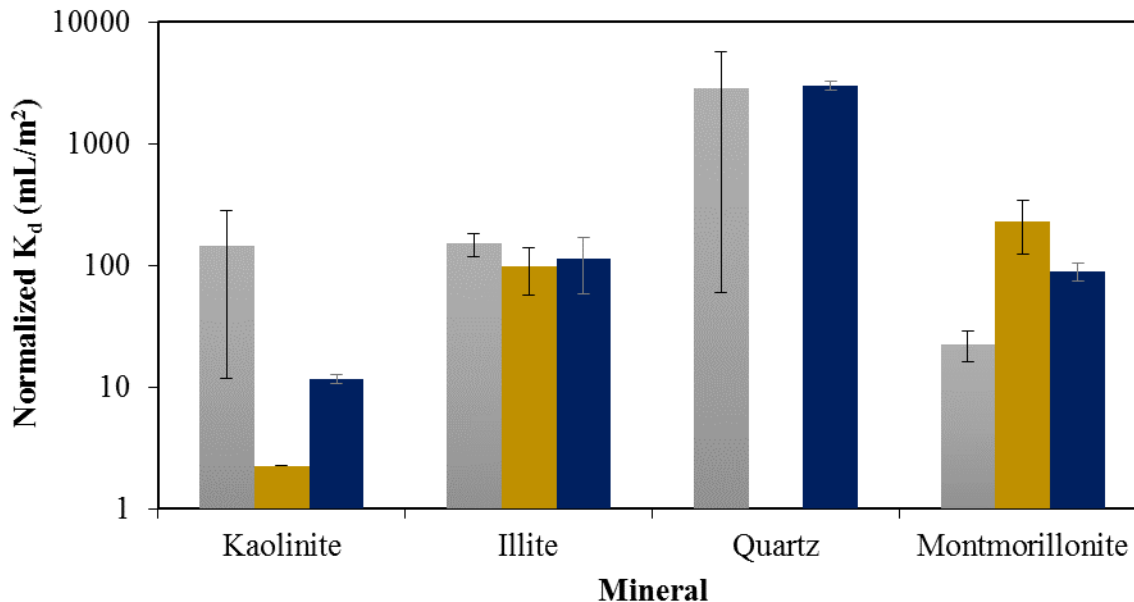
Figure 62. Normalized apparent K_d (mL/m^2) for U (500 ppb) removal in the presence of kaolinite (5 g/L), illite (5 g/L), quartz (100g/L) or montmorillonite (5 g/L) in 3.2 mM NaCl solution with pH at ~11.5 via adjustment with either NaOH (*yellow*) or NH$_4$OH (*gray*) or at ~7.5 to represent initial conditions prior to base treatment (*blue*), Note: NaOH treatment for quartz is still being analyzed.

Mineral Dissolution

Table 16, Figure 63, and Figure 64 represent the results for mineral dissolution in the presence of SGW for each of the minerals investigated with the exception of calcite as dissolution was measured by the Ca^{+2} ion. The greatest dissolution at elevated pH occurred for kaolinite and muscovite. Although at elevated pH due to the NaOH treatment, only 0.6% of calcite was dissolved into the aqueous phase, the greatest dissolution of any mineral occurred for calcite at neutral pH with 3.5% dissolution based on aqueous calcium measurements. It is possible that secondary minerals were formed at elevated pH in the calcite solutions as there is clear evidence that Ca^{+2} was removed from the aqueous phase with treatment. It is possible that co-precipitation of U also occurred explaining the nearly two order of magnitude increase in K_d for U partitioning with calcite in SGW following base treatment.

Furthermore, Figure 65 and Figure 66 represent the results for mineral in the presence of 0.0032 M NaCl solution for the following minerals: kaolinite, illite, quartz and montmorillonite. It should be noted that both figures indicate the same trend: an increase in Si and Al in the aqueous phase for NaOH-treated samples leading to a greater dissolution than the NH$_4$OH treatment. This effect can be explained by the different effects of the two treatments on the mineral solubility. The addition of NaOH adds singly charged ions (Na$^+$) to solution. However, the addition of NH$_4$OH adds greater than 99% molecular species (NH$_3$) at pH ~11.5 based on ammonia/ammonium speciation. For the charged ions (NaOH), solubility increases with ionic strength while molecular species (NH$_3$) decreases (Langmuir 1997). Therefore, it is expected that the increase in molecular species for the NH$_4$OH treatment would result in a significant decrease in solubility especially of Si as it is most likely to dissolve as a molecular species (H$_4$O$_4$Si).

Table 16. Mineral Dissolution Results for Silicate Layer Clays and Quartz Based on Aqueous Al^{3+} and H_4SiO_4 Measurements

Mineral	Conditions	pH	Al^{3+}	(error)	H_4SiO_4	(error)
Kaolinite	Initial	7.53	BDL	BDL	0.1481%	0.0289%
	NH_4OH	11.78	0.0301%	0.0048%	0.0774%	0.0128%
	NaOH	11.78	0.0190%	0.0007%	0.3862%	0.0043%
Illite	Initial	7.55	0.0300%	0.0054%	0.0429%	0.0268%
	NH_4OH	11.71	0.0377%	0.0018%	0.0134%	0.0007%
	NaOH	11.70	0.0568%	0.0054%	0.0203%	0.0019%
Montmorillonite	Initial	7.83	0.0351%	0.0095%	0.1970%	0.0079%
	NH_4OH	11.72	0.0515%	0.0048%	0.0247%	0.0023%
	NaOH	11.65	0.0488%	0.0021%	0.0234%	0.0010%
Muscovite	Initial	7.57	0.0018%	0.0008%	0.0641%	0.0052%
	NH_4OH	11.52	0.0957%	0.0044%	0.1799%	0.0132%
	NaOH	11.64	NM	NM	NM	NM
Quartz	Initial	7.61	-	-	0.0088%	0.0010%
	NH_4OH	0.00	-	-	0.0052%	0.0021%
	NaOH	0.00	-	-	0.0393%	0.0032%

BDL - below detection limits
NM - not yet measured
Note: Error is based on measurement of triplicate samples
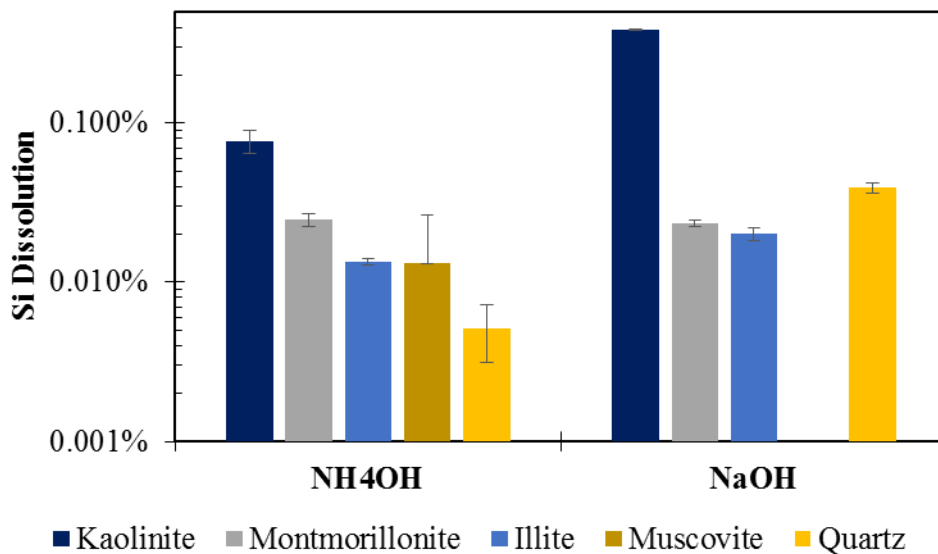
Figure 63. Dissolution of Si from layer silicate clays and quartz in the presence of synthetic groundwater based on aqueous measurements by ICP-OES, Note: samples for dissolution of muscovite following treatment with NaOH have yet to be analyzed.
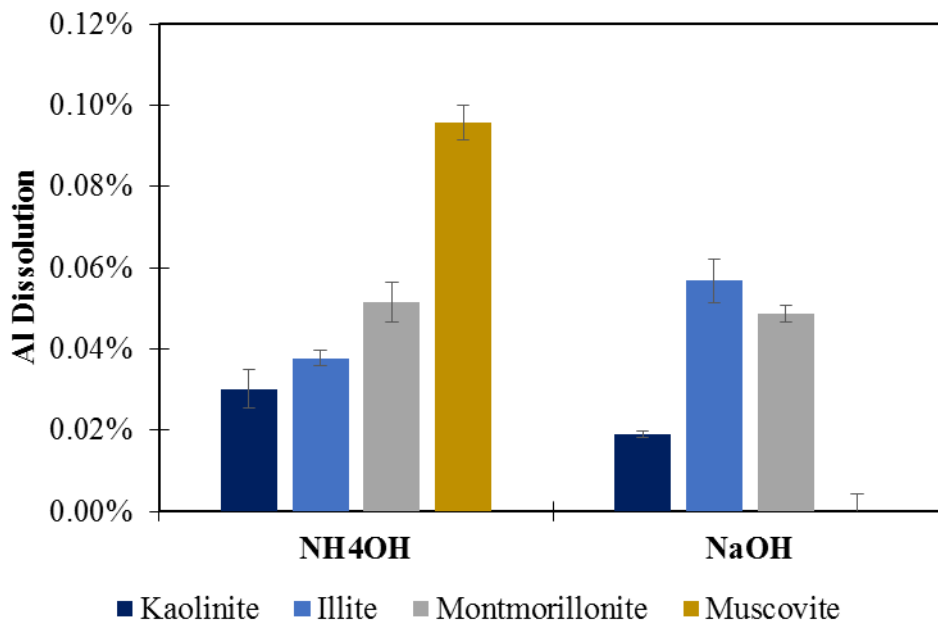
Figure 64. Dissolution of Al from layer silicate clays in the presence of synthetic groundwater based on aqueous measurements by ICP-OES, Note samples for dissolution of muscovite following treatment with NaOH have yet to be analyzed.
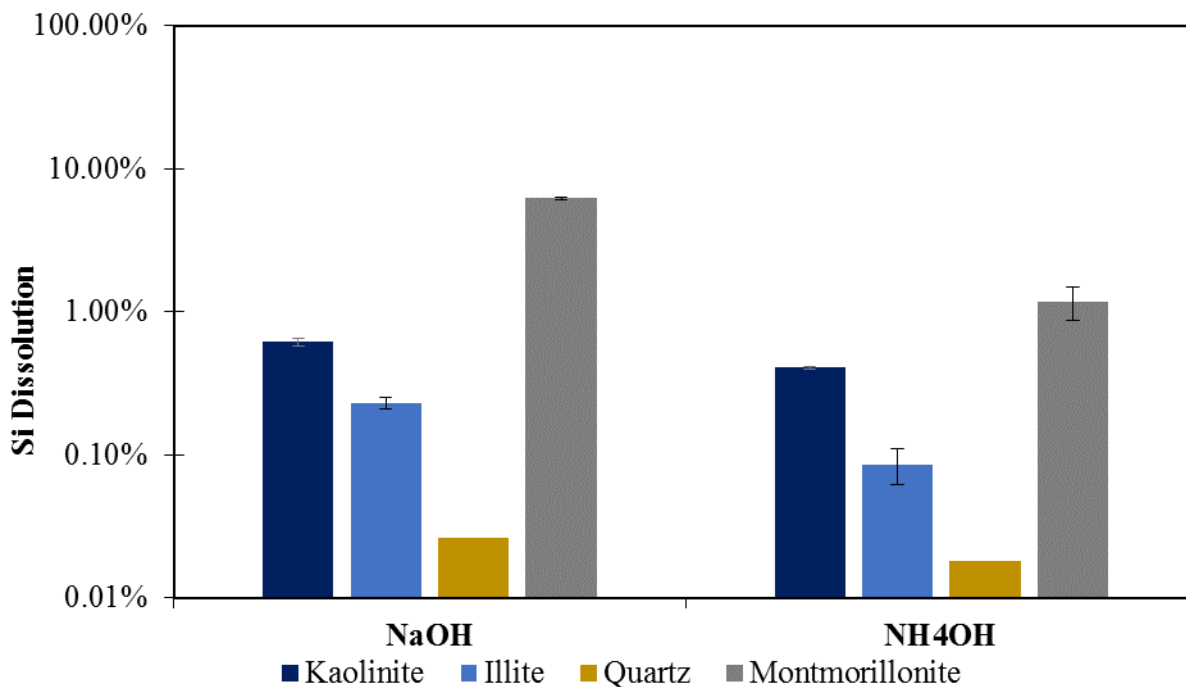
Figure 65. Dissolution of Si from layer silicate clays and quartz in the presence of 0.0032 M NaCl solution based on aqueous measurements by ICP-OES.
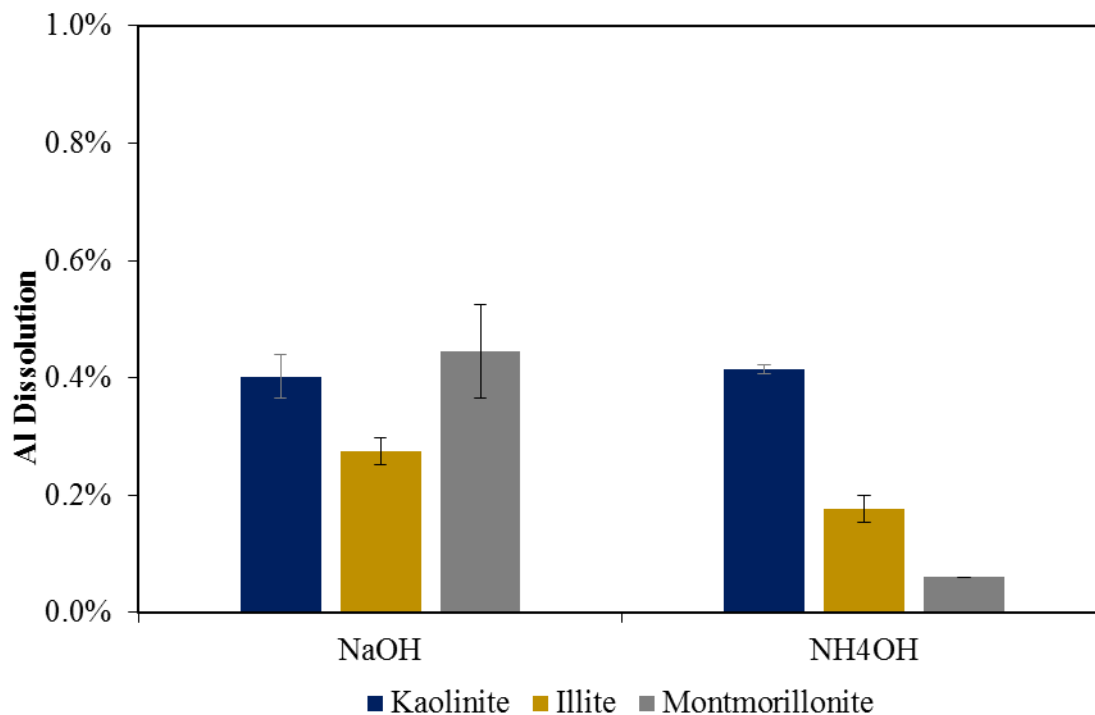
Figure 66. Dissolution of Al from layer silicate clays in the presence of in 0.0032 M NaCl solution based on aqueous measurements by ICP-OES.

Subtask 1.3.1: Future Work

Additional characterization of the solid phases is necessary including XRD, SEM-EDS and BET post experiments as the dissolution and precipitation processes likely affected the surface area of the original minerals and led to secondary mineral formation. Lastly, additional sampling may be completed following removal of ammonia from batch samples via air stripping.

Future experiments will be conducted with synthetic groundwater solutions with variable bicarbonate for comparison to the original 3.2 mM NaCl and synthetic groundwater solutions. Further, a similar set of experiments will be conducted with solutions initially equilibrated with ammonia gas (instead of adding NH_4OH solutions). An emphasis will be placed on understanding the differences in redox conditions with liquid versus gas addition to better understand how the vadose zone might be altered during remediation with ammonia gas. Further, experiments investigating mineral dissolution kinetics may help understand the complex processes occurring in these systems including the timing of secondary mineral formation.

Subtask 1.3.1: Acknowledgements

Subtask 1.3.1: References

Altmaier, M., X. Gaona and T. Fanghanel (2013). "Recent advances in aqueous actinide chemistry and thermodynamics." *Chem Rev* **113**(2): 901-943.

Alwan, A. K. and P. A. Williams (1980). "The aqueous chemistry of uranium minerals. Part 2. Minerals of the liebigite group." *Mineralogical Magazine* **43**(329): 665-667.

Baeyens, B. and M. H. Bradbury (2004). "Cation exchange capacity measurements on illite using the sodium and cesium isotope dilution technique: Effects of the index cation, electrolyte concentration and competition: Modeling." *Clays and Clay Minerals* **52**(4): 421-431.

Bernhard, G., G. Geipel, V. Brendler and H. Nitsche (1996). "Speciation of uranium in seepage waters of a mine tailing pile studied by time-resolved laser-induced fluorescence spectroscopy (TRLFS)." *Radiochimica Acta* **74**(s1): 87-92.

Bernhard, G., G. Geipel, T. Reich, V. Brendler, S. Amayri and H. Nitsche (2001). "Uranyl (VI) carbonate complex formation: Validation of the Ca2UO2 (CO3) 3 (aq.) species." *Radiochimica Acta International Journal for Chemical Aspects of Nuclear Science and Technology* **89**(8/2001): 511.

Bickmore, B. R., K. L. Nagy, J. S. Young and J. W. Drexler (2001). "Nitrate-cancrinite precipitation on quartz sand in simulated Hanford tank solutions." *Environmental Science & Technology* **35**(22): 4481-4486.

Boggs, M. A., Z. Dai, A. B. Kersting and M. Zavarin (2015). "Plutonium(IV) sorption to montmorillonite in the presence of organic matter." *Journal of Environmental Radioactivity* **141**: 90-96.

Catalano, J. G., S. M. Heald, J. M. Zachara and G. E. Brown (2004). "Spectroscopic and diffraction study of uranium speciation in contaminated vadose zone sediments from the Hanford site, Washington state." *Environmental Science & Technology* **38**(10): 2822-2828.

Corbin, R. A., B. C. Simpson, M. J. Anderson, W. F. Danielson, J. G. Field, T. E. Jones and C. T. Kincaid (2005). Hanford soil Inventory Model Rev.1. Richland, WA, CH2M Hill Hanford Group, Inc.

Denham, M. E. and B. B. Looney (2005). Gas: A Neglected Phase in Remediation of Metals and Radionuclides. Aiken, SC, Savannah River National Laboratory**:** 1-23.

Dong, W. and S. C. Brooks (2006). "Determination of the formation constants of ternary complexes of uranyl and carbonate with alkaline earth metals (Mg2+, Ca2+, Sr2+, and Ba2+) using anion exchange method." *Environmental Science & Technology* **40**(15): 4689-4695.

Dong, W., T. K. Tokunaga, J. A. Davis and J. Wan (2012). "Uranium(VI) Adsorption and Surface Complexation Modeling onto Background Sediments from the F-Area Savannah River Site." *Environmental Science & Technology* **46**(3): 1565-1571.

Dresel, P. E., D. M. Wellman, K. J. Cantrell and M. J. Truex (2011). "Review: Technical and Policy Challenges in Deep Vadose Zone Remediation of Metals and Radionuclides." *Environmental Science & Technology* **45**(10): 4207-4216.

Gorman-Lewis, D., P. C. Burns and J. B. Fein (2008). "Review of uranyl mineral solubility measurements." *The Journal of Chemical Thermodynamics* **40**(3): 335-352.

Gorman-Lewis, D., J. B. Fein, P. C. Burns, J. E. Szymanowski and J. Converse (2008). "Solubility measurements of the uranyl oxide hydrate phases metaschoepite, compreignacite, Na–compreignacite, becquerelite, and clarkeite." *The Journal of Chemical Thermodynamics* **40**(6): 980-990.

Grenthe, I., H. Wanner and I. Forest (1992). "Chemical thermodynamics of uranium."

Guillamont, R., T. Fanghanel, I. Grenthe, V. Neck, D. Palmer and M. Rand (2003). Update on the Chemical Thermodynamics of Uranium, Neptunium, Plutonium, Americium and Technetium. *Chemical Thermodynamics*, OECD Nuclear Energy Agency. **5:** 959.

Guo, X., S. Szenknect, A. Mesbah, N. Clavier, C. Poinssot, S. V. Ushakov, H. Curtius, D. Bosbach, R. C. Ewing and P. C. Burns (2015). "Thermodynamics of formation of coffinite, USiO4." *Proceedings of the National Academy of Sciences* **112**(21): 6551-6555.

Heidmann, I., I. Christl and R. Kretzschmar (2005). "Sorption of Cu and Pb to kaolinite-fulvic acid colloids: Assessment of sorbent interactions." *Geochimica Et Cosmochimica Acta* **69**(7): 1675-1686.

Heidmann, I., I. Christl, C. Leu and R. Kretzschmar (2005). "Competitive sorption of protons and metal cations onto kaolinite: experiments and modeling." *Journal of Colloid and Interface Science* **282**(2): 270-282.

Kalmykov, S. N. and G. R. Choppin (2000). "Mixed Ca2+/UO22+/CO32-complex formation at different ionic strengths." *Radiochimica Acta International journal for Chemical Aspects of Nuclear Science and Technology* **88**(9-11/2000): 603.

Kaplan, D. I., B. Powell, L. Gumapas, J. T. Coates, R. A. Fjeld and D. P. Diprete (2006). "Influence of pH on Plutonium Desorption/Solubilization from Sediment." *Environ Sci Technol* **40**(19): 5937-5942.

Kaplan, D. I., B. A. Powell, D. I. Demirkanli, R. A. Fjeld, F. J. Molz, S. M. Serkiz and J. T. Coates (2004). "Influence of Oxidation States on Plutonium Mobility during Long-Term Transport through an Unsaturated Subsurface Environment." *Environ Sci Technol* **38**(19): 5053-5058.

Kaplan, D. I., K. A. Roberts, K. A. Schwehr, M. Lilley, R. Brinkmeyer, M. E. Denham, D. P. Diprete, H. P. Li, B. Powell, C. Xu, C. Yeager, S. Zhang and P. H. Santschi (2011). "Evaluation of a Radioiodine Plume Increasing in Concentration at the Savannah River Site." *Environ Sci Technol* **45**: 489-495.

Lagaly, G. and S. Ziesmer (2003). "Colloid chemistry of clay minerals: the coagulation of montmorillonite dispersions." *Advances in Colloid and Interface Science* **100**: 105-128.

Langmuir, D. (1978). "Uranium solution-mineral equilibria at low temperatures with applications to sedimentary ore deposits." *Geochimica et Cosmochimica Acta* **42**(6): 547-569.

Langmuir, D. (1997). *Aqueous Environmental Geochemistry*. Upper Saddle River, New Jersey, Prentice Hall.

Moyes, L. N., R. H. Parkman, J. M. Charnock, D. J. Vaughan, F. R. Livens, C. R. Hughes and A. Braithwaite (2000). "Uranium uptake from aqueous solution by interaction with goethite, lepidocrocite, muscovite, and mackinawite: An X-ray absorption spectroscopy study." *Environmental Science & Technology* **34**(6): 1062-1068.

Powell, B. A., A. B. Kersting, M. Zavarin and P. Zhao (2008). "Development of a Composite Non-Electrostatic Surface Complexation Model Describing Plutonium Sorption to Aluminosilicates." Los Alamos National Laboratory.

Qafoku, N. P., C. C. Ainsworth, J. E. Szecsody and O. S. Qafoku (2003). "Aluminum effect on dissolution and precipitation under hyperalkaline conditions: I. Liquid phase transformations." *Journal of Environmental Quality* **32**(6): 2354-2363.

Qafoku, N. P., C. C. Ainsworth, J. E. Szecsody and O. S. Qafoku (2004). "Transport-controlled kinetics of dissolution and precipitation in the sediments under alkaline and saline conditions." *Geochimica et Cosmochimica Acta* **68**(14): 2981-2995.

Qafoku, N. P. and J. P. Icenhower (2008). "Interactions of aqueous U (VI) with soil minerals in slightly alkaline natural systems." *Reviews in Environmental Science and Bio/Technology* **7**(4): 355-380.

Richter, A., F. Bok and V. Brendler (2015). "Data compilation and evaluation for U (IV) and U (VI) for the Thermodynamic Reference Database THEREDA."

Serne, J. (2012). Hanford Site Vadose Zone Sediment Mineralogy - Emphasis on Central Plateau. Richland, WA, Pacific Northwest National Laboratory.

Serne, R. J., G. V. Last, G. W. Gee, H. T. Schaef, D. C. Lanigan, C. W. Lindenmeier, M. J. Lindberg, R. E. Clayton, V. L. Legore and R. D. Orr (2008). Characterization of vadose zone sediment: Borehole 299-E33-45 near BX-102 in the B-BX-BY waste management area, Pacific Northwest National Laboratory (PNNL), Richland, WA (US).

Shvareva, T. Y., L. Mazeina, D. Gorman-Lewis, P. C. Burns, J. E. Szymanowski, J. B. Fein and A. Navrotsky (2011). "Thermodynamic characterization of boltwoodite and uranophane:

Enthalpy of formation and aqueous solubility." *Geochimica et Cosmochimica Acta* **75**(18): 5269-5282.

Szecsody, J. E., K. J. Cantrell, K. M. Krupka, C. T. Resch, M. D. Williams and J. S. Fruchter (1998). Uranium Mobility During In Situ Redox Manipulation of the 100 Areas of the Hanford Site. D. o. Energy. Richland, WA, Pacific Northwest National Laboratory**:** 41.

Szecsody, J. E., M. J. Truex, N. P. Qafoku, D. M. Wellman, T. Resch and L. R. Zhong (2013). "Influence of acidic and alkaline waste solution properties on uranium migration in subsurface sediments." *Journal of Contaminant Hydrology* **151**: 155-175.

Szecsody, J. E., M. J. Truex, L. Zhong, N. Qafoku, M. D. Williams, J. P. McKinley, Z. Wang, J. Bargar, D. K. Faurie and C. T. Resch (2010). Remediation of Uranium in the Hanford Vadose Zone Using Ammonia Gas: FY 2010 Laboratory-Scale Experiments, Pacific Northwest National Laboratory (PNNL), Richland, WA (US), Environmental Molecular Sciences Laboratory (EMSL).

Szecsody, J. E., M. J. Truex, M. J. Zhong, T. C. Johnson, N. P. Qafoku, M. D. Williams, W. J. Greenwood, E. L. Wallin, J. D. Bargar and D. K. Faurie (2012). "Geochemical and Geophysical Changes during Ammonia Gas Treatment of Vadose Zone Sediments for Uranium Remediation." *Vadose Zone Journal*: 1-13.

Szenknect, S., A. Mesbah, T. Cordara, N. Clavier, H.-P. Brau, X. Le Goff, C. Poinssot, R. C. Ewing and N. Dacheux (2016). "First experimental determination of the solubility constant of coffinite." *Geochimica et Cosmochimica Acta* **181**: 36-53.

Thoenen, T., W. Hummel, U. Berner and E. Curti (2014). "The PSI/Nagra Chemical Thermodynamic Database 12/07."

Um, W., J. P. Icenhower, C. F. Brown, R. J. Serne, Z. M. Wang, C. J. Dodge and A. J. Francis (2010). "Characterization of uranium-contaminated sediments from beneath a nuclear waste storage tank from Hanford, Washington: Implications for contaminant transport and fate." *Geochimica Et Cosmochimica Acta* **74**(4): 1363-1380.

Wan, J. M., T. K. Tokunaga, J. T. Larsen and R. J. Serne (2004). "Geochemical evolution of highly alkaline and saline tank waste plumes during seepage through vadose zone sediments." *Geochimica Et Cosmochimica Acta* **68**(3): 491-502.

Wan, J. M., T. K. Tokunaga, E. Saiz, J. T. Larsen, Z. P. Zheng and R. A. Couture (2004). "Colloid formation at waste plume fronts." *Environmental Science & Technology* **38**(22): 6066-6073.

Xue, Y., C. Murray, G. Last and R. Mackley (2003). Mineralogical and bulk-rock geochemical signatures of Ringold and Hanford formation sediments. Richland, WA, Pacific Northwest National Laboratories.

Zachara, J. M., C. Brown, J. Christensen, J. A. Davis, E. Dresel, C. Liu, S. Kelly, J. Mckinley, J. Serne and W. Um (2007). "A site-wide perspective on uranium geochemistry at the Hanford Site."

Zavarin, M., B. A. Powell, M. Bourbin, P. Zhao and A. B. Kersting (2012). "Np(V) and Pu(v) ion exchange and surface-mediated reduction mechanisms on montmorillonite." *Environ Sci Technol* **46**(5): 2692-2698.

Zhao, H., Y. Deng, J. B. Harsh, M. Flury and J. S. Boyle (2004). "Alteration of Kaolinite to Cancrinite and Sodalite by Simulated Hanford Tank Waste and its Impact on Cesium Retention." *Clays and Clay Minerals* **52**(1): 1-13.

Zhong, L., J. E. Szecsody, M. J. Truex, M. D. Williams and Y. Liu (2015). "Ammonia gas transport and reactions in unsaturated sediments: Implications for use as an amendment to immobilize inorganic contaminants." *Journal of Hazardous Materials* **289**: 118-129.

Subtask 1.3.2: Spectral Induced Polarization Response of Biofilm Formation in Hanford Vadose Zone Sediment

Subtask 1.3.2: Introduction

FIU has begun column experiments relating to the spectral induced polarization response of biofilm formation within vadose zone sediment. Significant uranium contamination at the U.S. Department of Energy Hanford Site exists within the vadose zone (up to 76 m) in the form of mobile carbonate phases (rutherfordine, liebigite) and silicate phases (uranophane, Na-boltwoodite). Remediation of this zone requires *in situ* sequestration of mobile uranyl-carbonate species (Szecsody et al. 2012).

The primary goal of this work is to analyze the ability of geophysical electrical methods, particularly spectral induced polarization (SIP) and electrical resistance tomography (ERT), to detect subsurface microbial activity in a porous medium. Remote geophysical sensing of the subsurface allows scientists to forgo the drilling of expensive boreholes and rely instead on easily and cheaply deployed surface arrays in order to study processes occurring deep in the subsurface. Geophysical methods also allow the continuous collection of data autonomously, which can be remotely accessed and analyzed. The second goal of this work is to measure and record changes in pore water characteristics after microbe injection in columns.

Column experiments at FIU consist of 1-D columns which will run continuously for several months.

Overview of 200 Area Subsurface

The underlying bedrock beneath Hanford is the Columbia River Basalt Group; it is composed of hundreds of individual tholeiitic basalt flows that formed during the Miocene (23.03 – 5.3 Ma). Above that lies the Ringold formation which is composed of fluvial sediments approximately 125 m thick and is divided into three principal stratigraphic units: unit A (fluvial gravels), the lower mud unit, and unit E (fluvial gravels). The main aquifer under the 200 West Area is located mostly within unit E; the lower mud unit forms a low hydraulic conductivity base to this aquifer and confines groundwater stored in unit A. Between the Ringold Formation and the Hanford formation lies the Cold Creek Unit (formerly Plio-Pleistocene unit) which has a thickness up to 13.1 meters and is divided into two subunits: the upper CCUz (abundance of silt) and lower CCUc (abundance of pedogenic calcium-carbonate cement). Above the Plio-Pleistocene unit lies the Hanford formation which is composed of Pleistocene (2.58 – 0.0117 Ma) age deposits from cataclysmic floods during the Ice Age. The main constituents of the Hanford Formation are three distinct facies: a gravel dominated facie, a sand dominated facie, and a silt dominated facie (Serne et al. 2002, Xie et al. 2003).

The water within the principal unconfined aquifer under Hanford flows from recharge zones in the west towards the NE, E, and SE and eventually discharges into the Columbia River. Estimates of discharge from the Hanford aquifer into the river range from 1.1 to 2.5 m^3/s, which is considered to be relatively low. The hydraulic gradient of the water table is gentler under the 200 East Area compared to the 200 West Area due to the effects of a higher subsurface hydraulic conductivity. This is on account of the fact that the top of the aquifer in the 200 East area lies within the Hanford formation which is more permeable than the Ringold formation (Hartman, Morasch and Webber 2007).

Subsurface contamination is split between the river corridor (wastes derived from the operation of the reactors, mainly strontium-90 and hexavalent chromium) and the Central Plateau (plutonium extraction activities, more varied waste streams). While most subsurface contamination at the 100 Area is strontium-90 and hexavalent chromium, there is a large plume of nitrate and a smaller plume of trichloroethene under the 100-F Area. In addition, all of the areas have nitrate concentrations greater than the maximum contaminant level (MCL) of 45 mg/L. Contamination within the central plateau includes carbon tetrachloride, nitrate, tritium, iodine-129, technetium-99, hexavalent chromium, and uranium. Downward migration of contaminants into the vadose zone and the groundwater was facilitated by the intentional and accidental addition of water from wastewater ditches and cribs, water pipe leaks, and meteoric water. Contamination within the vadose zone continues to supply the underlying groundwater with contaminants. Figure 67 shows a map of major contaminant plumes under the 200 East and 200 West Areas (DOE/RL-2015-07 2015).
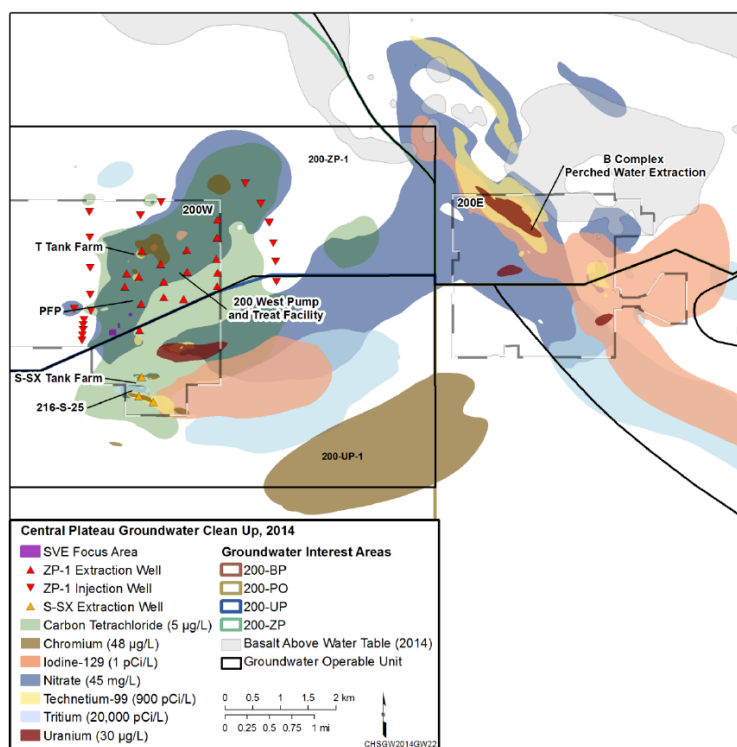
Figure 67. Contaminant plumes under the 200 Area taken from (DOE/RL-2015-07 2015).

Ammonia Injection

Contamination at the U.S. DOE Hanford Site has spread into the vadose zone and requires *in situ* remediation. The end goal of this remediation is the transformation of mobile uranium carbonate species into less mobile uranium silicates and phosphates. One proposed method is the injection of ammonia (NH_3) gas, which would partition into the pore water and cause an increase in the fluid pH. Ammonia gas injections are the preferred method over soluble amendments, such as injection of tripolyphosphate, due to the fact that liquid injections may lead to additional downward migration of contamination (Szecsody et al. 2012).

Szecsody et al. (2012) conducted experiments with ammonia gas injections using sediment samples collected from the Hanford Site 200 Area where uranium solid phases were identified as

Na-boltwoodite. Experimental results suggested that ammonia injections were most effective in reducing the mobility of aqueous and absorbed U species. This decrease is likely due to the incorporation of contaminants into precipitates formed during ammonia treatment. While the mobility of U(VI) in the Na-boltwoodite sample was lowered, XANES and EXAFS analysis conducted on the sample have not revealed any changes in the amount of Na-boltwoodite. This was interpreted as coating of some existing U-bearing solid phases by a low-solubility non-U precipitate, which would isolate them from the surrounding pore water. The sediment sample high in carbonates did not show a significant decrease in uranium mobility.

SIP Method

Electrical geophysical methods allow geophysicists to understand subsurface properties by measuring the voltage response to an electric current. Similar to standard DC resistivity methods, most induced polarization (IP) methods employ four electrodes in galvanic contact with the sediment. Two of the electrodes are current electrodes which act as source and sink for an electric current; the other two electrodes are potential electrodes which measure a voltage response. Spectral induced polarization (SIP) is a type of IP method that measures a phase shifted voltage at various injection frequencies. An impedance, in terms of magnitude and phase angle, is then obtained and used as a measure of charge transport and storage (Binley and Kemna 2005).

The SIP method allows geophysicists to quantitatively study charge storage and transport in porous media through the electrical complex conductivity. SIP has been used in the past to locate metallic ore bodies as well as subsurface zones rich in clay; however, recent work has focused on its applications in studying contaminant fate and transport. The injected current used for SIP measurements normally has a frequency below 1 kHz. The electrical complex conductivity (σ^*), the inverse of the complex resistivity ($\rho^*(\omega)$), is a function of ω (the angular frequency of the applied current). This can then be expressed in terms of σ' (the real part which represents charge transport) and σ'' (the imaginary part that represents charge storage). In the following equation defining the complex conductivity: $i = \sqrt{-1}$ (Hao et al. 2015)

$$\sigma^*(\omega) = \sigma'(\omega) + i\sigma''(\omega) \qquad \text{Eq 6}$$

The impedance can be obtained by measuring the difference between two voltage electrodes and is defined as:

$$Z^*(\omega) = \frac{U}{I} = |Z^*(\omega)|e^{i\varphi(\omega)} \qquad \text{Eq 7}$$

Where $Z^*(\omega)$ is the impedance, U is the voltage difference between the measuring electrodes (in V), I is the injected current (in A), ω is the angular frequency (in rad S^{-1}), and φ is the phase angle (in rad). The impedance can be related to the complex resistivity using a geometric factor K (in m) as:

$$\rho^*(\omega) = KZ^*(\omega) \qquad \text{Eq 8}$$

This geometric factor is based on the position of the electrodes, the size and shape of the samples, and boundary conditions on the grain surfaces. The complex conductivity is then just the inverse of the complex resistivity:

$$\sigma^*(\omega) = \frac{1}{\rho^*(\omega)} \qquad \text{Eq 9}$$

The conductivity magnitude can be expressed in terms of the real and imaginary components:

$$|\sigma| = \sqrt{(\sigma')^2 + (\sigma'')^2}$$ Eq 10

The phase angle can be described in terms of the components of the complex conductivity and an approximation can be made when the phase magnitude is less than 100 mrad. The phase angle is based on the ratio between the polarization and conduction (Okay et al. 2014):

$$\varphi(\omega) = \tan^{-1}\left[\frac{\sigma''(\omega)}{\sigma'(\omega)}\right] \cong \frac{\sigma''(\omega)}{\sigma'(\omega)}$$ Eq 11

There are two proposed mechanisms governing the low frequency polarization response, both relying on a structure known as the electrical double layer (EDL) at the solid-fluid interface. The EDL is formed when an electrolyte solution comes into contact with a charged surface; counterions from the solution are then attracted to the surface, forming two parallel charge layers of opposite polarity. Modern interpretation of the EDL actually designates three layers: the solid phase, the Stern layer, and the diffuse layer. The first theory asserts that at pore constrictions, where a pore becomes drastically thinner, the EDL comes together to form an ion selective membrane that would cause the charge to build up at those locations. The second theory argues that charge builds up when excess ions move at differing speeds in the Stern layer tangential to the solid surface (Scott 2006).

Scott (2006) conducted SIP measurements on sandstone samples saturated with an agar gel solution in order to prevent the motion of the bulk fluid during current injection. The results show that the quadrature conductivity is mainly unaffected by the use of an agar gel solution. This indicates that polarization is mainly controlled by grain surfaces rather than an ion selective membrane since ionic motion was constrained.

Skold et al. (2011) argues that there may exist a proton hopping mechanism at silica surfaces which may also contribute to polarization. This charge movement would be based on a Grotthuss cooperation mechanism where the charge moves along a surface through the breaking and reforming of hydrogen covalent bonds.

SIP Responses to Inorganic Factors

The specific surface area (S_p) is the ratio between the pore surface area and the pore volume. Generally, as grain size increases, specific surface area decreases due to the decreasing ratio between surface area and pore volume. There exists a positive correlation between the specific surface area and the imaginary conductivity (Lesmes and Friedman 2005).

Sediment clay content has been shown to have a positive correlation with both the in-phase and quadrature conductivities. Clays contribute greatly to the cation exchange capacity (CEC) of sediment, which is a measure of a sediments ability to absorb cations that in turn leads to higher quadrature conductivity. For kaolinite rich sediments, the quadrature conductivity increases in response to higher salinities; on the other hand, smectite rich sediments display a quadrature conductivity that is mostly independent of salinity (Okay et al. 2014).

Sediment grains generally have a negatively charged surface; however, if pH reaches the point of zero charge (PZC), the net surface charge becomes neutral, leading to reduced sorption of cationic groups. Reductions in pH below the PZC can lead to a positive surface charge as H^+ attaches to all negative sites on the grain surface. Low pH can reduce the effects of surface conductivity and polarization (Lesmes and Frye 2001).

SIP Responses to Subsurface Biofilm Formation

Bacteria in the subsurface are seldom found as solitary mobile organisms; rather, most microorganisms form interconnected immobile colonies known as biofilms. These biofilms are supported by extracellular polymers, which are the individual cells excrete and these polymers serve to strengthen attachment to a solid surface as well as to provide structural integrity to the biofilm. Biofilm formation can produce various changes in the physical and electrical properties of a porous medium; these changes include: clogging of pores (changes to porosity, permeability, and hydraulic conductivity), changes to overall shear strength and elastic moduli of media, production of proteinaceous extracellular appendages that facilitate electron transport and increase bulk electrical conductivity, alterations to pore fluid electrolyte concentrations, dissolution of minerals leading to increased surface roughness, and precipitation of magnetosomes (Atekwana and Slater 2009).

Modern research towards the direct detection of bacteria in subsurface porous media has placed a significant focus on the SIP method. Most bacteria have higher concentrations of anionic groups, which lead to a negatively charged cell wall; this in turn, when in the presence of an electrolyte solution, causes the formation of an EDL by counterions. Due to this effect, the bacterial surface can store charge when in the presence of a time-oscillating electric field in a fashion similar to charged mineral grains. Only bacteria that are alive contribute to the SIP response (Atekwana and Slater 2009).

Experiments using artificial biofilm consisting of alginate mixed with microbial cells in a silica bead packed column have shown significant low frequency (0.1 – 1 Hz) SIP responses to biofilm formation. By using artificial biofilm and silica gel beads with a very smooth surface area, this study isolated the SIP response to the actual presence of biofilm rather than grain roughness or changes in the chemical makeup of pore fluid (Ntarlagiannis and Ferguson 2008).

Methodology of Previous Column Experiments

Literature Research Overview

Johnson et al. (2013) used a column for the purpose of determining pore water saturation. The main focus of the geophysical measurements was to obtain bulk conductivity; however, a similar setup should be usable for SIP measurements. The column used plate electrodes at opposite ends as current source and sink; such a system allows for a homogeneous one dimensional current flow from source to sink along the length of the column. The potential gradient created by the current flow can then be measured using eleven Ag/AgCl electrodes placed flush along the column length. Since two potential electrodes are required for each measurement, this allowed for ten intervals for potential measurements. A standard resistor of known resistance was placed in the current loop in order to allow computation of resistance across electrodes using circuit analysis. The current used had a 1 Hz sinusoidal injection waveform.

Ntarlagiannis and Ferguson (2008) conducted column experiments on silica beads treated with artificial alginate biofilm. The experimental design used two Ag/AgCl coiled current electrodes at either end to supply current flow. The column had a length of 20 cm. Measurements were done using two pairs of potential electrodes, one pair 4 cm apart and a second pair 8 cm apart. In order to avoid polarization, the electrodes did not extend into the column. The artificial biofilm was a mix of alginate with a bacterial culture. The bacteria used were *Pseudomonas putida* 9816/11, which was cultured in 100 mL of nutrient broth at 37°C for 24 h. The general

methodology used for the experiments was as follows: before the experiments with the alginate/bacteria mix were conducted, a baseline SIP measurement was taken on a tap water saturated column as well as fluid flow measurements. Artificial biofilm was then injected with $CaCl_2$ to promote gelling (alginate requires Ca^{2+} to gel). The $CaCl_2$ was rinsed out using deionized water due to the fact that the presence of free Ca^{2+} and Cl^- ions would lead to an increase in the real conductivity. SIP measurements were then made on tap water saturated columns with the artificial biofilm present. The benefit of this approach is that it isolates the biological SIP response, although it may not properly represent the response in natural conditions.

Ntarlagiannis et al. (2005) studied the SIP response of iron and zinc sulfide biomineralization under anaerobic conditions in three columns. The three columns were as follows: one for electrical measurements (A), one for geochemical sampling (B), and a non-inoculated control (C). Both A and B were identical apart from the type of measurement being conducted. The geochemical sampling ports were extended into the center of the column and could affect current flow; so, the measurements were done on separate but identical columns. All three columns were 30.5 cm long with a diameter of 5.08 cm. The geochemical sampling column had seven ports positioned every 3.8 cm in order to coincide with the centers of each electrode pair on the electrical column; by extension, the electrical column had eight electrodes spaced 3.5 cm apart and flush against the surface, creating seven distinct measurement points. The electrodes were Ag-AgCl. The columns were filled with 20-30 mesh 99.8% quartz sand, which was packed by periodically tapping the column 15-20 times during filling. Since the experiment was designed to use anaerobic sulfate reducing bacteria, the columns were flushed with N_2 gas in order to evacuate any oxygen in the sand. The setup was contained within an anaerobic chamber.

Column Experiments at PNNL

PNNL column experiments, begun in spring 2016, were based on existing, currently operational columns, which were designed and constructed by a team under Dr. Brady Lee. The current setup uses a total of 14 columns; work at FIU uses only 6 columns. Using a large number of columns allows for testing of various variables simultaneously. Each column has one pair of potential electrodes for measurement at the middle of the column; there is also an injection point for the microbes under the lowermost electrode. The ends of each column contain two coiled Ag-AgCl current electrodes which provide homogeneous current flow parallel to the columns length. Figure 68 shows the basic setup of the electrodes on the column as well as an overview of the column construction. Figure 69 displays the makeup of the end caps that cover each end of the columns.

Figure 68. Structure of each column. C = Current Electrodes, P = Potential Electrodes, S = Microbe Injection Port.
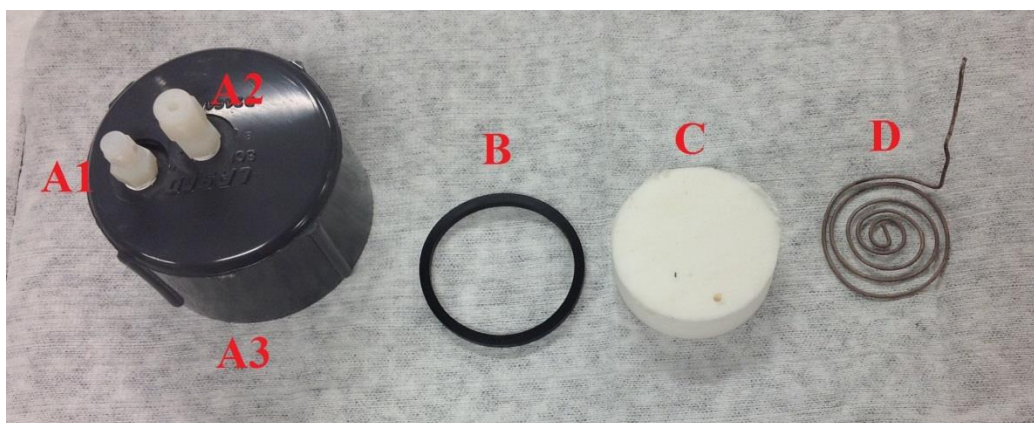
Figure 69. Various parts of end cap. A1 = current electrode port, A2 = influent/effluent port, A3 = end cap main body, B = rubber ring, C = porous plastic stopper, D = Coiled Ag-AgCl electrode.

Lessons Learned

Kemna (2014) provided several suggestions on the application of laboratory SIP experiments. From his overview, great care needs to be taken when working with unconsolidated sediments due to the fact that small differences in packing and water saturation can lead to significant differences in the SIP response even between identical samples. The samples should be saturated with solutions of known composition and enough time must elapse for chemical equilibrium to be established. At low frequencies (<1 kHz), a four electrode measurement array should be used.

Equipment should be calibrated against a reference resistor-capacitor circuit as well as water samples and the calibration should be thoroughly documented. Potential electrodes should not be within the current path; rather, they should be placed parallel to the path and flush against the sediment in electrolytic contact with the pore fluid.

Flow through the columns should be from bottom to top in order to ensure homogeneity in sediment fluid saturation over time. If the direction of the flow is from top to bottom, then fluid could penetrate at varying rates depending on the permeability of the sediment.

Electrodes should be non-polarizing and not penetrate into the sediment. Current electrodes should be placed at the ends of the column and should be plate or coiled electrodes in order to create a homogeneous flow of current from source to sink. Potential electrodes should be flush with the sediment. Experiments at PNNL use coiled Ag-AgCl for both current and potential electrodes.

In Ntarlagiannis et al. (2005), sulfate reducing bacteria migrated towards the nutrient source (influent from the bottom to the top of the column) and remained there, causing almost all sulfide mineral precipitation in the bottom of the column. This meant that although there were eight potential electrodes spaced throughout the column, only those near the bottom measured a significant change in the imaginary conductivity; electrode pairs closer to the effluent saw little change. It has also been noted during column experiments at PNNL that microbes can swim up the influent and potentially reach the source if barriers are not prepared in advance. The solution that scientists at PNNL devised was to connect IV drip tube air chambers (Figure 70) to the influent so that the solution would drip down rather than flow continuously and present a path for microbes to travel. Both these situations highlight that the movement of microbes introduced into columns should be considered in the experimental design.

When conducting geophysical column experiments, it is important to properly label all electrical and fluid connections to the columns; doing so reduces human error in regards to collecting data as well as injecting the correct solutions into the corresponding columns. Future column work will use six columns with five potential electrodes per column, including the current electrodes; this adds up to forty two electrical cables and twelve fluid tubes.

Figure 70. Air chambers used to prevent microbes swimming into influent; lines show flow of water through tubing. (A) Marks the pocket of air that prevents microbe migration.

Something to note is that experiments at PNNL have experienced some difficulty due to sediment from the column entering into the thin effluent tubing as well as the sample ports, blocking fluid flow and potentially creating excess back pressure. For future work, it would be beneficial to use some sort of filter on these ports that would allow water to pass through but not sediment. The sediment can clog up tubing and create high undesirable back pressure. This excess pressure can lead to the air chambers being filled with water, which could allow bacteria to swim up into the source; it can also cause tubing to pop off, creating small spills and allowing air bubbles to enter the column.

Subtask 1.3.2: Methodology

In June of 2016, researchers from PNNL arrived at FIU in order to build columns for SIP measurements. The general setup is pictured in Figure 71. There are six columns each with four potential electrodes and three sampling ports spaced equidistant on the sides. The potential electrodes are made from a silver wire encased within agar gel, this gel was prepared as a mix of agar and synthetic groundwater (Table 17) so that it would have a similar electrical conductivity to the adjacent pore water. The current electrodes are coiled Ag-AgCl and placed on either end. These columns contain approximately ~700 grams of sediments from the Hanford 200 Area. In in the center of each column is a region composed of 100 g autunite mixed with sediment. The body of the columns is composed of clear PVC. Within the ends of the columns are filters designed to stop sediment from entering the inlet tubing, there is also a 3D printed plastic disk with holes (~5 mm) at the ends to help support the filters.

Each column is fed solution from the bottom at a rate of 50 mL per day by an Ismatec peristaltic pump through a mix of flexible silicone and stiff Teflon tubing.. The solution that is pumped through the columns is sparged with Nitrogen for 10 minutes beforehand in order to remove dissolved gases, this is an effort to prevent gas bubbles from forming within the columns which can interfere with both geophysical measurements and pore water sampling.

There are four different solutions pumped through the columns (Table 17). These are: synthetic groundwater (column 1), synthetic groundwater + 3 mM HCO_3 (column 2), synthetic groundwater + 1 g/L glucose (columns 3 and 5), and synthetic groundwater + 3 mM HCO_3 + 1 g/L glucose (columns 4 and 6). The synthetic groundwater base solution is made using only stock solutions A + B since the current setup only has HCO_3 in three of the six columns. Each container has enough solution to last ten days at which point new solution needs to be made.

Table 17. Contents of Each Column

Column Contents	
Column 1	0 mM HCO_3
Column 2	3 mM HCO_3
Column 3	0 mM HCO_3 + 1g/L glucose
Column 4	3 mM HCO_3 + 1g/L glucose
Column 5	0 mM HCO_3 + 1g/L glucose+ Inoculum
Column 6	3 mM HCO_3 + 1g/L glucose+ Inoculum

The medium in which the microbes have been cultured is synthetic groundwater (SGW1). The table below shows the stock solutions (titled A, B, and C) used to make SGW1 and the process used to make SGW1 follows.

Table 18. Stock Solutions for SGW1

SGW1 Stock Solutions	Concentration (g/L)
A	
NaHCO₃	12.1
KHCO₃	1.6
B	
MgSO₄	3.06
CaSO₄	0.82
C	
Ca(NO₃)₂×4H₂O	5.43
CaCl₂×2H₂O	9.56

To create 1 L SGW1: Pipette 10 mL each of solutions A and C and 20 mL of solution B into 900 mL deionized water, then dilute to 1 L using deionized water. The SGW1 solution that was used also contained a concentration of yeast extract equal to 500 mg/L.

Microbes were cultured at PNNL in 50 mL SGW1 (with 500 mg/L yeast extract added beforehand) with approximately 500 mg Hanford sediment, 10 mg of autunite, and 50 mg glucose. On a weekly basis, a 1-mL sample of each culture is taken and transferred to a fresh container. Microbes originate from the sediment taken from a borehole and are naturally occurring in Hanford's vadose zone. Currently, the microbe species are unknown until DNA analysis can be conducted. These microbes were sent to FIU frozen and a new batch is being cultured at FIU in order to inject into columns five and six.

Spectral Induced polarization measurements are taken once a week. These measurements are taken using a National Instruments data acquisition card which is inserted in the PCI slot of a PC. The measurement is controlled by the proprietary software Signal Express made by National Instruments. Current is injected at twenty-one different frequencies spaced logarithmically ranging from 0.1 Hz to 10,000 Hz with an amplitude and phase measured for each. Signal Express records data for amplitude, phase, and frequency as ascii text files which are then analyzed using Python code written at FIU. In order to ensure reliability of measurements there is a reference resistor placed in circuit with the columns which has amplitude and phase measured in order to correct for measured amplitude and phase in the columns.

Pore water samples are taken once a week. These are taken by inserting a syringe into the sample ports and drawing water. Normally about 2 mL of sample is taken. Initial measurements are pH and conductivity (in mS/cm), samples are then stored in a fridge for future oxidation reduction potential (ORP) measurements.

Figure 71. Current experiment setup at FIU.
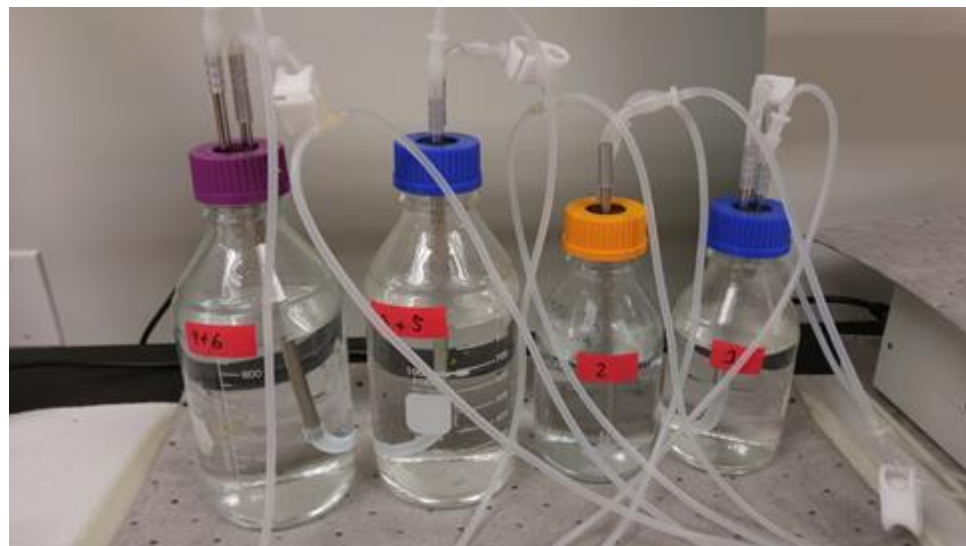
Figure 72. Containers with solution, each connected to a nitrogen bag and to the pump.

Subtask 1.3.2: Results and Discussion

Currently, no results have been obtained. Baseline measurements pre-microbe injection should be processed by the end of October and final results post-microbe injection by the end of calendar year 2016.

Subtask 1.3.2: Future Work

Bacteria are currently being cultured at FIU and will be injected in columns five and six during October 2016. During this period, both SIP and pore water samples will be taken which will allow comparison to pre-injection measurements.

Subtask 1.3.2: Acknowledgements

Subtask 1.3.2: References

Atekwana, E. A., and Slater, L. D., 2009, Biogeophysics: A new frontier in Earth science research: Reviews of Geophysics, v. 47, no. 4.

Binley, A., and Kemna, A., 2005, DC Resistivity and Induced Polarization Methods, *in* Rubin, Y., and Hubbard, S., eds., Hydrogeophysics, Volume 50, Springer Netherlands, p. 129-156.

DOE/RL-2015-07, R., 2015, Hanford Site Groundwater Monitoring Report for 2014, *in* U.S. Depertment of Energy, R. O. O., Richland, WA, ed.

Hao, N., Moysey, S. M., Powell, B. A., and Ntarlagiannis, D., 2015, Evaluation of Surface Sorption Processes Using Spectral Induced Polarization and a (22)Na Tracer: Environ Sci Technol, v. 49, no. 16, p. 9866-9873.

Hartman, M. J., Morasch, L. F., and Webber, W. D., 2007, Hanford Site groundwater monitoring for fiscal year 2006, Pacific Northwest National Laboratory Richland, WA.

Johnson, T. C., Oostrom, M., Truex, M. J., Thomle, J. N., and Wietsma, T. W., 2013, Determination of Water Saturation Using Gas Phase Partitioning Tracers and Time-Lapse Electrical Conductivity Measurements: Vadose Zone Journal, v. 12, no. 2, p. 0.

Kemna, A., 2014, An overview of the spectral induced polarization method for near-surface applications.

Lesmes, D. P., and Friedman, S. P., 2005, Relationships between the Electrical and Hydrogeological Properties of Rocks and Soils, *in* Rubin, Y., and Hubbard, S. S., eds., Hydrogeophysics: Dordrecht, Springer Netherlands, p. 87-128.

Lesmes, D. P., and Frye, K. M., 2001, Influence of pore fluid chemistry on the complex conductivity and induced polarization responses of Berea sandstone: Journal of Geophysical Research: Solid Earth, v. 106, no. B3, p. 4079-4090.

Ntarlagiannis, D., and Ferguson, A., 2008, SIP response of artificial biofilms: GEOPHYSICS, v. 74, no. 1, p. A1-A5.

Ntarlagiannis, D., Williams, K. H., Slater, L., and Hubbard, S., 2005, Low-frequency electrical response to microbial induced sulfide precipitation: Journal of Geophysical Research, v. 110, no. G2.

Okay, G., Leroy, P., Ghorbani, A., Cosenza, P., Camerlynck, C., Cabrera, J., Florsch, N., and Revil, A., 2014, Spectral induced polarization of clay-sand mixtures: Experiments and modeling: GEOPHYSICS, v. 79, no. 6, p. E353-E375.

Scott, J., 2006, The origin of the observed low-frequency electrical polarization in sandstones: GEOPHYSICS, v. 71, no. 5, p. G235-G238.

Serne, R. J., Bjornstad, B. N., Schaef, H. T., Williams, B. A., Lanigan, D. C., Horton, D. G., Clayton, R. E., Mitroshkov, A. V., Legore, V. L., and O'Hara, M. J., 2002, Characterization of vadose zone sediment: Uncontaminated RCRA borehole core samples and composite samples.

Szecsody, J. E., Truex, M. J., Zhong, L., Johnson, T. C., Qafoku, N. P., Williams, M. D., Greenwood, W. J., Wallin, E. L., Bargar, J. D., and Faurie, D. K., 2012, Geochemical and Geophysical Changes during Ammonia Gas Treatment of Vadose Zone Sediments for Uranium Remediation: Vadose Zone Journal, v. 11, no. 4, p. 0.

Xie, Y., Murray, C. J., Last, G. V., and Mackley, R., 2003, Mineralogical and bulk-rock geochemical signatures of Ringold and Hanford Formation sediments, Citeseer.

TASK 2: REMEDIATION RESEARCH AND TECHNICAL SUPPORT FOR SAVANNAH RIVER SITE

TASK 2: EXECUTIVE SUMMARY

Flow-through column experiments were conducted at the Florida International University (FIU) Applied Research Center (ARC) to estimate the sorption and desorption properties of humic acid onto Savannah River Site (SRS) sediment and to study the mobility of uranium through humic acid sorbed sediment. Previous studies have shown that humic acid sorbed to sediments will strongly bind with sediments at a mildly acidic pH. The use of humic acid could be applied to various DOE sites for contaminant stabilization; however, column studies are required to optimize this technology and prepare it for actual field deployment and regulatory acceptance. Experiments were designed to study the behavior of humic acid, specifically Huma-K, at different pH levels to help develop a model to predict the humic acid sorption/desorption. Furthermore, the application of sodium silicate for the restoration of alkalinity of acidic groundwater plumes at Savannah River Site F/H Area was investigated. The retention of U(VI) by SRS F/H area soil under circumenutral conditions (after sodium silicate application) was studied and the mechanism was elucidated. Last, desorption experiments were performed in order to research the potential re-mobilization of uranium under acidic and circumenutral conditions.

Subtask 2.1: Sodium Silicate Treatment For U(VI) Bearing Groundwater At F/H Area At Savannah River Site

Subtask 2.1: Introduction

The Savannah River Site (SRS) was established as one of the major sites for the production of materials related to the U.S. nuclear program during the early 1950s. An estimated 36 metric tons of plutonium were produced during the period 1953-1988. Since then, it has become a hazardous waste management facility responsible for nuclear storage and remediation of contaminated soil and groundwater from radionuclides. The groundwater at the F/H Area Seepage Basins Groundwater Operable Units at SRS was impacted by operations of the Hazardous Waste Management Facilities (HWMFs). Approximately 1.8 billion gallons (7.1 billion liters) and 1.6 billion gallons (6.0 billion liters) of low-level waste solutions have been received in the F and H areas, respectively, originating from the processing of uranium slugs and irradiated fuel at the separation facilities. The effluents were acidic (wastewater contaminated with nitric acid) and low-activity waste solutions containing a wide variety of radionuclides and dissolved metals. Waste solutions were transported approximately 3,000 feet from each processing area through underground vitrified clay pipes to the basins. After entering the basin, the wastewater was allowed to evaporate and to seep into the underlying soil. The purpose of the basins was to take advantage of the interaction with the basin soils to minimize the migration of contaminants to exposure points. Though the seepage basins essentially functioned as designed, the acidic nature of the basin influent caused mobilization of metals and radionuclides resulting in groundwater contaminant plumes.

Currently, more than 235 monitoring wells at the site are sampled for a variety of chemical and radioactive parameters. Groundwater monitoring results have indicated the presence of elevated levels of metals, radionuclides and nitrates. Significant chemical differences exist between the

groundwater from the two areas. The F Area groundwater contains higher concentrations of dissolved metals than that in the H Area. The constituents of concern (COCs) associated with the F Area HWMF groundwater plume are tritium, uranium-238, iodine-129, strontium-90, curium-244, americium-241, technetium-99, cadmium, and aluminum. The COCs in H Area are tritium, strontium-90, and mercury (Wan et al. 2012, Dong et al. 2012).

To remove contaminants from polluted groundwater, pump-and-treat and re-inject systems were implemented (Savannah River Nuclear Sloutions 2011). Downgrade groundwater within the system would be pumped up to a water treatment facility and then re-injected upgrade within the aquifer. This system was disconnected since the process incurred the risk of exposure to workers, generated a secondary waste stream that must be managed and was expensive, as well as time- and labor- intensive. In 2004, a funnel-and-gate process was implemented to carry out injections of alkaline solutions directly into the gates of the F-Area groundwater to raise pH levels. This approach allows for the creation of focused treatment zones and chemical stabilization of metals in those zones (*in situ* immobilization). Initial addition of sodium hydroxide revealed a decrease in uranium and strontium concentrations, but the concentration of iodine remained unaffected. Consequently, addition of carbonate solutions was investigated, but this solution eventually raised concerns about the re-mobilization of uranium previously contained within the treatment zone, due to the formation of highly soluble uranium-carbonate complexes. Furthermore, a systematic re-injection of carbonate solution would be required for the sustainability of circumneutral pH values in the treatment zone.

FIU-ARC is conducting research for the replacement of injection of carbonate alkaline solutions with sodium silicate. Sodium silicate is an alkaline solution that is favorable because it is environmentally benign with moderate to low cost (Baehr and Koehl 2007).

The main objective of these studies was to assess whether sodium silicate has sufficient alkalinity to restore the natural pH of the groundwater. Silica solutions have an inherent $pH \leq 10$, which complies with the regulatory constraints of injecting solutions of high pH values into subsurface systems. The optimal levels of sodium silicate for the restoration of circumneutral conditions were investigated, taking into account silica solubility levels in order to avoid clogging of the aquifer's permeability. Batch sorption and desorption kinetic experiments were performed, as well as experiments pertaining to soil characterization in an effort to elucidate the mechanism and provide further understanding of the process.

Subtask 2.1: Materials and Methods

Soil Samples, SRS Synthetic Groundwater and Other Stock and Working Solutions

Soil samples from the SRS F/H Area were sieved (USA Standard Testing Sieves, Fisher Scientific) and the fractions of mean diameter d<0.063, 0.063<d<0.18 and 0.18< d<2 mm were stored in a desiccator, which contains anhydrous calcium sulfate (Drierite, Drierite Company Inc), till further use .

Synthetic groundwater that mimics SRS groundwater characteristics was prepared according to Storm and Kabak (Storm and Kaback 1992) by dissolving 5.4771 g $CaCl_2$, 1.0727 Na_2SO_4, 3.0943 g $MgCl_2$, 0.3997g KCl and 2.6528g NaCl in 1 L of deionized water (Barnstead NANOpure water purification system). 1 mL of the stock solution was diluted into 1 L of deionized water acidified to pH 3.5 to create the working solution. Sodium silicate solutions

were created by dissolving the appropriate amount of $Na_2SiO_3 \cdot 9H_2O$ (reagent grade, MP Biomedicals) in deionized water. Sodium perchlorate and calcium chloride solutions were created by dissolving the appropriate amount of $NaClO_4$ and $CaCl_2 \cdot 6H_2O$ (Acros Organics, 99+%) analytical grade in deionized water. Similarly, Sr stock solution was prepared by dissolving the appropriate amount of $Sr(NO_3)$ (Fisher Scientific) in 2% HNO_3. Re working solutions were prepared by appropriate dilutions from a Rhenium standard for ICP (Fluka Analytical).

Sorption, Desorption and Sequential Extraction Experiments

All sorption experiments were performed by mixing solid (different fractions of SRS soil or mixtures of pure minerals in order to mimic SRS soil composition - Ottawa Sand standard 20-30 mesh by Fisher and $Al_2Si_2O_7 \cdot 2H_2O$ by Alfa Aesar) and SRS synthetic groundwater, resulting in a ratio of 20 g L^{-1} soil suspensions. Batch experiments of soil suspension in deionized water (pH 6.5) were also performed for comparison reasons. Each sample was spiked with the appropriate volume from a freshly prepared sodium silicate solution in order to achieve a final sodium silicate concentration of 70 mg L^{-1}. Preliminary experiments revealed that 70 mg L^{-1} sodium silicate is the appropriate amount in order to achieve circumneutral conditions. The initial concentration of uranium in all samples was 500 µg L^{-1}, whereas in the case of strontium and rhenium was 100 µg L^{-1}. Vials were agitated on a platform shaker at 120 rpm and all experiments were performed in triplicates. In order to study the effect of ionic strength, samples were spiked with the appropriate amount of $NaClO_4$, in order to obtain a final concentration of 0.001, 0.01 and 0.1 M. Similarly, in order to study the potential competition of uranium with calcium and magnesium as far as sorption is concerned, appropriate amounts of $CaCl_2$, $Ca(NO_3)_2$ and $Mg(NO_3)_2$ were added to the samples and a range of 0.0001-0.01 M Ca^{+2} and Mg^{2+} was achieved. Control samples (no addition of electrolyte) were also studied, which already contain concentrations of Ca^{2+} $2.5 \cdot 10^{-5}$ M and Mg^{2+} $1.5 \cdot 10^{-5}$ M.

Desorption experiments were performed by replacing the metal-bearing aqueous phase past the equilibration, by equal volume of deionized water or SRS synthetic groundwater.

Sequential extractions experiments followed BCR (Community Bureau of Reference) protocol. More specifically, after the initial sorption step, 1 g of the metal-laden bulk fraction of the solid (180µm<d<2mm) was suspended in 40 ml 0.11 M CH_3COOH and was shaken at room temperature for 16 h at 120 rpm. The extract was separated from the solid residue by centrifugation for 10 min (5000 rpm) and decanted into a polyethylene container and stored in a refrigerator at 4∘C for analysis. The residue was washed with 10 ml of deionized water by shaking for 10 min, centrifuged and the washings discarded. Step 1 aims to determine the exchangeable and acid soluble fraction of sorbed uranium. The second step involved the suspension of the solid in 40 mL of 0.5 M hydroxylamine hydrochloride ($H_2NO \cdot HCl$, Alfa Aesar), pH 1.5, acidified with HCl, and the extraction procedure was performed as described above. The goal of step 2 is the determination of uranium bound to Fe and Mn oxides. Subsequently, the solid was treated with 10 mL of H_2O_2 for 1h at room temperature, followed by 1 more hour treatment at 85 °C water bath, until the reduction of initial volume to less than 2 ml. 50 mL of $NH_4CH_3CO_2$ 1M, pH 2 adjusted with HNO_3 acid, were introduced. The suspension was shaken for 16 h at room temperature at 120 rpm and the extraction procedure was repeated, as described above. Step 3 provides information on the oxidisable fraction of sorbed uranium. The residual amount of retained uranium was calculated by subtracting the sum of the fractions

mentioned above from the total mass of sorbed uranium (Rauret et al. 1999). The steps are summarized in Table 19.

Table 19. Procedure of BCR Sequential Extraction (He et al. 2013, Zemberyova, Bartekova and Hagarova 2006)

Target phase	Reagents	Conditions
Exchangeable, water and acid-soluble	40 mL 0.11M CH$_3$COOH	16 h, room temperature
Reducible (Fe and Mn oxides)	40 mL 0.5M NH$_2$OH-HCl (pH 1.5)	16 h, room temperature
Oxidisable (Organic matter and sulfides)	10 mL 8.8M H$_2$O$_2$, 50 mL 1M NH$_4$CH$_3$CO$_2$ (pH2)	1 h, room temperature 1 h, 85°C
Residual	HNO$_3$-HCl digestion	

SEM-EDS & Specific Surface Analyses

The morphology and elemental composition of the SRS soil fractions were investigated using scanning electron microscopy equipped with energy dispersive spectroscopy (SEM-EDS) at the Florida Center for Analytical Electron Microscopy located on the Florida International University Modesto A. Maidique Campus (MMC). Samples were initially dried in a conventional oven at 30ºC for a period of 5 days. Specific amount of each SRS soil fraction was placed on a stainless steel stub and the exact weigh was recorded. Any required gold coating was done with an SPI-Module Control and Sputter unit for 2 minutes to produce a thin layer of gold. The SEM system used was a JOEL-5910-LV with acceleration potentials ranging from 10 to 20 kV. EDS analysis was produced using an EDAX Sapphire detector with UTW Window controlled through Genesis software.

Specific surface and pore size distribution for three different SRS soil fractions, namely d<63μm, 63<d<180μm and d>180μm, were determined by means of nitrogen gas adsorption and BET isotherm at the Department of Mechanical Engineering at FIU.

Elemental analysis

The residual uranium concentration in the samples was analyzed by means of kinetic phosphorescence analysis (KPA-11, Chemchek Instruments Inc.). Iron, calcium, magnesium, strontium and rhenium were determined by means of inductively coupled plasma - optical emission spectroscopy (ICP-OES 7300 Optima, Perkin Elmer). Rhenium (Re) was chosen as a chemical analog of technetium (Tc) under oxidizing conditions, due to their similarities in cationic radius and geochemical behavior (Icenhower et al. 2008).

Subtask 2.1: Results and Discussion

Kinetic Experiments with SRS Soil

SRS soil was sieved and the fractions of average particle diameter d<63 μm, 63 μm<d<180 μm and 180μm<d<2mm (called fine, intermediate and coarse fraction, respectively) were obtained and stored in a desiccator containing anhydrous calcium sulfate (Drierite, Drierite Company

Inc.), till further use. The results of uranium retention by each soil fraction as a function of time are presented in Figure 73.

The establishment of equilibrium is achieved within 24h for the coarse fraction; whereas the equilibrium for the fine and the intermediate fraction is almost instantaneous (equilibrium is achieved within 1h). Furthermore, the uranium removal efficiency at equilibrium varied: 60%, 80% and 100% for the coarse, intermediate and fine fraction, respectively. Despite having used the same amount of mass in each experiment, the surface area among the different fractions varies significantly. Hence, the results were expressed as per cent uranium removal and not as q (mg U(VI) sorbed per g of soil). Nevertheless, it is clear that in the case of intermediate and fine fractions, all the experimental points in the figure are part of the equilibrium, whereas in the case of the coarse fraction, there is a gradual increase of uptake up to 24 h.
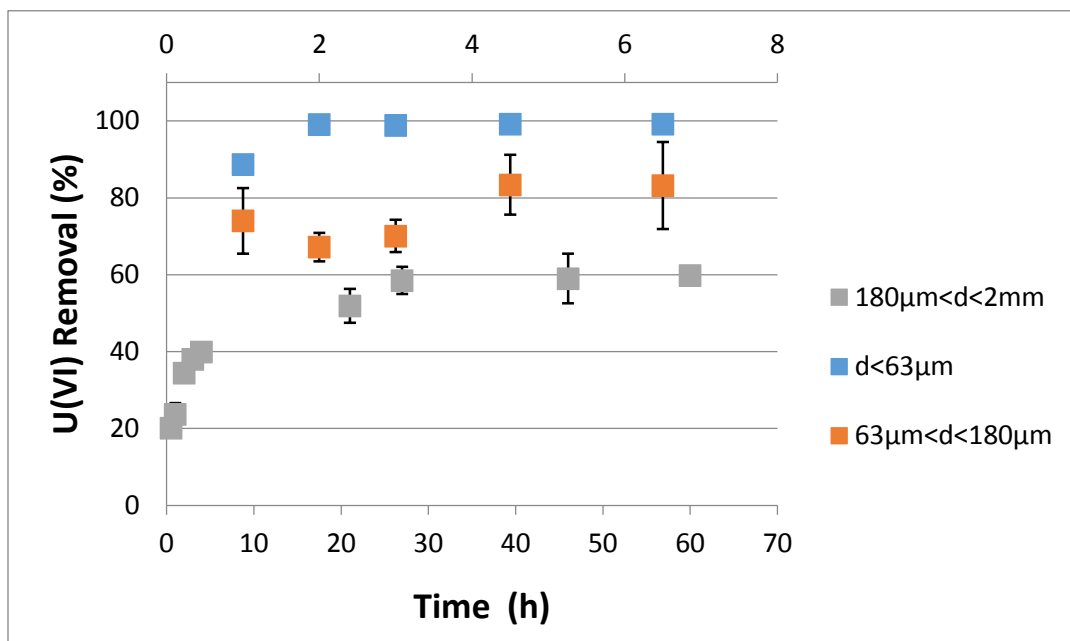
Figure 73. Uranium removal as a function of time for different fractions of SRS soil.

SEM-EDS Analysis of Different Soil Fractions

A specific amount of each soil fraction was placed on SEM stubs on an analytical scale and the exact mass was recorded. Triplicate homogeneous samples were prepared for each fraction and EDS analysis was performed in multiple locations of each sample. In Table 20, the elemental analysis of each fraction for Fe, Al and Si is presented.

**Table 20. Concentration of Fe, Al and Si for Each SRS Fraction
Followed by Relative Standard Deviation**

SRS Soil Fraction	U(VI) % Removed	[Fe] (mg/g)	[Al] (mg/g)	[Si] (mg/g)
d<63μm	99±0.2	89±2	72±4	396±3
63μm<d<180μm	79±8	70±11	71±5	389±4
180μm<d<2mm	59±1	40±4	54±13	416±37

The concentration of Fe differs significantly among the three fractions, whereas the concentration of Al and Si remains statistically the same throughout the fractions. The presence of Al and Si is due to kaolinite and quartz, whereas the presence of Fe is associated with goethite. Table 20 reveals a trend of higher uranium removal when the average particle diameter of the soil decreases. Nevertheless, the increase in uranium uptake could be attributed to two factors: the increase of iron concentration and/or the increase of surface area. It can be seen clearly in the SEM photos of different fractions that the smaller the average particle diameter, the larger the surface area (Figure 74), as evidenced by BET measurements (Table 24).
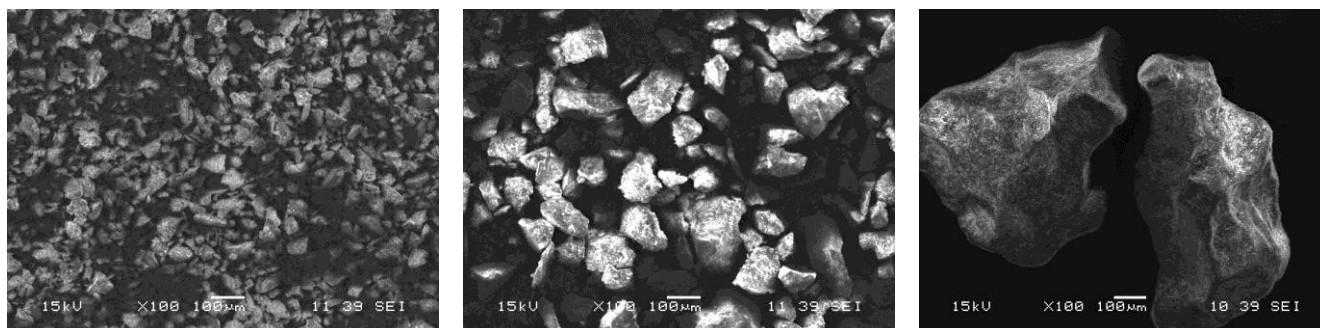
Figure 74. SRS soil fraction d<63 μm (left), 63<d<180 μm (middle) and 180 µm<d<2mm (right).

BCR Sequential Extraction Experiments

The theory behind sequential extraction protocols is that the most mobile metals are removed in the first fraction and continue in order of decreasing of mobility (Zimmerman and Weindorf 2010). In an attempt to provide an internationally accepted sequential extraction protocol, a modified BCR (Community Bureau of Reference or now the Standards, Measurements and Testing Program of the European Commission) sequential extraction procedure was developed (Rauret et al. 1999). This procedure is largely similar to that produced by Tessier (Tessier, Campbell and Bisson 1979), with the chief difference in the first fraction of the procedure. Instead of evaluating the exchangeable and carbonate bound separately, the BCR procedure combines both in the first fraction (Ure et al. 1993). The results of BCR sequential extraction for U(VI) sorbed on SRS soil (180μm<d<2mm) are presented in Table 21.

.

Table 21. Percentage of U(VI) Recovered in Each Stage of BCR Sequential Extraction Protocol

BCR target phase	U(VI) recovery %
Exchangeable, water and acid soluble	83 ± 7
Reducible form - bound to Fe and Mn oxides	10 ± 1
Oxidisable form – bound to organic matter and sulfides	2 ± 1
Residual	5 ± 4

The majority of the uranium that was retained by the bulk fraction of SRS soil (180μm<d<2mm) was recovered in the first step of the process, indicating that uranium that is uptaken by the soil is found mostly in acid soluble form. Nevertheless, the desorption experiments that involved uranium-loaded soil and deionized water (pH 6.5) as a desorbing agent, revealed practically no recovery of uranium. These results suggest that sorbed uranium on SRS soil may be re-mobilized only by acidic agents, such as 0.11 M CH_3COOH, that was used during step 1. Ten percent of the total uranium retained is associated to iron oxides (Table 21), since SRS background soil from the F/H area does not contain a significant amount of manganese oxides, as it can be seen in Table 22. The amount of uranium in oxidisable and residual form was practically found negligible, given the experimental error. The background soil from SRS F/H Area is a low organic, quartz dominated soil (Dong et al. 2012); hence, the experimental results were rather expected. Typically, metals of anthropogenic activity tend to accumulate in the first three phases and metals found in the residual fraction are metals of natural occurrence incorporated in the crystal lattice of the parent rock (Tessier et al. 1979, Ratuzny, Gong and Wilke 2008).

Table 22. Adaptation of Elemental Composition of SRS F/H Area Background Soil Obtained by Means of X-Ray Fluorescence, courtesy of Dr. Miles Denham

Mineral phase	SRS F/H area soil percentage (%)
Quartz	92 ± 4
Kaolinite	6 ± 2
Goethite	1.0 ± 0.5
MnO_2	<0.01

Kinetic Experiments with Mixtures of Pure Minerals

This set of experiments comprised of 2 different batches: the first contained plain quartz (Ottawa sand, 20-30 mesh) and the second contained 95% of quartz and 5% of kaolinite ($Al_2Si_2O_7 \cdot 2H_2O$), a concentration mimicking the ratio of quartz and kaolinite in the actual SRS F/H Area (Table 22). The results of the batch kinetic experiments are presented in Figure 75. The kinetic results, including those of the coarse fraction of the SRS soil (180 μm<d<2 mm) for comparison reasons, are presented in Figure 76.

The uranium removal efficiencies of quartz and the quartz and kaolinite mixture at equilibrium are quite close: 16% and 20%, respectively. Results suggest that the presence of kaolinite does not contribute significantly in uranium removal under the conditions studied (pH 6.7, 5%

kaolinite in the mineral mixture). In the case of quartz, equilibrium is established within 1 h, whereas in the case of the quartz and kaolinite mixture, equilibrium is gradually established after 3-4 h. The initial slope of the line before the establishment of equilibrium is 3.2 h^{-1} for quartz and kaolinite and 13 h^{-1} for plain quartz. The lower uptake rate for quartz and kaolinite, as well as the larger amount of time required to reach equilibrium, may be indications of diffusion phenomena, due to coating of the surface of quartz by fine kaolinite particles. Similarly, the uptake of U(VI) by the coarse fraction of SRS soil was even slower (equilibrium was reached after 24 h), but on the other hand, the removal efficiency at equilibrium was much higher (60%). This result suggests that the presence of goethite in SRS soil enhances the U(VI) uptake at circumneutral conditions.
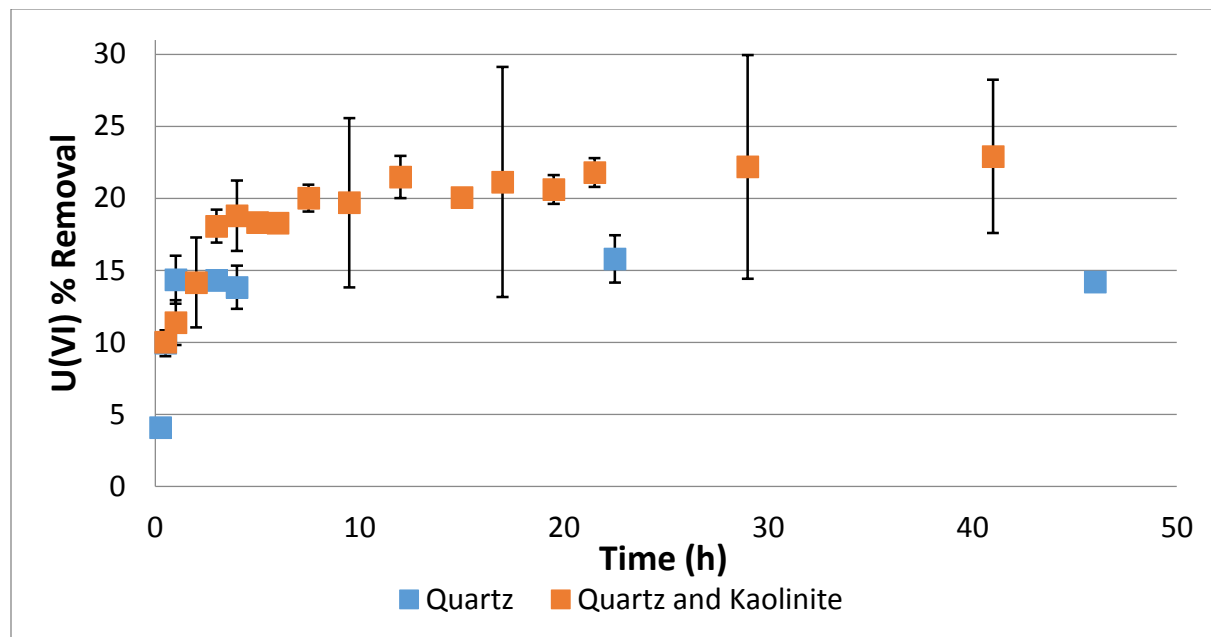
Figure 75. U(VI) percent removal as a function of time for pure quartz and quartz and kaolinite mineral mixtures.
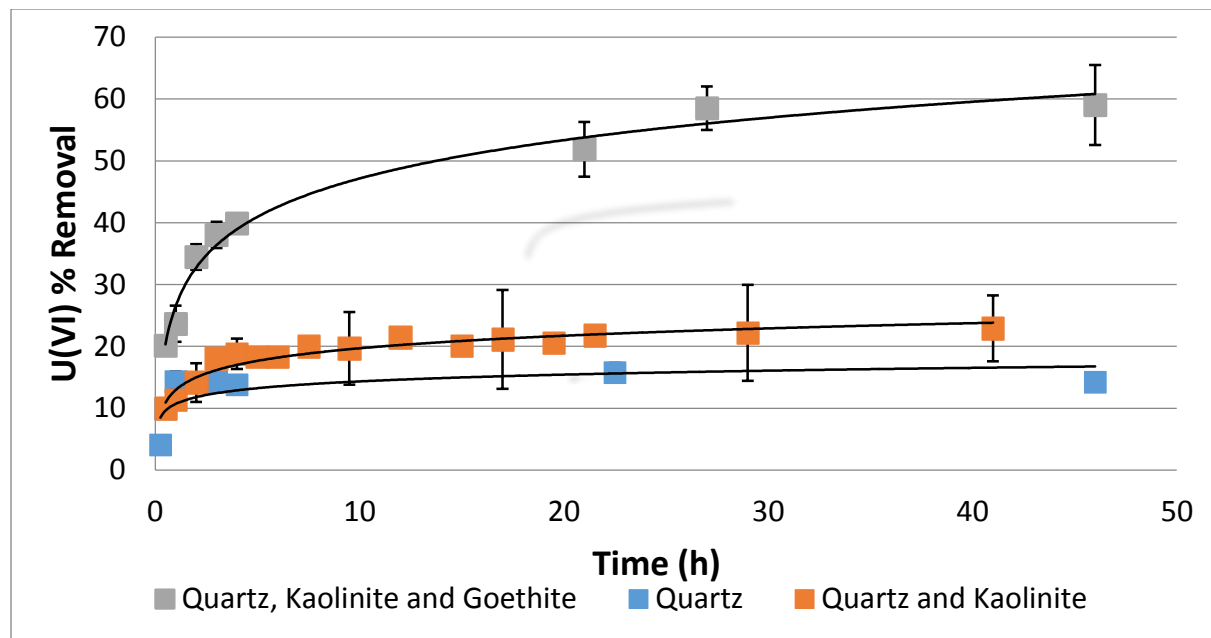
Figure 76. U(VI) per cent removal as a function of time for pure quartz and quartz and kaolinite mixtures, as well as SRS soil coarse fraction (180 μm<d<2 mm).

Desorption Experiments

After the establishment of the sorption equilibrium for the mixtures of pure minerals and the SRS coarse fraction, the supernatant was discarded and 10 ml of synthetic SRS groundwater were reintroduced. The new mixture was left to equilibrate for another 24 hours at room temperature and the U(VI) concentration released in the aqueous phase was determined. Similar experiments with deionized water (pH~6.5) in the place of synthetic groundwater were performed. Results are summarized in Table 23.

Table 23. U(VI) Removal by Each Experimental Set, Followed by the Percentage of U(VI) Released in the Aqueous Phase, as a Result of Contact with SRS Synthetic Groundwater (Desorption).

Soil Type	U(VI) % Removal	U(VI) % Recovery (SRS GW)
Quartz	16±2	109±13
Quartz and Kaolinite	22±1	99±12
Quartz, Kaolinite, Goethite (SRS soil, 180 μm<d<2 mm)	59±6	61±5

The results indicate that when the mineral mixture comprises of quartz and kaolinite, the amount of uranium removed is much lower compared to the removal percentage of SRS background soil. This suggests that goethite is the most reactive mineral phase towards U(VI) under circumneutral conditions, as discussed above. Furthermore, the amount of U(VI) sorbed is quantitatively released in the aqueous phase, upon contact with SRS synthetic groundwater in the case of quartz and quartz and kaolinite mixture. On the other hand, desorption was significantly less in the experiments with SRS background soil, which contains goethite as well, indicating that goethite contributes to stronger binding of U(VI). Possible reasons contributing to higher U (VI) sorption

and lower desorption may be the higher surface area provided by goethite particles, as well as Fe-U(VI) interactions (Cornell and Schwertmann 2003, Jolivet, Henry and Livage 2000).

The specific surface area of the different SRS soil fractions are summarized in Table 24. For comparison reasons, iron content of each SRS soil fraction and the corresponding sorption and desorption results are compiled in Table 25.

The results of Table 25 show that despite the 3- and 4- fold increase in the specific surface area among the different SRS soil fractions, sorption per surface unit decreases. These results imply that the phenomenon may not be dominated by physical sorption. If sorption was strictly a surface phenomenon (physical sorption, no specificity of the adsorbent towards the adsorbate), a positive, proportional correlation between surface and sorption efficiency would be expected, while the opposite case suggests the involvement, to some degree, of interaction between uranium species with active groups (Anagnostopoulos, Koutsoukos and Symeopoulos 2015, Anagnostopoulos et al. 2016).

Table 24. BET specific surface area results

SRS Soil Fraction	BET Surface Area
d<63μm	8.4 ± 0.12 m²/g
63μm <d<180μm	2.8 ± 0.1 m²/g
180μm<d<2mm	0.41 ± 0.01 m²/g

Table 25. Iron Concentration of Each SRS Fraction Alongside Sorption and Desorption Results for the Different Fractions

SRS Soil Fraction	[Fe] (mg/g)	Sorption		Desorption
		U(VI)% Removal	μg U(VI) Sorbed/ m² of soil	U(VI)% Recovered
d<63μm	89 ± 2	96 ± 0.4	3.1 ± 0.02	63 ± 3
63μm <d<180μm	70 ± 7	90 ± 2	8.7 ± 0.2	74 ± 4
180μm<d<2mm	40 ± 4	60±0.5	35 ± 0.4	61 ± 5

Furthermore, desorption remains practically the same when SRS groundwater (pH 3.5) is used.

Investigation of Ion Exchange Mechanism

In order to investigate if ion exchange is involved in the retention of U(VI) by SRS background soil from the F/H Area, different sets were prepared: batch experiments were conducted in the presence of sodium silicate (pH ~6.5) and without sodium silicate (pH ~3.5), as well as with and without uranium. The purpose was to track the amount of Ca, Mg, Al and Fe in the aqueous phase in the presence and absence of uranium to investigate if they affect the removal of uranium. The different sets are summarized in Table 26.

.

Table 26. Schematic Representation of the Different Batch Experiments Conducted in Order to Investigate the Effect of Cations on the Uranium Sorption onto SRS Sediment

Code	U(VI), 0.5 ppm	Sodium silicate (70 ppm) amendment	Medium	pH
A	x		SRS GRW	3.5
B	x	x	SRS GRW	6.5
C			SRS GRW	3.5
D		x	SRS GRW	6.5

In Table 27, the average concentration of Ca and Mg in the aqueous phase is presented, followed by the standard deviation for all samples (A-D). A comparison of the concentration of Ca and Mg reveals that there are significantly greater concentrations of these cations in the supernatant solution compared to the composition of synthetic SRS groundwater. This result suggests that amounts of Ca and Mg could leach from the soil into the aqueous phase, despite the fact that calcium and magnesium oxides comprise a very small fraction of SRS sediment. Furthermore, results suggest that the amount of calcium and magnesium in the aqueous phase is not pH dependent, since the pH for code samples A and C is 3.5 whereas for code samples B and D the pH value is 6.5 (sodium silicate amendment). Similarly, the presence of uranium in the samples does not seem to affect the amounts of magnesium in the aqueous phase (code samples C and D do not contain uranium). Uranium removal for the code A samples (pH 3.5) was found to be zero while for code B samples (pH 6.5) was found to be $60 \pm 4\%$, consistent with all the previous experiments. On the other hand, a small difference in the amount of calcium released in the aqueous phase was observed in the presence of uranium, implying that there may be some limited ion-exchange between calcium and uranium during uranium sorption. Finally, there seems to be no difference between the different time intervals (day 1 and 2), something rather expected since in previous kinetic experiments, the equilibrium was found to be established in less than 24 hours.

In Table 28, the average concentration of Al and Fe in the aqueous phase is presented, followed by the standard deviation for all samples (A-D). The presence of Al and Fe in solution can be traced back to the soil composition (kaolinite and goethite respectively), since SRS synthetic groundwater does not contain any of these elements.

Table 27. Ca and Mg Concentrations Detected in the Aqueous Phase followed by Relative Standard Deviation

		A	B	C	D
Day 1	**Ca (ppm)**	2.2 ± 0.1	2.6 ± 0.3	1.8 ± 0.1	1.7 ± 0.1
	Mg (ppm)	0.8 ± 0.01	0.8 ± 0.03	0.70 ± 0.01	0.70 ± 0.02
Day 2	**Ca (ppm)**	2.1 ± 0.3	2.0 ± 0.1	1.7 ± 0.01	1.6 ± 0.04
	Mg (ppm)	0.72 ± 0.01	0.71 ± 0.04	0.67 ± 0.01	0.68 ± 0.03
SRS.GRW	**Ca (ppm)**	0.50 ± 0.03			
	Mg (ppm)	0.35 ± 0.01			

Table 28. Al and Fe Concentration Detected in the Aqueous Phase Followed by Relative Standard Deviation

		A	**B**	**C**	**D**
Day 1	Al (ppm)	0.71 ± 0.08	0.66 ± 0.07	0.66 ± 0.09	0.56 ± 0.1
	Fe (ppm)	0.32 ± 0.1	0.39 ± 0.01	0.28 ± 0.1	0.41 ± 0.2
Day 2	Al (ppm)	0.51 ± 0.04	0.44 ± 0.05	0.51 ± 0.01	0.42 ± 0.1
	Fe (ppm)	0.12 ± 0.09	0.25 ± 0.1	0.13 ± 0.03	0.20 ± 0.1
SRS.GRW	Al (ppm)	0			
	Fe (ppm)	0			

The levels of iron and aluminum are similar across all the groups at day 1, indicating that the leaching of iron and aluminum into the aqueous phase is not pH dependent and is not affected by the presence of uranium in the aqueous phase. On the other hand, the levels of iron and aluminum during the second day, although similar across the samples, are lower than the respective values of the first day. A possible explanation for this pattern may be the secondary precipitation of iron and aluminum at the respective pH values.

Finally, identical batch experiments (pH 3.5 and 6.5 after sodium silicate amendment) were carried out, but instead of using SRS synthetic groundwater, deionized water (DIW) was introduced in the samples. In the sorption experiments of U onto SRS sediment in deionized water with and without the addition of sodium silicate (pH 3.5 and 6.5 respectively), U(VI) removal was very similar when compared to the experiment with SRS synthetic groundwater: at pH 3.5 removal was zero, while at pH 6.5 removal was found to be $64\pm7\%$. This implies that the presence of several cations, like Na^+, K^+, Ca^{2+} and Mg^{2+}, in the concentration range typical for the SRS groundwater, has little or no interference with U(VI) sorption onto the sediment. The amount of calcium, magnesium, aluminum and iron leached from the sediment in the aqueous phase (DI water) is summarized in Table 29.

Table 29. Ca, Mg, Al and Fe Concentrations in the Aqueous Phase Followed by Relative Standard Deviation for All the Samples

	pH 3.5	**pH 6.5**
Ca (ppm)	2.7 ± 0.3	2.8 ± 0.2
Mg (ppm)	0.75 ± 0.2	0.72 ± 0.1
Al (ppm)	0.40 ± 0.03	0.44 ± 0.01
Fe (ppm)	0.24 ± 0.08	0.36 ± 0.1

Effect of Ionic Strength and Divalent Cation Competition Studies

The experiments were conducted by bringing 400 mg of SRS soil of mean particle diameter 0.18<d<2mm in contact with 20 ml of SRS synthetic groundwater pH 3.5 bearing 500 ppb of U(VI). Seventy (70) ppm of sodium silicate was added to achieve circumneutral conditions and then different quantities from a stock solution of $NaClO_4$ were added in order to achieve the

desired electrolyte concentrations. The concentrations of NaClO$_4$ were 0.0001, 0.001. 0.01 and 0.1 M. The results are presented in Figure 77.
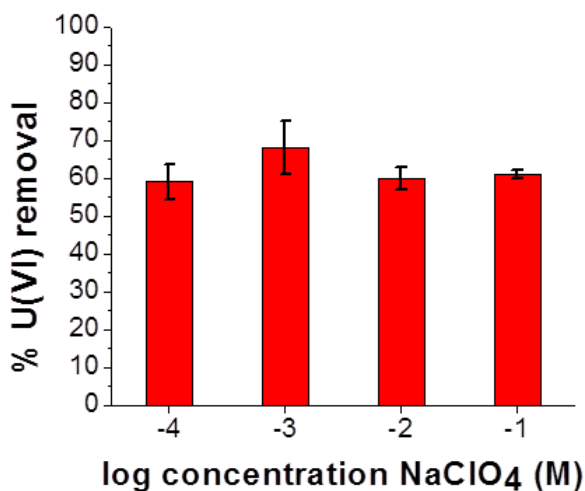
Figure 77. U(VI) per cent removal as a function of electrolyte concentration using NaClO$_4$ (x-axis is in logarithmic scale). Error bars represent relative standard deviation.

The retention of cations from mineral surfaces is frequently described by the surface complexation model. Surface complexation involves the formation of direct bonds between metal cations and surface –OH groups and/or O atoms and comprises of two different types of complexes: the outer-sphere complexes and the inner-sphere complexes (Wu, Laird and Thomson 1999). In the case of inner-sphere complexation, the ions are bound directly to the surface site (Figure 78). On the other hand, in outer-sphere complexation the ion is presumed to bind to the surface site by chemical bonds without losing the hydration shell, meaning that the water molecule is located between the ion and binding site (Figure 78). The distance to the surface is larger and the bond strength is weaker in comparison to inner-sphere complexation (Worch 2015). Outer-sphere complexation takes place in the double layer (as opposed to inner-sphere complexation, which takes place on the surface), where an excess of counter-ions are located, neutralizing surface charge. The double layer decreases with ionic strength (electrolyte concentration) increase and hence, outer-sphere complexes are presumed to be susceptible to coulombic interactions (Sherwood Lollar 2005).
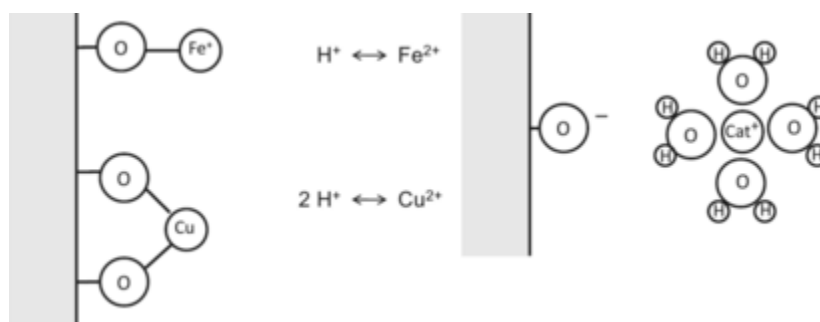
Figure 78. Example of inner-sphere complexation (left) and outer-sphere complexation (right), as adapted by Sigg and Stumm, Aquatic Chemistry (Sigg and Stumm 2011).

Hence, ions that form outer-sphere complexes exhibit reduced sorption with ionic strength increase whereas ions that form inner-sphere complexes are usually not affected by the fluctuation of ionic strength (Bachmaf and Merkel 2010). The removal of U(VI) by SRS soil remained unaffected when ionic strength was adjusted with the addition of $NaClO_4$, implying that U(VI) removal under the conditions studied may be mainly attributed to the formation of inner-sphere complexes. These results comply with results presented earlier, where the results of sorption per surface unit implied that retention is not a surface phenomenon. $NaClO_4$ was chosen because it is an inert electrolyte: it exhibits practically no complexation with metals present in the aqueous form and the sorption of ClO_4^- on oxide surfaces is minimal (Morales et al. 2011, Zebardast et al. 2014). Similar results were reported by Guo (Guo, Li and Wu 2009) who found that the sorption of U(VI) on goethite was insensitive to the fluctuation of ionic strength, adjusted with NaCl.

On the other hand, removal decreases significantly with the increase of calcium chloride concentration (Figure 79). The speciation of the soluble U(VI) species under the conditions studied is presented at Table 31 (10^{-5} M $CaCl_2$ is the concentration of SRS synthetic groundwater, without any further addition of calcium chloride). The speciation for most species remains the same across the range of concentrations studied, with the exception of the percentage of the $Ca_2UO_2(CO_3)_3$ species, between 0.001 and 0.01 M $CaCl_2$ concentrations.
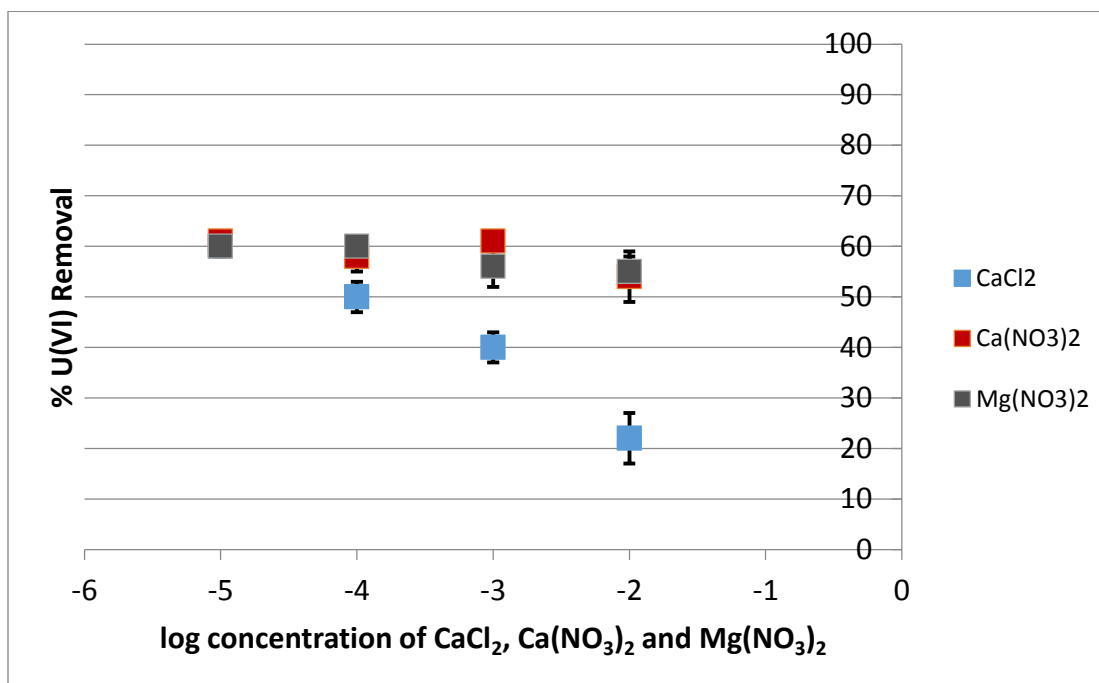
Figure 79. U(VI) per cent removal as a function of $CaCl_2$, $Ca(NO_3)_2$ and $Mg(NO_3)_2$ concentrations x-axis is in logarithmic scale). Error bars represent relative standard deviation.

Nevertheless, the decrease in the uranium removal across the wide range of concentrations studied is not likely to be largely dependent on speciation. A possible explanation for the reduced removal at high calcium chloride concentrations may be the interference of chloride ions with the analytical technique used for the determination of U(VI) (Kinetic Phosphorescence Analysis). The presence of chloride ions has been reported to incur quenching at the phosphorescence signal of the uranyl-complex (Brina and Miller 1992, Sowder, Clark and Fjeld 1998). When calcium nitrate and magnesium nitrate are used as electrolytes, U(VI) retention seems to be

unaffected by the presence of Ca and Mg in the range of $2.5 \cdot 10^{-5}$-0.01 M (Figure 79 and Table 30). The experimental findings imply that calcium and magnesium may bind in different sites than the ones that uranium is bound to. The uptake of calcium by goethite has been documented in literature and it has been found that calcium binds on goethite both as an outer- and inner-sphere complex (Rietra, Hiemstra and van Riemsdijk 2001, Rahnemaie, Hiemstra and van Riemsdijk 2006) based on the following scheme =SO-Ca$^+$ (Sverjensky 2006), where S stands for the solid surface and O is the oxygen atom.

Goethite may constitute only a small fraction of SRS soil, nevertheless it is very reactive towards metal cations in the solution. Guo (Guo et al. 2009) showed that when ionic strength is adjusted with NaCl, U(VI) sorption on goethite remains the same; it may be concluded that calcium and magnesium concentrations do not seem to hinder U(VI) sorption on SRS soil in circumneutral conditions. In the case of the counter-ion concentration effect in sorption, nitrates do not seem to affect sorption whereas for chloride ions results are not conclusive: reduction in sorption is due to analytical interference and/or chemical phenomenon. Calcium and magnesium concentrations higher than 0.01M were not investigated, since they were not in the scope of the present experimental work.

Table 30. U(VI) Retention by SRS Soil Under Circumneutral Conditions as a Function of Ca^{2+} and Mg^{2+} Concentration in the Aqueous Phase

Cation concentration	% U(VI) retention by SRS soil
Ca^{2+}	
0.000025 (SRS GRW)	63 ± 5
0.0001	54 ± 6
0.001	60 ± 2
0.01	55 ± 3
Mg^{2+}	
0.000015 (SRS GW)	63 ± 5
0.0001	64 ± 5
0.001	52 ± 9
0.01	50 ± 6

Table 31. Speciation of U(VI) Soluble Species for All the Calcium Concentrations Studied, as Provided by Visual Minteq.

CaCl$_2$ concentration (M)		
10^{-5}	10^{-3}	10^{-2}
47.3% (UO$_2$)$_3$(OH)$_5$$^+$	46.9 % (UO$_2$)$_3$(OH)$_5$$^+$	44.5 % (UO$_2$)$_3$(OH)$_5$$^+$
14.5 % UO$_2$OH$^+$	14.8 % UO$_2$OH$^+$	15.6 % UO$_2$OH$^+$
4.1% (UO$_2$)$_4$(OH)$_7$$^+$	4.0% (UO$_2$)$_4$(OH)$_7$$^+$	3.6 % (UO$_2$)$_4$(OH)$_7$$^+$
7.8 % UO$_2$H$_3$SiO$_4$$^+$	8.0 % UO$_2$H$_3$SiO$_4$$^+$	8.4 % UO$_2$H$_3$SiO$_4$$^+$
18.7 % UO$_2$CO$_3$	18.4 % UO$_2$CO$_3$	17.3 % UO$_2$CO$_3$
5.6 % UO$_2$(OH)$_2$	5.5 % UO$_2$(OH)$_2$	5.2 % UO$_2$(OH)$_2$
		1.9 % Ca$_2$UO$_2$(CO$_3$)$_3$

Multi-Contaminant Batch Sorption Experiments

In this set of experiments, the liquid phase contained 0.5 ppm of U(VI), 0.1 ppm of Sr and 0.1 ppm of Re. U(VI) removal was found 59 ± 5 %, whereas there was zero retention of strontium and rhenium. Rhenium under oxidizing conditions is found as perrhenate (ReO$_4$$^-$) and can be used as a chemical analog for technetium (TcO$_4$$^-$). Pertechnetate is highly soluble, does not sorb onto sediments and migrates at the same velocity as groundwater (Kaplan, Parker and Kutnyakov 1998). Hence, the experimental results for rhenium were rather expected. Strontium has similar physicochemical properties with calcium and although calcium has been reported to be retained by goethite (Rahnemaie et al. 2006, Sverjensky 2006, Rietra et al. 2001); no such behavior was observed for strontium under the conditions studied.

Subtask 2.1: Conclusions

The injection of sodium silicate seems to be a promising technology for the restoration of the alkalinity of the U(VI)-impacted treatment zone. U(VI) immobilization under circumneutral conditions after sodium silicate addition is 60% and the re-mobilization of U(VI) under neutral conditions is negligible. From a mechanistic point of view, this may be attributed mainly to the fact that U(VI) binds strongly to SRS soil and most specifically, through inner-sphere complexation onto goethite. Furthermore, the experiments revealed no signs of ion-exchange between the soil and uranium in the aqueous phase. As far as re-mobilization is concerned, acidic conditions (pH 3.5) may assist prior-contained-U(VI) to re-enter the aqueous phase up to 50%; hence, the maintenance of alkaline conditions is an important factor. The presence of divalent ions such calcium and magnesium does not affect the U(VI) retention for concentrations as high as 0.01M. This could denote the applicability of the method to other U(VI) impacted systems, apart from SRS F/H Area, since SRS groundwater is rather poor in those metals.

Subtask 2.1: Acknowledgements

Subtask 2.1: References

Anagnostopoulos, V., Symeopoulos, B., Bourikas, K., Bekatorou, A. 2016. Biosorption of U(VI) from aqueous systems by malt spent rootlets. Kinetic, equilibrium and speciation studies. *International Journal of Environmental Science and Technology*, **13**(1), 285-296.

Anagnostopoulos, V.A., Koutsoukos, P.G., Symeopoulos, B.D. 2015. Removal of U(VI) from Aquatic Systems, Using Winery By-Products as Biosorbents: Equilibrium, Kinetic, and Speciation Studies. *Water, Air, & Soil Pollution*, **226**(4), 1-14.

Bachmaf, S., Merkel, B.J. 2010. Sorption of uranium(VI) at the clay mineral–water interface. *Environmental Earth Sciences*, **63**(5), 925-934.

Baehr, C.H., Koehl, W. 2007. Soluble silicates - highly versatile and safe. *International Journal of Applied Science*, **133**, 88-94.

Brina, R., Miller, A.G. 1992. Direct detection of trace levels of uranium by laser-induced kinetic phosphorimetry. *Anal. Chem.*, **64**, 1413-1418.

Cornell, R.M., Schwertmann, U. 2003. *The iron oxides. Structure, properties, reactions, occurences and uses*. Wiley-VCH GmbH & Co. KGaA, Weinheim.

Dong, W., Tokunaga, T.K., Davis, J.A., Wan, J. 2012. Uranium(VI) adsorption and surface complexation modeling onto background sediments from the F-Area Savannah River Site. *Environ Sci Technol*, **46**(3), 1565-71.

Guo, Z., Li, Y., Wu, W. 2009. Sorption of U(VI) on goethite: Effects of pH, ionic strength, phosphate, carbonate and fulvic acid. *Applied Radiation and Isotopes*, **67**(6), 996-1000.

He, Q., Ren, Y., Mohamed, I., Ali, M., Hassan, W., Zeng, F. 2013. Assessment of trace and heavy metal distribution by four sequential extraction procedures in a contaminated soil. *Soil & Water Res.*, **8**(2), 71-76.

Icenhower, J.P., Martin, W.J., Qafoku, N.P., Zachara, J.M. 2008. The geochemistry of technetium: a summary of the behavior of an artificial element in the natural environment. PNNL.

Jolivet, J.P., Henry, M., Livage, J. 2000. *Metal oxide chemistry and synthesis*. John Wiley and Sons Ltd., Paria.

Kaplan, D.I., Parker, K.E., Kutnyakov, I.V. 1998. Radionuclide distribution coefficients for sediments collected from borehole 299-E17-21: Final report for subtask 1a. Pacific Northwest National Laboratory.

Morales, J.W., Galleguillos, H.c.R., Hernández-Luis, F., Rodríguez-Raposo, R. 2011. Activity Coefficients of NaClO4in Aqueous Solution. *Journal of Chemical & Engineering Data*, **56**(8), 3449-3453.

Rahnemaie, R., Hiemstra, T., van Riemsdijk, W.H. 2006. Inner- and outer-sphere complexation of ions at the goethite-solution interface. *Journal of Colloid and Interface Science*, **297**(2), 379-388.

Ratuzny, T., Gong, Z., Wilke, B.-M. 2008. Total concentrations and speciation of heavy metals in soils of the Shenyang Zhangshi Irrigation Area, China. *Environmental Monitoring and Assessment*, **156**(1), 171-180.

Rauret, G., F. Lopez-Sanchez, J., Sahuquillo, A., Rubio, R., Davidson, C., Ure, A., Quevauviller, P. 1999. Improvement of the BCR three step sequential extraction procedure prior to the certification of new sediment and soil reference materials. *Journal of Environmental Monitoring*, **1**(1), 57-61.

Rietra, R.P.J.J., Hiemstra, T., van Riemsdijk, W.H. 2001. Interaction between Calcium and Phosphate Adsorption on Goethite. *Environmental Science & Technology*, **35**(16), 3369-3374.

Savannah River Nuclear Sloutions, L. 2011. Savannah River Site Groundwater Management Strategy and Implementation Plan (U).

Sherwood Lollar, B. 2005. *Environmental Geochemistry*. Elsevier Science, Italy.

Sigg, L., Stumm, W. 2011. *Aquatic Chemistry*. Vdf Hochschulverlag, Zurich.

Sowder, A.G., Clark, S.B., Fjeld, R.A. 1998. The effect of sample matrix quenching on the measurement of trace uranium concentrations in aqueous solutions using kinetic phosphorimetry. *J Radioanal Nucl Chem*, **234**(1-2), 257-260.

Storm, R.N., Kaback, D.S. 1992. SRP Baseline Hydrogeologic Investigation: Aquifer Characterization, Groundwater Geochemistry of the Savannah River Site and Vicinity (U). Westinghouse Savannah River Company, Savannah River Laboratory.

Sverjensky, D.A. 2006. Prediction of the speciation of alkaline earths adsorbed on mineral surfaces in salt solutions. *Geochimica et Cosmochimica Acta*, **70**(10), 2427-2453.

Tessier, A., Campbell, P.G.C., Bisson, M. 1979. Sequential extraction procedure for the speciation of particulate trace metals *Analytical Chemistry* **51**(7), 844-851.

Ure, A.M., Quevauviller, P., Muntau, H., Griepink, B. 1993. Speciation of Heavy Metals in Soils and Sediments. An Account of the Improvement and Harmonization of Extraction Techniques Undertaken Under the Auspices of the BCR of the Commission of the European Communities. *International Journal of Environmental Analytical Chemistry*, **51**(1-4), 135-151.

Wan, J., Tokunaga, T.K., Dong, W., Denham, M.E., Hubbard, S.S. 2012. Persistent Source Influences on the Trailing Edge of a Groundwater Plume, and Natural Attenuation Timeframes: The F-Area Savannah River Site. *Environmental Science & Technology*, **46**(8), 4490-4497.

Worch, E. 2015. *Hydrochemistry: Basic Concepts and Exercises*. De Gruyter, Berlin, Germany.

Wu, J., Laird, D., Thomson, M. 1999. Sorption and desorption of copper on soil clay components. *Journal of Environmental Quality*, **28**, 334-338.

Zebardast, H.R., Pawlik, M., Rogak, S., Asselin, E. 2014. Potentiometric titration of hematite and magnetite at elevated temperatures using a ZrO2-based pH probe. *Colloids and Surfaces A: Physicochemical and Engineering Aspects*, **444**, 144-152.

Zemberyova, M., Bartekova, J., Hagarova, I. 2006. The utilization of modified BCR three-step sequential extraction procedure for the fractionation of Cd, Cr, Cu, Ni, Pb and Zn in soil reference materials of different origins. *Talanta*, **70**(5), 973-8.

Zimmerman, A.J., Weindorf, D.C. 2010. Heavy Metal and Trace Metal Analysis in Soil by Sequential Extraction: A Review of Procedures. *International Journal of Analytical Chemistry*, 2010.

Subtask 2.2: Monitoring of U (VI) Bioreduction after ARCADIS Demonstration at F-Area

Subtask 2.2: Introduction

Enhanced *in situ* anaerobic bioremediation can be an effective means for the degradation and/or retardation of contaminants found in groundwater. Due to the fact that it is *in situ*, this process leaves little impact on site and facility operations and generates no waste. Because it relies on microorganisms already present in the soil, it is also relatively low-cost when compared to active engineered remediation. The enhanced anaerobic reductive precipitation (EARP) process is one of these bioremediation methods. EARP utilizes a carbohydrate-substrate such as whey, molasses or high fructose corn syrup, for example, to serve as an electron donor and drive down the oxidation-reduction potential of the groundwater to a more reduced state. By doing this, the reductive precipitation of dissolved metals and dissolved radionuclides into less reactive forms is likely to occur. This has been proven to be a useful way to control transport of contaminants via groundwater flows.

In 2010, ARCADIS demonstrated the use of *in situ* injections of a carbohydrate substrate, molasses, to create reactive zones for uranium (VI) remediation via the EARP process at the F-Area of the Savannah River Site (SRS). The addition of the molasses substrate solution to groundwater was done to produce anaerobic conditions conducive to uranium reduction and then precipitation as uranium (IV) (Dennis and Suthersan 1998). This remediation strategy relies on changing the geochemical conditions in a direction that is opposite of their natural evolution. The important aspect of any *in situ* remediation technology is to prove the longevity of contaminant immobilization. The SRS soil features very unique environmental conditions due to the naturally low alkalinity. The sediments at the F-area are classified as weathered sands with very high quartz content in composition and a presence of kaolinite, montmorillonite, and goethite to a lesser degree (Dong et al. 2012). A microcosm study, prepared with sieved SRS sediments and augmenting the solution mixture with molasses, was designed to provide evidence for the capabilities of this remediation technology for SRS conditions. The objective of these microcosm experiments was to replicate the anaerobic conditions created as a result of injections of molasses combined with sulfate ions similar to the EARP process that was performed at SRS and investigate if any mineralogical changes could occur in the soil due to the addition of molasses. Specifically, the study aimed to determine if forms of reduced iron such as siderite and pyrite would be created, as this would indicate that the EARP process had created the bioreductive zone that was desired. An understanding of the technology will be useful to determining if it is a viable option for remediation.

The acidic pH and naturally low soil alkalinity in the F-Area sediments are believed to be major factors contributed to the deficiency of ferrous iron solid phases during experimentation. In the experiment, the media solution was amended with molasses and sulfate to stimulate sulfate-reducing bacteria. Sulfate reduction occurs extensively in the redox conditions occurring after iron reduction and before methanogenic conditions at $E_h^o = -220$. These conditions are considered the second most reducing condition in natural groundwater systems. Sulfate reducing bacteria (SRB) are a very diverse group of obligatory anaerobes, which have an ability to dissimilate sulfate to sulfide while oxidizing various growth substrates (Willis et al. 1997). Molasses is one of the substrates that have been described as an electron donor and carbon source for the cultivation of SRB (Annachhatre and Suktrakoolvait 2001, Hussain, Qazi and Shakir 2014).

Under environmental conditions, sulfate reduction, mediated exclusively by prokaryotic sulfate-reducing bacteria, results in chemical reactions in which the organic substrate is oxidized while sulfate is reduced (Eq.1) (Canfield 2001, Berner et al. 2002, Aravena and Mayer 2009):

$$SO_4^{2-} + 2CH_2O \rightarrow H_2S + 2HCO_3^- \hspace{3cm} Eq.1$$

These anaerobic bacteria gain energy for growth from the oxidation of organic substrates using sulfate as the electron acceptor (Hao et al. 1996, Barton and Tomei 1995). The microbial reduction of sulfate produces hydrogen sulfide and releases of HCO_3^-, resulting in an increase in alkalinity and pH (Richards and Pallud 2016, Mormontoy and Hurtado 2013). After sulfate reduction, sulfide is sequestered by ferrous iron by creating blackish precipitates of pyrite (Boonchayaanant et al. 2010). It was expected that, in the anaerobic conditions, sulfate would be reduced to sulfide and bind to ferrous iron because of the abundance of iron in the SRS sediments. It was also expected that the release of bicarbonate ions, which are produced out of the sulfate reduction reaction, would lead to an increase in pH, causing the aqueous phase to become saturated with respect to ferrous carbonate. The research conducted for this subtask can shed light into the limiting factors for the EARP process in an environment such as the one at the F-Area.

Subtask 2.2: Methodology

Uncontaminated background sediment samples collected from the SRS F-Area from the well FSB 91C, the closest well to the molasses injection site, were selected to conduct the batch experiments. Fine fractions were first separated from SRS sediments through 2 mm, 180 µm, 125 µm and 63 µm sieves in order to remove larger quartz particles. Soil fractioning also helped to decrease the presence of quartz in the samples (suggested by the large intensity peaks shown through X-ray diffraction (XRD) analysis) which overshadows goethite and kaolinite in fine fractions. Before creating any of the samples for the microcosm experiment, XRD analysis was conducted for the 180 µm, 125 µm and 63 µm fractions to obtain a reference for comparison if any mineralogical changes in the microcosms after sediment treatment with molasses. The sediment composition was predominantly quartz, kaolinite and goethite, which agrees with previous results (Dong et al. 2012).

The experiment consisted of two batches of microcosm tubes, prepared to mimic conditions at the SRS F-Area. To simulate the anaerobic conditions present in the saturated zone of the SRS F-Area, a vinyl anaerobic airlock chamber was used. The chamber (Coy Lab products) was vacuumed and purged several times with pure nitrogen gas to establish anaerobic conditions, which were then confirmed by the oxygen and hydrogen gas analyzer installed inside the chamber. The glove box environment was continuously monitored to ensure that oxygen level conditions remained anaerobic.

For the first batch, 4 sets of samples were prepared in triplicate for a total of 12 samples. In the second batch, 4 single samples were created due to the low amount of fine fractions collected from the SRS sediments. It should also be noted that Batch 1 was started 42 days prior to Batch 2. In Batch 2, the same basal-molasses solution was used except that the pH was adjusted to a neutral level before the addition of any sediment. All batches followed similar preparation steps and the same types of analysis.

All of the samples for Batches 1 and 2 were prepared in 50-mL polypropylene tubes and were treated using a basal medium solution augmented with sulfate and molasses. The basal medium

solution consisted of (in g L^{-1} deionized water): 1.5 NaHCO$_3$, 0.2 NH$_4$Cl, 0.1 K$_2$HPO$_4$ 3H$_2$O, 0.055 KH$_2$PO$_4$, 0.001 resazurin as a redox indicator, 0.039 Na$_2$S 9H$_2$O as a sulfur source and reductant, and 0.1 MgCl$_2$ 6H$_2$O. In addition, 5 mL L^{-1} trace metal solution was added. The trace metal solution consisted of (in g L^{-1}): 0.005 FeCl$_2$ 4H$_2$O, 0.005 MnCl$_2$ 4H$_2$O, 0.001 CoCl$_2$ 6H$_2$O, 0.0006 H$_3$BO$_3$, 0.0001 ZnCl$_2$, 0.0001 NiCl$_2$ 6H$_2$O, 0.0001 Na$_2$MoO$_4$ 2H$_2$O, and 0.002 CaCl$_2$ 2H$_2$O (Freedman and Gossett 1989). Magnesium sulfate anhydrous (MgSO$_4$) salt was used as a source of sulfate for the augmented samples; it was combined with the basal medium solution to a concentration of 500 ppm. The anaerobic process is very slow; to speed up the molasses fermentation process, Sets 1 and 4 were inoculated with 0.5 mL of anaerobic sludge collected from the anaerobic digester of the Miami-Dade South wastewater treatment plant. The complete composition of each tube in Batch 1 and Batch 2 is presented in Table 32.

Table 32. Sample Composition for Batch 1 and Batch 2

Batch 1				
Sample Composition	**Set #1**	**Set #2**	**Set #3**	**Set #4**
Soil, mL	20	20	20	15
Basal Medium, mL	20	20	20	15
Sulfate, ppm	500	500	-	-
Molasses, % by weight	5-10%	5-10%	5-10%	5-10%
Anaerobic sludge, mL	0.5	-	-	0.5
Batch 2				
Soil, mL	20	20	20	15
Basal Medium, mL	12	12	12	12
Sulfate, ppm	500	500	-	-
Molasses, % by weight	5-10%	5-10%	5-10%	5-10%
Anaerobic sludge, mL	0.5	-	-	0.5

Throughout the experiment, all samples underwent a pH evolution study to determine the effects of the additions to the sediments. After the samples were created and given time to react in the anaerobic chamber, sub-samples were taken from both of the microcosm batches to be used for XRD analysis. For Batch 1, a small sub-sample was taken from each of the samples and combined to create a representative sample for each set, with a total of 4 sub-samples. Sub-samples for Batch 1 were taken at week four (4) and week eight (8). For Batch 2, sub-samples were taken directly from each of the tubes for a total of 4 sub-samples. The Batch 2 sub-samples

were taken after four (4) weeks in the anaerobic chamber. Each of the dried sub-samples was placed individually onto a plastic sample-holder for the XRD analysis.

XRD analyses were performed using a Bruker 5000D XRD instrument set to 35 kV and 40 mA. Diffraction patterns were obtained using a copper Cu Kα radiation source (λ=0.154056 nm) with a tungsten filter. The XRD was programmed to run over a 2-theta (2θ) range from 3° to 70° with a 0.02° step size and 3 second counting per step. Obtained XRD patterns were analyzed and compared against known XRD patterns for siderite and pyrite minerals.

In addition, inductively coupled plasma optical emission spectrometry (ICP-OES) analysis was conducted on the supernatant solutions to determine the ferrous iron concentrations. Five (5) mL of deionized water (DI) was added to each of the samples and the samples were centrifuged in tubes at 2700 rpm for 20 minutes. The supernatant was collected from each sample and filtered through a 45 mm filter syringe. Standards were prepared for iron analysis with a calibration curve between 1 to 100 ppm. The supernatant was collected and diluted by a factor of 200 in 1% nitric acid (HNO_3). Three (3) mL of each of the diluted samples were placed into 15 mL tubes for iron analysis via ICP-OES.

Sulfate analyses were conducted via a Metrohm ion chromatograph equipped with a Metrosep a Supp 5 - 150/4.0 separation IC column. The calibration curve was prepared by using the sulfate standards for 1 ppm, 7 ppm, 17 ppm, 20 ppm and 25 ppm with R^2 of 0.9948. All samples were diluted 20 times before analyses.

Geochemist's Workbench (GWB) 10.0 (Bethke 2007) React Module was used for the geochemical equilibrium modeling to predict the formation of siderite and pyrite solid phases expected to be present as a result of molasses and sulfate additions into the microcosms. For comparison, this modeling was conducted for both an open and closed system. The model for a closed system was constructed by fixing the fugacity of CO_2 and an open system was built in equilibrium with atmospheric CO_2. The synthetic groundwater solutions were formulated using cations and anions concentrations. The experimental conditions were simulated using the React Module, which allowed for varying the pH values in the range of 3 to 8 at which the reductive precipitation of iron can occur. This modeling would determine if the EARP process would create a bio-reductive zone in a similar experiment at a range of different pH values.

Subtask 2.2: Results and Discussion

pH evolution

During the monitoring of the Batch 1 samples, a sharp decrease in the pH from week 1 to week 2 was noted and an investigation was conducted to determine the cause. Previous reports from ARCADIS indicated that the EARP process often results in a decrease in pH (Lutes et al. 2003). It was concluded through an elimination process that the addition of molasses had caused the initial drop in pH. Prior to the molasses addition, the basal media solution with and without sulfate, exhibited more basic pH values ranging between 8.7- 8.8. These values shifted significantly to below pH 5.0 (4.57-4.85) after the molasses addition (Table 33).

Table 33. Measured pH Values

Solution amended with sulfate, basal medium and molasses	Solution amended with basal medium and molasses	Basal medium	Solution amended with basal medium and 500 ppm of sulfate
4.85	4.57	8.7	8.82

Due to the pH reduction in the samples of Batch 1, it was decided that a second batch would be prepared with solutions that were first brought to a neutral pH before the addition of the sediments. The pH measurements suggested that almost all of the samples, in either batch, have followed a similar trend, with a decline in the pH value (Figure 80). This can be attributed to the fermentation process of molasses and the natural acidity of SRS soil used for the microcosm study. It has been found that the fermentative bacteria that thrive in these low pH conditions can out-compete sulfate-reducing and methanogenic bacteria. Lowering of pH to below 5 standard units may inhibit growth of sulfate reducers and methanogens bacteria (Maillacheruvu and Parkin 1996). In addition, the naturally low alkalinity of the SRS soils provides little buffering capacity to the pH changes caused by the molasses. Despite the fact that the fermentative bacteria out-competed the sulfate-reducing bacteria, there was still a slightly higher pH in the sulfate-augmented samples. In general, the pH values for all of the samples inoculated with bacteria were lower than 5 and the difference between sulfate-amended and sulfate-free samples was insignificant.

Both batches received an addition of a small quantity of neutral solution in order to keep the microcosm tubes from drying out. Two solutions were prepared for this purpose for the Batch 2 samples. The first solution consisted of 45 mL of basal medium and 7.1 g molasses. This solution was adjusted to a pH of 7.03 before it was added in the amount of 2 mL per sample to the samples in set 3 and set 4 samples. The second solution consisted of 45 mL of basal medium augmented with 500 ppm of sulfate and 7.1 g molasses. This solution was adjusted to a pH of 6.99 before it was added in the amount of 2 mL per sample to the set 1 and set 2 samples. These additions account for a small increase in the pH evolution graphs at Day 60 for Batch 1 and at Day 18 for Batch 2 (Figure 80). Regardless of initial pH adjustments to neutral, the solutions' pH dropped in all of the Batch 1 and Batch 2 samples. The pH was measured on the level of 4.7 after keeping the samples inside the anaerobic chamber for three weeks and then dropped to 4.0 after keeping the samples inside the chamber for two months (Figure 80).

Figure 80. pH evolution for Batch 1 and Batch 2 samples based on measurements of triplicate samples for each set.

X-ray diffraction analysis

The initial XRD analyses on the background samples indicated that the sediments contained quartz, kaolinite, montmorillonite, and goethite. The most prominent peak for quartz was observed at 2θ 26.65 degrees, montmorillonite at 5.89 degrees, goethite at 21.37 degrees, and kaolinite at 12.37 degrees (Figure 81-Figure 84). In the molasses treated samples, there were no visible peaks for reduced forms of iron such as siderite and pyrite. The maximum intensity peaks for siderite would occur at 32.49 2-theta value and for pyrite at 28.74 (100%) and 56.75 (84.7%) 2-theta values, respectively. In addition, mackinawite at 2-theta 17.62 (100%) and ankerite at 30.83 (100%) was also tested, but haven't produced any measurable results (Figure 85, Figure 86). Due to the fact that no matches to siderite or pyrite were found in any sample, only a few of the XRD graphs have been displayed. All samples in both batches displayed nearly identical XRD patterns when compared against XRD results of the background sediment before beginning the microcosm experiment.

SRS soil is very low in the carbonate alkalinity needed for the formation of ferrous carbonate and the acidic pH of the samples might play a role in the lack of ferrous iron solid phases formation.

Figure 81. Background sample vs. quartz.

Figure 82. Background sample vs. montmorillonite.

Figure 83. Background sample vs. goethite.

Figure 84. Background sample vs. kaolinite.

Figure 85. XRD data to identify ferrous minerals in Batch 1 samples treated with molasses; A) Set 1; B) Set 3. No matches were found to ferrous iron minerals in any of samples.

Figure 86. XRD data to identify ferrous minerals in Batch 2 samples treated with molasses; A) Set 1; B) Set 3. No matches to ferrous iron minerals were found in any of samples.

Samples analysis for sulfate and iron

In the acidic iron-rich sediments, the microbial reduction of Fe(III) is the dominant electron-accepting process for the oxidation of organic matter (Küsel 2003). Potential Fe(III) reduction was measured by the accumulation of Fe(II) during incubation in an anaerobic glove box. Iron analyses of the supernatant solutions extracted from the samples were conducted via ICP-OES. The samples varied significantly in iron concentration, with the greatest reaching 7808 µg/L in Batch 1/Set 1 samples. It was found that the samples amended with sulfate (Sets 1 and 2) did not display a significant difference in average iron concentration in comparison to the samples which contained no sulfate, 5726.54 µg/L vs. 4907.53 µg/L, respectively. This suggests that the ferrous iron most likely doesn't complex with sulfide ions to create pyrite solid phase due to the hindering of sulfate reduction in the acidic conditions. The variation in iron concentrations is most probably due to slight differences in the soil composition upon preparation of the microcosm tubes.

It was also noted that the Batch 1 samples containing anaerobic bacteria (Sets 1 and 4) had higher average iron concentrations in comparison to those which were not inoculated. It is believed that the samples inoculated with anaerobic sludge contain an adequate amount of active iron-reducing bacteria that may have biodegraded the molasses using ferric iron as a terminal electron acceptor, leading to the higher concentrations of soluble ferrous iron in these samples.

Figure 87. Iron concentrations detected in supernatant solutions of (A) Batch 1 and (B) Batch 2 samples.

Sulfate analyses were conducted via ion chromatography for the liquid samples collected from the microcosm experiments. All samples collected for analysis were kept under anaerobic conditions in the anaerobic glove box until time of assay. A calibration curve was prepared by using a sulfate standard in the concentration range from 1 ppm to 25 ppm (Figure 88).

The figure shows a scatter plot with regression line. The y-axis is labeled "Peak Area" ranging from 0 to 300, and the x-axis is labeled "Sulfate concentration, ppm" ranging from 0 to 30. The regression equation shown is:

$$y = 10.498x + 8.8612$$
$$R^2 = 0.9948$$
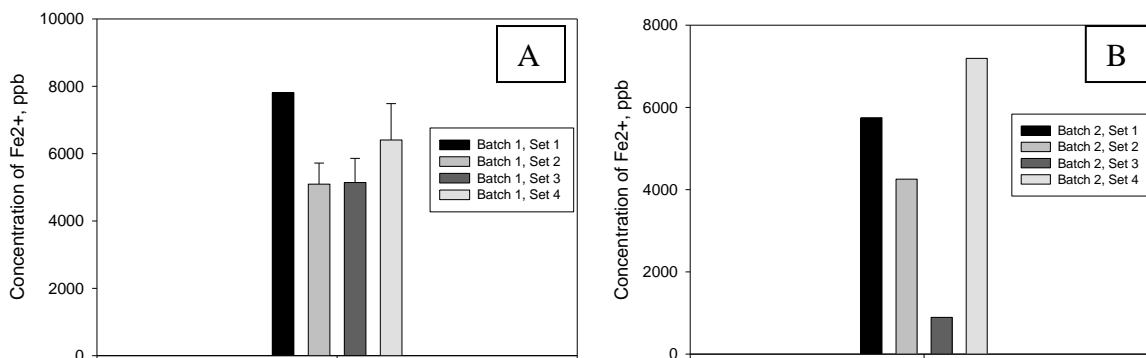
Legend: ● Sulfate concentration. ppm vs area; — Plot 1 Regr
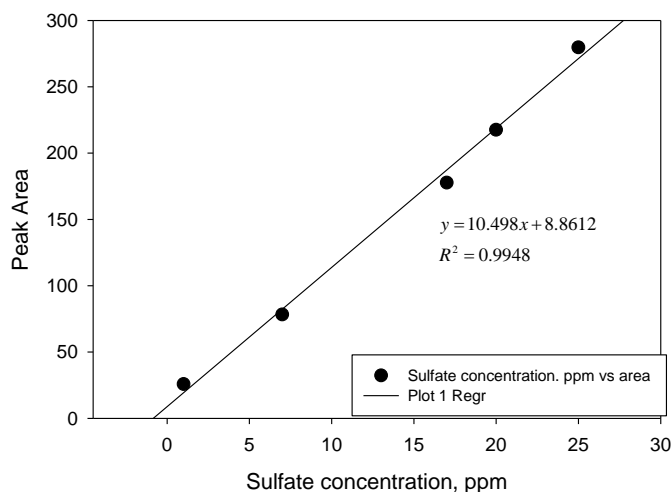
Figure 88. Calibration curve for sulfate analysis.

Analytical results showed that there was no sulfate reduction in any of samples augmented with sulfate and the concentration remained on the level of 500 ppm as originally added to the initial solutions (518-542±14.5 ppm). This might explain why XRD analysis hasn't revealed the formation of pyrite phases. Literature suggests that SRB microorganisms are very adaptable to many environmental conditions, including acid mine drainages and acidic sediments (Costa and Duarte 2005, Muyzer and Stams 2008, Fauque and Ollivier 2004, Hussain et al. 2016). Meier et al. (2004) reported that sulfate reduction rates were much lower in the slightly acidic sediment than in the pH-neutral sediment because of reduced microbial activity (Meier, Babenzien and Wendt-Potthoff 2004). Moreover, in the zone of ferric iron reduction in sediments, sulfate reduction is a competitive mechanism, leading to the inhibition of sulfate reduction on the level of 86% to100% (Lovley and Phillips 1987). Literature data demonstrated that Fe(III)-reducing bacteria can outcompete sulfate-reducing food chains for organic matter in acidic sediment (Peine et al. 2000). Fe(III) phases doesn't have a direct toxic effect on sulfate-reducing bacteria and the inhibition of sulfate reduction is more a result of organic substrate limitation (Lovley and Phillips 1987). Apparently, if electron donors are not limiting the iron and sulfate reduction processes, they can take place simultaneously. Iron in SRS sediments is present as oxide minerals that exist as a coating on clay and quartz minerals surfaces. The abundance of biologically available Fe(III) allows Fe(III) reducers outcompete sulfate-reducing bacteria using molasses as an electron donor.

Speciation modeling

Speciation modeling was conducted via Geochemists Workbench (GWB) software. Aqueous speciation and saturation indices of solid phases are presented in Figure 89. Iron is mostly present as soluble ferrous iron ions.
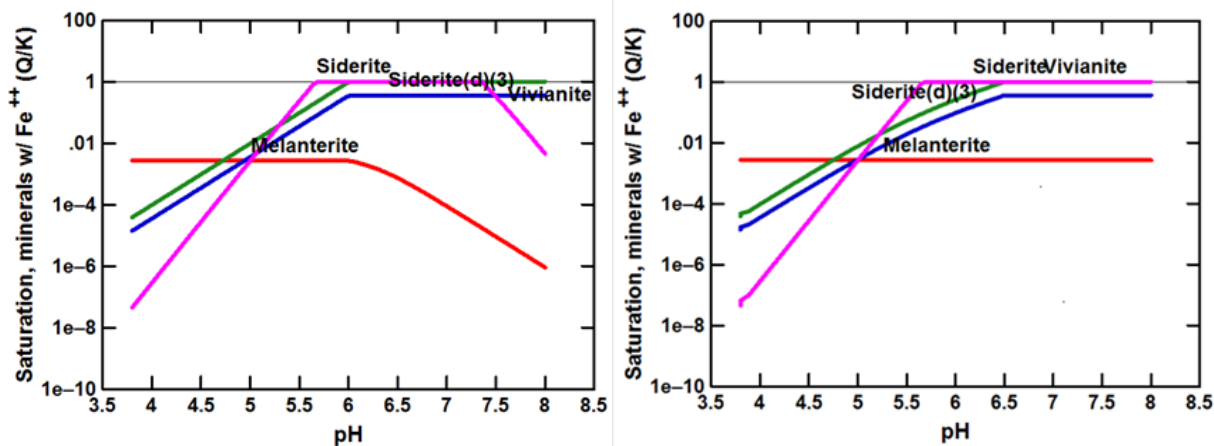
Figure 89. GWB simulations conducted for open (right) and closed systems (left) for conditions mimicking the enhanced anaerobic reductive precipitation (EARP) remediation method previously tested at SRS F- Area.

Speciation modeling suggested that the formation of siderite is observed at pH ~6.5 for the modeled closed system and at pH 6 for the open system, both well above the pH values measured after molasses fermentation in the microcosms. Modeling predicated very small concentrations of siderite created at neutral conditions in soil. In the closed system, the concentration of siderite was about 0.002 g/kg of sediment. In the open system, due to equilibrium with atmospheric pH, the concentration of siderite was predicted to be higher, on the level of 13.8 g/kg. No pyrite formation was observed at any of the pH values tested. Since there was no formation of reduced iron solid phases in the molasses-treatment zone, dissolved ferrous iron (Fe^{2+} and $FeCl_2$) will most likely be easily flushed out from the Fe(III)-reducing zone and then rapidly oxidize to insoluble ferric (Fe^{3+}) iron under aerobic conditions in the aquifer sediments.

Subtask 2.2: Conclusion

Microcosm experiments were performed to investigate the addition of molasses to create anaerobic conditions in the acidic SRS sediments collected from the F-Area. In the anaerobic conditions, microbially-mediated Fe(III) reduction resulted in an increase of ferrous iron concentrations that in the acidic conditions is mostly present in solution as soluble Fe^{2+} ions. These conditions open up the potential for reduction of highly mobile uranyl (UVI) ions to insoluble reduced U(IV) phases. This process of uranyl reduction can be catalyzed by ferrous iron (Liger, Charlet and Van Cappellen 1999, Boland et al. 2011, Tsarev, Waite and Collins 2016) over a limited pH range, which could result in the immobilization of uranium. However, if no mineralogical changes occur in the acidic soil forming ferrous iron minerals due to the addition of molasses, soluble ferrous iron can be oxidized to ferric iron as molasses is rapidly fermented or flushed out from the treatment zone with groundwater. This would affect the stability of the reduced uranium species and lead to their re-oxidation to highly soluble and mobile uranyl ions.

An abstract on this research was submitted for presentation at the Waste Management 2017 (WM17) Symposia. This research has been completed and will not be continued next year.

Subtask 2.2: Acknowledgements

valuable input and support of this research. XRD analyses were conducted at FIU AMERI facilities.

Subtask 2.2: References

Annachhatre, A. P. & S. Suktrakoolvait (2001) Biological sulfate reduction using molasses as a carbon source. *Water Environment Research,* 73**,** 118-126.

Aravena, R. & B. Mayer (2009) Isotopes and processes in the nitrogen and sulfur cycles. *Environmental isotopes in biodegradation and bioremediation***,** 203-246.

Barton, L. L. & F. A. Tomei. 1995. Characteristics and activities of sulfate-reducing bacteria. In *Sulfate-reducing bacteria*, 1-32. Springer.

Berner, Z. A., D. Stüben, M. A. Leosson & H. Klinge (2002) S-and O-isotopic character of dissolved sulphate in the cover rock aquifers of a Zechstein salt dome. *Applied geochemistry,* 17**,** 1515-1528.

Boland, D. D., R. N. Collins, T. E. Payne & T. D. Waite (2011) Effect of amorphous Fe (III) oxide transformation on the Fe (II)-mediated reduction of U (VI). *Environmental science & technology,* 45**,** 1327-1333.

Boonchayaanant, B., B. H. Gu, W. Wang, M. E. Ortiz & C. S. Criddle (2010) Can microbially-generated hydrogen sulfide account for the rates of U(VI) reduction by a sulfate-reducing bacterium? *Biodegradation,* 21**,** 81-95.

Canfield, D. E. (2001) Isotope fractionation by natural populations of sulfate-reducing bacteria. *Geochimica et Cosmochimica Acta,* 65**,** 1117-1124.

Costa, M. & J. Duarte (2005) Bioremediation of acid mine drainage using acidic soil and organic wastes for promoting sulphate-reducing bacteria activity on a column reactor. *Water, air, and soil pollution,* 165**,** 325-345.

Dennis, E. & A. G. Suthersan. 1998. Microbial Precipitation of Dissolved Metals Using Molasses. EPA 542-N-98-010.

Dong, W., T. K. Tokunaga, J. A. Davis & J. Wan (2012a) Uranium (VI) adsorption and surface complexation modeling onto background sediments from the F-Area Savannah River Site. Environmental science & technology, 46, 1565-1571.

Dong, W., T. K. Tokunaga, J. A. Davis & J. Wan (2012b) Uranium(VI) Adsorption and Surface Complexation Modeling onto Background Sediments from the F-Area Savannah River Site. Environmental Science & Technology, 46, 1565-1571.

Fauque, G. & B. Ollivier (2004) Anaerobes: the sulfate-Reducing Bacteria as an Example of Metbolic Diversity. *Microbial Diversity and Bioprospecting,* 17**,** 169-176.

Freedman, D. L. & J. M. Gossett (1989) Biological reductive dechlorination of tetrachloroethylene and trichloroethylene to ethylene under methanogenic conditions. *applied and Environmental Microbiology,* 55**,** 2144-2151.

Hao, O. J., J. M. Chen, L. Huang & R. L. Buglass (1996) Sulfate-reducing bacteria. *Critical reviews in environmental science and technology,* 26**,** 155-187.

Hussain, A., A. Hasan, A. Javid & J. I. Qazi (2016) Exploited application of sulfate-reducing bacteria for concomitant treatment of metallic and non-metallic wastes: a mini review. *3 Biotech,* 6**,** 1-10.

Hussain, A., J. I. Qazi & H. A. Shakir (2014) Implication of molasses as electron donor for biological sulphate reduction. *American Journal of Environmental Engineering,* 4**,** 7-10.

Küsel, K. (2003) Microbial cycling of iron and sulfur in acidic coal mining lake sediments. *Water, Air and Soil Pollution: Focus,* 3**,** 67-90.

Liger, E., L. Charlet & P. Van Cappellen (1999) Surface catalysis of uranium (VI) reduction by iron (II). *Geochimica et Cosmochimica Acta,* 63**,** 2939-2955.

Lovley, D. R. & E. J. Phillips (1987) Competitive mechanisms for inhibition of sulfate reduction and methane production in the zone of ferric iron reduction in sediments. *Applied and Environmental Microbiology,* 53**,** 2636-2641.

Lutes, C. C., P. Angela Frizzell, T. A. Thornton & J. M. Harrington. 2003. In-situ chemical stabilization of metals and radionuclides through enhanced anaerobic reductive precipitation. Arcadis Geraghty & Miller, Inc.(US).

Maillacheruvu, K. Y. & G. F. Parkin (1996) Kinetics of growth, substrate utilization and sulfide toxicity for propionate, acetate, and hydrogen utilizers in anaerobic systems. *Water Environment Research,* 68**,** 1099-1106.

Meier, J., H.-D. Babenzien & K. Wendt-Potthoff (2004) Microbial cycling of iron and sulfur in sediments of acidic and pH-neutral mining lakes in Lusatia (Brandenburg, Germany). *Biogeochemistry,* 67**,** 135-156.

Mormontoy, J. & J. E. Hurtado. 2013. Hydrogen sulphide production at alkaline, neutral and acid pH by a bacterial consortium isolated from Peruvian mine tailing and wetland. In *Integration of Scientific and Industrial Knowledge on Biohydrometallurgy,* eds. N. Guiliani, C. Demergasso, R. Quatrini, F. Remonsellez, C. DavisBelmar, G. Levican, P. Parada, C. Barahona & R. Zale, 384-387. Stafa-Zurich: Trans Tech Publications Ltd.

Muyzer, G. & A. J. Stams (2008) The ecology and biotechnology of sulphate-reducing bacteria. Nature Reviews Microbiology, 6, 441-454.

Peine, A., A. Tritschler, K. Küsel & S. Peiffer (2000) Electron flow in an iron-rich acidic sediment—evidence for an acidity-driven iron cycle. *Limnology and Oceanography,* 45**,** 1077-1087.

Richards, C. M. & C. Pallud (2016) Kinetics of sulfate reduction and sulfide precipitation rates in sediments of a bar-built estuary (Pescadero, California). *Water Research,* 94**,** 86-102.

Tsarev, S., T. D. Waite & R. N. Collins (2016) Uranium reduction by Fe (II) in the presence of montmorillonite and nontronite. *Environmental Science & Technology.*

Willis, L. C., H. J. Cummings, G. Neale & R. G. Gibson (1997) Nutritional Aspects of Dissimilatory Sulfate Reduction in the Human Large Intestine. *Current Microbiology,* 35**,** 294-298.

Subtask 2.3: The Sorption Properties of the Humate Injected Into the Subsurface System

Subtask 2.3: Introduction

Savannah River Site (SRS), located 13 miles south of Aiken in South Carolina, was a defense nuclear processing facility owned by the U.S. government. During the Cold War, from 1953 to 1988, SRS produced a large amount of radioactive and hazardous acidic waste from the production of plutonium and irradiated fuel. The acidic waste solutions containing low-level radioactivity from numerous isotopes were discharged into a series of unlined seepage basins in the F/H Area. At that time, it was believed that most of the radionuclides present in the waste solution would bind to the soil, precluding the migration of the radionuclides. However, sufficient quantities of uranium isotopes, ^{129}I, ^{99}Tc, and tritium migrated into the groundwater, creating an acidic plume with a pH between 3 to 5.5. In an effort to remove the contaminants from the groundwater, pump-and-treat and re-inject systems were implemented in 1997. Downgradient contaminated groundwater was pumped up to a water treatment facility, treated to remove metals (through osmosis, precipitation/flocculation, and ion exchange), and then re-injected upgradient within the aquifer. The pump-and-treat water treatment unit eventually became less effective generating large amounts of radioactive waste. The maintenance of the pump-and-treat water treatment unit was very expensive, and this prompted the research for new remedial alternatives. In 2004, the pump-and treat system was replaced by a funnel and gate system in order to create a treatment zone via injection of a solution mixture composed of two components, sodium hydroxide and carbonate. The injections were done directly into the gates of the F-Area groundwater to raise pH levels. The purpose of the treatment zone was to reverse the acidic nature of the contaminated sediments, thereby producing a more negative net charge on the surface of sediment particles and enhancing the adsorption of cationic contaminants. This system of remediation required a systematic re-injection of the base to raise the pH to near neutral values. However, the continuous use of high concentrations of a carbonate solution to raise the pH creates a concern of possible re-mobilization of uranium that was previously adsorbed within the treatment zone since U(VI) in the presence of bicarbonate ions forms soluble aqueous uranyl-carbonate complexes, though this has not been observed in monitoring data.

Savannah River National Laboratory (SRNL) has been testing an unrefined, low cost humic substance known as Huma-K as an amendment that can be injected into contaminant plumes to enhance sorption of uranium and Sr-90. The advantage of using an unrefined humic substance is that it is inexpensive, and can be used for full scale deployment of remediation technologies.

Humic substances (Figure 90) are ubiquitous in the environment, occurring in all soils, waters, and sediments of the ecosphere. Humic substances consist of complex organic compounds formed by the decomposition of plant and animal tissue. This decomposition process is known as humification, where the organic matter is transformed naturally into humic substances by microorganisms in the soil. Humic substances are divided into three main fractions: humic acid (HA), fulvic acid (FA), and humin. Their size, molecular weight, elemental composition, structure, and the number and position of functional groups vary.
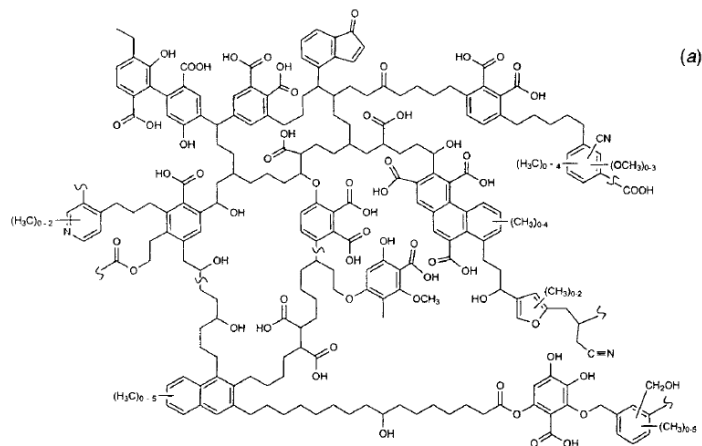
Figure 90. Soil humic acid structure proposed by Schulten and Schnitzer.

Some studies have shown that HA is as an important ion exchange and metal-complexing ligand, carrying a large number of functional groups with high complexing capacity that can greatly affect the mobility behavior of actinides in natural systems (Davis, 1982; Choppin, 1998; Plancque et al., 2001). pH and concentration are the main factors affecting the formation of complexes between humic molecules and metals. It is generally considered that the sorption of metal ions on the mineral surfaces in the presence of HA is enhanced at low pH and reduced at high pH (Ivanov et al., 2012). For example, Keprelova et al. showed that U(VI) prefers to be adsorbed onto kaolinite as a uranyl-humate complex (Krepelova et al., 2007).

This study used Huma-K, an organic fertilizer used by farmers to stimulate plant growth and facilitate nutrient uptake. It is a water soluble potassium salt of humic and fulvic acids that comes from the alkaline extraction of leonardite (a low-rank coal). Leonardite has a very high content of humic substances due to decomposition by microorganisms. Also, compared to other sources of humic substances, leonardite has a higher humic/fulvic acid content. The extraction of humic/fulvic acid from leonardite is performed in water with the addition of potassium hydroxide (KOH), and the resulting liquid is freeze-dried to produce the amorphous crystalline black powder/shiny flakes as seen in Figure 91.

Figure 91. Huma-K black powder/shiny flakes.

Subtask 2.3: Methodology

Characterization of SRS sediments

For the Fourier Transform Infrared (FTIR) analysis, a Perkin Elmer Spectrum 100 FT-IR Spectrometer coupled with an Attenuated Total Reflectance (ATR) was used. The spectrum of the samples were collected from 4000 to 600 cm-1. Before the analysis, SRS sediments were

sieved to a particle size less than 63 µm in order to analyze the fine fraction which contains more clay. Also, the sample had to have a powder structure in order to generate a high quality spectrum. After the sieving, the < 63 µm collected fraction was brought in contact with a solution of Huma-K in order to compared SRS sediments that were previously coated with Huma-K with SRS sediments without the coating.The samples were placed in an oven at 80° C for 48 hours to remove any adsorbed water. Then, the samples were stored in a dessicator until analysis. Before the analysis, the ATR crystal of the FTIR was cleaned with ethanol, and the background was collected. Just enough sample was placed on top of the crystal to cover the whole area. The pressure clamp was lowered and pressure was applied to ensure that there was good contact between the sample and the crystal. After that, the spectrum of the sample was collected.

Potentiometric titration of SRS sediments (< 63 µm fraction) was performed in order to determine the protonation-deprotonation behavior of sediments. The potentiometric titration consisted of placing a certain amount of SRS sediments dissolved in $NaNO_3$ in a closed beaker. The setup is shown in Figure 92. The solution was stirred constantly and nitrogen was introduced in order to get rid of CO_2 and to create an inert atmosphere. Once the pH of the solution containing the material was stable, NaOH was added to raise the pH to 11 in order to deprotonate the functional groups present in the material. Once the pH was stabilized again, the titration was started by adding small quantities of HNO_3. After each addition of HNO_3, the pH and the volume were recorded. The titration was ended at a pH around 3. After the titration was finished, the supernatant was collected by vacuum filtration and titrated again. The purpose of titrating the supernatant was to estimate the functional groups that may have leached from the sediment and could consume hydrogen ions. In order to get just the hydrogen ions consumed by the material, it was necessary to subtract the titration curve of the electrolyte ($NaNO_3$) from the material dissolved in the electrolyte using a data analysis software (OriginPro 8).

Figure 92. Setup for the potentiometric titration.

Desorption Experiment of Huma-K

Kinetic Experiment of Huma-K desorption at pH 4

In this study, SRS sediments (FAW-1 70-90ft) collected from the F-Area were used. All the experiments were done at laboratory ambient temperature (between 20 and 23°C). The desorption experiment was conducted at a 20:1 liquid to soil ratio.

First, several centrifuge tubes were prepared to contain the same amount of SRS sediments (1 gram). A known concentration of Huma-K (500 ppm) was pipetted into each centrifuges tube.

The pH was adjusted to pH 4 for all the samples by using either 0.1 M HCL or 0.1 M NaOH. DI water was added to a final volume of 20 mL in each tube (Figure 93). The samples were then placed on a shaker table until equilibrium was reached (Figure 94). Second, the supernatant of the samples was replaced by deionized water at pH 4. pH was monitored daily and adjusted with 0.1 M HCl or 0.1 M NaOH. Samples were placed on the shaker table. At predetermined time intervals, samples were withdrawn and centrifuged at 2700 RPM (Figure 95). The concentration of the supernatant was measured by UV-vis spectrophotometer in order to determine the quantity of Huma-K that was desorbed at different time intervals (Figure 96).
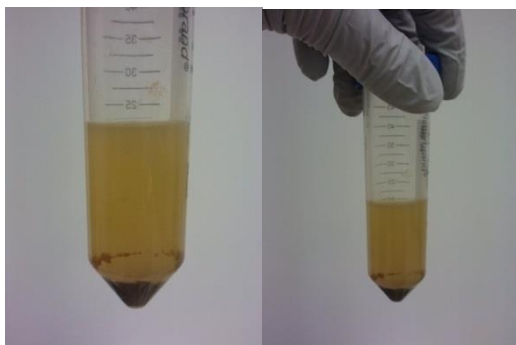
Figure 93. Centrifuge tube with sediment and humate solution.

Figure 94. Shaker table with samples.

Figure 95. Centrifugation.

Figure 96. UV-Vis spectrophotometer.

Desorption of Huma-K at differenst pH values

A batch desorption experiment was conducted at pH range 4-8. Initially, 20 mL of Huma-K solution (Cin 500 mg L^{-1}) at pH 4 was brought in contact with 1 g of SRS soil at 25 $^{\circ}$C. After five days of rotation, samples were centrifuged, the residual Huma-K concentration in the supernatant was determined and the supernatant was replaced with deionized water at different pH values (4-8). pH was monitored daily and adjusted with 0.1 M HCl or 0.1 M NaOH. Samples were rotated and centrifuged in the same exact way as previously described. The desorbed Huma-K concentration in the aqueous phase was determined by UV-vis spectrophotometer.

Subtask 2.3: Results and Discussion

Characterization of SRS sediments

Fourier Transform Infrared Spectroscopy

Figure 97 shows the spectrum that was collected for SRS sediments before adsorption and after adsorption of Huma-K. First, spectrum of SRS sediments with a particle size < 63 µm was collected. The peak at 3695 cm^{-1} is attributed to the stretching vibration of the surface hydroxyl groups while the peak at 3620 cm^{-1} is attributed to the inner-surface OH group stretching vibration (Djomgoue, 2013; Müller et al., 2014). Also the SRS sediment spectrum shows a shoulder of absorption band at 1164 cm^{-1}, which is attributed to the Si-O stretching. The peaks at 1030 and 1006 cm^{-1} correspond to the in-plane Si-O stretching vibration. Another interesting characteristic peak is found at 912 cm^{-1} which corresponds to the OH bending vibration of the inner surface OH groups (Vaculíková et al., 2011). Finally, the peaks at 776 cm^{-1} and 692 cm^{-1} correspond to the Si-O symmetrical stretching and bending vibration, respectively.

The interactions between Huma-K and SRS sediment was confirmed in Figure 97 (red line). As can be seen, some bands decreased in the 1000 cm^{-1} region probably due to the interaction between the functional groups (COOH, OH) of Huma-K and the surface hydroxyl groups of SRS soil. One possible explanation for the reduction of the peaks is due to the formation of a complex between the carboxyl groups in Huma-K and the OH groups present in the sediments.
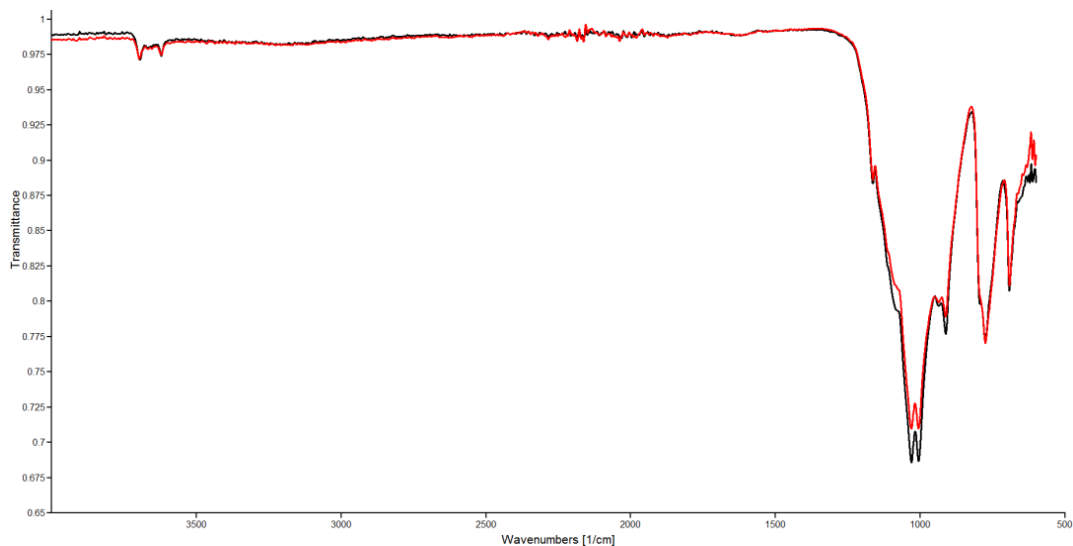
Figure 97. FTIR spectra of SRS sediment (< 63 μm) before (black line) and after adsorption (red line) of Huma-K.

Potentiometric Titrations

Potentiometric titrations provide useful information on the protonation/deprotonation properties of SRS sediments. Reverse peaks correspond to the pK values of the surface sites that have acid/base properties and can be ionized.

The differential potentiometric titration curve of SRS sediments (< 63 µm) revealed reverse peaks only in the region between pH 3-4 (Figure 98) which can be attributed to the acid basic properties of the silanol (Si-OH) groups. These results suggest that for pH values higher than 4, the surface charge of the sediments will be predominantly negative due to the deprotonation of the silanol groups (Si-O-). Other studies have reported similar pK values (4.5 and 8.5) for the acid /base behavior of silica interaction with water. Also, the potentiometric titration curve of SRS sediments revealed a small peak around pH 6.8 that could correspond to the silanol groups of amorphous silica. Some studies have shown that when the quartz surface is in contact with water, an amorphous layer is formed.
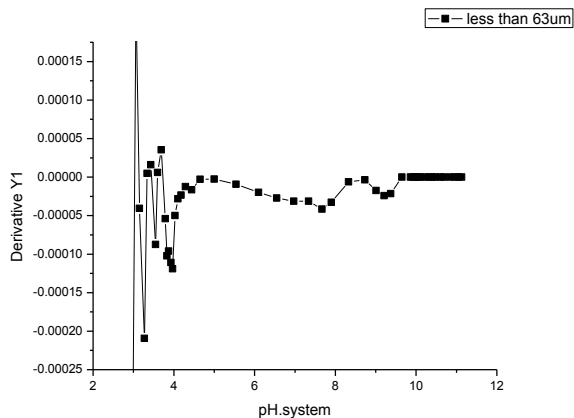
Figure 98. Differential potentiometric curve of SRS sediments (< 63 µm).

Desorption Experiment of Huma-K

Kinetic Experiment of Huma-K desorption at pH 4

The kinetic experiment of Huma-K desorption from SRS sediments is shown in Figure 99. The initial concentration (C_0) correspond to the initial concentration adsorbed to SRS sediments before desorption. The results from the kinetic experiment show that the concentration of HumaK sorbed after the desorption is constant from day 3 to day 30, and it did not decrease during that period. A possible explanation for this behavior is that since the pH of the DI water that replaced the supernatant was the same (pH 4), the interactions in the adsorbed layer remains relatively the same. Therefore, there is no increase in negative charges in humic molecules or the surface charge of sediments that could stimulate the desorption process. Also, humic molecules that are adsorbed strongly will not be desorbed easily, and the humic molecules that have a weak interaction with sediments (either physical or reversible adsorption) will be desorbed more easily.
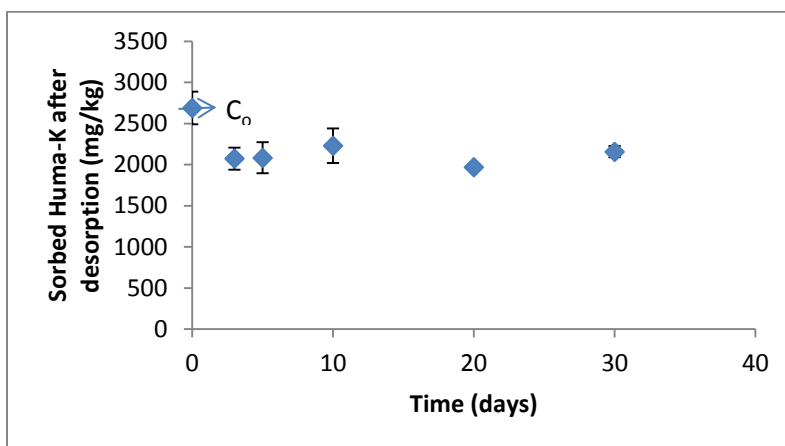
Figure 99. Kinetic Experiment of Huma-K Desorption.

Desorption of Huma-K at different pH values

The results of the desorption study between Huma-K and SRS sediments at a pH range 4-8 is shown in Figure 100. At pH 4, the desorption was 25% but as the pH of the solution increased to pH 8, the desorption increased significantly to 65%. The complete desorption process of the previously adsorbed Huma-K onto SRS soil was not reached, meaning that still there is a fraction of Huma-K strongly bound to the soil that resists desorption. Probably the fraction of Huma-K being desorbed corresponds to the fraction of Huma-K that was precipitated at pH 4 due to the functional groups in humic substances being mostly protonated; there is also a contribution of hydrophobic interactions. A possible explanation for the increase of desorption is that as the pH is increased, there is a larger presence of hydroxyl ions than can be exchanged with the carboxyl groups of the humic molecules, detaching these molecules from the surface of the sediment.. Also, with the increase of pH, there is an increase in the negative charges of the humic substances due to the deprotonation of the carboxyl groups and other functional groups; this leads not only to mutual repulsion of humic molecules adsorbed at the surface, enhancing the desorption, but also increases their solubilization.
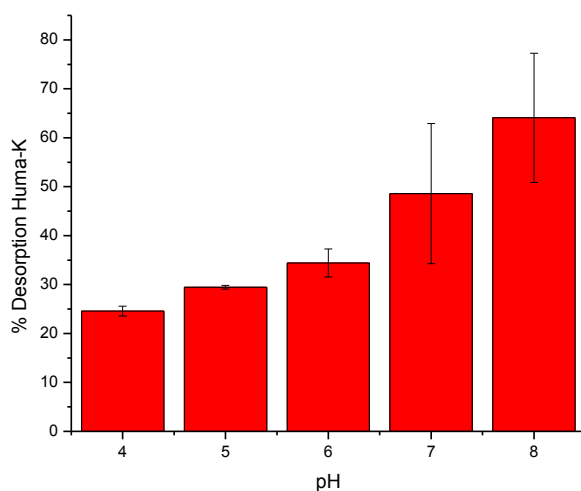
Figure 100. Desorption of Huma-K at different pH values.

Subtask 2.3: Future Work

Future work will focus on the batch experiments, exploring the removal of uranium using Huma-K as a low-cost remediation method. This will be investigated by exploring the following conditions:

- Savannah River Site sediments + uranium
- Savannah River Site sediments + uranium + Huma-K
- Sediments coated with Huma-K + uranium
- Uranium + Huma-K

By using the conditions shown above, the removal of uranium will be better understood if Huma-K is used as a remediation method. Also, other factors that may affect the removal of uranium using Huma-K will be investigated as well such as pH and desorption.

Subtask 2.3: Acknowledgements

Funding for this research was provided by U.S. DOE Cooperative Agreement DE-EM0000598. We truly appreciate Dr. Miles Denham and Dr. Brian Looney from the SRNL for their valuable contributions and support of this research.

Subtask 2.3: References

Aguayo-Villarreal, I., Bonilla-Petriciolet, A., Hernández-Montoya, V., Montes-Morán, M., Reynel-Avila, H. 2011. Batch and column studies of Zn^{2+} removal from aqueous solution using chicken feathers as sorbents. *Chemical Engineering Journal*. 167: 67-76.

Anagnostopoulos, V., Koutsoukos, P., Symeopoulos, B. (2015). Removal of U(VI) from Aquatic Systems, Using Winery By-Products as Biosorbents: Equilibrium, Kinetic, and Speciation Studies. *Water Air Soil Pollut*. 226: 107.

Anagnostopoulos, V., Manariotis, I., Karapanagioti, H., Chrysikopoulos, C. (2012). Removal of mercury from aqueous solutions by malt spent rootlets. *Chemical Engineering Journal*. 213: 135-141.

Appel, C., Ma, L., Rhue, R., Kennelley, E. (2003). Point of zero charge determination in soils and minerals via traditional methods and detection of electroacoustic mobility. *Geoderma*. 113:77-93.

Balan, E., Lazzeri, M., Saitta, M., Allard, T., Fuchs, Y., Mauri, F. (2005). First-principles study of OH-stretching modes in kaolinite, dickite, and nacrite. *American Mineralogist*. 90: 50-60.

Balcke, G., Kulikova, N., Hesse, S., Kopinke, F., Perminova, I., Frimmel, F. (2002). Adsorption of humic substances onto kaolin clay Related to their structural features. *Soil Science Society of America*. **66**: 1805-1812.

Balnois, E., Wilkinson, K., Lead, J., Buffle, J. (1999). Atomic force miscroscopy of humic substances: effect of pH and ionic strength. *Environ. Sci. Technol.* 33: 3911-3917.

Benedetti, M., Van Riemsdijk, W., Koopal, L. (1996). Humic substances considered as a heterogeneous donnan gel phase. *Environmental Science and Technology*. **30**: 1805-1813.

Bourikas, K., Kordulis, C., Lycourghiotis, A. (2005). Differential Potentiometric Titration: Development of a Methodology for Determining the point of Zero Charge of Metal (Hydr)oxide by One Titration Curve. *Environ. Sci. Technol*. 39: 4100-4108.

Bourikas, K., Kordulis, C., Lycourghiotis, A. (2006). How metal (hydr)oxides are protonated in aqueous media: The (n + 1) rule and the role of the interfacial potential. *Journal of Colloid and Interface Science.* 296: 389-395.

Bourikas, K., Kordulis, C., Lycourghiotis, A. (2006). The mechanism of the protonation of metal (hydr)oxides in aqueous solutions studied for various interfacial/surface ionization models and physicochemical parameters: A critical review and a novel approach. *Advances in Colloid and Interface Science.* 121: 111-130.

Bourikas, K., Vakros, J., Kordulis, C., Lycourghiotis, A. (2003). Potentiometric Mass Titrations: Experimental and Theoretical Establishment of a New Technique for Determining the Point of Zero Charge (PZC) of Metal (Hydr)Oxides. *J. Phys. Chem. B*. 107: 9441-9451.

Chen, Y., Senesi, N., Schnitzer. (1977). Information provided on humic substances by E_4/E_6 ratios. *Soil Science Society of America*. **41**: 352-358.

Choppin, G.R., 1992. The role of natural organics in radionuclide migration in natural aquifer systems. *Radiochim. Acta* 58/59, 113.

Choppin, G.R., 1998. Humics and radionuclide migration. *Radiochim. Acta* 44/45, 23-28.

Da Costa Saab, S., Carvalho, E., Bernardes Filho, R., de Moura, M., Martin-Neto, L., Mattoso, L. (2010). pH effect in aquatic fulvic acid from a Brazilian river. *J. Braz. Chem. Soc*. 21: 1490-1496.

Davis, J.A., 1982. Adsorption of natural dissolved organic matter at the oxide/water interface. *Geochim. Cosmochim. Acta* 46, 2381-2393.

Davis, J.A., 1984. Complexation of trace metals by adsorbed natural organic matter. *Geochim. Cosmochim. Acta* 48, 679-691.

Djomgoue, P., Njopwouo, D. (2013). FT-IR Spectroscopy Applied for Surface Clays Characterization. *Journal of Surface Engineered Materials and Advanced Technology*. 3: 275-282.

Dong, W., Tokunaga, T. K., Davis, JA., Wan, J., 2011. Uranium(VI) Adsorption and Surface Complexation Modeling onto Background Sediments from the F-Area Savannah River Site. *Environmental Science & Technology*

Dong, W., Wan, J. (2014). Additive Surface Complexation Modeling of Uranium(VI) Adsorption onto Quartz-Sand Dominated Sediments. *Environ. Sci. Technol.* 48: 6569-6577.

E. A. Ghabbour and G. Davies , Eds., Humic Substances: Structures, Models and Functions, Royal Society of Chemistry, Cambridge, 2001, p. 26.

Erdogan, S., Baysal, A., Akba, O., Hamamci, H. (2007). Interaction of Metals with Humic Acid Isolated from Oxidized Coal. *Polish J. of Environ. Stud*. 16(5): 671-675.

Fairhurst, A. J.; Warwick, P.; Richardson, S. 1995. The influence of humic acid on the sorption of europium onto inorganic colloids as a function of pH. *Colloids Surf., A*, 99, 187-199.

Fein, J., Boily, J., Güçlü, K., Kaulbach, E. (1999). Experimental study of humic acid adsorption onto bacteria and Al-oxide mineral surfaces. *Chemical Geology*. **162**: 33-45.

Fuentes, M., González-Gaitano, G., García-Mina, J. (2006). The usefulness of UV-visible and fluorescence spectroscopies to study the chemical nature for humic substances from soils and composts. *Organic Geochemistry*. **37**: 1949-1959.

Gan, D., Kotob, S. Walia, D. (2007). Evaluation of a spectrophotometric method for practical and cost effective quantification of fulvic acid. *Annals of Environmental Science*. **1**: 11-15.

Giovanela, M., Crespo, J.S., Antunes, M., Adamatti, D.S., Fernandes, A.N., Barison, A., da Silva, C.W.P., Guegan, R., Motelica-Heino, M., Sierra, M.M.D. (2010). Chemical and spectroscopic characterization of humic acids extracted from the bottom sediments of a Brazilian subtropical microbasin. *Journal of Molecular Structure*. 981: 111-119.

Giovanela, M., Parlanti, E., Soriano-Sierra, E.J. Soldi, M.S., Sierra, M.M.D. (2004). Elemental compositions, FT-IR spectra and thermal behavior of sedimentary fulvic and humic acids from aquatic and terrestrial environments. *Geochemical Journal*. 38: 255-264.

Hameed, B., Mahmoud, D., Ahmad, A. 2008. Equilibrium modeling and kinetic studies on the adsorption of basic dye by a low-cost adsorbent: Coconut (Cocos nucifera bunch waste. *Journal of Hazardous Materials.* 158: 65-72.

Illés, E., Tombácz, E. (2004). The role of variable surface charge and surface complexation in the adsorption of humic acid on magnetite. *Colloids and Surfaces A: Physicochem. Eng. Aspects*. **230**: 99-109.

Ivanov, P., Griffiths, T., Bryan, N.D., Bozhikov, G. and S. Dmitriev, 2012. The effect of humic acid on uranyl sorption onto bentonite at trace uranium levels. *J. Environ. Monit*., 14, 2968 - 2975.

Jacques Berthelin, P.M. Huang, J-M. Bollag, Francis Andreux. Effect of Mineral-Organic-Microorganism Interactions on Soil and Freshwater Environments. Springer Science & Business Media, 2012, p. 136.

Janot, N., Reiller, P., Zheng, X., Croué, J., Benedetti, M. (2012). Characterization of humic acid reactivity modifications due to adsorption onto α-Al$_2$O$_3$. *Water Research*. **46**: 731-740.

Khambhaty, Y., Mody, K., Basha, S., Jha, B. (2009). Kinetics, equilibrium and thermodynamic studies on biosorption of hexavalent chromium by dead fungal biomass of marine Aspergillus niger. *Chemical Engineering Journal*. 145: 489-495.

Klucakova, M., Kolajova, R. (2014). Dissociation ability of humic acids: Spectroscopic determination of pKa and comparison with multi-step mechanism. *Reactive and Functional Polymers*. 78: 1-6.

Krepelova, A., Brendler, V., Sachs, S., Baumann, N., Bernhard, G., 2007. U(VI)-Kaolinite Surface Complexation in Absence and Presence of Humic Acid Studied by TRLFS. *Environ. Sci. Technol*. 2007, 41, 6142-6147.

Kumar, K. (2006). Linear and non-linear regression analysis for the sorption kinetics of methylene blue onto activated carbon. *Journal of Hazardous Material*. B137: 1538-1544.

L.K. Koopal, Y. Yang, A.J. Minnaard, P.L.M. Theunissen, W.H. Van Riemsdijk, 1998. Chemical immobilization of humic acid on silica. *Colloids and Surfaces A: Physicochemical and Engineering Aspects* 141, 385-395.

Labonne-Wall, N., Moulin, V., Vilarem, J.P., 1997. Retention properties of humic substances onto amorphous silica: consequences for the sorption of cations. *Radiochim. Acta*, 79, 37-49.

Leung, K., Nielsen, I., Criscenti, L. (2009). Elucidating the Bimodal Acid-Base Behavior of the Water-Silica Interface from First Principles. *J. Am. Chem. Soc*. 131: 18358-18365.

Liao Jiali, Wen Wei, LI Bing, Yang Yuanyou, Zhang Dong, Kang Houjun, Yang Yong, Jin Jiannan, Liu Ning, 2013. Interaction between uranium and humic acid (II): complexation, precipitation and migration behavior of U(VI) in the presence of humic substances. *Nuclear Science and Techniques* 24, 030301

Liu, X., Cheng, J., Lu, X., Wang, R. (2014). Surface acidity of quartz: understanding the crystallographic control. *Phys. Chem. Chem. Phys*. 16: 26909-26916.

Liu, Y., Liu, Y. 2008. Biosorption isotherms, kinetics and thermodynamics. *Separation and Purification Technology*. 61: 229-242.

Madejová, J., Komadel, P. (2001). Baseline studies of the clay minerals society source clays: infrared methods. *Clays and Clay Minerals*. 49: 410-432.

Müller, C., Molinelli, A., Karlowatz, M., Aleksandrov, A., Orlando, T., Mizaikoff, B. (2012). Infrared Attenuated Total Reflection Spectroscopy of Quartz and Silica Micro- and Nanoparticulate Films. *J. Phys. Chem. C*. 116: 37-43.

Müller, C., Pejcic, B., Esteban, L., Piane, C., Raven, M., Mizaikoff, B. (2014). Infrared Attenuated Total Reflectance Spectroscopy: An Innovative Strategy for Analyzing Mineral Components in Energy Relevant Systems. *Sci. Rep*.

Murphy, R. J., Lenhart J. J. and B. D. Honeyman, The sorption of Th(IV) and U(VI) to hematite in the presence of natural organic matter, *Colloids Surf., A*, 1999, 157, 47.

Ong, S., Zhao, X., Eisenthal, K. (1992). Polarization of water molecules at a charged interface: second harmonic studies of the silica/water interface. *Chemical Physics Letters*. 191: 327-335.

Palayangoda, S., Nguyen, Q. (2012). An ATR-FTIR procedure for quantitative analysis of mineral constituents and kerogen in oil shale. *Oil Shale*. 29: 344-356.

Perminova, I.V, Hatfield, K., Hertkorn, N., 2002. Use of humic substances to remediate polluted environments: from theory to practice. In the proceedings of the NATO Advance Research Workshop, Springer, P.O Box 17, 3300 AA Dordrech, The Netherland.

Plancque, G., Amekraz, B., Moulin, V., Toulhoat, P., Moulin, C., 2001. Molecular structure of fulvic acids by electrospray with quadrupole time-of-flight mass spectrometry. *Rapid Commun. Mass Spectrom.* 15, 827-835.

Prélot, B., Charmas, R., Zarzycki, P., Thomas, F., Vlliéras, F., Piasecki, W, Rudziński, W. (2002). Application of the Theoretical 1-pK Approach to Analyzing Proton Adsorption Isotherm Derivatives on Heterogeneous Oxide Surfaces. *J. Phys. Chem. B*. 106: 13280-13286.

Qiu, H., LV, L., Pan, B., Zhang, Q., Zhang, W., Zhang, Q. 2009. Critical review in adsorption kinetic models. *Journal of Zhejiang University*. 10(5): 716-724.

Rajamohan, N., Rajasimman, M., Rajeshkannan, R., Saravanan, V. 2014. Equilibrium, kinetic and thermodynamic studies on the removal of Aluminum by modified Eucalyptus camaldulensis barks. *Alexandria Engineering Journal*. 53: 409-415.

Rudzinski, W., Plazinski, W. 2006. Kinetics of Solute Adsorption at Solid/Solution Interfaces: A Theoretical Development of the Empirical Pseudo-First and Pseudo-Second Order Kinetic Rate Equations, Based on Applying the Statistical Rate Theory of Interfacial Transport. *J. Phys. Chem. B*. 110: 16514-16525.

Saikia, B., Parthasarathy, G., Sarmah, N. (2008). Fourier transform infrared spectroscopic estimation of crystallinity in SiO2 based rocks. *Bull. Mater. Sci*. 31: 775-779.

Shaker, A., Komy, Z., Heggy, S, El-Sayed, M. (2012). Kinetic Study for Adsorption Humic Acid on Soil Minerals. *J. Phys. Chem. A*. 116: 10889-10896.

Shmeide, K., Pompe, S., Bubner, M., Bernhard G. and H. Nitsche, 2000. Uranium(VI) sorption onto phyllite and selected minerals in the presence of humic acid, *Radiochim. Acta*, 88, 723

Strawn, D., Sparks, D. (2000). Effects of Soil Organic Matter on the Kinetics and Mechanisms of Pb(II) Sorption and Desorption in Soil. *Soil Sci. Soc. Am. J.* 64: 144-156.

Stumm, Werner, and James J. Morgan. Aquatic Chemistry: Chemical Equilibria and Rates in Natural Waters. New York: Wiley, 1996, p. 141.

Thurman, E. M. Organic Geochemistry of Natural Waters. Dordrecht: M. Nijhoff, 1985, p. 90.

Tinnacher, R., Nico, P., Davis, J., Honeyman, 2013. Effects of Fulvic Acid on Uranium(VI) Sorption Kinetics. *Environ. Sci. Technol.* 47, 6214-6222.

Vaculíková, L., Plevová, E., Vallová, S., Koutník, I. (2011). Characterization and differentiation of kaolinites from selected Czech deposits using infrared spectroscopy and differential thermal analysis. *Acta Geodyn. Geomaster*. 8: 59-67.

Vakros, J., Kordulis, C., Lycourghiotis, A. (2002). Potentiometric mass titrations: a quick scan determining the point of zero charge. *Chem. Commun*. 1980-1981.

Vieyra, F., Palazzi, V., Sanchez de Pinto, M., Borsarelli, C. (2009). Combined UV-vis absorbance and fluorescence properties of extracted humic substances-like for characterization of composting evolution of domestic solid wastes. *Geoderma.* **151**: 61-67.

Wan, J., Dong, W., Tokunaga, T. (2011). Method to attenuate U (VI) mobility in acidic waste plumes using humic acids. *Environmental Science and Technology*. **45**: 2331-2337.

Wang, J., Dong, W., Tokunaga, T, 2011. Method to Attenuate U(VI) Mobility in Acidic Waste Plumes Using Humic Acids. *Environ. Sci. Technol*. 45, 2331-2337.

Zachara, J.M., Resch, C.T., Smith, S.C., 1994. Influence of humic substances on Co^{2+} sorption by a subsurface mineral separate and its mineralogical components. *Geochim. Cosmochim. Acta* 58, 553-566.

Subtask 2.4: Synergetic Interactions between Humic Acid and Colloidal Silica for the Removal of Uranium

Subtask 2.4: Introduction

Constructed during the 1950s, the Savannah River Site (SRS) became one of the major producers of plutonium for the United States during the Cold War. Beginning with the implementation of the environmental cleanup program in 1981, SRS has become a hazardous waste management facility responsible for the storage and remediation of contaminated soil and groundwater from radionuclides. Approximately 1.8 billion gallons of acidic waste containing radionuclides and dissolved heavy metals was disposed in F/H Area seepage basins, which led to the unintentional creation of highly contaminated groundwater plumes consisting of radionuclides and chemicals with an acidic pH of 3 to 5.5. The acidity of the plumes contributes to the mobility of several constituents of concern (COC) such as tritium, uranium-238, iodine-129, and strontium-90 for the F-Area plume as well as tritium, strontium-90 and mercury for the H-Area plume. This investigation will focus on uranium (VI), which is a key contaminant of concern in the F-Area groundwater plume.

Initially, removal of contaminates from the groundwater was implemented with a pump-and-treat and re-inject system constructed in 1997. Downgrade groundwater within the system would be pumped to the water treatment facility and re-injected upgrade within the aquifer. The effectiveness and sustainability of this process diminished over time and it was discontinued in 2004, replaced with a funnel-and-gate process. This new process would inject sodium hydroxide directly into the gates of the F-Area groundwater to effectively raise pH levels. By raising the pH of the groundwater, a treatment zone would be created by reversing the acidic nature of the contaminated sediments and producing a negative net charge on the surface of sediment particles, enhancing the adsorption of cationic contaminants. This process resulted in a decrease in concentration of Sr and U, though the concentration of iodine was unaffected by this treatment. The solution used for the injections contained high carbonate alkalinity in order to overcome the surface acidic conditions and natural partitions in the groundwater system. To maintain the neutral pH in the treatment zone, systematic injections are required. The continuous use of high concentrations of a carbonate solution to raise pH could re-mobilize uranium previously adsorbed within the treatment zone, though this has not been observed in the monitoring data.

Humic substances (HS) are major components of soil organic matter with the ability to influence migration behavior and fate of heavy metals. Essentially, HS are polyfunctional organic macromolecules formed by the chemo-microbiological decomposition of biomass or dead organic matter. Being organic substances, HS are able to interact with both metal ions and organic compounds, and based on their solubility, HS are usually divided into three fractions (Chopping, et al. 1992). The three fractions are humin, humic acid and fulvic acid. Humin is insoluble at all pH values; HA represents the fraction which is soluble at pH greater than 3.5 and fulvic acid is soluble at all pH values.

Humic acid, which carries a large number of functional groups, provides an important function in ion exchange and as a metal complexing ligand, with a high complexation capacity being able to affect the mobility of actinides in natural systems (Davis, 1982; Plancque et al., 2001). Various studies have suggested that the retention of U(VI) via sorption in the presence of HA is a complex process due to HA forming organic coatings by sorbing on the surface of oxides and

minerals, thus modifying the sorption capabilities of these metal ions (Davis, 1984; Zachara et al., 1994; Labonne-Wall et al., 1997; Perminova et al., 2002). The sorption of metal ions is considered to be enhanced at low pH and reduced at high alkaline pH (Ivanov et al., 2012). This sorption capability is also affected by the concentration of HA in the system (Chen and Wang, 2007). The U(VI) sorption onto kaolinite is influenced by the pH, U(VI) concentration, presence of inorganic carbon species and naturally occurring HA. It has also been shown that U(VI) prefers to be adsorbed onto kaolinite as a uranyl-humate complex (Krepelova et al., 2007).

This investigation analyzed any synergistic interactions between U(VI) ions, HA and colloidal silica under varying pH conditions from 3 to 8 and the presence of sediment collected from SRS FAW1. Multi-component batch systems were constructed to effectively analyze the removal behavior of U(VI).

Subtask 2.4: Materials and Methods

Removal behavior of U(VI) was studied through multi-component batch systems with a pH range from 3 to 8 in order to evaluate adsorption affected by the pH. FIU previously investigated the synergetic effect of colloidal silica and HA (10 ppm and 50 ppm) on uranium removal by preparing seven batches with various combinations of Si and HA (Lagos, et al., 2014). Expanding on this research, FIU prepared samples with 30 ppm HA to study the sorption behavior of uranium at an intermediate HA concentration. Sediment samples used in the experiments were collected at SRS from FAW1 at a depth of 70-90 feet and shipped to FIU. The sediment was sifted through a 2-mm sieve to remove gravel and larger sediment particles. Control samples were prepared in triplicate, containing deionized water (DIW) and 0.5 ppm U(VI), to account for any sorption of uranium to the container.

- Batch 1: Si (3.5 mM) + U(VI) (0.5 ppm)
- Batch 2: Si (3.5 mM) + U(VI) (0.5 ppm) + HA, (no sediments)
- Batch 3: U(VI) (0.5 ppm) + HA, (no Si or sediments)
- Batch 4: Si (3.5 mM) + U(VI) (0.5 ppm) + sediments
- Batch 5: Sediments + Si (3.5 mM) +U (VI) (0.5 ppm) + HA
- Batch 6: Sediments + U(VI) (0.5 ppm) + HA, (no Si)
- Batch 7: Sediments + U(VI) (0.5 ppm)
- Control: U(VI) (0.5 ppm), (no SI, HA, or sediments)

Fumed colloidal silica, silicon (IV) oxide 99%, and humic acid sodium salt (50-60% as humic acid) were obtained from Fisher Scientific. Stocks of HA and Si were prepared in DIW at 2000 ppm and 100 ppm, respectively. A commercial 1000 ppm uranyl nitrate stock solution in 2% nitric acid (Fisher Scientific) was used as a source of U(VI). The resulting sample mixtures were spiked with uranium to yield a concentration within a solution matrix of 0.5 ppm. Table 34 and Table 35 present the amount of stock solutions needed to yield 50 ppm and 30 ppm of HA, respectively, with 3.5 mM of Si and 0.5 ppm of U(VI). Triplicate samples for each batch were prepared; uranium was added to each sample prior to adjusting the pH. The pH of the mixture was then adjusted to the required value using 0.01 M HCl or 0.1 M NaOH (Figure 101). Control samples were prepared in DIW amended with U(VI) at a concentration of 0.5 ppm U(VI) to test for U(VI) losses from the solutions due to sorption to the tube walls and caps. All volumes of solutions were prepared to initially have 20 mL of total volume in the sample tube. All control

and experimental tubes were vortexed and then kept on the shaker at 100 rpm for 48 hours at room temperature.

Table 34. Experimental Matrix with Components for 50 ppm Humic Acid Experiments

Batch #	Constituents					
	SiO$_2$ ml	Humic Acid ml	Uranium ml	Sediment mg	Water ml	Total Volume ml
Batch No. 1	2.1	0	0.01	0	17.89	20
Batch No. 2	2.1	10	0.01	0	7.89	20
Batch No. 3	0	10	0.01	0	9.99	20
Batch No. 4	2.1	0	0.01	400	17.89	20
Batch No. 5	2.1	10	0.01	400	7.89	20
Batch No. 6	0	10	0.01	400	9.99	20
Batch No. 7	0	0	0.01	400	19.99	20

Table 35. Experimental Matrix with Components for 30 ppm Humic Acid Experiments

Batch #	Constituents					
	SiO$_2$ ml	Humic Acid ml	Uranium ml	Sediment mg	Water ml	Total Volume ml
Batch No. 1	2.1	0	0.01	0	17.89	20
Batch No. 2	2.1	6	0.01	0	11.89	20
Batch No. 3	0	6	0.01	0	13.99	20
Batch No. 4	2.1	0	0.01	400	17.89	20
Batch No. 5	2.1	6	0.01	400	11.89	20
Batch No. 6	0	6	0.01	400	13.99	20
Batch No. 7	0	0	0.01	400	19.99	20

Figure 101. Experimental setup.

After being shaken for 48 hr at 100 rpm, the samples with 50 ppm HA were centrifuged at 2700 rpm at 22°C for 30 minutes (Figure 102). All samples, after being centrifuged, were filtered using a 0.45 μm syringe filter, yielding a 3-mL aliquot. Aliquots for KPA [U(VI) analysis] and ICP-OES (Fe and Si analysis) were prepared by taking a 300-μL aliquot for KPA and a 500-μL aliquot for ICP-OES from the filtered solutions and doing a 10x dilution with 1% HNO_3. Samples with 30 ppm HA were placed on a platform shaker over a period of time until the pH of the sample was stable; pH of the samples was measured daily and readjusted with addition of an acid or base to the original pH. After the sample pH stabilized, the samples were centrifuged, following the same procedure used for the 50 ppm HA samples. Filtered and unfiltered samples were then prepared for analysis via KPA and ICP.

Figure 102. Shaker and centrifuge experimental setup.

Subtask 2.4: Results and Discussion

Unfiltered samples from batches 1, 4, and 7 containing uranium, colloidal silica and/or sediment with no humic acid were analyzed using the KPA instrument; uranium removal data at different pH is shown in Figure 103. Batch 1 showed a decreasing trend starting at 60.90% removal at pH 4 to 20.97% removal at pH 8. Batch 4 also gave a decreasing trend to a lesser degree, beginning

at 74.40% removal at pH 4 and 57.72% removal at pH 8. Unlike batches 1 and 4, batch 7 had a maximum removal at pH 5 (93.98%) then decreased to 65.93% at pH 8. Batch 7 yielded the highest removal among the samples, with U(VI) being able to bind to the sediment; unlike batch 4, which contains U(VI), sediment and silica and uranium could bind to silica, sediment or both. If uranium is bound to silica, it may remain in solution; this could be the reason for less removal for batch 4 and higher removal for batch 7. It might be possible that some of the U(VI) is adsorbed to the colloidal Si and cannot be measured without sample filtration. Batch 1, which only contained silica, showed significantly less removal than both batches 4 and 7. In this case, any removal would be due to silica aggregation or coagulation and positive uranyl ions present in the solution at pH 4 can interact with the negatively charged silica surface. Silica particles have a negative surface charge, the magnitude of which increases with increasing pH and increasing ionic strength (Kobayashi 2005). Krestou and Panias (2004) reported that as pH increases, the positively charged uranyl ions become negatively charged; this limits the interaction of uranium with silica particles, leading to less uranium removal. Batch 1, 4 and 7 samples were filtered through a 0.45-µm syringe filter and were also analyzed via KPA to estimate uranium removal from the samples; this data is shown in Figure 104. Uranium removal for batches containing silica, batch 1 and batch 4, are in the range of 88% - 99%, while the percent of uranium removal for batch 7 with uranium and sediment are in the range of 75% - 99%. The higher removal of uranium in the case of filtered samples can be attributed to removal of uranium from the solution that is bound to silica, which is removed during the filtration process.

Figure 103. Uranium removal for unfiltered samples for batches 1, 4, and 7.
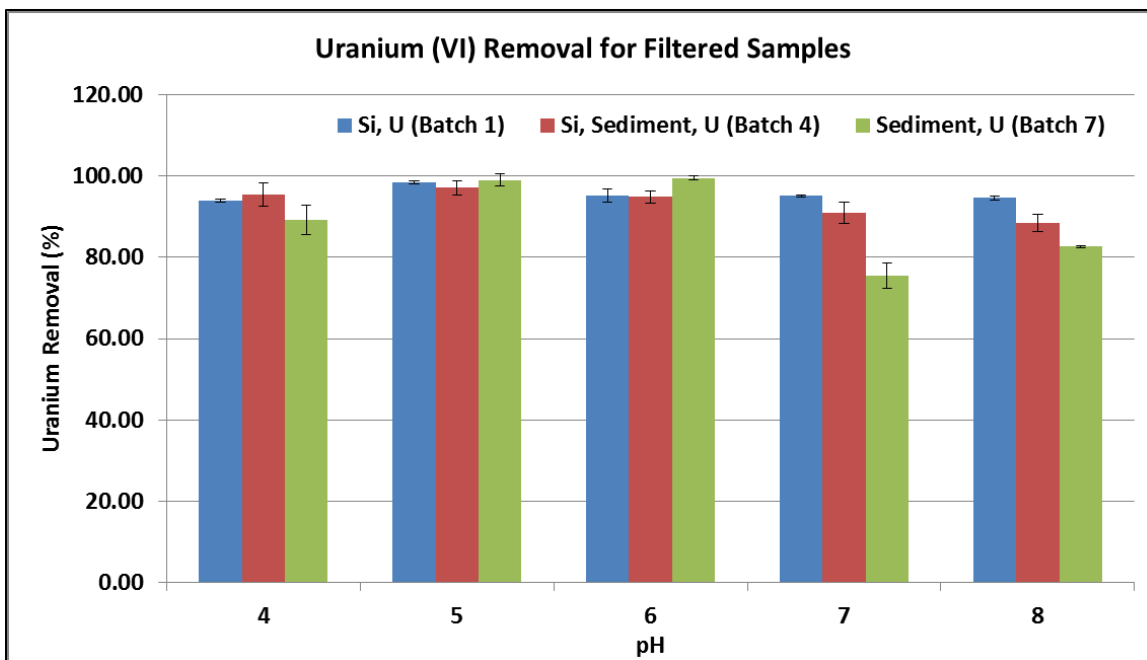
Figure 104. Uranium removal for filtered samples for batches 1, 4, and 7.

Batches 1, 4, and 7 containing uranium, silica and/or sediment with no humic acid were analyzed using ICP-OES in order to determine silica and iron concentrations. Unfiltered samples were analyzed; silica removal data obtained during this analysis is shown in Table 36. Batch 1 showed approximately 50% of silica removal while batch 4 data was inconsistent; most of batch 4 samples showed no detectable concentration of silica. Data obtained for filtered sample from batches 1, 4, and 7 containing uranium, silica, and/or sediment with no humic acid are shown in Table 36.

Batch 1 filtered samples, which contain only silica and uranium, revealed a high silica percent removal with pH 4, yielding the highest removal at 98% and subsequently decreasing until pH 8, with a removal percent of 88%. Batch 4 (silica, uranium, sediment) filtered samples had an average removal of ~97% between all pH values. Batch 7 was analyzed and revealed no silica presence, as expected; batch 7 does not contain fumed silica particles and only contains sediment and uranium; no Si release from sediment was observed.

Table 36. Silica Removal for Unfiltered and Filtered Samples

Batch#/pH	Unfiltered Samples		Filtered Samples	
pH 4	Si Avg Removal, %	Std Deviation	Si Avg Removal, %	Std Deviation
Batch 1	54.6	7.77	97.74	2.05
Batch 4	Not Detected	Not Detected	96.36	0.55
Batch 7	-	-	-	-
pH 5	Si Avg Removal, %	Std Deviation	Si Avg Removal, %	Std Deviation
Batch 1	55.6	1.55	96.4	1.72
Batch 4	Not Detected	Not Detected	97.06	0.93
Batch 7	-	-	-	-
pH 6	Si Avg Removal, %	Std Deviation	Si Avg Removal, %	Std Deviation
Batch 1	48.20	4.35	92.3	1.61
Batch 4	45.10	9.06	96.41	1.44
Batch 7	-	-	-	-
pH 7	Si Avg Removal, %	Std Deviation	Si Avg Removal, %	Std Deviation
Batch 1	51.30	6.48	88.72	3.89
Batch 4	Not Detected	Not Detected	98.67	0.64
Batch 7	-	-	-	-
pH 8	Si Avg Removal, %	Std Deviation	Si Avg Removal, %	Std Deviation
Batch 1	41.60	2.89	88.13	2.12
Batch 4	Not Detected	Not Detected	97.72	0.10
Batch 7	-	-	-	-

FIU completed synergy experiments with 30 ppm of humic acid; fresh stock solutions of 30 ppm humic acid and 3.5 mM of silica were prepared. Triplicate samples of batches containing HA, Si, sediment and uranium were prepared by mixing a known amount of various constituents. Uranium was added prior to the pH adjustment and precautions were taken to add the appropriate amount of DIW so that the addition of the acid/base resulted in a total volume of approximately 20 ml. pH of the samples was adjusted with 0.01M HCl or 0.1M NaOH to the desired pH and the samples were placed on a platform shaker. The pH of the samples was measured periodically and readjusted to the original pH as needed. The unfiltered and filtered batch samples were analyzed using the KPA instrument to measure uranium concentration to estimate the percent removal of uranium at varying pH levels (3-8), data from filtered and unfiltered samples are shown in Figure 105 and Figure 106. All batches showed maximum uranium at pH 4 with batch 6 having the highest removal of all with 89% uranium removal. Percent of uranium removal followed a decreasing trend with increase in pH and the average uranium removal at pH 8 was observed to

be around 50%. Batch 5 and 6 samples containing sediment showed the highest removal compared to non-sediment samples. Filtered samples had more removal than the unfiltered samples at the varying pH levels. There is a possibility that some of the uranium ions are absorbed to the colloidal silica and can only be removed via filtration; hence, higher uranium was observed for filtered samples. For both filtered and unfiltered samples, pH 4 had the highest percent removal. It can be seen that the filtration with used filters has less of an effect on the results of the U(VI) sorption in the pH range greater than pH 5. The sorption of uranium onto sediment decreases at higher pH conditions.
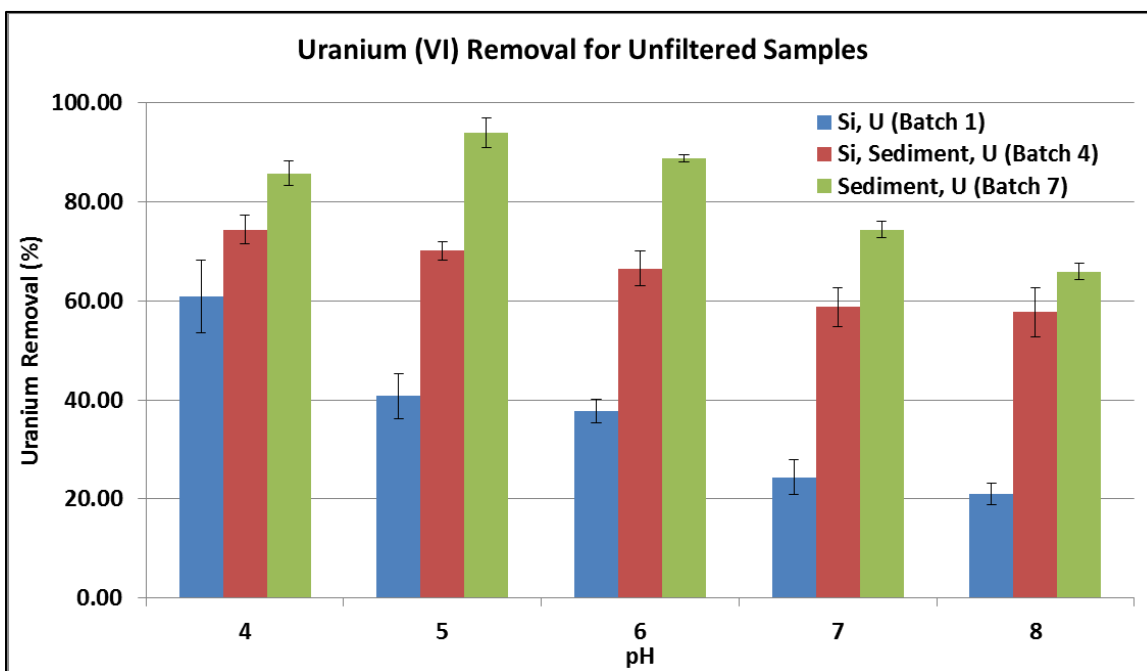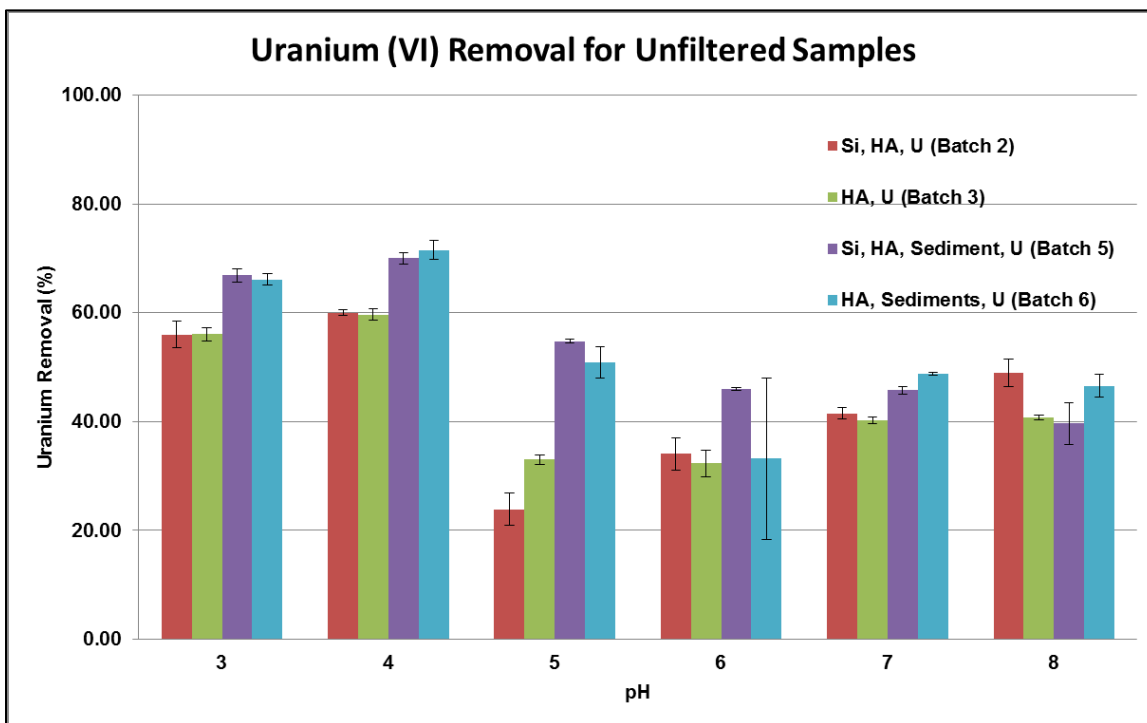

Figure 105. Uranium removal for unfiltered samples for batches 2, 3, 5 and 6.
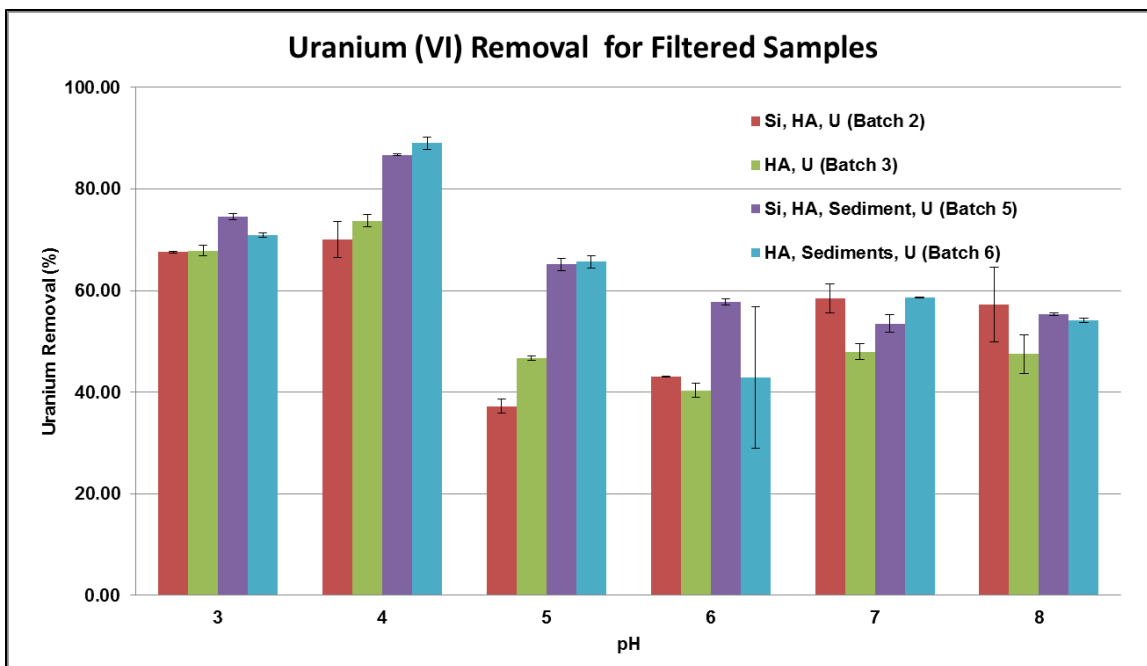
Figure 106. Uranium removal for filtered samples for batches 2, 3, 5 and 6.

pH 3 and pH 4

Percent of uranium removal for batches 2, 3, 5 and 6 at pH 3 and 4 were estimated by determining the uranium concentration of the samples via KPA. Uranium removal was calculated using the uranium concentration from the control samples. Table 37 shows the average U(VI) percent removal from the triplicate samples. The percent removal of uranium for batches 2 & 3 (with no sediment) and batches 5 & 6 (amended with sediment) was found to be between 56-60% and 66-70%, respectively. Solubility of HA is low at low pH while U(VI) is present as highly soluble uranyl ions (Krepelova, 2007b). Krepelova et al. (2007a) reported that HA enhances the U(VI) sediment uptake in acidic pH conditions. The high percent removal can be attributed to the competition of solubilizing negative functional groups (deprotonated carboxyl groups) with hydrophobic groups; at low pH, the hydrophobic group is the stronger force, causing aggregation/coagulation of the uranyl cations (Tipping, 2002). U(VI) interaction with silica colloids is found to be negligible as the batches with and without silica have similar uranium removal for both filtered and unfiltered samples. Addition of sediment contributed to around 10 -15 % uranium removal, possibly due to the availability of a greater number of binding sites for U(VI). The high solubility of uranium allows the cations to easily come into contact with negatively charged sediment particles and interact successfully, increasing the percent of U(VI) removal.

Table 37. Uranium Removal of Unfiltered and Filtered Batch Sample at pH 3 and 4.

	Unfiltered Samples		Filtered Samples	
pH 3	U(VI) % removal	Std. Dev	U(VI) % removal	Std. Dev
Batch 2	56.01	2.46	67.58	0.18
Batch 3	56.06	1.25	67.88	0.99
Batch 5	66.85	1.16	74.49	0.64
Batch 6	66.10	1.01	70.95	0.39
pH 4	U(VI) % removal	Std. Dev	U(VI) % removal	Std. Dev
Batch 2	60.04	0.52	70.04	3.60
Batch 3	59.68	1.03	73.75	1.27
Batch 5	70.01	0.99	86.73	0.24
Batch 6	71.53	1.69	88.99	1.18

pH 5 and 6

The average uranium removal for all batches at pH 5 and 6 is shown in Table 38. The uranium removal for batches 2 and 3 at both pH values are within the statistical error for both filtered and unfiltered samples. Similar to pH 3 and 4, batch samples with sediment were shown to improve uranium removal compared to non-sediment batches. At circumneutral pH, the number of uranyl cations in solution decreases, which ultimately limits the interactions between uranium and HA. Krepelova (2007a) reported that once the pH reaches 6, the dominant species in solution is $UO_2(OH)HA(I)$ with minimal presence of uranyl cations and $UO_2HA(II)$. Similarly, due to the increased solubility of HA, fewer binding sites are available for interactions.

Table 38. Uranium Removal of Unfiltered and Filtered Batch Sample at pH 5 and 6.

	Unfiltered Samples		Filtered Samples	
pH 5	U(VI) % removal	Std. Dev	U(VI) % removal	Std. Dev
Batch 2	23.88	2.92	37.21	1.40
Batch 3	33.06	0.87	46.73	0.46
Batch 5	54.77	0.38	65.12	1.13
Batch 6	50.89	2.83	65.63	1.29
pH 6	U(VI) % removal	Std. Dev	U(VI) % removal	Std. Dev
Batch 2	34.07	2.91	43.04	0.08
Batch 3	32.30	2.40	40.36	1.37
Batch 5	45.97	0.20	57.83	0.62
Batch 6	33.20	14.77	42.90	13.95

pH 7 and 8

Uranium removal at pH 7 and 8 for all unfiltered and filtered batches was observed to be in the range of 40 - 49% and 48 - 59%, respectively (Table 39). The uranium removal at pH 7 and 8 seemed to not be greatly affected by the presence of sediments. At high pH, the proton-binding sites of HA molecules are sufficiently dissociated to carry any significant charge, thus reducing any binding potential (Tipping 2002). The major species is $(UO2)_3(OH)_8^{2-}$, a negatively charged complex, limiting interaction with the dissociated functional groups of HA.

Table 39. Uranium Removal of Unfiltered and Filtered Batch Sample at pH 7 and 8.

	Unfiltered Samples		Filtered Samples	
pH 7	U(VI) % removal	Std. Dev	U(VI) % removal	Std. Dev
Batch 2	41.52	1.01	58.45	2.82
Batch 3	40.30	0.60	47.98	1.59
Batch 5	45.78	0.72	53.52	1.74
Batch 6	48.77	0.31	58.63	0.01
pH 8	U(VI) % removal	Std. Dev	U(VI) % removal	Std. Dev
Batch 2	48.89	2.53	57.21	7.34
Batch 3	40.77	0.51	47.48	3.79
Batch 5	39.64	3.82	55.37	0.31
Batch 6	46.58	2.03	54.16	0.42

Subtask 2.4: Future Work

The focus of this research was to study the influence of varying HA concentration on uranium removal at constant U(VI) concentration. However, it is important to study the effect of varying uranium concentration in the presence of HA and colloidal silica at variable pH. FIU will study the synergetic interactions between HA and colloidal silica on uranium removal at varying uranium concentrations in the system.

Subtask 2.4: Acknowledgements

Subtask 2.4: References

Chen, C., and X. Wang, 2007. Sorption of Th (IV) to silica as a function of pH, humic/fulvic acid, ionic strength, electrolyte type. *Applied Radiation and Isotopes* 65, 155-163.

Choppin, G.R., 1992. The role of natural organics in radionuclide migration in natural aquifer systems. *Radiochim. Acta* 58/59, 113.

Davis, J.A., 1982. Adsorption of natural dissolved organic matter at the oxide/water interface. *Geochim. Cosmochim. Acta* 46, 2381-2393.

Davis, J.A., 1984. Complexation of trace metals by adsorbed natural organic matter. *Geochim. Cosmochim. Acta* 48, 679-691.

Ivanov, P., Griffiths, T., Bryan, N.D., Bozhikov, G. and S. Dmitriev, 2012. The effect of humic acid on uranyl sorption onto bentonite at trace uranium levels. *J. Environ. Monit.,* 14, 2968 - 2975.

Kobayashi M., Juillerat F., Galletto P., Bowen P., and Borkovec M., 2005. Aggregation and Charging of Colloidal Silica Particles: Effect of Particle Size, Langmuir, 21 (13), 5761-5769 DOI: 10.1021/la046829z

Koopal, LK, Y. Yang, A.J. Minnaard, P.L.M. Theunissen, W.H. Van Riemsdijk, 1998. Chemical immobilisation of humic acid on silica. Colloids and Surfaces A: Physicochemical and Engineering Aspects 141, 385-395.

Krepelova, A., 2007a. Influence of Humic Acid on the Sorption of Uranium(VI) and Americium(III) onto Kaolinite (Dissertation).

Krepelova, A., Brendler, V., Sachs, S., Baumann, N., Bernhard, G., 2007b. U(VI)-Kaolinite Surface Complexation in Absence and Presence of Humic Acid Studied by TRLFS. Environ. Sci. Technol. 2007, 41, 6142-6147.

Krestou A., Panias D., 2004, Uranium (VI) speciation diagrams in the $UO_2^{2+}/CO_3^{2-}/H_2O$ system at 25^oC, The European Journal of Mineral Processing and Environmental Protection, Vol.4, No.2, 1303-0868, 2004, pp. 113-129.

Labonne-Wall, N., Moulin, V., Vilarem, J.P., 1997. Retention properties of humic substances onto amorphous silica: consequences for the sorption of cations. *Radiochim. Acta,* 79, 37-49.

Lagos, L., Katsenovich, P., Gudavalli, R., et al., 2014. Rapid Deployment of Engineered Solutions for Environmental Problems at Hanford. Year End Technical Report, June 30, 2014, U.S. Department of Energy Office of Environmental Management Office of Science and Technology under Cooperative Agreement No. DE-EM0000598.

Perminova, I.V, Hatfield, K., Hertkorn, N., 2002. Use of humic substances to remediate polluted environments: from theory to practice. In the proceedings of the NATO Advance Research Workshop, Springer, P.O Box 17, 3300 AA Dordrech, The Netherland.

Plancque, G., Amekraz, B., Moulin, V., Toulhoat, P., Moulin, C., 2001. Molecular structure of fulvic acids by electrospray with quadrupole time-of-flight mass spectrometry. *Rapid Commun. Mass Spectrom*. 15, 827-835.

Tipping, E., 2002. Cation Binding by Humic Substances. Vol. 12. Cambridge UP, p. 266.

Wang, X. K.; Dong, W. M.; Dai, X. X.; Wang, A. X.; Du, J. Z.; Tao, Z. Y. 2000, Sorption and desorption of Eu and Yb on alumina: mechanisms and effect of fulvic acid. Appl. Radiat. Isot. 52, 165-173.

Zachara, J.M., Resch, C.T., Smith, S.C., 1994. Influence of humic substances on Co^{2+} sorption by a subsurface mineral separate and its mineralogical components. *Geochim. Cosmochim. Acta* 58, 553-566.

Subtask 2.5: Investigation of the Migration and Distribution of Natural Organic Matter Injected into Subsurface Systems

Subtask 2.5: Introduction

The Savannah River Site (SRS) was established as one of the major U.S. Department of Energy (DOE) facilities for the production of materials related to the U.S. nuclear program during the early 1950s. The F-Area Hazardous Waste Management Facility (HWMF) consists of three unlined, earthen surface impoundments, referred to as seepage basins. From 1955 to 1988, the F-Area seepage basins received approximately 1.8 billion gallons of low level waste solutions generated by uranium slug and irradiated fuel processing in the F-Area Separations Facility. The effluents were acidic due to the presence of nitric acid and a contained a wide variety of radionuclides and dissolved metals (Dong et al., 2012). The waste solutions were moved approximately 3,000 feet from each processing area through underground clay pipes to the basins. Once the wastewater entered the basin, it was allowed to evaporate and seep into the underlying soil. The basins were intended to minimize contaminant migration to exposure points through the interactions with the basin soils. Although they performed as designed, due to the acidic nature of the basin influent, there was mobilization of some metals and radionuclides of uranium isotopes, ^{129}I, ^{99}Tc, and tritium, which migrated into the groundwater to create an acidic plume with a pH between 3 and 5.5.

Beginning in the late 1950s, the groundwater at the basins has been monitored and assessed. Remediation efforts and assessments have been applied through the years using various types and numbers of wells, seepline monitoring points and surface water locations. Although the site has gone through years of active remediation, the groundwater remains acidic, with pH as low as 3.2 around the basins and increasing to pH 5 down gradient. In addition, U(VI) and other radionuclide concentrations remain above their maximum contaminant levels. In an effort to remove the contaminants from the groundwater, pump-and-treat and re-inject systems were implemented in 1997. Down gradient contaminated groundwater was pumped to a water treatment facility, treated to remove metals (through osmosis, precipitation/flocculation, and ion exchange), and then re-injected upgradient within the aquifer. The pump-and-treat water treatment unit eventually became less effective, generated large amounts of radioactive waste and was expensive to maintain, prompting research for new remedial alternatives. In 2004, the pump-and treat system was replaced by a funnel and gate system in order to create a treatment zone via injection of a solution mixture composed of two components, sodium hydroxide and carbonate. The injections were done directly into the gates of the F-Area groundwater to raise pH levels. The purpose of the treatment zone was to reverse the acidic nature of the contaminated sediments, thereby producing a more negative net charge on the surface of sediment particles and enhancing adsorption of cationic contaminants. This system of remediation required a systematic re-injection of the base to raise the pH to near neutral values. However, the continuous use of high concentrations of a carbonate solution to raise pH creates a concern of possible re-mobilization of uranium that was previously adsorbed within the treatment zone since U(VI) in the presence of bicarbonate ions forms soluble aqueous uranyl-carbonate complexes.

Savannah River National Laboratory (SRNL) has been testing an unrefined, low cost humic substance known as Huma-K as an amendment that can be injected into contaminant plumes to enhance sorption of uranium, Sr-90, and I-129. A field test of the humic acid technology for uranium and iodine-129 (I-129) was conducted by Millings et al. (2013) at the F-Area Field Research Site. Humic substances are ubiquitous in the environment, occurring in all soils,

waters, and sediments of the ecosphere. Humic substances are complex heterogeneous mixtures of polydispersed materials formed by biochemical and chemical reactions during the decay and transformation of plant and microbial remains. Humic substances (HS) account for 50-80% of the organic carbon in the soil or sediment and are known for their excellent binding capacity for metals, while being insoluble or partially soluble. This makes HS a strong candidate for remediation efforts to reduce the mobility of uranium (VI) in the subsurface. Three main fractions of HS are identified based on their solubility in dilute acids and bases. Their size, molecular weight, elemental composition, structure, and the number and position of functional groups vary.

> *Humic acids:* the fraction of humic substances that is not soluble in water under acidic conditions (pH < 2) but is soluble at higher pH values. They can be extracted from soil by various reagents, which are insoluble in dilute acid. Humic acids are the major extractable component of soil humic substances. They are dark brown to black in color.

> *Fulvic acids:* the fraction of humic substances that is soluble in water under all pH conditions. They remain in solution after removal of humic acid by acidification. Fulvic acids are light yellow to yellow-brown in color.

> *Humin:* the fraction of humic substances that is not soluble in water at any pH value and in alkali. Humins are black in color.

The Huma-K commercially available dry flake organic amendment was used as a source of humic acid for these experiments. Huma-K is high in humic and fulvic compounds and is just one of several brands produced for large scale use as soil conditioners to boost productivity in organic agriculture and used by farmers to stimulate plant growth and facilitate nutrient uptake. Huma-K is made from leonardite, an organic rich mineral formed due to decomposition by microorganisms, by extracting the raw material with a potassium hydroxide base solution and then drying it. The high pH solubilizes the humic acid molecules and generates a dark-brown highly-concentrated solution, rich in humic acid, which can be diluted for use. Importantly, while such solutions are commonly called soluble humic acid, they are actually basic with pH greater than 7.

Subtask 2.5: Materials and Methods

Sediment Characterization

Sediment previously obtained from SRS and characterized during characterized by FIU during 2014 was used in the experiments. The sediment sample was obtained from SRS's FAW-1 at a depth of 60'-70'. Sediment was disaggregated with minimal force to avoid creating new mineral surfaces due to fracturing and abrasion using a 2-mm sieve to collect sediment of particle size ≤2 mm.

Column Experiments

A glass column (25 mm x 300 mm) obtained from Ace Glass Inc. was used to conduct the flow-through column experiment to study the sorption/desorption of humic acid onto SRS sediment and to study the mobility of uranium through humic acid sorbed sediment. The column, fitted with Teflon® adapters containing 350 micron screen support and a layer of glass wool (Figure 107), was filled with a known mass of oven dried sediment obtained from SRS (Figure 108).
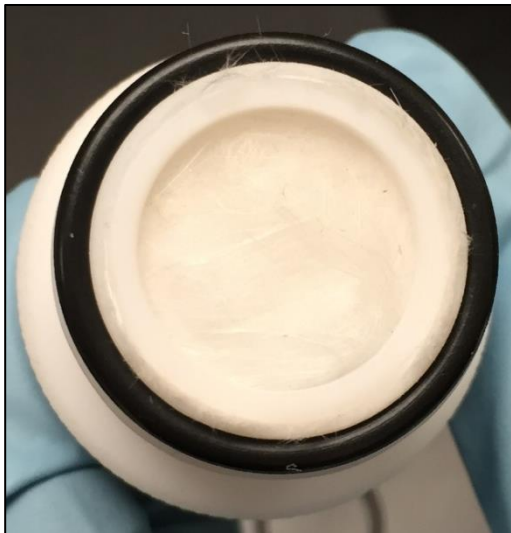
Figure 107. Teflon ® adapter with layer of glass wool.
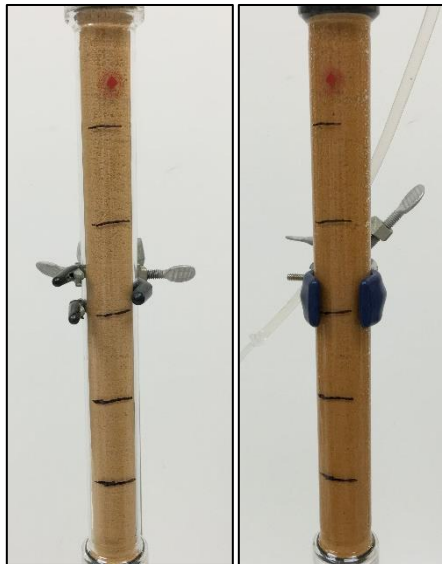
Figure 108. Column with SRS sediment before and after saturation with DIW.

Column Tracer Test

A bromide tracer test was performed to obtain transport parameters; prior to performing the tracer tests, the column was saturated with deionized water (DIW) from the bottom of the column to the top in order to remove air bubbles. Flow of DIW was continued until the effluent flow rate of 2 ml/min was achieved. After flow was equilibrated, 4 ml of a 1000 ppm bromide solution was injected at the top of the column. Samples of effluent were collected in pre-weighed containers at regular intervals. After each interval, the containers with samples were re-weighed and the bromide concentration was measured using a Thermo Scientific Orion Bromide Electrode (9635BNWP). Samples were collected until the bromide effluent readings reached equilibrium. Data collected allow for the determination of mean residence time, as well as the pore volume of the column. Prior to measuring the bromide concentration using a bromide electrode, the electrode was calibrated using bromide standards in the range of 0.5 - 100 ppm (Figure 109).
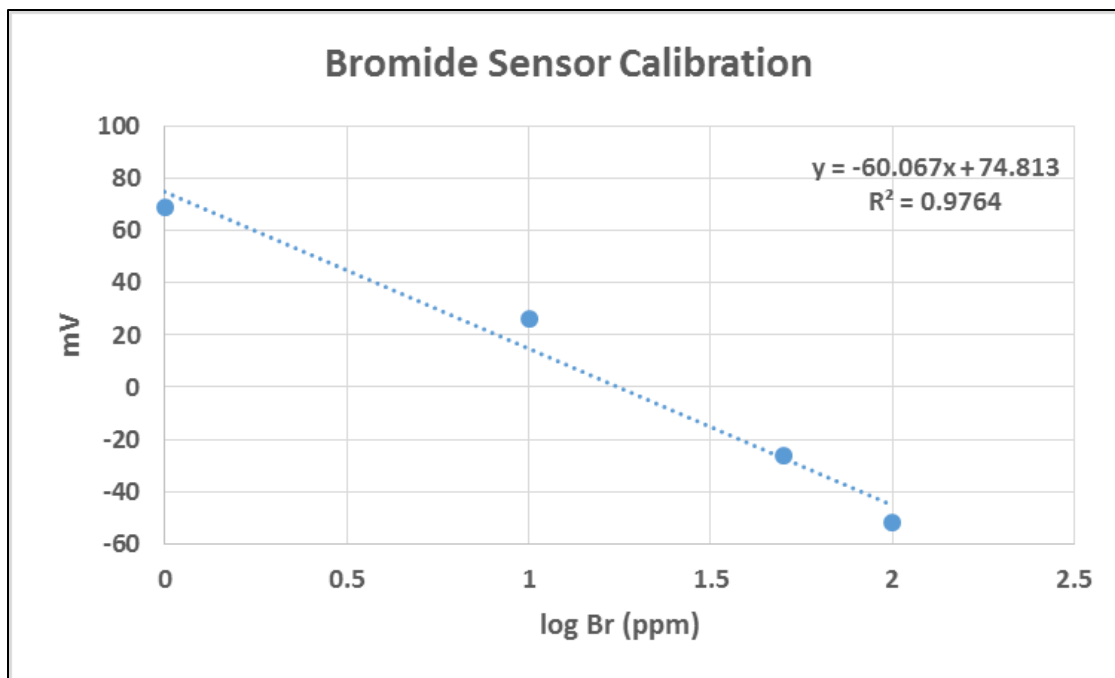
Figure 109. Calibration curve for bromide electrode.

The residence distribution function, E(v), as a function of volume fractions (Levenspiel, 1972) was calculated using Eq. 12:

$$E(v) = \frac{C(v)}{\int_0^\infty C(v)\,dv}$$

Eq 12

Where:
v - Volume of effluent
C(v) - Concentration of bromide

Mean residence time (t_m), and pore volume (V_p) (Shook et al., 2005) were estimated using Eq. 13 and Eq. 14:

$$t_m = \frac{\int_0^\infty t\,E(t)\,dt}{\int_0^\infty E(t)\,dt} = \int_0^\infty t\,E(t)\,dt$$

Eq 13

$$V_p = \frac{\int_0^\infty v\,E(v)\,dv}{\int_0^\infty E(v)\,dv} = \int_0^\infty v\,E(v)\,dv$$

Eq 14

Where:
t - Time
E(t) - Residence distribution function in terms of time
v - Volume of effluent
E(v) - Residence distribution function in terms of volume

Variance and the dimensionless Peclet number (P_e), which represents the ratio of the rate of transport by convection to the rate of transport by diffusion or dispersion, were determined by

solving the 1D dispersion/advection equation (Bischoff et al., 1963; Fogler et al., 1992; Mibus et al., 2007):

$$Variance\ \left(\sigma^2\right) = \int_0^\infty \left(v - v_p\right)^2 E(v)\,dv \qquad \text{Eq 15}$$

$$\frac{\sigma^2}{t_m^2} = \frac{2}{P_e^2}\left(P_e - 1 + e^{-P_e}\right) \qquad \text{Eq 16}$$

Where:
v - Volume of effluent
v_p - Pore volume
E(v) - Residence distribution function in terms of volume

Sorption/Desorption of Huma-K

After the tracer test, the column was preconditioned using pH adjusted artificial groundwater (AGW). Artificial groundwater that mimics SRS groundwater characteristics was prepared according to Storm and Kabak (Storm & Kaback, 1992) by dissolving 5.4771 g $CaCl_2$, 1.0727 Na_2SO_4, 3.0943 g $MgCl_2$, 0.3997 KCl, and 2.6528 NaCl in 1 L of deionized water (Barnstead NANOpure water purification system). 0.84995 g $NaNO_3$ was dissolved to obtain a 0.01M $NaNO_3$ solution. One (1) mL of the stock solution was diluted into 1 L of deionized water acidified to the desired pH to create a working solution. AGW pH adjusted to 3.5 was pumped from the bottom of the column until the pH of the effluent solution reached equilibrium at pH 3.55. Once the pH of the effluent reached equilibrium, approximately one pore volume (PV) of 10,000 ppm Huma-K solution, pH adjusted to 9 using 0.1 M HNO_3, was pumped at the same flow rate (2 ml/min) used during the tracer test. After injecting 1 PV of the Huma-K solution, pH 3.5 adjusted AGW solution was pumped into the column until the effluent concentration reached approximately 2% of the initial concentration; effluent samples were collected to measure the change in pH and concentration of Huma-K. The concentration of Huma-K in the effluent was measured immediately after collecting the sample to ensure the desired end point of the desorption phase was achieved. Samples were analyzed using a Thermo Scientific Genesys 10S UV-Vis spectrophotometer; calibration of the UV-Vis was performed using standards in the range of 1 to 25 ppm and at wavelength of 254 nm (Figure 110). Also, the E4/E6 ratio (ratio between the absorbance at 465 nm and 665 nm) and the E_{Et}/E_{Bz} ratio (ratio of absorbance at 253 nm and 220 nm) was measured using the UV-Vis spectrophotometer.

Sorption/Desorption of Uranium

After sorption and desorption of Huma-K, 2 PV of 100 ppb uranium prepared with AGW at pH 3.5 was injected through the column with Huma-K sorbed sediment to study the mobility of uranium. The desorption of uranium was studied by injecting 2 PV of 3.5, 4.5 and 5.5 pH adjusted AGW solutions, respectively.
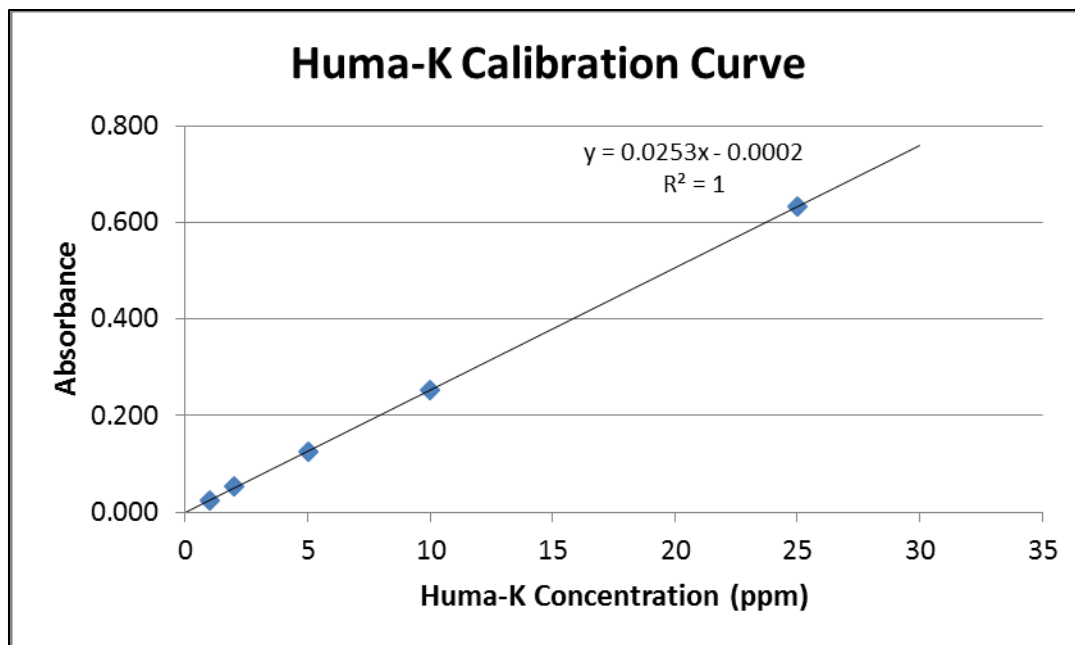
Figure 110. Humic acid calibration curve.

Subtask 2.5: Results and Discussion

Bromide Tracer Tests

The column was filled with 256.31 g of oven-dried SRS sediment that was sieved through a 2-mm sieve. After the column was filled and saturated with DI water, a bromide tracer test was performed by following the procedure detailed in the methodology section. The data obtained from the tracer test is presented in Figure 111 and Table 40. Figure 111 shows the change in concentration of bromide versus the volume of collected effluent fractions. The pore volume, variance and Peclet number were calculated using the five equations as described in the methodology section and the data is presented in Table 40 and Table 41. The results show that the column has a pore volume of 87.72 ml and a greater variance value positively correlates with a greater distribution spread.

Table 40. Tracer Test Results

Sediment weight (g)	Flow rate (ml/min)	Bromide added (mg)	Bromide recovered (mg)	Recovery (%)	Total fluid collected (mL)	Pore volume (ml)
256.31	2.0	4.0	3.72	93	371.85	87.72
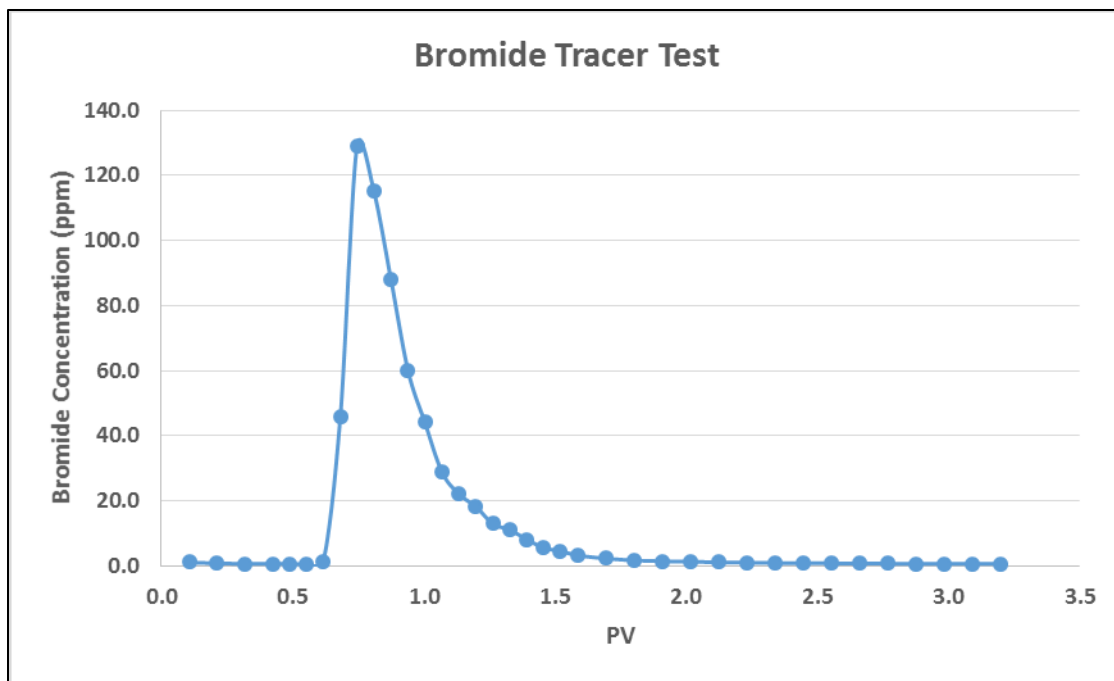
Figure 111. Concentration of measured bromide.

The dimensionless Peclet number (Pe) is defined as the ratio of the rate of transport by convection to the rate of transport by diffusion or dispersion (Eq. 17). Pe, found experimentally from the tracer test, was used to calculate effective dispersion (Table 41); the values of the Peclet number were used to correlate the effect of dispersion on the effluent tracer concentration.

$$Pe = \frac{rate\ of\ transport\ by\ convection}{rate\ of\ transport\ by\ diffusion\ or\ dispersion} = \frac{UL}{D_a}$$

Eq 17

Where:
L - characteristic length term (m)
D_a - effective dispersion coefficient (m^2/s)
U - average interstitial velocity (m/s)

Table 41. Transport Parameters Determined by Bromide Tracer Injection

U (m/s)	Variance, σ^2	Pe	Dispersion (m^2/s)	1/Pe=D/uL	Dispersion
4.09×10^{-4}	263.9	14.0	8.76×10^{-6}	0.071	High

Sorption and Desorption of Humic Acid

Following the bromide tracer test, AGW with pH adjusted to 3.5 was pumped from the bottom of the column until the pH of the effluent solution reached equilibrium (at pH 3.55). One (1) PV of 10,000 ppm of Huma-K with pH adjusted to 9 was then pumped at a flow rate of 2 ml/min. The humic solution was stirred continuously while pumping to avoid settling. After injecting approximately 1 PV of the humic solution, AGW at pH 3.5 was injected into the column until the concentration of Huma-K reached approximately 2% of the initial concentration while collecting effluent samples at 4 minute intervals. The concentration of humic acid in the effluent samples

was measured immediately after sample collection in order to ensure that the desired end point of the desorption phase was achieved. It was observed that approximately 2.2 PV of AGW with pH adjusted to 3.5 was required to reach 2% of the initial humic acid concentration. The effluent sample pH was also measured and recorded.

Figure 112 shows the breakthrough curve of humic acid sorption and desorption in the column and the change in pH. It is evident from the curve that most of the humic acid injected into the column was retained in the column and no humic acid was observed in the effluent solution until after 0.75 pore volumes. After 0.75 pore volumes, the concentration of humic acid increased and reached a peak value of approximately 5,700 ppm while the pH started to rise. When HA at pH 9 was injected into the pH 3.5 column, precipitation and re-dissolution of HA might have occurred as the pH of the solution increased; this would explain the spread of the breakthrough curve compared to that of the non-reactive bromide breakthrough curve. Because of precipitation, the amount of HA sorbed is inconclusive and the term "retained" is used over "sorbed" in this report. Around 2 PV, the concentration of HA started to decrease and the concentration of humic acid in the effluent reached 197 ppm after injecting approximately 2.2 PV of AGW at pH 3.5. Table 42 shows the results obtained from sorption and desorption of Huma-K; the pH of the column changed from 3.55 to 8.79 while retaining approximately 189 mg of humic acid out of 829 mg of humic acid, resulting in a retention total of 738 mg of humic acid per kg of sediment.
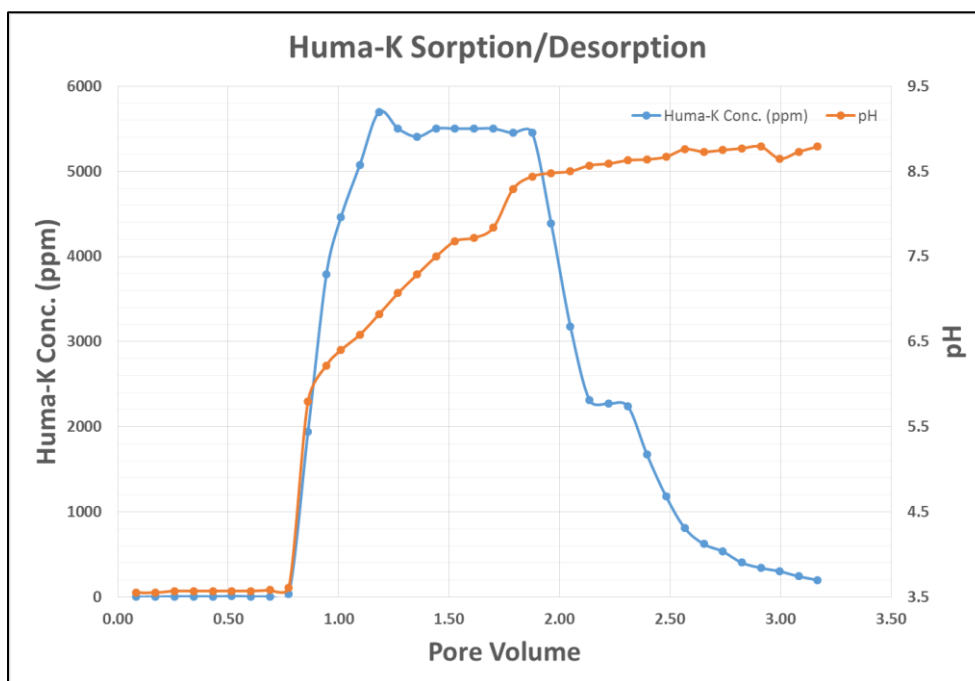
Figure 112. Concentration profile of HA in the effluent of the column.

Table 42. Soprtion/Desorption of Humic Acid

Sediment weight (g)	pH		Humic acid			
	Initial	Final	Volume injected (ml)	Injected (mg)	Recovered (mg)	Retained (mg/kg)
256.31	3.55	8.79	82.9	829.00	639.77	738.29

Since the humic acid solution was prepared from unrefined Huma-K, the humic solution was composed of humic acid and fulvic acid of different sizes and molecular weights; the E_4/E_6 ratio was used to determine which humic fraction sorbed onto the sediments. The E_4/E_6 ratio was calculated by dividing the absorbance of the sample at 465 nm by 665 nm. Researchers have found that the E_4/E_6 ratio increases as the average molecular weight of humic substances decreases. The range of values of the E_4/E_6 ratio from a wide variety of literature sources for humic acids and fulvic acids are 3.8-5.8 and 7.6-11.5, respectively; however, the E_4/E_6 ratios obtained during the experiment were in the range of 1.0 - 7.0. Where the concentration of humic acid in the effluent was high, the experimental E_4/E_6 ratios were in the range of 3.5 - 7.0, meaning that the fraction of humate bound to the sediments consists of humic acid molecules.

The E_{ET}/E_{BZ} ratio was calculated in order to determine the degree and possible nature of substitution. The ratio was calculated by measuring the absorbance at 253 nm and 220 nm, corresponding to the electron-transfer band and the benzenoid band, respectively. The intensity of the absorbance, especially the electron-transfer band, has a significant increase when substitution increases. The benzene band is almost unaffected. A low E_{ET}/E_{BZ} ratio indicates scarce substitution in the aromatic rings or substitution with aliphatic functional groups, while a high E_{ET}/E_{BZ} ratio indicates the presence of O-containing functional groups (hydroxyl, carbonyl, carboxyl, and ester groups) on the aromatic ring. The ratios vary from 0.03 (benzene ring), to between 0.25-0.35 for phenolic compounds and above 0.40 for aromatic rings with carbonyl and carboxylic groups. The values of the E_{ET}/E_{BZ} ratios were observed to be around 0.8 - 0.9, indicating that the aromatic structures in these humic molecules probably have a higher degree of substitution with oxygen-containing functional groups.

Sorption and Desorption of Uranium

Sorption and desorption of uranium in the humate sorbed column was studied by injecting 2 PV of a 100 ppb uranium solution prepared with SRS AGW at pH 3.5 followed by injection of 2 PV of AGW at pH 3.5, 4.5 and 5.5. Figure 113 shows the change in the concentration of uranium and change in pH while injecting the uranium solution through the column. The pH of the column decreased from 8.8 to 7.79 while 100 ppb of uranium at pH 3.5 was injected into the column.
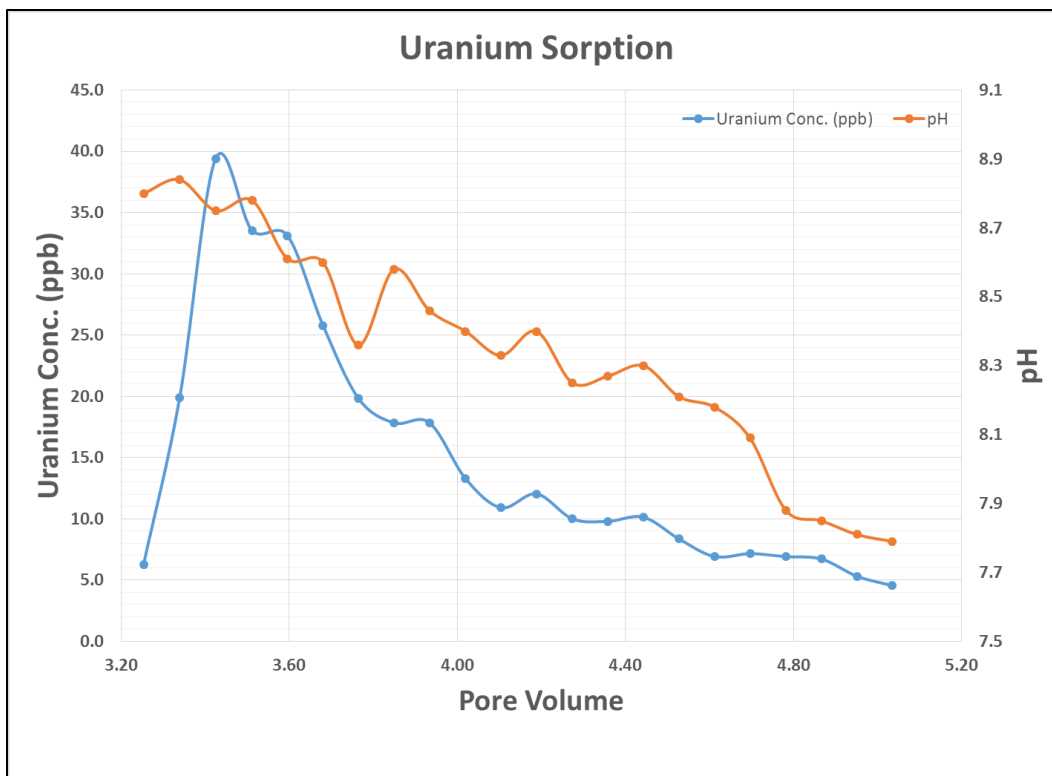
Figure 113. Change in uranium concetration and pH during uranium injection.

Figure 114 and Figure 115 show the change in humic acid concentration during injection of uranium and AGW solution at pH 3.5, respectively. Approximately 15 mg of humic acid was recovered from the effluent solution during the uranium injection, and total of 2.4 mg of humic acid was recovered during injection of the AGW solution with pH 3.5; no humic acid was recovered during injection of pH 4.5 and 5.5 AGW.

Table 43. Soprtion/Desorption of Humic Acid after Uranium Injection

sediment weight (g)	pH		Humic acid					
	Initial	Final	Volume injected (ml)	Injected (mg)	Recovered (mg)	Retained (mg/kg)	Total Recovered (mg)	Total Retained (mg/kg)
256.31	3.55	8.79	82.9	829.00	639.77	738.29	657.44	669.33
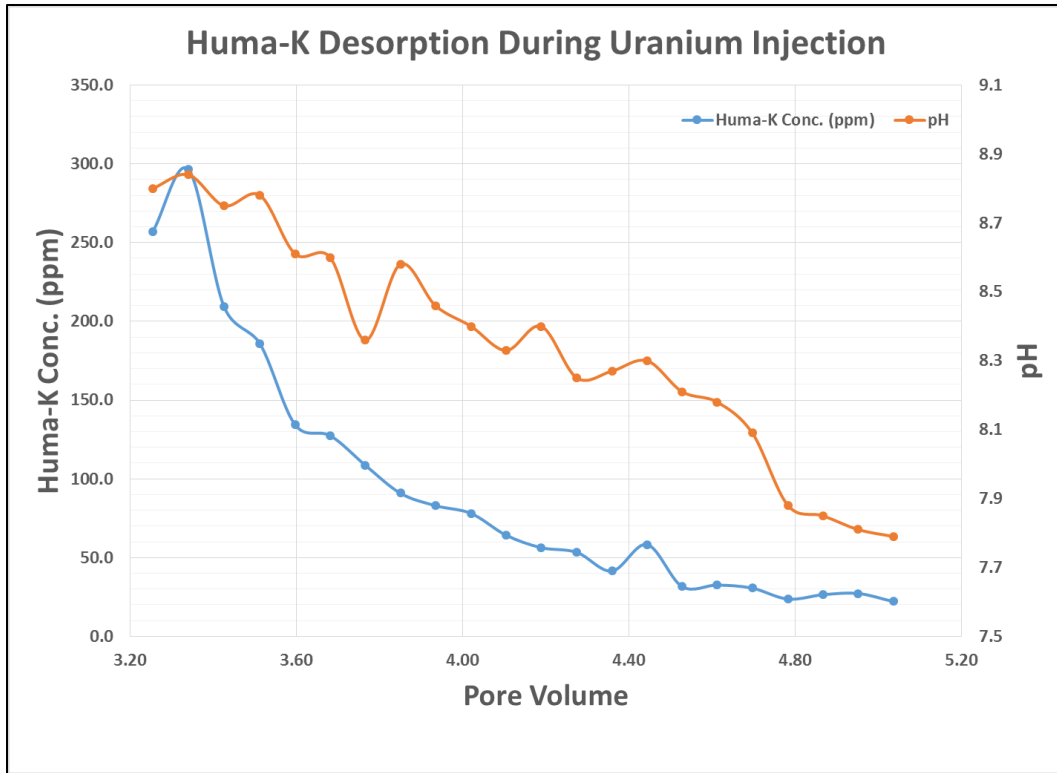
Figure 114. Change in Huma-K concentration during uranium injection.
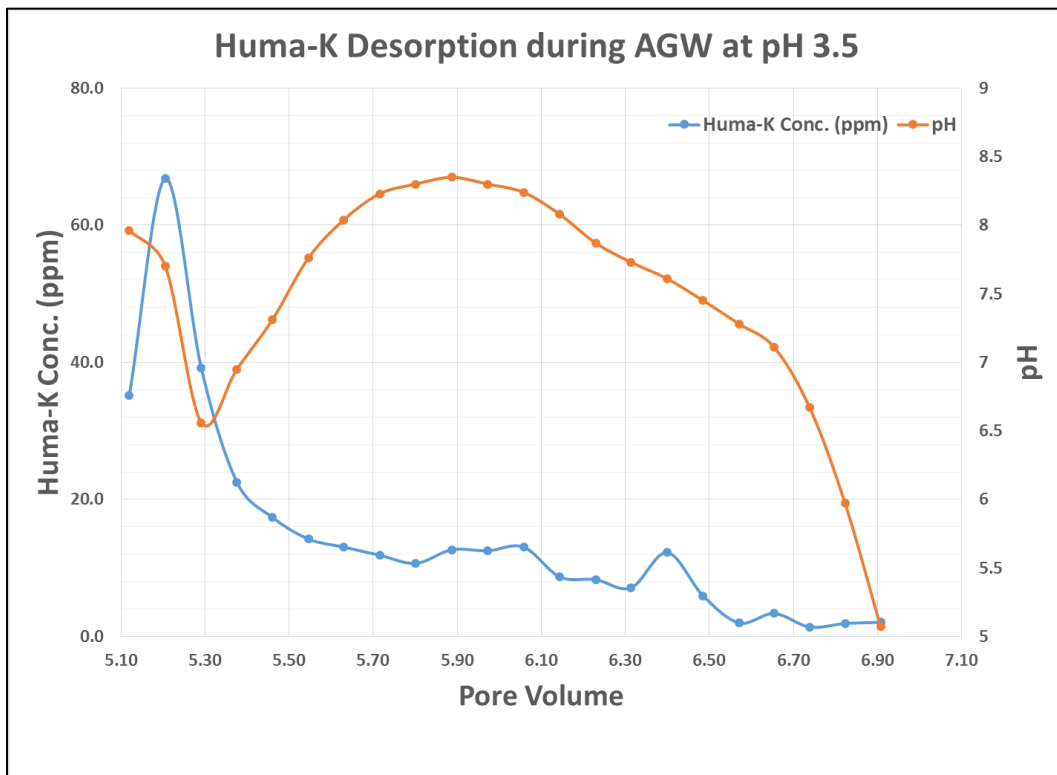
Figure 115. Humic acid recovery after uranium injection.

Figure 116 shows the change in uranium concentration and pH in the effluent solution during injection of the uranium solution and AGW (pH adjusted to 3.5 - 5.5). Approximately 16.4 µg of uranium was injected into the column; the amount of uranium recovered during the uranium injection and AGW at pH 3.5 were 2.43 µg and 0.568 µg, respectively. The concentration of uranium in the effluent solution during the injection of pH 4.5 and 5.5 AGW was below the detection limit of KPA. Samples collected during this phase of experiments were spiked with a known amount of 100 ppb uranium solution and reprocessed to obtain the concentration of uranium in the samples. The amounts of uranium recovered at this stage of the experiment were 0.026 µg and 0.03 µg, respectively. Table 44 shows the results obtained from sorption and desorption of uranium; overall, approximately 52 µg/kg of uranium was sorbed on to Huma-K sorbed sediment.
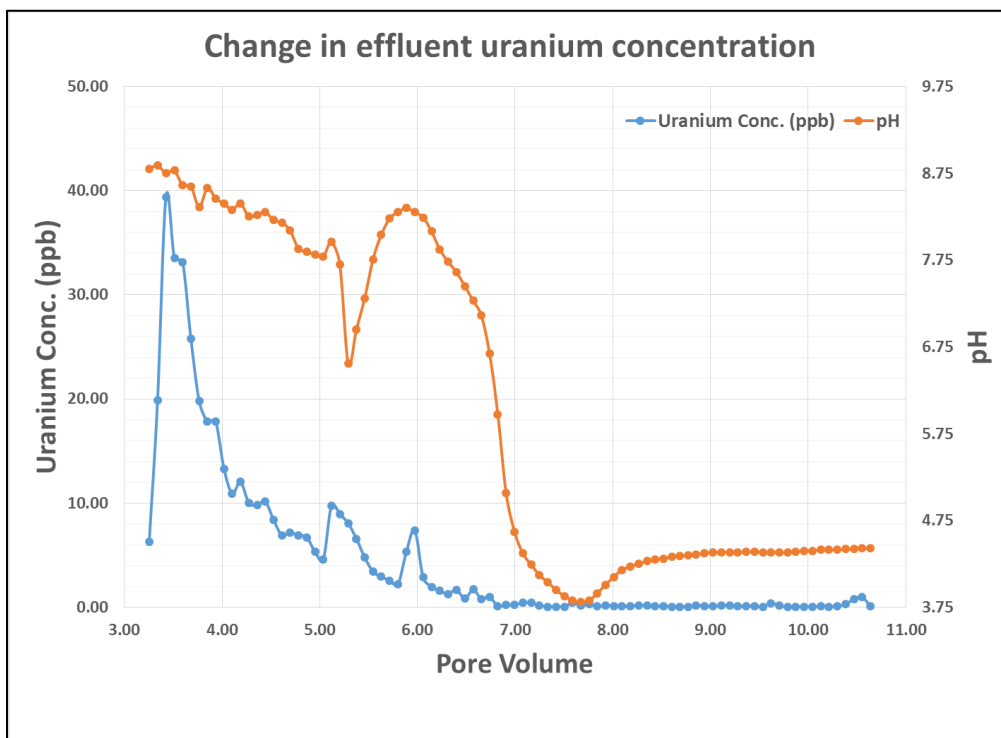
Figure 116. Change in uranium concentraion during sorption and desoprtion of uranium.

Table 44. Soprtion/Desorption of Uranium

Sediment weight (g)	pH		Humic acid		Uranium		
	Initial	Final	Retained (mg)	Retained (mg/kg)	Injected (µg)	Recovered (µg)	Retained (µg/kg)
256.31	8.79	4.43	171.56	738.29	16.39	3.05	51.95

Subtask 2.5: Future Work

FIU will continue to perform the humic acid sorption/desorption experiments at varying pH levels and varying humic acid concentrations to study uranium mobility though the humate sorbed columns.

Subtask 2.5: Acknowledgements

Subtask 2.5: References

Bear, Jacob, Hydraulics of Groundwater, McGraw-Hill Book Company, New York 1979.

Bischoff K., Levenspiel O., (1963) Adv. Chem. Eng. 4, p. 95.

Blake, G.R., and Hartge, K.H., (1986). Bulk Density. In: Klute, A. (Ed.), Methods of Soil Analysis. Part 1. Physical and Mineralogical Methods. American Society of Agronomy-Soil Science Society of America, 677 South Segoe Road, Madison, WI, 363-375.

Blake, G.R., and Hartge, K.H., (1986). Particle Density. In: Klute, A. (Ed.), Methods of Soil Analysis. Part 1. Physical and Mineralogical Methods. American Society of Agronomy-Soil Science Society of America, 677 South Segoe Road, Madison, WI, 377-382.

Danielson, R.E., and Sutherland, P.L., (1986). Porosity. In: Klute, A. (Ed.), Methods of Soil Analysis. Part 1. Physical and Mineralogical Methods. American Society of Agronomy-Soil Science Society of America, Madison, WI, 443-450.

Dong, W., Tokuanga, T. K., Davis, J. A., Wan, J., (2012). Uranium(VI) Adsorption and Surface Complexation Modeling onto Background Sediments from the F-Area Savannah River Site. Environ. Sci. Technol. 46, 1565-1571.

Fogler, H., S., (1992). Elements of Chemical Reaction Engineering, PTR Prentice-Hall, Inc., 837p.

Levenspiel, O., Chemical Reaction Engineering, 2nd Ed., (1972), John Wiley &Sons.

Mibus, J., Sachs, S., Pfingsten, W., Nebelung, C., Bernhard, G., (2007). Migration of Uranium (IV)/(VI) in the Presence of Humic Acids in Quartz Sand: a Laboratory Column Study, Journal of Contaminant Hydrology, Volume 89, Issues 3-4, Pages 199-217.

Milling, M. R., Amidon, M. B., Denham M. E., Looney B. B., (2013). Preliminary Data Report: Humate Injection as an Enhanced Attenuation Method at the F-Area Seepage Basins, Savannah River Site (U). (SRNL-STI-2013-00514).

Ptak, T., Piepenbrink, M., Martac E. (2004). Tracer Tests for the Investigation of Heterogeneous Porous Media and Stochastic Modelling of Flow and Transport - a Review of some Recent Developments, Journal of Hydrology, 122 - 163.

Shook, G. M., Forsmann, J. H., (2005). Tracer Interpretation Using Temporal Moments on a Spreadsheet (INL/EXT-05-00400).

Storm, R.N., Kaback, D.S. 1992. SRP Baseline Hydrogeologic Investigation: Aquifer Characterization, Groundwater Geochemistry of the Savannah River Site and Vicinity (U). Westinghouse Savannah River Company, Savannah River Laboratory.

Wan, J., Dong, Wenming, and Tokunaga T. K., (2011) Method to Attenuate U(VI) Mobility in Acidic Waste Plumes Using Humic Acids, Environ. Sci. Technol. 2011, 45, 2331–2337

Wan, J., Tokuanga, T. K., Dong, W., Denham M. E., Hubbard, S. E., (2012). Persistent Source Influences on the Trailing Edge of a Groundwater Plume, and Natural Attenuation Timeframes: The F-Area Savannah River Site. Environ. Sci. Technol. 46, 4490-4497.

TASK 3: SURFACE WATER MODELING OF TIMS BRANCH

TASK 3: EXECUTIVE SUMMARY

This task involves the development of a hydrological model to be used as a tool for predicting the fate and transport of sediment and contaminants in Tims Branch at SRS. Tims Branch has been impacted by contaminant discharges from process and laboratory facilities in the SRS A/M Area as a result of anthropogenic events associated with nuclear weapons research. The principal objective of Task 3 is to create a flow and contaminant transport model to examine the response of the Tims Branch system to historical discharges and environmental management remediation actions. The research under this task will directly support interpretation of historical data on the trends in contaminant concentrations in Tims Branch biota, and support planning and execution of future biota sampling in this important ecosystem, particularly considering the effect of extreme hydrological events on stream flow and the transport of sediment and contaminants

During FIU Performance Year 6, FIU continued development of the surface water model of Tims Branch that was initiated in Year 5 by first revising the model domain and then implementing the MIKE SHE overland flow, evapotranspiration, unsaturated and saturated flow modules. Development of a MIKE 11 stream flow model was also initiated which involved delineation of the stream network and cross section profiles using ArcGIS and MIKE 11 tools. This report provides a summarized description of the three interrelated subtasks: Subtask.3.1, Modeling of Surface Water and Sediment Transport in the Tims Branch Ecosystem; Subtask 3.2, Application of GIS Technologies for Hydrological Modeling Support; and Subtask 3.3, Biota, Biofilm, Water and Sediment Sampling in Tims Branch Watershed. These subtasks outline the preliminary development of the Tims Branch hydrological model using MIKE SHE, and the extensive pre-processing that was carried out using geographic information systems (GIS) tools to prepare the data for input into the model.

Subtask 3.1: Modeling of Surface Water and Sediment Transport in the Tims Branch Ecosystem

Subtask 3.1: Introduction

This research is part of continued efforts to correlate the hydrology of SRS and Tims Branch watershed (TBW) with the distribution of tin within the overland and river sub-domains. Tims Branch is a small braided, marshy, second-order stream that starts at the northern portion of SRS, passes through Beaver Ponds 1-5 and Steed Pond, and eventually discharges into Upper Three Runs (Figure 117). Its drainage area is nearly 16 km^2 (Batson et al., 1996). The average width of the stream varies between 2 to 3 m. Two major tributaries of Tims Branch are A014 and A011 outfalls which are approximately 230 m apart. They combine with the main stream of Tims Branch 1,400 m from the A014 outfall (Hayes, 1984). Flow in Tims Branch is strongly influenced by groundwater discharge (Mast and Turk, 1999). Because of the water table elevation and Tims Branch bed elevation, it is considered to be a losing stream (surface water discharges into the groundwater) near the A/M outfalls and a gaining stream (groundwater discharges into the stream) further south toward the confluence with Upper Three Runs (Looney et al., 2010; Varlik, 2013).
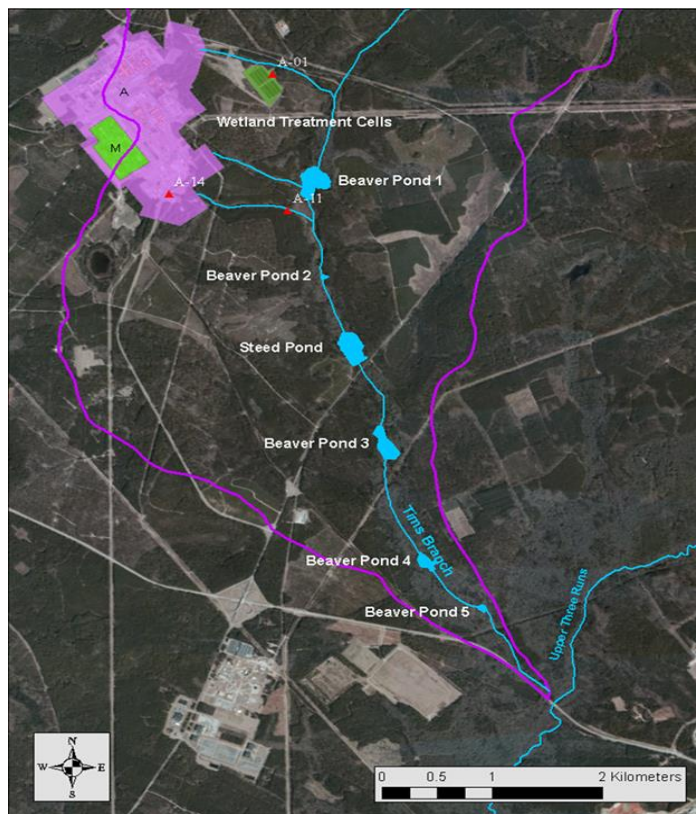
Figure 117. Tims Branch stream in the vicinity of the SRS A/M Area.

Environmental remediation actions were implemented in the SRS A/M Area in 2007 by injecting stannous (tin) chloride prior to air stripping in a pump and treat operation, which effectively removed trace levels of mercury (Hg) present in Tims Branch but resulted in concomitant discharge of inorganic tin (precipitated as small micro particles and nanoparticles of tin dioxide) into the A-014 outfall which discharges directly into Tim Branch stream at SRS. Although precipitated tin is mostly deposited as sediment, scientists postulate remobilization during episodic extreme events, such as storms or heavy rainfall. In these cases, sediment can be resuspended in the water column and deposited further downstream. The introduction of tin as a step function with high quality records on the quantity and timing of release provides a unique opportunity to study TBW as a complex full-scale ecosystem that experienced controlled step changes in its boundary conditions. Monitoring the fate and transport of tin compounds will contribute to the overall understanding of the behavior and movement of contaminants in TBW, particularly during heavy rainfall.

The principal objective of this task, therefore, is to develop and test a hydrological model which simulates stream flow and predicts the fate and transport of sediment and contaminants such as tin in the Tims Branch watershed, in order to examine the system's response to extreme hydrological events and monitor the long-term response to innovative EM-developed remediation treatment technologies. Performing simulations of extreme storm events provides DOE-EM/SRS with information that can assist in: (a) understanding the potential impact on flow depth and velocity in Tims Branch, (b) determining the potential for contaminant transport due to the resuspension and remobilization of sediment during such extreme events, and (c) identifying areas where sediment/contaminants might further be deposited.

Subtask 3.1: Methodology

During FIU Performance Year 6, FIU continued collaboration with SRNL and SREL scientists to develop an integrated spatially distributed hydrology model to analyze the tin cycle in the environment and to provide forecasting capabilities for the fate and transport of tin and other contaminants in Tims Branch watershed over time. ARC researchers completed the development of the main hydrological modules and components of the TBW overland flow model using MIKE SHE. The modeling application uses historical precipitation, groundwater levels, geological data, and river discharges that were retrieved from government databases and input to the model. The model was developed to simulate flow discharges and water levels and can determine spatial and temporal distribution of suspended particles or contaminants in the area when storms or heavy rainfalls occur. The model couples hydrology of the watershed with contaminant transport and provides a tool for analysis of spatiotemporal variation of tin concentration as a function of hydrology. Currently, the model includes the main hydrology cycle components: 2-D overland flow, 3-D groundwater flow, 1-D river flow, precipitation, and evapotranspiration.

Evapotranspiration (ET) Module Setup and Simulation

1. The ET module was developed using two methods: Richards Equation, and Two Layer Evapotranspiration/Unsaturated Zone (ET/UZ).
2. Two methods were used in module development: (a) uniform data of reference ET, Leaf Area Index, and Root Depth; and (b) station-based timeseries, which require timeseries of reference ET and station-based rainfall records.
3. Timeseries of rainfall records were acquired from the SRS database.
4. Station-based timeseries of rainfall data from various stations within South Carolina were obtained to generate rainfall grids in MIKE SHE. This data was processed prior to input into the relevant MIKE SHE module.
5. Station-based timeseries of reference ET was acquired from stations within Aiken County near SRS and processed in accordance with MIKE SHE requirements.
6. Table 45 shows some of the parameters used in the ET module, which are based on numerical stability criteria and experimental measurements reported in the literature.

Table 45. Evapotranspiration Parameters Used For ET Module Setup and Simulation

Parameter	Value	Units
Detention Storage	2.5	mm
Surface-Subsurface Leakage Coefficient	0.0001	1/sec
Reference Evapotranspiration	2.22	mm/day
Leaf Area Index	1.3 – 6.3	m^2/ m^2
Root Depth	0.0 – 4000	mm

Unsaturated Zone (UZ) Module Setup

1. The UZ module was developed using two methods: Richards Equation and Two Layer Unsaturated Zone.
2. The Richards equation was used for the preliminary simulation setup.

3. The spatial soil profile definition was developed using both uniform and distributed methods. Currently, the model is set up with a uniform spatial distribution with soil profile data acquired from a report generated specifically for the Tims Branch watershed from the US Department of Agriculture (USDA) Web Soil Survey website (http://websoilsurvey.sc.egov.usda.gov/App/WebSoilSurvey.aspx).

4. Each soil profile is comprised of several layers (horizons). The thickness of each layer varies from one soil type to another ranging from 0 – 80 in. Soil profiles consist of layers such as sand, sandy loam, loamy sand, and sandy clay loam. A complete report of the various soil profiles was created using MS Excel.

5. Vertical discretization was defined according to soil layer thickness, with finer discretization closer to the ground surface and coarser discretization for deeper layers.

6. In the current model set up, the uniform soil profile is classified into 4 different uniform soil horizons. A MIKE SHE unsaturated flow file (.uzs) for each soil horizon was created and a total of 4 horizons were prepared. Default parameters were used for preliminary setup of the soil characterization. Vertical discretization was set to represent 8 cell layers with various heights. Table 46 shows details of the UZ vertical discretization (values in meters).

Table 46. UZ Vertical Discretization (Values in Meters)

From depth	To depth	Cell height	No. of cells
0	0.076	0.076	1
0.076	0.584	0.254	2
0.584	0.762	0.178	1
0.762	1.762	0.2	5
1.762	2	0.238	1
2	4	1	2
4	20	2	8
20	50	3	10

7. In SRS, the depth of the unsaturated zone (also known as vadose zone) varies from 7 ft to 179 ft (Aadland et al., 1995; Hiergesell, 2004). In this model set up, 179 ft (~50 m) is assumed as the thickness of the unsaturated zone.

8. Station-based timeseries data of the groundwater table was acquired from 4 stations. Only one station was found inside the SRS boundary. The other remaining stations are within the neighboring counties (Aiken and Barnwell). Groundwater head timeseries data was processed and converted to the format accepted by the MIKE SHE model.

9. Uniform groundwater table depth was also tested as an additional option for UZ set up.

Saturated Zone (SZ) Module Setup

1. The SZ module was developed in two ways: one as a simplified configuration of a two-layer aquifer (shallow aquifer and aquifer), and another using an actual geologic layer configuration within the SRS A/M Area. The two-layer model will help in determining if a simplified groundwater flow representation would be adequate to capture the watershed hydrologic response. Furthermore, the two-layer model will run much faster, allowing the accommodation of running additional simulation scenarios in shorter timeframe. A more

complex integration of the actual soil layers significantly slows down the model and may not provide much more insight about the rainfall-runoff dynamics of TBW.

2. It was assumed that the shallow aquifer and aquifer are both uniform.
3. Each layer required values for geological parameters to be set in the model. These parameters were as follows:
   a. Lower Level
   b. Horizontal Hydraulic Conductivity (Kx)
   c. Vertical Hydraulic Conductivity (Ky)
   d. Specific Yield
   e. Specific Storage

The values for these parameters were mostly empirical, reported in various articles (Aadland et al., 1995; Miller et al., 2000; Rasmussen et al., 2003). Table 47 below shows the values assigned to these parameters.

Table 47. Geological Parameters Used for SZ Module Setup

	Lower Level (m)	K_x (m/s)	K_y (m/s)	Specific Yield	Specific Storage
Shallow Aquifer	-30	0.001	0.0001	0.2	0.0001
Aquifer	-100	0.001	0.0001	0.2	0.0001

4. It was assumed that the geologic layers are homogeneous and isotropic. Therefore, the values of horizontal and vertical hydraulic conductivities are uniform in space.
5. No geologic lens was considered.
6. Two computation layers were set up: Shallow Aquifer and Aquifer. Both layers were assumed to have closed outer boundaries. For simplicity, no internal boundaries were assigned at this stage of the model development.
7. Each computational layer in the SZ module requires an initial potential head. A GIS shapefile of groundwater head contour lines (2003) was prepared and used as the initial potential head. This file was internally interpolated in MIKE SHE to generate a model specific DFS2 grid file which then used to replace the original groundwater contour shapefile used in the SZ module. Figure 118 shows the 2003 groundwater head elevation that was used as the initial condition in the SZ flow module.
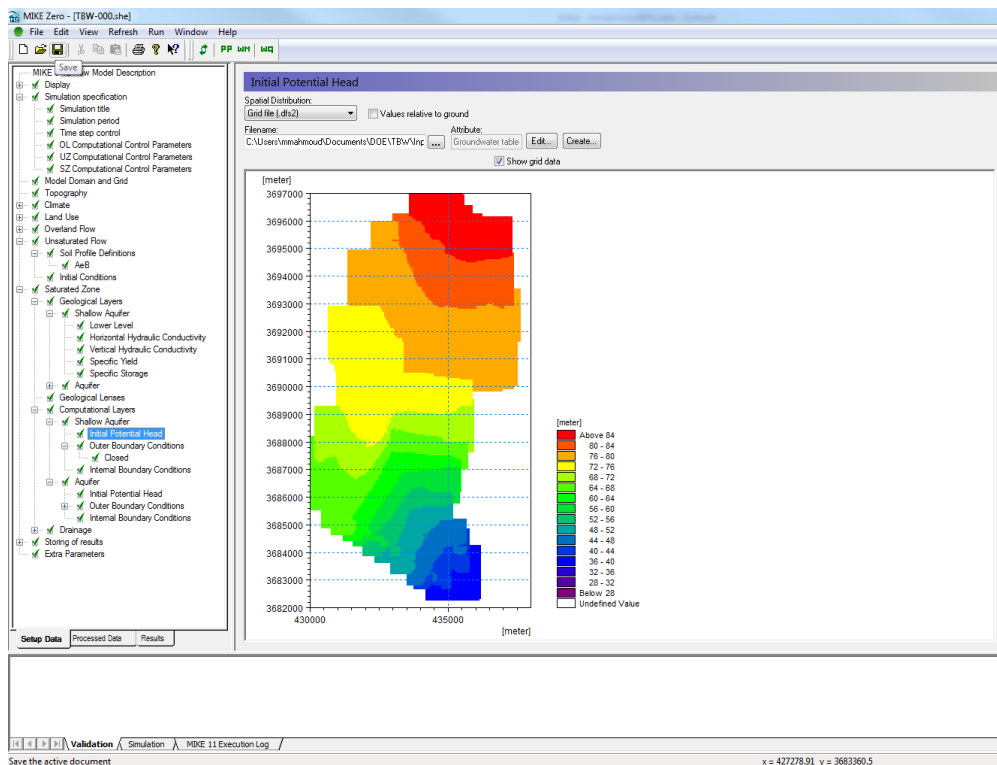
Figure 118. DFS file of groundwater head that was used as the initial condition in computation layers within MIKE SHE model.

Subtask 3.1: Results and Discussion

Simulation of overland flow in the Tims Branch watershed was performed after each hydrology module was completed. The first set of simulations of overland flow was only based on rainfall. The Evapotranspiration (ET) and Unsaturated Zone (UZ) modules were completed simultaneously and a second set of preliminary results of overland flow simulations was prepared. The third set of overland flow simulations was executed after the completion of Saturated Zone (SZ) module. The results are presented in an attached progress report (see Appendices). It should be taken into consideration that the above mentioned results are inconclusive due to the fact that no model calibration has yet been performed. Figure 119 illustrates a single simulation with and without the SZ module.
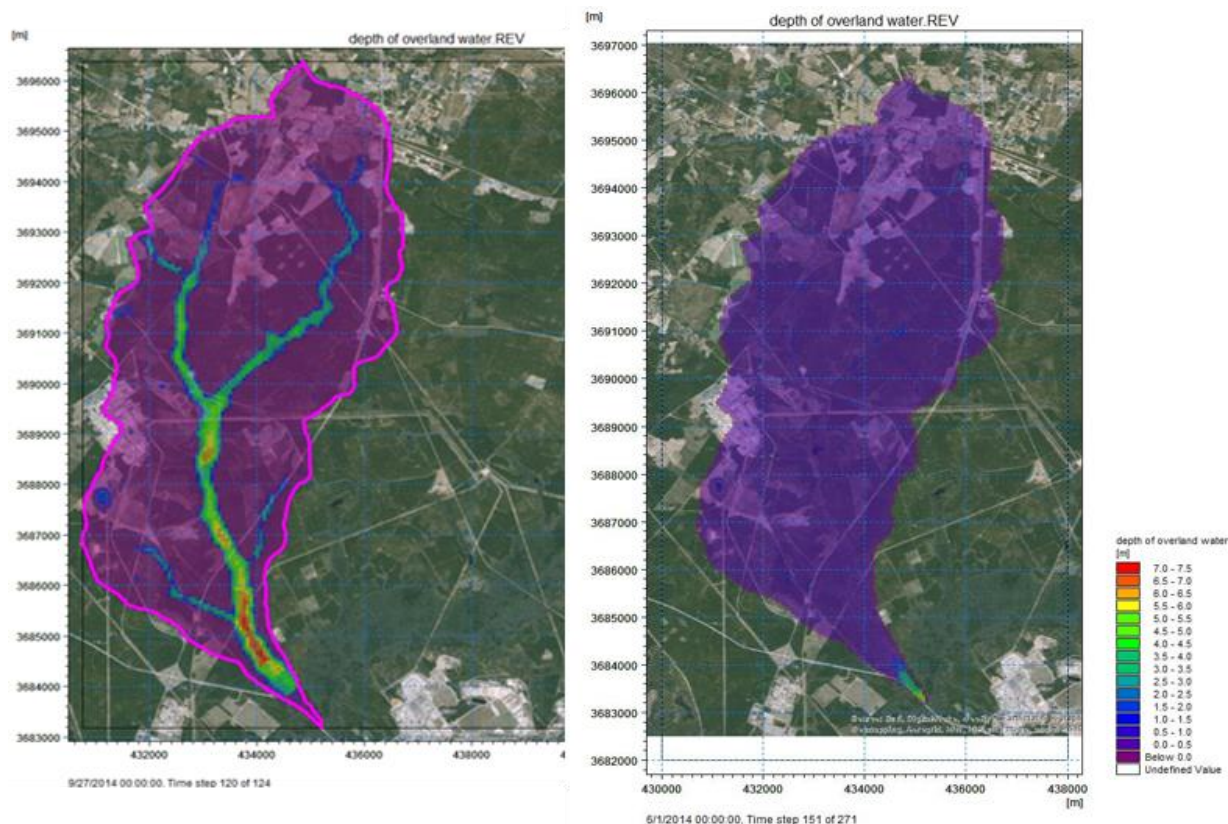
Figure 119. Simulation of overland flow in TBW without saturated zone (SZ), evapotranspiration (ET) and unsaturated zone (UZ) (left), and with all the hydrological modules (SZ, ET & UZ) activated (right).

Although the model is still in the development stage, it indicates relatively significant loss when the saturated zone is included for a long term simulation. The effect of surface water loss through infiltration may be minimal when simulating for a single rainfall event in a short period of time. Further simulation and calibration is required to verify the short term and long term effect of saturated zone on the simulation results.

In addition to model development, the following tasks were also accomplished:

- A draft Project Technical Plan was submitted to DOE on October 16, 2015 outlining the tasks planned for FIU Performance Year 6.
- A poster and associated paper entitled "Development of an Integrated Hydrological Model for Simulation of Surface Runoff and Stream Flow in Tims Branch Watershed" were submitted to the 2016 Waste Management Symposium held on Phoenix, AZ in March 2016.
- Three milestones were submitted outlining the model modification, and updates.
- A technical progress report for this subtask was submitted on June 29, 2016 outlining the process of model development and data preparation.
- In addition, the initial set up of MIKE 11 stream flow model for A-014 outfall and Tims Branch stream were started. These models will run as stand-alone and will be coupled with Tims Branch watershed overland flow model later on.

Subtask 3.1: Conclusion

Preliminary simulations indicate the model's capability in capturing overland water movement in Tims Branch watershed. Comparison between simulations for several short term rainfall events shows how the model responds to rainfall intensity and duration. Further investigation is required to understand the model's sensitivity to various hydrological parameters. Model calibration and validation will be performed to ensure model accuracy and to decrease the uncertainty of simulation results. Sensitivity analysis will also be performed to evaluate calibration factors and the effect of hydrological modules on simulation results.

Subtask 3.2: Application of GIS Technologies for Hydrological Modeling Support

Subtask 3.2: Introduction

An ArcGIS geodatabase was developed to support development of the hydrological model of the Tims Branch watershed at SRS. The SRS geodatabase has an advanced spatial data structure that facilitates storage and management of large spatiotemporal data sets derived from multiple sources that are required for model configuration and numerical model calibration. The MIKE SHE/MIKE 11 hydrological modeling package being used has a built-in user interface that directly accepts data in GIS format. The use of GIS data is significant not just for the spatial representation of hydrologic features, but particularly because of its integration with timeseries data attributes such as flow rates and directions, contaminant concentrations, water levels, precipitation, etc. Availability of data in this format shortens the time for model-specific data preparation and ultimately model development. The geodatabase developed is based on the ArcHydro and ArcGIS Base Map data models with modifications made for project-specific input parameters. The significance of this approach was to ensure its replicability for potential application at other DOE sites. Application of GIS tools has aided in the pre-processing and analysis of the hydrological model data; automation of repetitive geoprocessing tasks; and production of maps for visualization of the surface water hydrology of the Tims Branch watershed.

Subtask 3.2: Methodology

This subtask has involved the utilization of GIS software and tools to store, manage and process data required for the development of a surface water contaminant fate and transport model of the Tims Branch watershed at Savannah River Site. Model development required preprocessing of surface topography, rainfall and evapotranspiration time series, unsaturated and saturated zone parameters (soil characteristics, groundwater table time series, hydraulic conductivities, geologic formation, etc.), land cover, and land use data (vegetation coverage, impervious surface, manning coefficient, etc.) using GIS tools. Efforts during FIU Performance Year 6 were primarily focused on:

1. Downloading model-specific geospatial and timeseries configuration parameters such as precipitation, hydrology, geology, land use, vegetation cover and topography, to fill in data gaps for the revised Tims Branch watershed model domain.
2. Updating the original ArcGIS geodatabase developed for SRS in 2015 with the additional downloaded data.
3. Using ArcGIS tools to process the downloaded data to ensure that it is in the required model-specific format, that the appropriate coordinate system is assigned and that the data is clipped to the new model domain.

4. Reapplying previously developed process flow models using ArcGIS ModelBuilder to automate repetitive geoprocessing tasks and batch process data in order to save time, improve overall efficiency and document geoprocessing workflows.
5. Reproducing GIS maps of Tims Branch hydrology, geology, land use, vegetation cover, topography, etc. for the expanded model domain for visualization and reporting purposes.
6. Conducting geospatial analyses that can further support hydrological modeling results.
7. Using geoprocessing tools for preliminary creation of the Tims Branch stream network required for development of the MIKE 11 stream flow model.

Subtask 3.2: Results and Discussion

Download of Model-Specific Geospatial and Timeseries Configuration Parameters for Expanded Model Domain

GIS data used to initiate the Tims Branch model development in 2015 was often limited in extent to the Savannah River Site boundary. In 2016, a decision was made to extend the study area to the entire Tims Branch watershed, as opposed to only the portion of the watershed that lies within the SRS boundary. This therefore required additional spatiotemporal data to be downloaded to fill in data gaps for the revised Tims Branch watershed model domain. Work in 2016 was therefore focused upon modification of the SRS geodatabase to incorporate the downloaded data, and the use of ArcGIS tools to process the data using the expanded model domain for input into the hydrological model being developed for the Tims Branch watershed.

Data was derived from online databases of federal agencies such as the U.S. Geological Survey (USGS), the U.S. Department of Agriculture Natural Resources Conservation Service (USDA NRCS) State Soil Geographic (STATSGO) and Soil Survey Geographic (SSURGO) databases and the U.S. Geological Survey (USGS)/U.S. Department of the Interior (DOI) Multi-Resolution Land Characteristics Consortium (MRLC) national land cover database (NLCD). FIU ARC researchers also utilized several reports and journal publications provided by Savannah River National Laboratory (SRNL) and conducted an extensive literature review in order to characterize the study area and retrieve additional data required for model development and calibration.

Update of the SRS Geodatabase

The geodatabase developed for SRS in 2015 was updated to incorporate the recently downloaded data derived from the federal online databases described above for the expanded model domain of the Tims Branch watershed. As the data was collected from various sources, it was often necessary to conduct preprocessing in order to convert the files to compatible formats that could be uploaded into the ArcGIS geodatabase into the appropriate preconfigured feature datasets or raster catalogs. Pre-processing often involved alteration of tabular data from pivot tables to simple spreadsheets, conversion of data units (e.g., feet to meters), modification of tabular field properties (e.g., short integer to scientific notation) and renaming of tabular field names as there is a 10-character limit in ArcGIS geodatabases. This process of data conversion and standardization prepared the data for direct input into the MIKE SHE/MIKE 11 model.

Geoprocessing of Updated Model Data using ArcGIS

With the expanded Tims Branch watershed study domain, hydrological model data had to be collected from multiple sources which often resulted in data with different spatial references, that were at different scales, and that were from different time periods. ESRI's ArcGIS 10.2

geoprocessing tools were used to process the downloaded data to ensure that it was in the required model-specific format, that the appropriate coordinate system was assigned and that the data was clipped to the new model domain.

Application of Process Flow Models using ArcGIS ModelBuilder

Development of process flow models using ArcGIS ModelBuilder which has built-in ArcGIS tools helps to automate repetitive geoprocessing tasks and batch process data in order to save time, improve overall efficiency and document geoprocessing workflows which visually represent the tools and scripts (if any) that have been incorporated in the data model. ArcGIS ModelBuilder is a scalable and reusable application that can iterate over the hydrological model configuration parameters, perform geoprocessing actions, calculate statistical parameters and generate maps and reports.
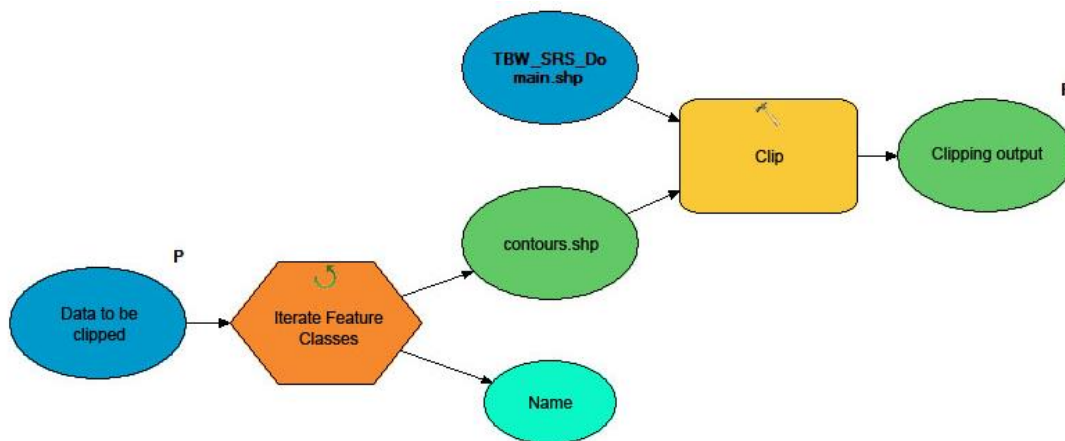
Figure 120. ArcGIS ModelBuilder workflow diagram for clipping GIS data to the study domain.
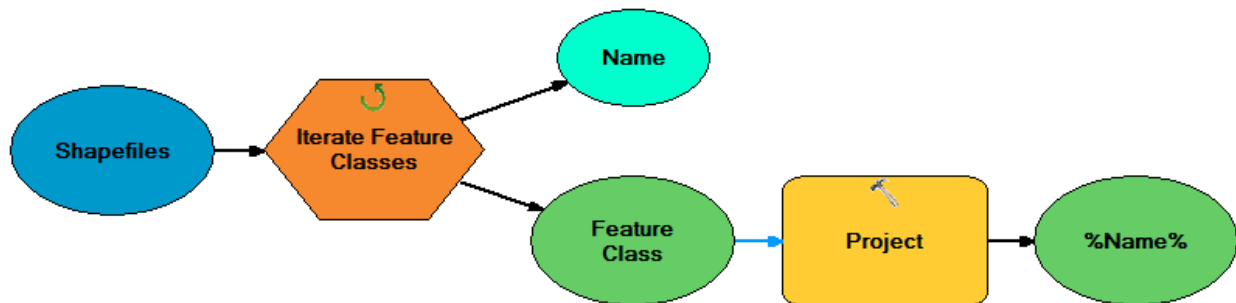
Figure 121. ArcGIS ModelBuilder workflow diagram for projecting GIS data to UTM coordinates.

Several ModelBuilder models (Figure 120 and Figure 121) were developed by FIU ARC researchers in 2015 during preliminary hydrological model development, in order to clip all of the GIS data to the study domain being used in the MIKE SHE model and project them into the appropriate coordinate system being used (i.e., NAD 1983 UTM Zone 17N); however, with the expansion of the study domain, it was necessary to reapply these models using the newly downloaded GIS data in order to clip them to the new Tims Branch watershed domain and project them into the UTM coordinate system. The process flow models developed were created so that they can also be implemented for other DOE sites by simply altering the study domain, the input files and the coordinate system.

Development of Model-Specific Input Files

New GIS shapefiles and maps were created for the expanded study domain which now incorporates the entire Tims Branch watershed as opposed to just the portion that lies within the SRS boundary. Some of the significant model input parameters that were generated for the new revised study domain are presented below.

Tims Branch Watershed Boundary (Model Domain)

Preliminary model development in 2015 involved the use of a model domain that only covered the portion of the Tims Branch watershed that lies within the SRS boundary. In order to study contaminant fate and transport along the full length and reaches of the Tims Branch stream, the model domain was expanded to cover the entire Tims Branch watershed (Figure 122).
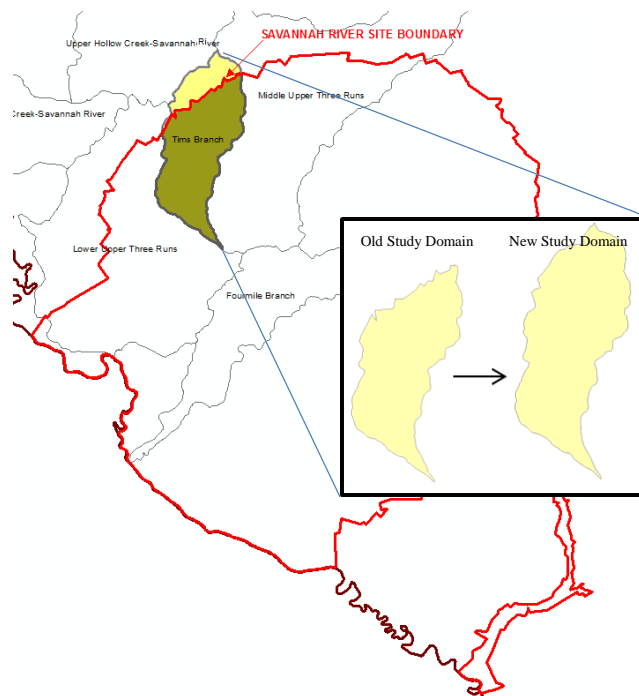
Figure 122. Expanded Tims Branch watershed study domain.

Land Use

MIKE SHE uses land use/land cover data to calculate ponded water and the spatial and temporal distribution of evapotranspiration (ET). ArcGIS tools were used to clip the downloaded GIS data to the revised Tims Branch watershed study domain and project the data into the appropriate coordinate system. Figure 123 depicts maps of the 1992 land cover classification for the old and new study domains.
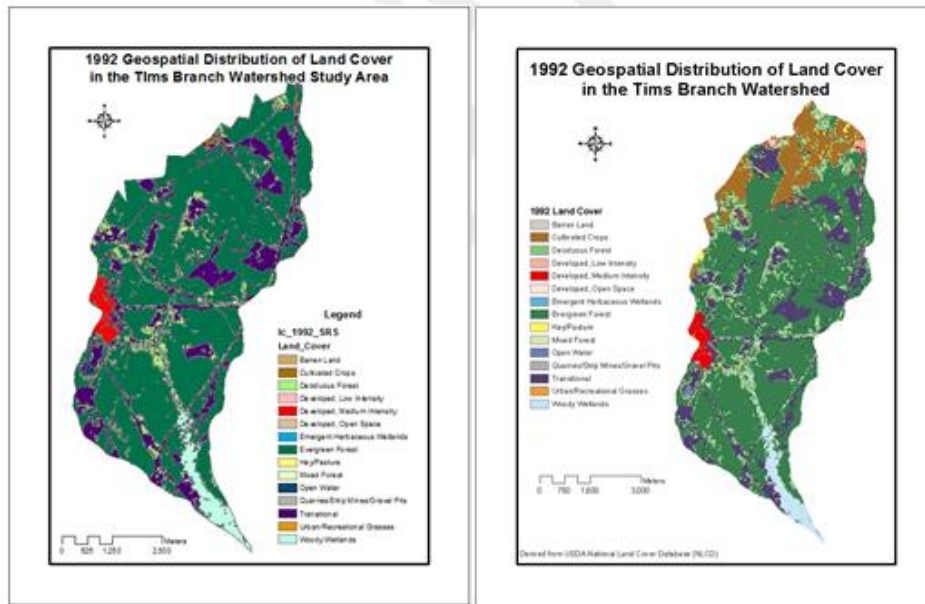
Figure 123. Map of the 1992 land cover classification in the Tims Branch watershed for the original study domain (left) and the new revised study domain (right).

Manning's Roughness Coefficient

The revised land cover GIS data was also used as the basis for generating shapefiles which represent other configuration parameters required for development of the MIKE SHE model with the expanded study boundary, such as the Manning's roughness coefficient seen below in Figure 124.
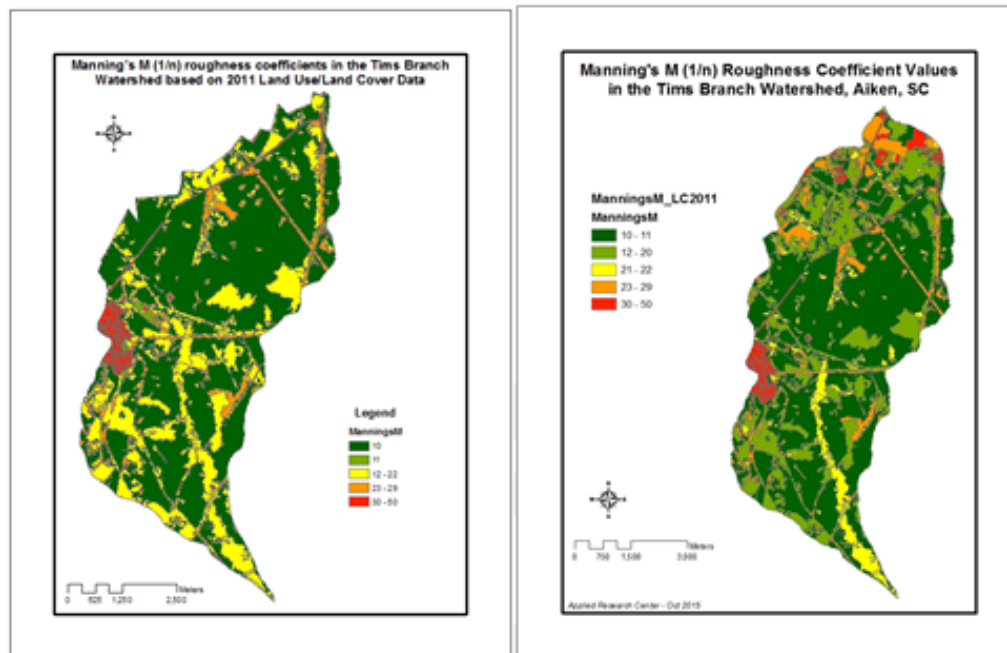
Figure 124. Map of the Manning's M (1/n) roughness coefficients in the Tims Branch watershed for the original study domain (left) and the new revised study domain (right).

Soils

Soil profile GIS data was acquired from the U.S. Department of Agriculture (USDA) Web Soil Survey website (http://websoilsurvey.sc.egov.usda.gov/App/WebSoilSurvey.aspx). Soil textures within the Tims Branch watershed were identified by investigating soil map units on the basis of geologic formation, geomorphology, and soil parent material at SRS. Figure 125 shows GIS maps of the soil classification for the old and revised Tims Branch study domains. The soil data was reclassified into 6 classes which include 4 dominant soil types (sand, sandy loam, loam, and loamy sand) as well as urban areas and open water (Figure 126).
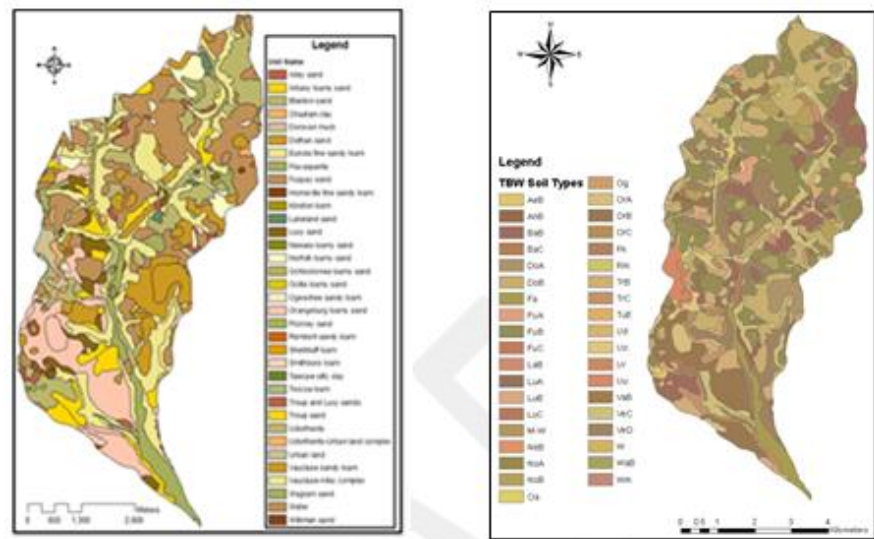
Figure 125. Soil classification maps of the Tims Branch watershed for the original study domain (left) and the new revised study domain (right).
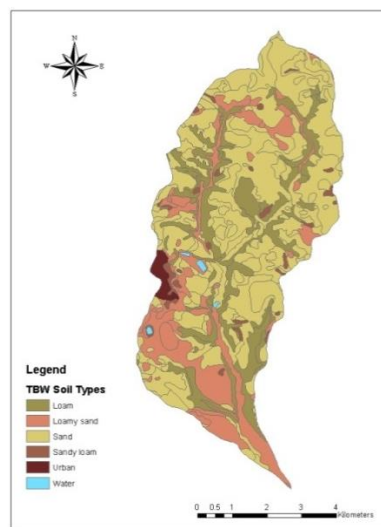
Figure 126. Map of the re-classified soil data in the Tims Branch watershed.

Preliminary Development of the MIKE 11 Stream Network

Development of a MIKE 11 stream flow model is targeted for FIU Performance Year 7 (2016-2017); however, ARC researchers decided to begin preliminary preparation by delineating the Tims Branch stream network and cross sections (Figure 127) using a combination of ArcGIS and

MIKE 11 tools and a digital elevation model (DEM) derived from 3m resolution LIDAR satellite imagery. More than 80% of the cross sections for the Tims Branch study area were prepared, but problems arose in areas along the various tributaries where the stream width was smaller than the mesh size of the grid being used. As such, ARC researchers and students decided to visit Savannah River Site in August 2016 to collect cross section measurements in several locations along Tims Branch. This data will be used to regenerate better representative cross sections and profiles of the Tims Branch stream and the A-014 outfall tributary thereby improving model accuracy.
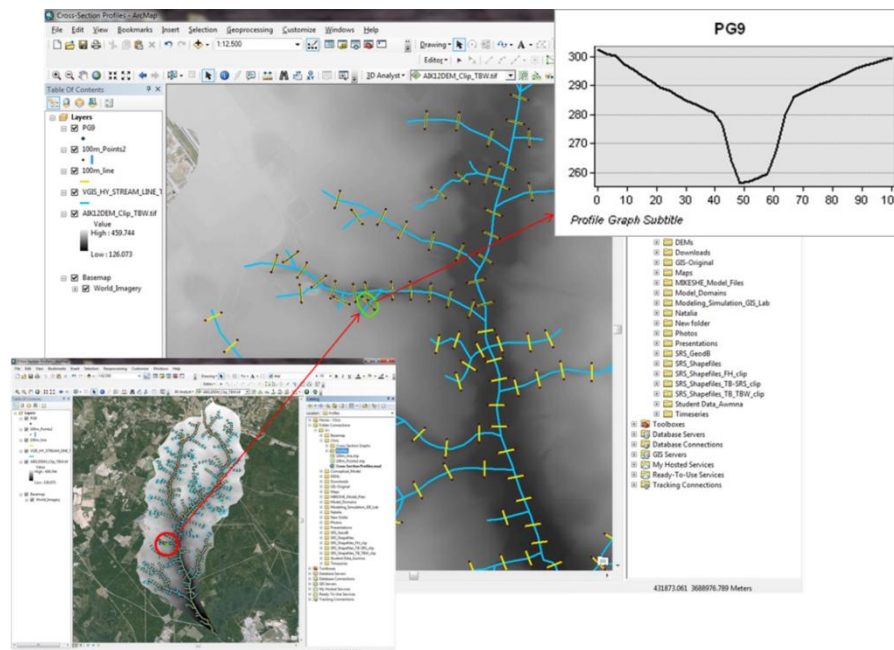
Figure 127. An ArcMap view of the preliminary delineated cross sections Tims Branch (left and center); the cross section profile of the cross section #PG9 (right).

Geospatial Analysis of Land Cover Change in the Tims Branch Watershed

FIU ARC researchers and students began a preliminary geospatial analysis of land cover and land use change due to urbanization in the Tims Branch watershed based on a methodology that calculates "projected urban growth" using ArcGIS geoprocessing and statistical analysis tools. as this can have an impact on the watershed hydrology. The geospatial analysis conducted involved:

1. Downloading land cover datasets for different years from the NLCD online database.
2. Clipping the data to the Tims Branch watershed study domain.
3. Converting the downloaded grid files from the NLCD database to GIS shapefiles.
4. Extracting regions within Tims Branch watershed where land cover change occurred.
5. Projecting the data to the appropriate coordinate system.
6. Calculating the area of land cover change from 1992 to 2011 due to urbanization.

Figure 128 depicts the analysis results which show only the extracted features that changed from non-urban to urban land use from 1992 to 2011. An inconsistency was noted during the analysis between the classifications of the 1992 and 2011 shapefiles. For the purpose of this preliminary exercise, and in order to compare the 1992 and 2011 shapefiles, the classification type "Urban/

Recreational Grasses" in the 1992 shapefile was changed to "Developed Medium Intensity". It is noted on the NLCD website that "the NLCD 1992 is not recommended for direct comparisons with any subsequent NLCD data products (i.e. NLCD 2001, NLCD 2006, NLCD 2011). The typical result of direct comparison will result in a change map showing differences between legends and mapping methods rather than real changes on the ground." This study will therefore need to be repeated to compare data from the 2001, 2006 and 2011 NLCD datasets.
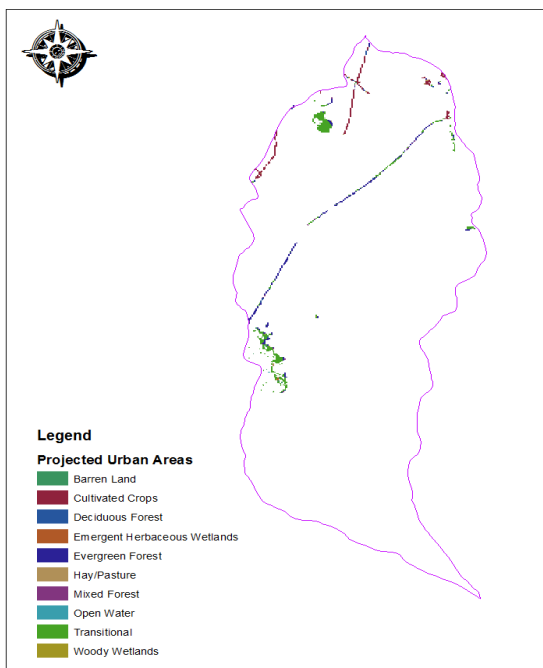
Figure 128. Map of the land cover in the Tims Branch watershed depicting only the extracted features that changed from non-urban to urban land use from 1992 to 2011.

Subtask 3.2: Conclusion

An ArcGIS geodatabase was developed by ARC researchers for the Savannah River Site and the Tims Branch watershed as a foundation for management, storage, processing, analysis and visualization of environmental and hydrological parameters, and for potentially building GIS-based water resources applications. The geodatabase possesses a spatial relational database management system (RDBMS) schema and relationship structure primarily based on the ArcHydro data model that is specific to hydrologic systems. This makes it a significant tool for conducting contaminant flow and transport analyses that require large amounts of high-quality spatial and temporal data in order to ensure reliability and validity of modeling results. ArcGIS tools significantly reduce the time needed for data preparation and improve overall efficiency by automating and batch processing model-specific geospatial and timeseries data via the development and implementation of process flow models. Utilization of the ArcGIS platform will continue to provide ARC researchers with a basis for management and geoprocessing of model configuration parameters, documenting process workflows, conducting geospatial analyses and visualizing model results. In addition, the SRS hydrologic geodatabase infrastructure enables linkage with other hydrologic modeling tools and applications to model hydrologic systems, and is scalable and replicable for implementation at other DOE sites.

Subtask 3.3: Biota, Biofilm, Water and Sediment Sampling in Tims Branch Watershed

Subtask 3.3: Introduction

To support the hydrology and contaminant transport modeling research, an *in situ* sampling and data collection exercise was conducted along the Tims Branch stream, A-014, and A-011 outfalls, to obtain data and parameters including flow velocity, depth, stream cross sections, suspended particle concentration, and other water quality data (pH, temperature, turbidity, etc.) required for model calibration and validation. Sampling methodology was developed prior to the fieldwork. The main goals were to generate cross-section profiles along the Tims Branch stream, A-014 and A-011 outfalls, at various locations and to quantify the suspended particle concentration at the same locations. Other water quality data were also measured during sample collection and cross-section profiling. A full report detailing the procedure, methodology, and results was prepared (see Appendices).

The data collection conducted at SRS was performed in collaboration with SREL and under full supervision of SREL staff and scientists. This fieldwork provided a great opportunity for FIU undergraduate and graduate STEM students (DOE fellows) to gain hands-on experience and technical training on the use of *in situ* measurement equipment. The data derived from their fieldwork will be implemented into the hydrology/hydraulic model as initial and boundary conditions.

Subtask 3.3: Methodology

To minimize system disturbance and particle suspension in the streams and channels, samples and measurements were collected starting from downstream of Tims Branch and A-011, gradually moving upstream. Figure 129 shows the locations along A-014, A-011, and Tims Branch where cross section measurements and samples were taken. Other water quality parameters were also measured at these same locations.
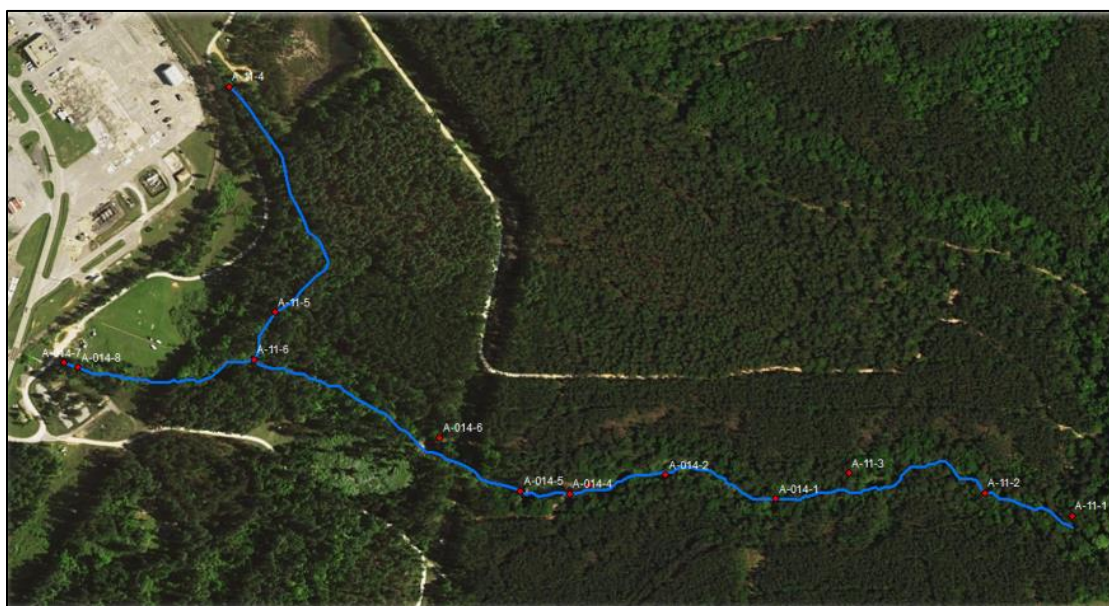

Figure 129: Sampling locations along A-014 and A-011, SRS, SC.

Figure 130: Profiling the cross section at one of the locations along A-014.

Subtask 3.3: Results and Discussion

The results indicate that flow velocity in A-014 ranges from 4 cm/s to 13 cm/s, but it is mostly constant at 4 cm/s; however velocity up to 27 cm/s was measured after rainfall occurred. This indicates that flow in A-014 is highly affected by a single rainfall event. High suspended particle concentration was also observed after the rainfall event which confirms the effect of a single storm event on resuspension and remobilization of sediment. Although the sampling and data collection was done only once, the results can relatively represent the flow and water quality parameters that occur in SRS naturally. The data will be used as initial parameters in hydrology and transport model development. The complete results are available in a separate report (see Appendices).

Subtask 3.3: Conclusion

Cross-section profiles and stream flow data are basic input parameters required when developing a detailed river flow model that can represent the natural system with certainty. Field data collection is an important step in providing accurate data for model development, calibration, and validation.

In the recent field data collection exercise, various data such as flow velocity, depth, and suspended particle concentration were measured in Tims Branch, Outfalls A-011, and A-014. A total of 33 water samples were taken and 21 cross-sections were profiled. The collected water samples were prepared and processed in an SREL laboratory to estimate the tin-rich suspended particle concentration in the water column. Analysis of the suspended particle concentration showed elevated levels after a rainfall event that occurred during the data collection. The significant increase in particle concentration confirms that rainfall indeed creates disturbance which causes the resuspension and remobilization of sediment in A-014 and Tims Branch. Therefore, continuous *in situ* data collection and performing numerical simulations are necessary to investigate the fate and transport of tin-rich sediment when a storm occurs.

TASK 3: FUTURE WORK

In FIU Performance Year 7, development of the hydrological model will be continued to simulate stream flow and sediment and contaminant transport in Tims Branch based on the

modeling work scope defined in Figure 131 below. The sampling and analysis activities identified under this task will be dependent on the availability of SRNL/SREL funds in order for them to provide support to FIU for site-required permitting and oversight activities as well as sample preparation and analysis costs.
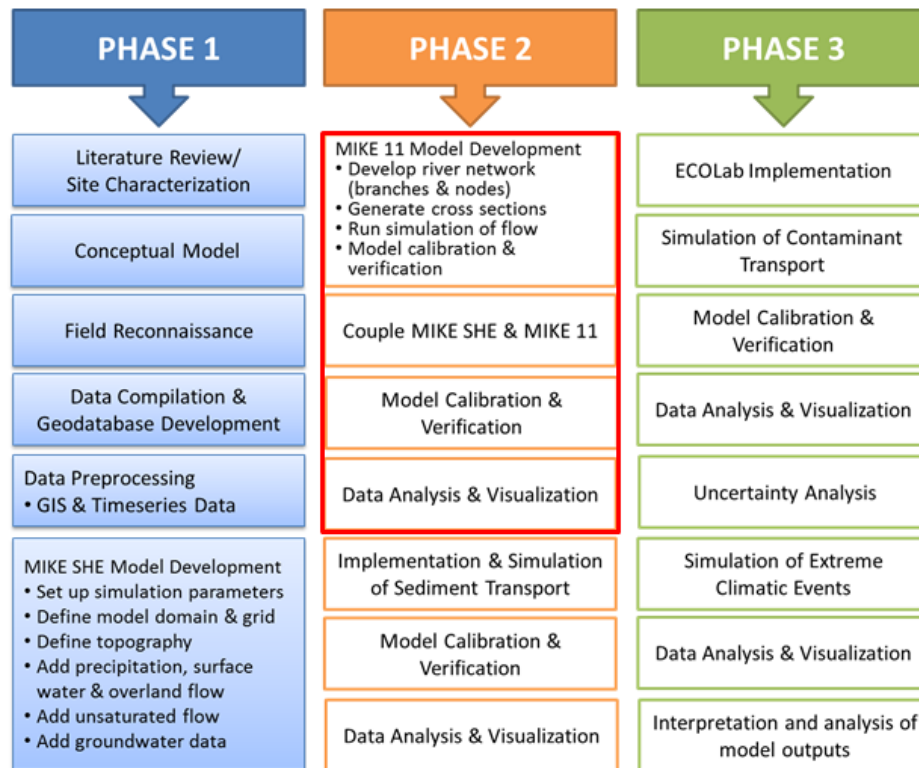
Figure 131. Hydrological modeling phases and detailed future plans.

The future modeling tasks to be performed include:

1. Running the UZ/SZ/ET modules simultaneously within MIKE SHE domain for prediction of the water balance of the TBW.
2. Calibration of the model to evaluate and refine parameter values by comparing simulated and observed values in an attempt to develop a model that represents the watershed. Different statistical evaluation methods will be employed to ensure the accuracy of the calibration results. This calibration and validation exercise helps to improve the predictive capability and reliability of the model. The main steps used for model calibration include: identification of calibration parameters, sensitivity analysis and numerical optimization.
3. Developing a 1-D river model using MIKE 11 for Tims Branch.
4. Calibration and validation of the MIKE 11 river model of Tims Branch in accordance with the MIKE SHE simulation of TBW.
5. Coupling the MIKE SHE watershed model and the MIKE 11 river model.
6. Integration of the developed model with the ECO Lab module to simulate contaminant transport in the TBW and Tims Branch stream.

GIS technology will be continuously utilized throughout the project to support the hydrological model development. Application of GIS technology is a key component in hydrological modeling that helps to prepare data, display results and conduct further spatial analyses. The use

of GIS technology has supported the preliminary development of the MIKE SHE and MIKE 11 models. In FIU Performance Year 7, ARC will continue to support hydrological model development with pre- and post-processing of data. GIS tools will support the development of the MIKE SHE/MIKE 11 model for delineation of the stream network and generation of cross-sections and profiles of the major and minor tributaries of Tims Branch. Advanced geospatial analyses will also be conducted for the Tims Branch watershed. This will include the examination of timeseries land use and land cover maps of the Tims Branch watershed to evaluate if there is any impact of land use/land cover change on the watershed hydrology. In addition, topographical changes as a result of the implementation of man-made structures along the A-014 outfall tributary will be examined to determine any hydrological impacts on the Tims Branch watershed.

FIU graduate and undergraduate students will be mentored and trained on how to update and query the existing geodatabase within the ArcGIS environment, perform geoprocessing tasks, conduct geospatial analyses and generate maps and graphs for reporting purposes.

TASK 3: ACKNOWLEDGEMENTS

TASK 3: REFERENCES

Aadland, R. K., Gellici, J. A., Thayer, P. A., and Carolina, S., 1995, Hydrogeologic Framework of West-Central South Carolina, State of South Carolina, Department of Natural Resources.

Abbott, M., and Refsgaard, J., 1996, Distributed Hydrologic Modeling, Kluwer Academics, Norwell.

Amouroux, D., Tessier, E., and Donard, O. F., 2000, Volatilization of organotin compounds from estuarine and coastal environments: Environmental Science & Technology, v. 34, no. 6, p. 988-995.

Arcement Jr., G., and Schneider, V., 1989, Guide for Selecting Manning's Roughness Coefficients for Natural Channels and Flood Plains, United States Geological Survey Water-Supply, Paper 2339.

Batson, V. L., Bertsch, P., and Herbert, B., 1996, Transport of anthropogenic uranium from sediments to surface waters during episodic storm events: Journal of Environmental Quality, v. 25, no. 5, p. 1129-1137.

Beven, K., and Kirkby, M., 1979, A physically based, variable contributing area model of basin hydrology: Hydrological Sciences Journal, v. 24, no. 1, p. 43-69.

Clarke, J. S., and West, C. T., 1998, Simulation of ground-water flow and stream-aquifer relations in the vicinity of the Savannah River Site, Georgia and South Carolina, predevelopment through 1992: US Dept. of the Interior, US Geological Survey; Branch of Information Services [distributor].

Conrads, P. A., Roehl, E. A., Daamen, R. C., and Kitchens, W. M., 2006, Simulation of water levels and salinity in the rivers and tidal marshes in the vicinity of the Savannah National Wildlife Refuge, Coastal South Carolina and Georgia: U. S. Geological Survey.

Dai T., A. R., Alvi, K., Wool, T., Manguerra, H., Choski, M., Yang, H., and Kraemer, S., 2005, Characterizing spatial and temporal dynamics: Development of a grid-based watershed mercury loading model. American Society of Civil Engineers Conference Proceedings. Managing Watersheds for Human and Natural Impacts: Engineering: Ecological, and Economic Challenges, Williamsburg, Virginia, USA.

Denham, M., 1999, SRS Geology/Hydrogeology Environmental Information Document: Savannah River Site (US).

Donard, O., and Weber, J., 1985, Behavior of methyltin compounds under simulated estuarine conditions: Environmental Science & Technology, v. 19, no. 11, p. 1104.

Faye, R. E., and Prowell, D. C., 1982, Effects of late Cretaceous and Cenozoic faulting on the geology and hydrology of the Coastal Plain near the Savannah River, Georgia and South Carolina: US Geological Survey, 2331-1258.

Feaster, T. D., Benedict, S. T., Clark, J. M., Bradley, P. M., and Conrads, P. A., 2014, Scaling up watershed model parameters: flow and load simulations of the Edisto River Basin, South Carolina, 2007-09: United States Geological Survey.

Feaster, T. D., Golden, H. E., Conrads, P. A., and Bradley, P. M., 2012, Simulation of Streamflow in the McTier Creek Watershed, South Carolina, Using TOPMODEL and GBMM.

Hallas, L., and Cooney, J., 1981, Tin and tin-resistant microorganisms in Chesapeake Bay: Applied and environmental microbiology, v. 41, no. 2, p. 466-471.

Halverson, N., 2008, Final Report on the Aquatic Mercury Assessment Study: SRS.

Hayes, D., 1984, Uranium studies in the Tims Branch and Steed Pond system: Westinghouse Savannah River Co., Aiken, SC (United States).

Kristensen, K., and Jensen, S., 1975, A model for estimating actual evapotranspiration from potential evapotranspiration: Nordic Hydrology, v. 6, no. 3, p. 170-188.

Lanier, T., 1997, Determination of the 100-year flood plain on Fourmile Branch at the Savannah River Site, South Carolina, 1996, US Department of the Interior, US Geological Survey.

Looney, B., 2001, Ultralow Concentration Mercury Treatment Using Chemical Reduction and Air Stripping: Savannah River Site (US).

Looney, B., Jackson, D., Peterson, M., Mathews, T., Southworth, G., Paller, M., Bryan, L., Eddy-Dilek, C., and Halverson, N., 2010, Assessing Potential Impacts of Stannous Chloride Based Mercury Treatment on a Receiving Stream Using Real-World Data from Tims Branch, Savannah River Site: SRS.

Looney, B., Larry, B., Mathews, T. J., Peterson, M. J., Roy, W. K., Jett, R. T., and Smith, J. G., 2012, Interim Results from a Study of the Impacts of Tin (II) Based Mercury Treatment in a Small Stream Ecosystem: Tims Branch, Savannah River Site: Oak Ridge National Laboratory (ORNL).

Maguire, R., Tkacz, R., Chau, Y., Bengert, G., and Wong, P., 1986, Occurrence of organotin compounds in water and sediment in Canada: Chemosphere, v. 15, no. 3, p. 253-274.

Maidment, D. R., 2002, Arc Hydro: GIS for Water Resources. ESRI Press.

Mast, M. A., and Turk, J. T., 1999, Environmental characteristics and water quality of hydrologic benchmark network stations in the midwestern United States, 1963-95, US Geological Survey.

van Genuchten, M. T., 1980, A Closed-form Equation for Predicting the Hydraulic Conductivity of Unsaturated Soils: Soil Science Society of America Journal, v. 44, no. 5, p. 892-898.

Varlik, B., 2013, Total Maximum Daily Load Document Tims Branch SV-324 and Upper Three Runs SV-325 Hydrologic Unit Codes 030601060501, 030601060502, 030601060503, 030601060504, 030601060505, 30601060506.

Wolock, D., 1993, Simulating the variable-source-area concept of streamflow generation with the watershed model TOPMODEL: US Geological Survey, Water Resources Division; US Geological Survey, Books and Open-File Reports [distributor].

Yan, J., and Smith, K. R., 1994, Simulation of Integrated Surface Water and Ground Water Systems-Model Formulation: Journal of the American Water Resources Association, v. 30, p. 879-890.

TASK 4: SUSTAINABILITY PLAN FOR THE A/M AREA GROUNDWATER REMEDIATION SYSTEM

TASK 4: EXECUTIVE SUMMARY

The research and analysis under this task was performed in support of what was formerly DOE EM-13 (Office of D&D and Facilities Engineering) under the direction of Mr. Albes Gaona, program lead for DOE's Sustainable Remediation Program. Sustainable remediation analyses require the collection and analysis of historical site remediation system design and performance including electrical energy usage, contaminant recovery per well, optimized air stripper operation, and more. During FIU Performance Year 5, FIU researchers began a sustainable remediation analysis of the Savannah River Site (SRS) M Area groundwater remediation system (GWRS). The first stage involved an extensive analysis of contaminant recovery per well which was published in reports and publications. During FIU Performance Year 6, FIU continued the research by analyzing the equipment, processes, hydraulic containment of contamination, and developed a set of recommendations for the existing infrastructure of the groundwater remediation system that will reduce the environmental burden of the A/M Area groundwater remediation system.

TASK 4: INTRODUCTION

DOE sites are developing sustainability programs, projects and initiatives in order to help meet the goals as set out in individual Site Sustainability Plans and the overall U.S. DOE 2013 Strategic Sustainability Performance Plan. There are many benefits of implementing sustainable practices, including reducing costs as well as fostering better engagement and acceptance of improved remediation strategies and sustainable practices by regulators, the public, and other stakeholders. These benefits are in addition to the more obvious ones of reducing energy consumption, improving air and water quality, minimizing impact to the environment, reducing carbon footprints, and reducing waste generation. In support of Savannah River Site's sustainability goals, FIU began a sustainable remediation analysis of the SRS M Area groundwater remediation system in 2014. The analysis was focused on the M1 Air Stripper: its mechanical systems, volume flow rate of water and contaminant concentration, performance of the packing material, and the blower motor. The intent was to determine the existing environmental burden associated with operating the A/M Area groundwater remediation system. This baseline then served as the basis for identifying opportunities for improving sustainability.

TASK 4: OBJECTIVES

The goal of the SRS M Area groundwater remediation system is to provide hydraulic containment of the contaminated groundwater. The focus of FIU's sustainable remediation analysis was to provide analyses and recommendations for improving the electro-mechanical components and operations of this remediation system (e.g., air stripper, pumps). These improvements should result in a more sustainable system that saves energy, cuts greenhouse gas emissions, and saves financial and other resources.

TASK 4: METHODOLOGY

Recovery wells in the A/M Area groundwater remediation system have been operated with constant speed pumps since the system began operation. The constant speed pumps produce line pressures that range from 35 – 95 psig. In some cases, the pumps may be producing excess pressure that is not required and as a result are continuously consuming energy that is not necessary for operation. FIU executed a study of the piping diagram and operating pressure throughout the system to identify wells which may be able to operate using a smaller pump while still maintaining the same flow rate.

In addition, the M1 Air Stripper has operated at a constant air/water ratio since it began operation. The air/water ratio was set to treat the prevailing influent contaminant concentrations existing at start-up. Contaminant concentrations have decreased significantly over the last 27 years of operation and, as a result, the air/water ratio can likely be decreased. The water flow rate is set by the hydraulic containment objective and is not considered to be an option for improvement. The air flow rate, however, is based on the influent contaminant concentration. It is believed that the air flow rate can be reduced and still meet the discharge limits at the outfall receiving effluent from the A1 air stripper. Reducing the air flow rate would significantly reduce the energy demand since the A1 air stripper operates constantly. FIU's aim was to use current influent concentrations with published design guidelines for air strippers to determine the minimum air flow rate that would meet treatment specifications and recommend a new blower based on the outcome of the air stripper analysis.

The sustainable remediation analysis of the M1 Air Stripper included:

- Analysis of available data of air mass flow rates and contaminant removal efficiency to determine the overall system efficiency and provide recommendations for the optimal air flow rates which will provide the lowest overall cost of operation.

- Analysis of the contaminant concentration from all recovery wells feeding the M1 air stripper and the current packing material and recommendations for component and process changes to improve the efficiency, lower the electrical energy usage and lessen the environmental footprint of the stripper operation.

- Analysis of a renewable energy system to power the M1 air stripper to include solar and/or wind. This would include costs for components properly sized and for installation.

TASK 4: RESULTS AND DISCUSSION

Details of the sustainability analysis for the A/M Area groundwater remediation system are provided in a separate technical report entitled, *A Sustainability Analysis for the M1 Air Stripper and Pumps of the M Area Groundwater Remediation System at the Savannah River Site*. This report consists of the following:

- Analysis of Historic Contaminant Recovery
- Solar Power Option for Powering the A/M Groundwater Remediation System
- Packing Material Design and Optimization of Operation
- Pump Replacement Upon Failure Strategy
- Use of Variable Frequency (or Speed) Drives
- Optimization of Pumping Rate and Schedule for each Recovery Well

TASK 4: CONCLUSION

FIU developed a set of actions for the existing infrastructure of the groundwater remediation system that will reduce the environmental burden of the A/M Area groundwater remediation system while potentially reducing the duration of operation for the treatment system. Analyses and modifications are suggested for the A/M-Area groundwater remediation system that would offer the potential for less electrical power consumption and lower total groundwater pumping rates. Specific recommendations include:

1. A solar photovoltaic system for powering the A/M Area groundwater remediation system;

2. The determination and use of an optimal speed for the blower motor that is sufficient to run the countercurrent stripper and removes the volatile organic contaminants to below the 1 ppb required;

3. A groundwater modeling analysis be completed to optimize the pumping rate for each recovery well and for the entire system that provides hydrologic containment and maximizes the concentration of contaminants pumped to the stripper with possible lower total groundwater and air flow rates in the stripper; and

4. Replacement of groundwater pumps when they fail with new efficient pumps with power that matches the required pump rate of the recovery well (e.g., possibly more lower powered 1-5 hp pumps).

TASK 4: FUTURE WORK

This task was completed during FIU Performance Year 6 and a technical report was submitted to DOE and SRNL. This task is not continuing to FIU Performance Year 7.

TASK 4: ACKNOWLEDGEMENTS

Our sincere appreciation is extended to Mr. Albes Gaona (DOE EM) and Dr. Ralph Nichols (SRNL) for their support while conducting this research.

TASK 4: REFERENCES

Llewellyn F. Boone, Robert Lorenz, Carl F. Muska, J. L. Steele, and LeVerne P. Fernandez, A Large-Scale High-Efficiency Air Stripper and Recovery Well Network for Removing Volatile Organic Chlorocarbons from Ground Water, E.I. du Pont de Nemours and Co., Savannah River Plant, Aiken, SC, Sixth National Symposium and Exposition on Aquifer Restoration and Ground Water Monitoring, May 1986.

Personal communication, Dennis Jackson, SRNL, Dec. 2015.

Betancourt, A. (2011). *Tin Distributution and Fate in Tims Branch at the Savannah River Site.*DOE Fellows Summer Internship Technical Report, Applied Research Center, Florida International University, https://fellows.fiu.edu/wp-content/uploads/2015/06/Amaury-Betancourt-Internship-Rpt-Summer-2011-Rev-0-1.pdf

Braden Kramer, James Kupar, Jeff Ross, Joao Cardosa-Neto, SRNS and Dennis Jackson and Brian Looney, SRNL, Concluding a Steam Injection Remediation Project at a DNAPL Zone at SRS, Waste Management 2015, March 2015.

Huang, J. C., & Shang, C. (2006). Air Stripping. In *Advanced Physicochemical Treatment Processes handbook of Environmental Engineering* (Vol. 4, pp. 47-79).

Srinivasan, A., Chowdhury, P., & Viraraghavan, T. *Air Stripping in Industrial Wastewater Treatment.* University of Regina, Canada, Faculty of Engineering.

Melin, G. (2000). *Treatment Technologies for Removal of Methyl Tertiary Butyl Ether (MTBE) from Drinking Water.* National Water Research Institute.

Beranek, D. A. (2001). *Engineering and Design Air Stripping.* U.S. Army Corps of Engineers, Department of the Army, Washington, D.C.

El-Behlil, M., Sead M, E.-G., & Adma, S. A. (2012). *Simplified Packed Tower Design Calculation for the Removal of VOC's from Contaminated Water.* Istambul: Sixteenth International Water Technology Conference.

El-Behlil, M., Sead M, E.-G., & Adma, S. A. (2012). *Volatile Organic Chemicals Removal from Contaminated Water.* Istambul: Sixteenth International Water Technology Conference.

Faust, S. D., & Aly, O. M. (1998). *Chemistry of Water Treatment* (2nd ed.). Boca Raton, Fl: Lewis Publishers.

Handbook of Public Water Systems (Second ed.). (n.d.). HDR Engineering, Inc.

Huang, J.-C., & Shang, C. (2006). *Air Stripping.* Totowa, NJ: Humana Press.

Personal communication, Ralph Nichols, SRNL, Feb. 2015.

Modeling and Quantitative Assessment of Green and Sustainable Remediation Options for the M1 Air Stripper System at DOE's SRS, David Roelant and Natalia Duque, Florida International University, and Ralph Nichols, Savannah River National Laboratory, Waste Management 2015, March 2015.

Quote from Southern Atlantic Solar Company for a 894 kW solar photovoltaic system for M1 air stripper and associated well network, Nov. 2015.

Waide, Paul; Brunner, Conrad U. (2011). "Energy-Efficiency Policy Opportunities for Electric Motor-Driven Systems."

Bose, B. K. (Feb 2009). "Power Electronics and Motor Drives Recent Progress and Perspective". *IEEE Transactions on Industrial Electronics* **56** (2): 581–588. doi: 10.1109/tie.2008.2002726

Campbell, Sylvester J. (1987). *Solid-State AC Motor Controls*. New York: Marcel Dekker, Inc. pp. 79–189. ISBN 0-8247-7728-X.

Interim Action Record of Decision Remedial Alternative Selection, A/M Area Groundwater Operable Unit, SRS, WSRC-RP-92-744, June 25, 1992.

Geraghty & Miller Inc, Apr. 1983, Tuscaloosa Aquifer Pumping Test, M-Area, Savannah River Site Plant, prepared for E.I. du Pont de Nemours and Co., Savannah River Plant, Aiken, SC.

Geraghty & Miller Inc, Aug. 1986, Hydraulic Properties of the Tertiary Aquifer System Underlying M Area, prepared for E.I. du Pont de Nemours and Co., Savannah River Plant, Aiken, SC.

Trescott, P.C. and Larson, S. P., 1976, Supplement to Open-File Report 75-438, Documentation of the Finite Difference Model Simulation of Three-Dimensional Ground-Water Flow, U.S. Geological Survey Open-File Report 76-591.

Westinghouse Savannah River Company. (1998). *3Q/4Q99 Annual M-Area and Metallurgical Laboratory Hazardous Waste Management Facility Groundwater Monitoring and Corrective-Action Report, Third and Fourth Quarters 1999, Volume I and II.* Aiken, SC.

Savannah River Nuclear Solutions, LLC. (2012). *Annual 2011 M-Area and Metallurgical Laboratory Hazardous Waste Management Facilities Groundwater Monitoring and Corrective Action Report, Volume I.* Aiken, SC.

Westinghouse Savannah River Company. (1993). *Fourth Quarter 1992 and 1992 Summary M-Area Hazardous Waste Management Facility Groundwater Monitoring Report, Volume I.* Aiken, SC.

Westinghouse Savannah River Company. (1997). *M-Area and Metallurgical Laboratory Hazardous Waste Management Facility Groundwater Monitoring and Corrective-Action, Third and Fourth Quarters 1996, Volume I.* Aiken, SC.

Westinghouse Savannah River Company. (1998). *M-Area and Metallurgical Laboratory Hazardous Waste Management Facility Groundwater Monitoring and Corrective-Action, Third and Fourth Quarters 1997, Volume I.* Aiken, SC.

Westinghouse Savannah River Company. (1995). *M-Area Hazardous Waste Management Facility Groundwater Monitoring and Corrective-Action Report, Fourth Quarter 1994.* Aiken, SC.

Westinghouse Savannah River Company. (1996). *M-Area Hazardous Waste Management Facility Groundwater Monitoring and Corrective-Action Report, Third and Fourth Quarters 1995.* Aiken, SC.

Westinghouse Savannah River Company. (1990). *M-Area Hazardous Waste Management Facility Post-Closure Care Permit Groundwater Monitoring and Corrective Action Program.* Aiken, SC.

Savannah River Nuclear Solutions, LLC. (2011). *Annual 2010 M-Area and Metallurgical Laboratory Hazardous Waste Management Facilities Groundwater Monitoring and Corrective Action Report, Volume I.* Aiken, SC.33. Interstate Technology & Regulatory Council. (2011). *Green and Sustainable Remediation: State of the Science and Practice.* Washington, DC.

TASK 5: REMEDIATION RESEARCH AND TECHNICAL SUPPORT FOR THE WASTE ISOLATION PILOT PLANT

TASK 5: EXECUTIVE SUMMARY

The following task is a new collaboration begun in spring 2016 with Los Alamos National Laboratory's field office at the Carlsbad Environmental Monitoring and Research Center (LANL CEMRC) which is a part of New Mexico State University. Hilary Emerson spent ten weeks working at the LANL CEMRC laboratories as a visiting scientist to kick off this new task in collaboration with Drs. Tim Dittrich and Donald Reed. The goal is to generate accurate sorption data for the trivalent actinides to minerals and under conditions relevant to the Waste Isolation Pilot Plant as previous risk assessment models are based on conservative assumptions. DOE Fellow Frances Zengotita (B.S. Chemistry and English) also supported this project task. In addition, abstracts were submitted to be presented at the American Geophysical Union Conference in December 2016 by collaborator Tim Dittrich entitled "Role of bring chemistry and geologic sorption on potential long-term storage of radioactive waste: Experimental evaluation of sorption parameters" and at the FIU McNair Scholars Research Conference in October 2016 by Frances Zengotita entitled "Role of ionic strength on sorption of neodymium on dolomite."

TASK 5: INTRODUCTION

The Waste Isolation Pilot Plant (WIPP) was authorized by the U.S Congress in 1979 for 'the express purpose of providing a research and development facility to demonstrate the safe disposal of radioactive waste from the defense activities and programs of the U.S exempted from regulation by the NRC' (U.S.DOE 1995, U.S.DOE 1996). The WIPP has successfully disposed of waste from nuclear weapons production and nuclear activities during WWII and the Cold War although disposal operations are currently stopped.

At this time, the WIPP is re-evaluating their risk assessment models as they are planning to begin accepting waste again by the end of this year. The site has currently disposed of 90,000 m^3 contact-handled transuranic waste (CHTRU) and 360 m^3 remote-handled transuranic waste (RHTRU), reported as of Feb. 2014. The chemical behavior of radionuclides in the actinide series is a major concern for the WIPP. The actinide series elements being disposed of at the WIPP are from the transuranic waste produced during the development of nuclear weapons and account for 90% of alpha activity. A complete assessment of the chemical behavior of radionuclides is fundamental for safe operation of the WIPP.

In the WIPP release scenario, human intrusion (cuttings, cavings, spallings) can lead to direct and/or long-term brine release (U.S.DOE 1995, U.S.DOE 1996, Perkins, Lucero et al. 1999). Once the brine is released, it may proceed through the Rustler formation (the most transmissive layer) and pose a potential threat to the environment (Perkins, Lucero et al. 1999). Due to the potential threat in the future for radioactive contamination, risk assessment models must be updated. The significance of the investigation of Nd sorption processes will report both the speed and transmissive properties of the hypothetical outbreak (brine release).

TASK 5: OBJECTIVES

Updating experimental data on the behavior of radionuclides at WIPP is of fundamental significance because it will help the site update their risk assessment models. In this work, neodymium (Nd) will be used as an analog to Americium. The chemical similarities of trivalent actinide series (i.e. Am^{+3}) and naturally occurring rare earth elements (such as the lanthanide Nd) have been established previously and can be used as chemical analogues for the actinide series elements (Hodge et al., 1995). These chemical analogues have similar chemical behaviors, ionic radii and valence states as trivalent actinides. Chemical analogues such as Nd can be used to model "geochemical behavior" (i.e as mobility, speciation) for the trivalent actinides without the manipulation of radioactive materials.

Previous experimental sorption data for trivalent actinides and lanthanides to dolomite had difficulties with precipitation and many works did not investigate the high ionic strength conditions relevant to the WIPP (Brush and Storz 1996; Brady, Papenguth et al. 1999; Perkins, Lucero et al. 1999). Since there is a lack of appropriate experimental data for sorption processes for the trivalent actinides, there is a need for a better understanding of radionuclide sorption in deep geologic repositories at the WIPP.

The purpose of this subtask is to conduct column and batch experiments to observe the sorption of neodymium to the dolomite mineral at variable total ionic strength (NaCl + 3 mM bicarbonate) up to 5 M. The batch experiments of the dolomite with the background electrolyte (NaCl +3 mM bicarbonate + 20 ppb Nd) will help in updating the DOE risk assessment models for the WIPP site. The significance of the batch and column sorption experiments is that it investigates the kinetics and saturation of neodymium to the dolomite mineral, which would update risk assessment models for the WIPP.

TASK 5: MATERIALS AND METHODS

Materials

Synthetic brine: 0.1, 2 M and 5.0 M total ionic strength [3mM $NaHCO_3$ + NaCl], 20 ppb Nd

Mini-Columns:

Continuous injection mini-columns

- Teflon columns are 2.2 cm length (1 cm length of dolomite + fitting)
- 1 cm column (~1 gram dolomite, porosity 0.32)
- Synthetic brine 2 and 5 M total ionic strength [3 mM $NaHCO_3$ + NaCl] + 20ppb Nd
- 1/16" Teflon tubing
- Syringe pump
- Humidity Chamber
- Fraction collector (for effluent)
- 13x100 mm polystyrene tubes
- 2 mL polypropylene vials
- 2% Nitric Acid
- pH electrode and meter

Batch Kinetics:

- End-over-end mixer

- Variable concentrations of dolomite (12.5, 25, 125 g/L dolomite)
- Background electrolyte of 2 M and 5.0 M total ionic strength [3mM NaHCO$_3$ + NaCl] + 20 ppb Nd
- 2 mL polypropylene vials
- 50 mL polypropylene centrifuge tubes
- 2% Nitric Acid
- pH electrode and meter

Methods

Mini-Column Experiments

A mini column experiment was started for the 5 M electrolyte background [3 mM bicarbonate + NaCl] + 20 ppb Nd. The mini column experiment is investigating the sorption processes of neodymium (Nd) to the dolomite mineral. A Kloehn pump pushes the 5 M electrolyte solution [3 mM bicarbonate + NaCl + 20 ppb Nd] into the column at a 1.5 mL/hr flow rate through 2.2 cm length (1 cm length of dolomite + fittings) columns. The effluent is collected every 4 hours into 13x100 mm polystyrene tubes in an Eldex fraction collector.

The tubes that were collected from the column experiment, weighed, analyzed for pH and then placed into 2 mL vials for the ICP-MS analysis with a 1:5 dilution in 2% HNO$_3$. An additional dilution of at least 1:10 (for a total of 1:50) will be completed to further dilute the total salts to acceptable limits for ICP-MS analysis. Nitric acid was added in order to preserve the solution for ICP-MS analysis.

The column has been running for approximately two months with continuous effluent collection and pH analysis of each effluent tube. The mini column experiment will be measured until breakthrough (i.e., when the dolomite mineral is saturated with Nd and the effluent concentration reaches the initial spike influent concentration).

Batch Experiments

The batch sorption experiments included variable concentrations of dolomite (12.5, 25 and 125 g/L dolomite) along with a background electrolyte that consisted of 2 M or 5 M total ionic strength [3 mM NaHCO$_3$ + NaCl]. The batch kinetics experiment measurements were taken over a two day period with measurements at 15 minutes as well as 1, 4, 8, 24 and 48 hours. The kinetic batch experiment investigates the saturation concentration and the sorption processes of neodymium to the dolomite mineral.

At each time interval for the batch kinetic experiment, the tubes were allowed to settle for 15 minutes to ensure that the dolomite mineral was not present in the aqueous phase prior to sampling as solids could damage the ICP-MS during analysis. While the six mixtures (0.5g-dol-1,2,3; 1.0g-dol-1,2,3) were left to sit, the pH was measured and the time was recorded. Once the seventh batch kinetics data was collected, the final mass of each tube was taken to ensure that total volume losses throughout the experiment were minimal (i.e. <2%).

The batch samples collected from the tubes were weighed and placed into 2-mL vials for ICP-MS analysis with a 1:10 dilution in 2% HNO$_3$. Nitric acid was added in order to preserve the solution for the ICP-MS analysis. The batch experiments were conducted at 2 and 5 M total ionic strength [3 mM NaHCO$_3$ + NaCl].

Sample Analysis

All samples from the column and batch are currently awaiting analysis by ICP-MS as the instrument is not currently operational. However, the samples will continue to be prepared and stored until the ICP-MS analyses is performed. If the needed ICP-MS repairs continue to delay the analyses, the ICP-OES will be used.

TASK 5: RESULTS AND DISCUSSION

The final results for these experiments are still being collected and analyzed at this time. They will be presented in future monthly reports as soon as they are available. All results collected during the time that Hilary Emerson was a visiting scientist at LANL CEMRC have been submitted as a separate technical report.

TASK 5: FUTURE WORK

During FIU Performance Year 7, mini-column and kinetic batch sorption experiments begun in Year 6 will be continued with Nd(III) as an analog for the actinide(III) oxidation state and dolomite to refine the procedures for the experiments with radioactive elements. Ionic strength will be varied from 0.01 – 5.0 M with NaCl to ensure investigation of conditions relevant to brines from both the near field and far field which may be transported through the dolomite formation. Relevant ligands will also be considered in batch and mini column experiments. Experiments will also begin with Am(III) to confirm the use of Nd(III) as an analog for the trivalent oxidation state.

TASK 5: ACKNOWLEDGEMENTS

TASK 5: REFERENCES

Brady, P. V., H. W. Papenguth and J. W. Kelly (1999). "Metal sorption to dolomite surfaces." Applied Geochemistry 14(5): 569-579.

Brush, L. H. and L. J. Storz (1996). Revised Ranges and Probability Distributions of Kds for Dissolved Pu, Am, U, Th, and Np in the Culebra for the PA Calculations to Support the WIPP CCA. S. N. Laboratories. Albuquerque, NM.

Perkins, W. G., D. A. Lucero and G. O. Brown (1999). Column Experiments for Radionuclide Adsorption Studies of the Culebra Dolomite: Retardation Parameter Estimation for Non-Eluted Actinide Species. S. N. Laboratories. Albuquerque, NM: 163.

U.S.DOE (1995). Inventory WIPP Baseline Inventory Report. U. S. D. o. Energy. Carlsbad, NM.

U.S.DOE (1996). Title 40 CFR Part 191 Compliance Certification Application for the Waste Isolation Pilot Plant. U. S. D. o. Energy. Carlsbad, NM, Carlsbad Area Office.

APPENDICES

The following reports are available at the DOE Research website for the Cooperative Agreement between the U.S. Department of Energy Office of Environmental Management and the Applied Research Center at Florida International University: http://doeresearch.fiu.edu

1. Florida International University, *Project Technical Plan,* Project 2: Environmental Remediation Science and Technology, October 2015.

2. Florida International University, *Application of GIS Technologies for Hydrological Modeling Support*, Technical Progress Report, May 2016.

3. Florida International University, *A Sustainability Analysis for the M1 Air Stripper and Pumps of the M Area Groundwater Remediation System at the Savannah River Site*, Technical Progress Report, December 2015.

4. Florida International University, *Research and Technical Support for WIPP: Trivalent Actinide and Lanthanide Partitioning in Culebra Dolomite*, Technical Progress Report, August 2016.

The following documents are included in this report as separate attachments:

1. Appendix A: Florida International University, *Modeling of Surface Water and Sediment Transport in the Tims Branch Ecosystem*, Technical Progress Report, submitted June 2016 and updated October 2016.

2. Appendix B: Florida International University, *In-Situ Data Collection and Water Quality Sampling in Tims Branch, Savannah River Site, Aiken, SC*, Trip Report, August 2016.